Analysis of the function and regulation of the conserved Mef2 transcription factor in muscle differentiation and maintenance in *Drosophila melanogaster*

Robert John Mitchell-Gee

March 2024

This thesis is submitted for the degree of Doctor of Philosophy

Acknowledgements

Firstly, I want to thank my supervisor Dr Michael Taylor, for his unwavering support and guidance throughout the entirety of my PhD. Your enthusiasm for science is infectious, and your expertise, patience and mentorship have been instrumental in shaping this thesis and my academic growth. I have enjoyed many of our discussions about this project over the years, particularly those that were accompanied by fine French cuisine!

I am also indebted to my colleagues within Cardiff's fly community, many of whom I now count as friends, for their constant encouragement and camaraderie during both the challenging and rewarding moments of this project. Frequent collaborative trips to Brodie's and Gregg's have ensured my brain is well fed with a constant supply of caffeine and sausage rolls, without which this project would have greatly suffered.

Thank you to my parents, Rob & Sandi, and my sister, Lily, for always cheering me on, and for their patience and understanding when I haven't visited for a while. I am also grateful to my Auntie Susie, Uncle Brian and my Nan, who have always ensured that this poor student has had plenty to eat.

To my partner, Tilly; ever since our first date to Kongs, where I regaled you with tales of *Drosophila* spermatogenesis, you have been nothing other than supportive of me on this journey. Your shear belief that I can do this has kept me going, even when the road seemed long and arduous.

Finally, thank you to Zorra the dog. Your excitement to see me every time I get home from the lab has always cheered me up, even after the longest of days.

Funding

This work was generously supported by the John Ryder Memorial Trust and Cardiff University School of Biosciences.

List of Abbreviations

***Drosophila* gene name**	**Human ortholog(s)**
Ama – Amalgam	No clear ortholog
bnl - branchless	*Fibroblast growth factor-10 (FGF10)*
β3-tubulin	*TUBB* (β -tubulin Class I)
ct – cut	*Cut-like homeobox 1* (*CUX1*)
dpp – decapentaplegic	*Bone Morphogenetic protein 2/4 (BMP2/4)*
Doc – Dorsocross	T-box transcription factors (*TBX1-3*)
duf - dumbfounded	*KIRREL* (Nephrin-like protein)
eve – even-skipped	Even-skipped homeobox genes (*EVX1, EVX2*)
gro – groucho	Transducin-like enhance of split (TLE) family
gsb – (gooseberry)	Paired-box transcription factors (*PAX3, PAX7*)
hbs – hibris	*NEPH1*
Him – Holes in muscle	No clear ortholog
Kr – Kruppel	Kruppel-like factors (KLFs)
lmd – lame duck	*LMO4*
l'sc – lethal of scute	*ASCL1*
Mhc – myosin heavy chain	Myosin heavy chain family (MYH)
nau - nautilus	Myogenic regulatory factors (MRFs)
pnr – panier	GATA transcription factors
rst – roughest	*KIRREL*
sd – scalloped	TEA domain transcription factors (TEAD)
sing – singles bar	No clear ortholog
slp – sloppy paired	*NR2E1*
sls - sallimus	*TITIN*
sns – sticks and stones	*KIRREL* (Nephrin-like proteins)
Su(var)2-10 – Suppressor of variegation 2-10	PIAS family
svp – seven up	COUP-TF nuclear receptors
tinman – tin	*NKX2-5*
Ubc9	*UBC9*
vg – vestigial	VGLL (vestigial-like proteins)
wg – wingless	WNT family
zfh1	*ZEB1*

Muscle Terminology

AMP – adult muscle progenitor
DFM – direct flight muscles
DLM – dorsal longitudinal muscle
DOM – dorsal oblique muscle
DVM – dorsal ventral muscle
FC – founder cell
FCM – fusion competent myoblast
IFM – indirect flight muscle
MuSC – muscle satellite cell
TDT – tergal depressor of the trochanter (or jump muscle)

Other Abbreviations

AP – anterior-posterior
APF – after pupal formation
DV – dorsal-ventral
Gal80ts – temperature-sensitive Gal80
GOF – gain-of-function
LiOAc – Lithium Acetate
LOF – loss-of-function

Summary

Understanding the mechanisms that govern the transition from undifferentiated precursor cell types, to fully differentiated, functioning tissues is critical to many aspects of biology. These mechanisms include cell signalling, cell migration, morphogenesis, tissue patterning and growth regulation; and form the basis for research into stem cells, regeneration, wound healing, cancer and other diseases. At the molecular level, determining how transcription factors regulate gene expression is fundamental to understanding their physiological role in ensuring correct developmental patterning and specifying cell types. Clear links exist between many human diseases and transcription factor dysregulation, thus continued efforts into understanding how they function, and how their activity is modulated, is paramount.

Here, I use the model organism *Drosophila melanogaster* to investigate several aspects of the function and regulation of the conserved transcription factor Mef2, during the process of muscle development. I describe Mef2's expression pattern in the wing imaginal disc-associated adult muscle progenitor cell (AMP) population, and then go on to show that overexpression of Mef2 in these cells results in a striking phenotype: the precocious formation of 'mini-muscles' as a result of premature AMP differentiation. These prematurely developed myofibres express a panel of sarcomeric proteins, and are resemblant of differentiated muscle. Using this system, I have developed an assay to quantify Mef2's transcription factor activity, which can be used to determine how addition of co-factors/repressors, or mutation to conserved residues of interest, can impact upon its behaviour.

One route by which Mef2 activity is thought to be modulated is through Him, an inhibitor of myogenesis. In wing disc associated AMPs, I demonstrate that the Him protein is expressed in a highly localized pattern, which potentially represent a particularly naïve subpopulation of progenitor cells. Overexpression of Him can inhibit Mef2-overexpression induced premature differentiation, demonstrating that Him can repress Mef2 activity in this cell-type. I show that this is likely through a direct protein-protein interaction, as in a Yeast2Hybrid assay, these two proteins can physically interact with one another. I then explored the role of *Him* through loss-of-function experiments, describing novel jump muscle and pericardial cell patterning phenotypes.

Sumoylation is an additional mechanism by which Mef2's transcription factor activity can be altered. For the first time in an animal model, I demonstrate that myogenesis cannot proceed without the sumoylation pathway through RNAi-knockdown experiments. To explore Mef2-specific effects, I generated a series of overexpression constructs in which a well conserved Mef2 C-terminal sumoylation motif was mutated. Using this novel toolkit, I demonstrate that sumoylation can significantly repress Mef2 activity, in both the context of the wing imaginal disc premature differentiation assay, and during the process of flight muscle development.

The recent discovery of muscle satellite cells (MuSCs) in *Drosophila*, inspired experimentation into Mef2 function in muscle homeostasis and repair; a separate but related process to muscle development. I have identified Him as just the second marker of MuSCs in *Drosophila*, and describe a putative leg muscle-associated MuSC population; two core results which will help drive the field forwards. Mef2 function in these cells was explored by MuSC-specific knockdown, which resulted in an exacerbation of age-associated decline in flight ability, suggestive of a novel function for Mef2 in *Drosophila* muscle maintenance.

The findings presented here are directly relevant to mammalian biology, because of the general conservation of the underlying mechanisms that underpin muscle tissue differentiation. In particular, I build on the current understanding of Mef2 regulation, whose function is central to both *Drosophila* and vertebrate muscle development. Moreover, I further establish *Drosophila* as a model for studying how muscle is maintained post-developmentally. This newly emerging model could prove an effective direction for building on the field of muscle satellite cell biology.

Table of Contents

List of Figures

Chapter 1

Chapter 2

Chapter 3

Chapter 4

Chapter 5

Chapter 6

List of Tables

Chapter 1 - Introduction

1.1 *Drosophila* as a model organism

For over 100 years, the fruit fly, *Drosophila melanogaster,* has been used as a model system for topics ranging from fundamental genetics, to tissue and organ development, to parasitology and behavior. Several of its characteristics make it an ideal model for basic research, including its rapid 10-day life cycle, inexpensive culture techniques and simple 4-chromosome genome. The advent of balancer chromosomes in the early 20th century (Muller 1918), allowed researchers to maintain complex, mutant chromosomes over generations, representing a significant advantage over other model systems for decades to come. In the time that has followed, *Drosophila*'s genetic toolkit has diversified dramatically, and the humble fruit fly still remains at the forefront of biological research today.

Despite the obvious differences between *Drosophila melanogaster* and *Homo sapiens*, there is a great deal of overlap between the fundamental biological processes that control their development and survival. 60% of all human genes, and 75% of disease-associated genes have a *Drosophila* homolog, which makes the fly a useful model for exploring the genetic basis of disease (Bier 2005). A wide spectrum of human diseases have already been modelled in the fly, including developmental and degenerative disorders, as well as a variety of different cancers (Mirzoyan *et al.* 2019; Verheyen 2022; Zhao *et al.* 2023). The *Drosophila* system has also been used to identify key players in vertebrate development. *tinman* (*tin*), the homolog of human *Nkx2-5*, is an example of this. It was the first known regulator of heart development to be discovered, opening many avenues of research into its vertebrate counterpart (Bodmer 1993; Komuro and Izumo 1993; Lints *et al.* 1993). *Drosophila* research has made a considerable contribution to our knowledge of human biology, with many aspects of modern medicine based upon discoveries made in the fly. A particularly compelling example of this is the recent development of 'fly avatars', whereby personalized *Drosophila* strains are developed to model particular mutations a cancer patient has. These can then be robotically screened to determine effective drug combinations for treatment specific to that patient (Bangi *et al.* 2021).

A huge advantage to the *Drosophila* system is the relative ease with which it is possible to perform genetic manipulations such as the knockdown or overexpression

of a gene of interest. Experiments that would take months, or even years, in more complex vertebrate models, can be performed in just a few weeks in the fly. Over the past couple of decades, the technologies used for generating new transgenic flies have evolved dramatically. Initially, P-element mediated transgenesis resulted in random integration of transgenes into the *Drosophila* genome, requiring considerable effort to map their location (Spradling and Rubin 1982). This also has the significant disadvantage of genomic position effect, whereby the expression level of the transgene depends upon its landing site, rendering precise analyses of protein structure and function practically impossible. An optimized ΦC31-integrase based system was developed in 2007 to overcome these issues, allowing transgene insertion into well characterized AttP landing sites with consistent expression levels (Bischof *et al.* 2007). More recently, CRISPR has been adapted for use in *Drosophila*, to allow extremely precise manipulations of genes at their endogenous locus, including gene editing, deletion, replacement and tagging (Gratz *et al.* 2013; Port *et al.* 2014).

A crucial tool to the Drosophilist researcher is the Gal4/UAS system; based on the principal that the yeast transcription factor Gal4 can bind to a UAS promoter sequence and drive expression of an associated gene (Brand and Perrimon 1993). Entire libraries of Gal4 drivers are available to the researcher, meaning the system can be employed across a diverse range of tissue and cell types. This tool can provide temporal and spatial control of overexpression or RNAi UAS-constructs, permitting loss- or gain-of-function experiments to study how this affects a specific process of interest (Figure 1.1). The system can also be used in conjunction with UAS-reporter lines, to determine where and when specific Gal4 promoters are active. More recently, the development of temperature-sensitive Gal80 (Gal80ts) allows even more precise control over the timing of Gal4 induced expression (McGuire *et al.* 2003). Gal80ts inhibits Gal4 expression at permissive temperatures, but is inactivated at 29°C, allowing the researcher to switch Gal4 expression on and off by changing the temperature at which the flies are incubated. This adaptation of the system is necessary if the researcher needs to restrict Gal4 expression to particular life stages of the fly. The Gal4/UAS toolkit is constantly being adapted to increase the resolution at which gene expression is manipulated, including the development of a Split-Gal4 system, auxin inducible Gal4 and Photo-Gal4; a light

activated driver (Luan *et al.* 2006; de Mena and Rincon-Limas 2020; McClure *et al.* 2022).

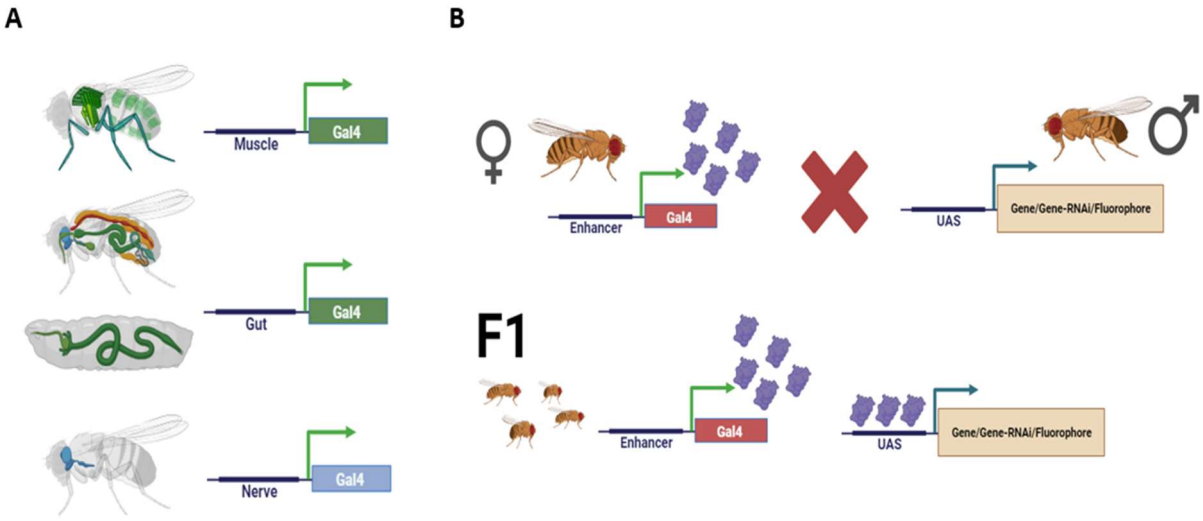

Figure 1.1 – The Drosophila Gal4/UAS System for tissue-specific genetic manipulations.

The Gal4/UAS system has been adapted from yeast for *Drosophila* to allow tissue or cell-type specific manipulations of a gene of interest. This is a bipartite system, consisting of separate Gal4 and UAS expressing strains, which when combined by performing a genetic cross results in Gal4 driven expression of a UAS construct in F1 progeny.

(A) Gal4 lines have been created that express yeast-derived Gal4 under the control of a specific promoter sequence, resulting in expression of Gal4 protein in the chosen tissue or cell-type, such as muscle, the gut or nervous system. (B) When crossed to flies harboring UAS-constructs, the F1 progeny contain both the Gal4 and UAS transgenes. Consequently, Gal4 drives expression by binding the UAS-promoter, resulting in transcription of the associated sequence. This can be a protein of interest, RNAi against a specific gene, or a fluorophore to study localization of specific Gal4 drivers.

Another major advantage of the *Drosophila* system is its short 10-day life cycle. This, and its relatively small size, allows it to be cultured in extremely large numbers within the laboratory environment. Females can lay up to 100 eggs per day, with embryonic development lasting only 24 hours. Upon hatching as an L1 larva, the animal undergoes two molts approximately 24 hours apart, progressing through the L2

stage and onto L3, during which time a substantial amount of feeding and growth occurs. The L3 stage lasts approximately 48 hours, spending the last few hours wandering up the culture vial to find a place to pupate. During pupation, the larva undergoes an almost complete histolysis, with the majority of adult structures forming from larval imaginal disc progenitor cells. Pupation lasts for 3-4 days, until a fully developed adult fly emerges from the pupal case. The length of this life cycle can be manipulated by varying the temperature in which the flies are is maintained, providing researchers with a mechanism to slow down culture development and decrease the hands-on time required for their maintenance, or speed it up when experiments demand it.

1.2 *Drosophila* Myogenesis

Over the years, *Drosophila* has proven an invaluable model for researchers to explore the genetic and cellular basis for muscle development, many aspects of which are well conserved in the vertebrate system (Taylor 2013). Furthermore, the recent discovery of muscle satellite cells (MuSCs) in *Drosophila* (Chaturvedi *et al.* 2017; Boukhatmi and Bray 2018) provides a promising new direction of research into muscle homeostasis and repair following injury, with the potential to provide insight into why vertebrates gradually lose muscle during ageing, or to model conditions such as muscular dystrophies in which satellite cell dysfunction is implicated (Boukhatmi 2021).

As with all holometabolous insects, the fruit fly undergoes two waves of myogenesis during its life cycle. The first, during embryogenesis, gives rise to the larval musculature, which is well adapted to suit the crawling and burrowing behaviors that characterize this life stage (Figure 1.2A). During pupation, the adult musculature develops (Figure 1.2B). This is a completely different set of muscles which power the insect's flight, jumping and walking abilities. Many of the key genes and cellular processes that contribute to fruit fly muscle development are well conserved in vertebrates. Because of this, the *Drosophila* system represents a viable model to explore myogenesis and extrapolate findings to vertebrate systems. For example, *Drosophila* myoblast fusion has been extensively studied as a powerful *in vivo* model for cell-cell fusion to identify key conserved mechanisms and genes such as *dumbfounded (duf)*, *sticks and stones (sns)* and *WASp* (Bour *et al.* 2000; Ruiz-Gómez *et al.* 2000; Schäfer *et al.* 2007). *Drosophila's* relative speed, low cost and

ease with which genetic manipulations can be performed, make it an attractive system to address many of the open questions that remain about muscle differentiation, homeostasis and repair over the coming decades.

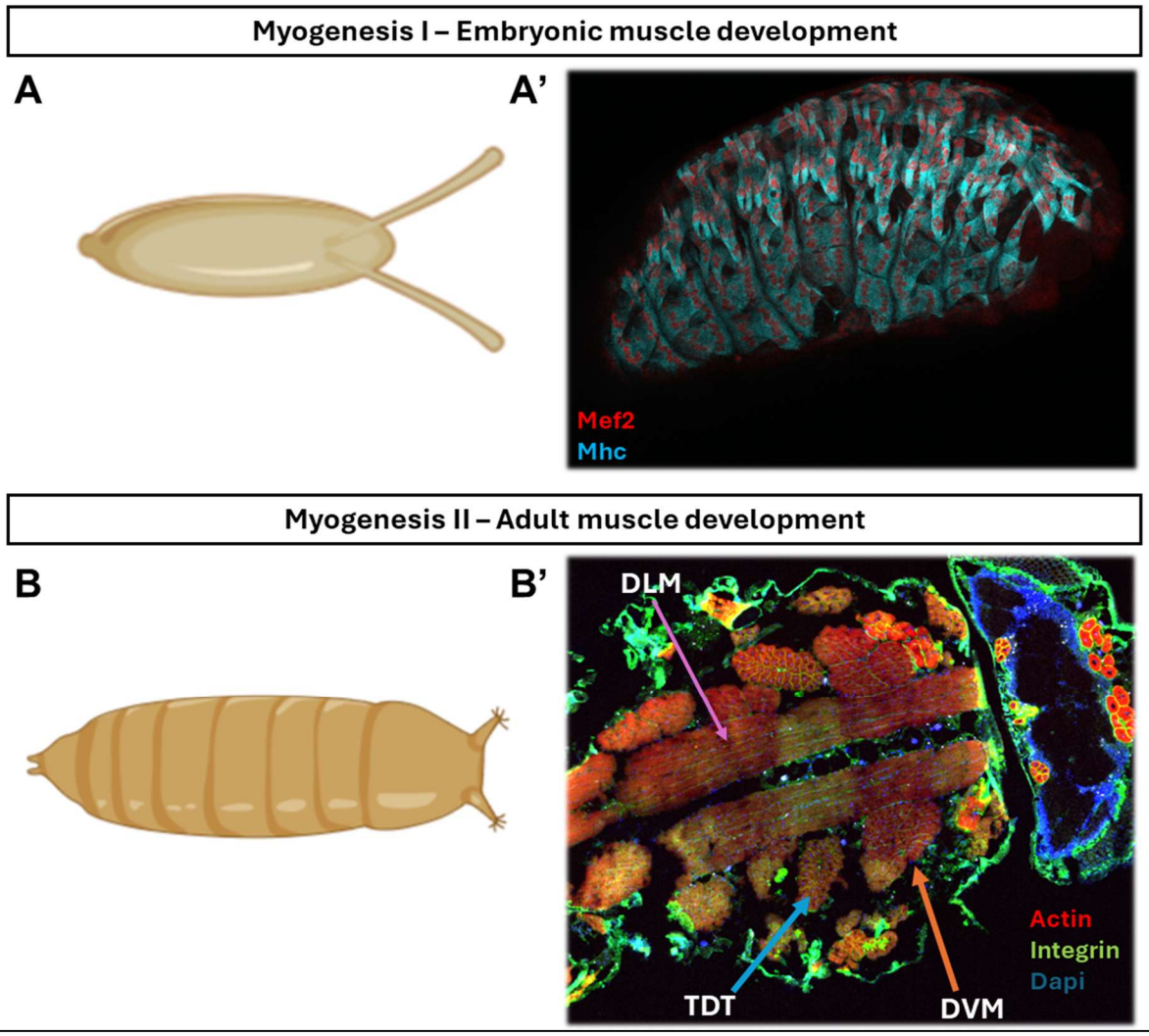

Figure 1.2 - Drosophila undergoes two waves of myogenesis during its life-cycle.

(A-A') The first wave of *Drosophila* muscle development occurs during its embryonic phase, giving rise to the highly stereotyped, repeating pattern of larval muscles found in each segment of the animal. An immunostaining of a late-stage embryo, shows myosin-heavy-chain (cyan) labelling of the developed fibres, and Mef2 (red) positive muscle fibre nuclei.

(B-B') Following the larval stage of the life-cycle, the animal pupates during which time a second wave of muscle development occurs. The larval musculature undergoes histolysis, and the adult muscles develop from imaginal disc-associated muscle progenitor cells. This includes a variety of specialized muscles, including the fibrillar dorsal longitudinal muscles (DLMs) and dorsal-ventral muscles (DVMs) which power flight, and the tubular tergal depressor of the trochanter (TDT aka jump) muscles. (B') A cryosection of an adult fly shows longitudinal sections of the DLMs, and transverse sections of the TDT and DVMs.

1.21 *Drosophila* embryonic muscle development

Drosophila's first wave of myogenesis to generate the larval musculature occurs during its embryogenesis. There are three types of muscle generated at this stage – cardiac, visceral and somatic, all of which develop from the embryonic mesoderm. Cardiac muscle includes the contractile cardiomyocytes which form the dorsal heart tube. The visceral musculature includes interwoven circular and longitudinal muscles which surround the midgut of the digestive system. The somatic muscles form the body-wall musculature of the developed larva, which power its ability to burrow and crawl.

The mesoderm which gives rise to the larval musculature is initially derived from the ventral-most cells of the early embryo, which express a high level of Dorsal (Simpson 1983). Dorsal expression activates the expression of the transcription factors *twist* (*twi*) and *snail* (*sna*), required for specification of the mesoderm. During gastrulation, Twi and Sna positive cells invaginate, forming the ventral furrow (Boulay *et al.* 1987; Kosman *et al.* 1991; Leptin 1991). These cells then undergo an epithelial-mesenchymal transition, spreading along the dorsal side of the embryo underneath the ectoderm, giving rise to the mesodermal germ layer (Leptin and Grunewald 1990; Leptin 1991). This later differentiates into a variety of different tissue types, dependent on subsequent patterning events.

Following gastrulation, the mesoderm becomes subdivided into segments and is patterned along both its anterior-posterior (AP) and dorsal-ventral (DV) axes. Even skipped (Eve) and Sloppy-paired (Slp) regulate the AP patterning of each segment, resulting in alternating high and low Twi expression domains (Baylies *et al.* 1998, Figure 1.3). TGFβ signaling though Decapentaplegic (Dpp) from the overlying ectoderm contributes to DV patterning, with the dorsal mesoderm receiving a higher level of Dpp than the ventral mesoderm (Staehling-Hampton *et al.* 1994; Frasch 1995; Maggert *et al.* 1995). This subdivision of mesoderm segments into different expression domains along these two axes, determining the tissue type that will develop from them;

1) The dorsal region of the posterior hemi-segment gives rise to visceral muscle and fat body.

2) The ventral region of the posterior hemi-segment gives rise to mesodermal glial cells.
3) The dorsal region of the anterior hemi-segment gives rise to cardiac muscle.
4) The ventral region of the posterior hemi-segment gives rise to the somatic muscle (Dobi *et al.* 2015).

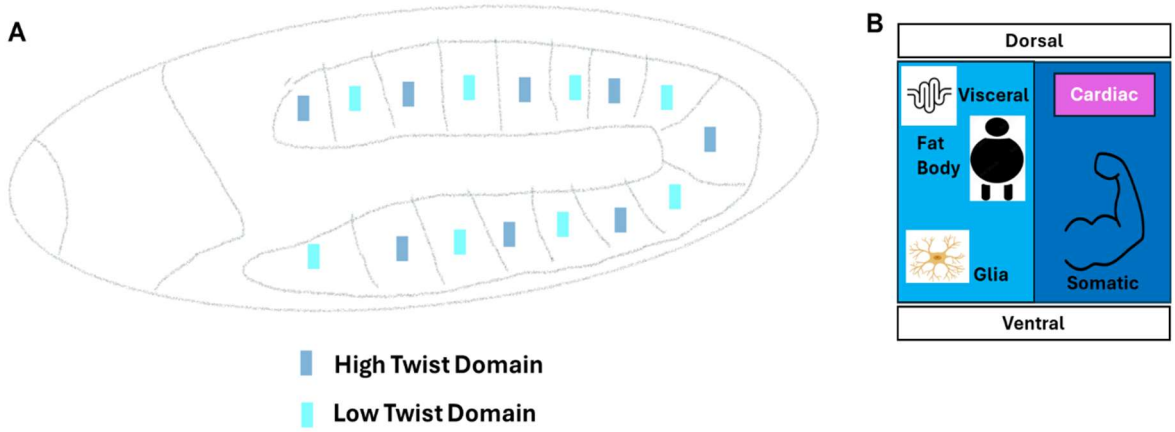

Figure 1.3 – Anterior-posterior and dorsal-ventral patterning of the embryonic mesoderm. (A) Following gastrulation, the mesoderm is subdivided into high vs low Twist expressing hemi-segments along its anterior-posterior axis. (B) Further patterning of each hemisegment along its dorsal-ventral axis determines the tissue type that will develop. In low Twist expressing hemi-segments, dorsal cells will give rise to the visceral musculature and fat body, whereas more ventrally located cells will form mesodermal glial cells. In high Twist expressing hemi-segments, dorsal cells will form cardiac musculature, and ventral cells the somatic muscles.

Clusters of myogenic precursor cells, referred to as equivalence groups, are specified by activation of Lethal of scute (L'sc) expression, which soon becomes restricted to a single progenitor via Notch mediated lateral inhibition (Carmena *et al.* 1995; Carmena, Gisselbrecht, *et al.* 1998). There are 18 equivalence groups per abdominal hemi-segment, which represent the lineages for the somatic musculature and pericardial cells. Once specified, the progenitor cell divides to give rise to two founder cells (FCs), or one FC and one AMP, or specifically in the dorsal hemi-segment, a FC and pericardial precursor (Gómez and Bate 1997; Carmena,

Murugasu-Oei, *et al.* 1998; Carmena, Gisselbrecht, *et al.* 1998). In total, 30 somatic FCs are formed, each of which has its own transcriptional identity, giving rise to one of the 30 unique muscles per abdominal hemi-segment. The remaining cells of the cluster develop into fusion competent myoblasts (FCMs), characterized by expression of the transcription factor Lame duck (Lmd) (Duan *et al.* 2001; Ruiz-Gómez *et al.* 2002; Cunha *et al.* 2010).

Myoblast fusion begins in the stage 11 embryo, initially involving just a single FC and a single FCM, followed by several more rounds of fusion to each growing syncytium. The number of fusion events depends, with the smaller ventral muscles requiring as few as 3 FCMs, and the larger dorsal muscles up to 30 (Haralalka and Abmayr 2010). Correct recognition and adhesion between FC & FCM is dependent on the function of a number of genes from the immunoglobulin superfamily (IgSF), including *duf*, *sns*, *hibris* (*hbs*) and *roughest* (*rst*) (Bour *et al.* 2000; Ruiz-Gómez *et al.* 2000; Artero *et al.* 2001; Strünkelnberg *et al.* 2001). Myotube formation is complete by stage 14, by which point the mature fibres are attached to the relevant sites of the epidermis (Rushton *et al.* 1995).

The *Drosophila* larval heart develops from cells originally located in the dorsal mesoderm. Expression of *tin*, a master regulator of heart development, is activated in the dorsal compartment of the mesodermal hemi-segments by the collective action of Wingless (Wg) and Dpp signaling during embryonic stage 10 (Frasch 1995; Lockwood and Bodmer 2002). By stage 11, additional cardiac transcription factors including the GATA homologs *panier* (*pnr*) and *Dorsocross* (*Doc*), are also expressed (Gajewski *et al.* 2001; Reim and Frasch 2005). The two rows of tin-positive cardioblasts align and migrate dorsally towards one another to form the cardiac tube, in a process called dorsal closure which is complete by stage 15 (Young *et al.* 1993).

The final heart tube stretches across two thoracic and seven abdominal segments, consisting of repetitive units of cardioblasts. The late-stage embryo has six cardioblasts per segment, of which four express Tin and two Seven-up (Svp). The heart tube is flanked by a row of pericardial cells on either side; non-myogenic cells thought to act as nephrocytes, which filter heamolymph and help stabilize cardiac outflow (Das *et al.* 2008).

1.22 Drosophila adult muscle development

Drosophila adults have a variety of different muscles, specialized for performing a variety of different functions. These can be divided into two major subsets: the fibrillar and the tubular muscles (Snodgrass, 1935). Tubular muscles are most often compared to vertebrate skeletal muscle, both structurally and functionally. They consist of laterally aligned sarcomeres and contract synchronously in response to Ca^{2+} influx from the sarcoplasmic reticulum following neural stimulation (Peckham *et al.* 1990). Tubular muscles include the direct flight muscles (DFMs), leg muscles and jump muscle (or TDT), each of which requires fine motor co-ordination to perform functions such as orienting wings during flight, walking and jumping. Conversely, *Drosophila's* fibrillar muscles are more similar to vertebrate cardiac musculature. These comprise the indirect flight muscles (IFMs), which consist of two opposing sets of muscles; the dorsal-ventral muscles (DVMs) and the dorsal-longitudinal muscles (DLMs). They contract asynchronously and consist of non-aligned myofibrils. These are stretch-activated muscles that undergo extremely high contraction frequencies in the absence of calcium flux, generating the speed and power required for insect flight (Josephson *et al.* 2000). Similarly, stretch activation is thought to play a role in the autonomous control of the vertebrate heartbeat (Campbell and Chandra 2006).

The muscles of adult *Drosophila* develop during pupation, from adult muscle progenitor cells (AMPs), which are set aside embryonically and remain undifferentiated. The AMPs that give rise to the adult DFMs and IFMs localize in the developing embryonic mesothoracic segment (T2), and later become associated with the wing imaginal disc tissue by the end of embryogenesis (Gunage *et al.* 2014). During larval stages, the AMPs proliferate dramatically to generate a pool of approximately 2,500 cells. Gunage *et al.* propose a model whereby proliferation is initially via a symmetrical mode of division to generate a pool of progenitors. During the larval L3 stage, there is then a switch to asymmetric division, to generate postmitotic myoblasts which will later form the adult fly musculature. This results in a multi-stratified organization of AMPs, with the post-mitotic myoblasts sat in more distal layers on the wing imaginal disc relative to their actively dividing parents, which are located more closely to the disc epithelium. Throughout their amplification, the

AMPs depend on interactions with the wing disc notum epithelium, which is thought to act as niche from which Notch and Wg signals emanate (Gunage *et al.* 2014).

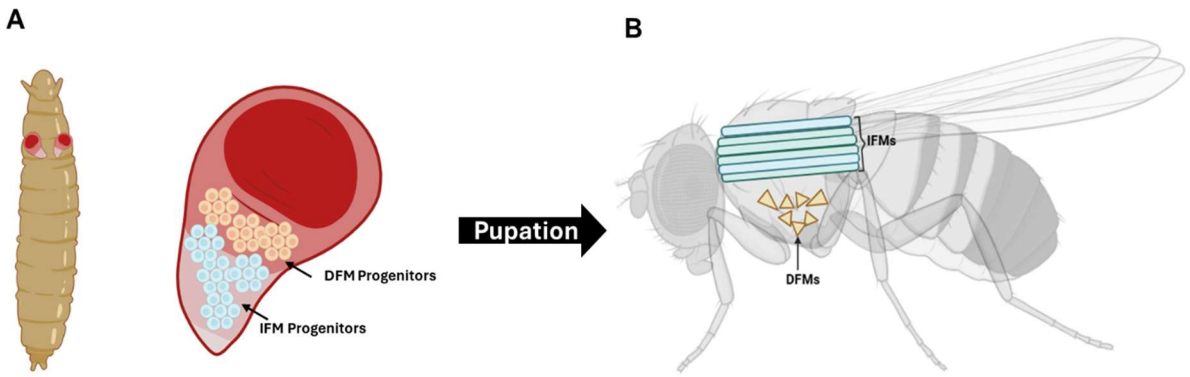

Figure 1.4 – Larval wing imaginal disc-associated adult muscle progenitors give rise to the adult indirect flight muscles.

(A) A schematic of a L3 larvae showing the placement of the wing imaginal disc near the anterior end of the animal. The associated adult muscle progenitors are subdivided into two main populations: the more ventrally located direct flight muscle (DFM) progenitors (orange) and the dorsally located indirect flight muscle (IFM) progenitors (blue). (B) A schematic of the adult fly, showing a major subset of the IFMs (blue) that develop from the IFM-progenitor population, and the DFMs (orange) that develop from the DFM-progenitor population.

The wing imaginal disc AMP population is subdivided into progenitors that will give rise to both the DFMs and IFMs (Figure 1.4). These are separated both spatially, with the DFM-AMPs situated more ventrally than the IFM-AMPs, and by differential patterns of gene expression. For example, whilst all AMPs express the transcription factor Cut (Ct), Vestigial (Vg) is specific to the IFM progenitors, and Amalgam (Ama) is specific to DFM progenitors. Within these IFM and DFM populations, a scRNAseq dataset further subdivides these into seven separate clusters based on gene expression profile; DFM1-2 and IFM1-5 (Zappia *et al.* 2020). These are proposed to represent a gradient of cellular differentiation state, from undifferentiated progenitors, to differentiation-primed myoblasts. Undifferentiated clusters display a high level of *twi* and *Him* RNA, known repressors of myogenesis (Anant 1998; Soler and Taylor 2009), whereas the differentiating cell clusters have a reduction in these markers and an increase in pro-myogenic signals such as *hoi-polloi* (Zappia *et al.* 2020). Immunostainings of markers for IFM_1 and IFM_2 suggest that these more naïve cells localize to a specific region in the anterior presumptive lateral heminotum of the

wing disc, contrasting with the layer-based model proposed by Gunage *et al.* Nonetheless, both studies point towards AMPs existing not as a uniform population of cells, but rather consisting of differentiation primed myoblasts and the progenitors they are derived from.

The Notch signaling pathway is thought to play an important role in maintaining these AMPs in their undifferentiated state. Notch directly regulates expression of the anti-differentiation signal *twi*, which in turn co-operates with Notch to activate *Him* to repress myogenesis (Anant *et al.* 1998; Soler and Taylor 2009; Bernard *et al.* 2010). Consistent with this, Zappia *et al* (2020) found differential expression of the *E(spl)* genes in the AMP clusters, which are indicative of Notch signaling activity. Clusters with a low level of *E(spl)* also have reduced *twi* and *Him* and therefore have increased capacity to differentiate.

Adult muscle development starts at the beginning of pupation. Research to date has largely focused on the development of the adult fibrillar DLMs rather than other muscle types, in part due to their size and ease of access compared to other muscles. At the onset of pupation, the vast majority of larval muscles undergo rapid histolysis, aside from three dorsal oblique muscles (DOMs) in larval segment T2, which act as templates for the development of the future DLMs. The wing disc derived myoblasts migrate from their original position at about 8hr APF, and fuse to the larval template muscles to form the adult DLM fibres (Roy and VijayRaghavan 1998; Bernard *et al.* 2003). During migration, it has been proposed that myoblasts are maintained in an only partially differentiated state by Notch signaling. Upon arrival at the myotube, Notch signaling decays and the myoblast can now terminally differentiate by undergoing fusion to the template muscle fibre (Gildor *et al.* 2012). Whilst myoblast fusion is underway, the three template muscles split to form the six developing DLMs, shortly after which time myoblast fusion is complete. These immature myofibres spend the rest of pupation undergoing substantial growth, and by 90hr APF span the entire length of the thorax. In contrast, the DVMs develop *de novo*, with myoblasts fusing with one another rather than to a template, more similar to vertebrate muscle development (Fernandes *et al.* 1991).

Tubular muscle development is less well studied in *Drosophila.* In contrast to the IFMs, the myoblasts that give rise to the tubular leg and jump muscles are

associated with the leg imaginal discs (Soler *et al.* 2004; Jaramillo *et al.* 2009). There are three leg discs, the T1 prothoracic, the T2 mesothoracic and T3 metathoracic, each of which gives rise to a particular leg and its associated musculature. The TDT progenitors are associated specifically with the T2 leg disc. The developmental processes that give rise to these muscle types is thought to be more resemblant of embryonic myogenesis, whereby a *duf* positive founder-cell like progenitor seeds formation of the muscle fibre (Soler *et al.* 2004; Jaramillo *et al.* 2009). However, founder cell selection seemingly contrasts with that of embryonic muscle development, which is dependent on lateral inhibition mediated by Notch signaling. Adult muscle founder cell specification is instead reliant on the TGFβ and FGF signaling pathways (Jaramillo *et al.* 2009; Dutta *et al.* 2005).

1.23 *Drosophila* satellite cell biology

Muscle satellite cells (MuSCs) are a type of quiescent stem cell located on the periphery of the differentiated muscle fibre, implicated in the homeostasis and repair of the tissue. Upon stimulation, these cells proliferate and give rise to myoblasts which can fuse to existing muscle to contribute to its maintenance or repair. Until relatively recently, it had been assumed that insects lacked this cell type, leading to questions about how it maintained its own, extensively used, musculature over its life-span. Almost simultaneously, Chaturvedi *et al.* and Boukhatmi and Bray, identified that *Drosophila* do indeed possess MuSCs that perform an equivalent function to their vertebrate counterparts, contributing to muscle homeostasis and repairing damage. These pioneering studies characterized DLM-associated MuSCs, but whether similar populations exist for other muscle types is currently unknown.

Drosophila DLM-associated MuSC's are derived from a subset of wing imaginal disc associated AMPs that escape differentiation during pupation, localizing on the periphery of the developing IFMs. Mechanistically, this is achieved by a switch in *zfh1* isoforms, from a *zfh1*-long variant, which is downregulated by miR-8 in differentiation-bound myoblasts, to a *zfh1*-short variant lacking the miR-8 target site, maintaining the AMPs in which it is expressed in an undifferentiated state (Boukhatmi and Bray 2018). Presently, Zfh1 is the only published marker of *Drosophila* satellite cells, although it is known that MuSCs express Mef2 at a much lower level than the differentiated muscle fibre nuclei (Chaturvedi *et al.* 2017; Boukhatmi and Bray 2018). The mammalian homolog of *zfh1*, *ZEB1*, has been

shown to be implicated in the regeneration of vertebrate muscle following damage, suggesting there may be overlap in the mechanisms that modulate muscle repair (Siles *et al.* 2019).

Similar to its role in the wing imaginal disc-associated AMP population, Notch signaling is thought contribute to *Drosophila* MuSC maintenance. Post muscle development, the Notch pathway is active in the MuSCs, but not in the mature muscle fibres. Within the MuSC population, Notch signaling is thought to contribute to regulation of *zfh1* expression via two Su(H) binding motifs in its promoter region. Consistent with this, mutation to these motifs compromises *zfh1* expression (Boukhatmi and Bray 2018).

In addition to exploring the mechanisms by which MuSCs are maintained in an undifferentiated state, the *Drosophila* model has also been used to investigate muscle repair following injury, by inducing damage mechanically and studying the response over the followings days and weeks. Localized stab wounds of the DLMs can regenerate, with an almost complete recovery seen by day 10. Following injury, the Zfh1+ satellite cell population proliferates and localizes to the injury site (Chaturvedi *et al.* 2017). This proliferative response is thought to be dependent on Notch signaling. Upon injury, muscle fibres upregulate expression of the Notch ligand Delta, which is required for proliferation of the MuSCs during the repair response. This mechanism may be conserved, as Notch signaling is also implicated in the proliferative response of the vertebrate MuSC population. For example, pathway inhibition leads to premature activation of the MuSCs, whereas pathway activation prevents MuSC activation (Philippos *et al.* 2012; Wen *et al.* 2012).

Since the field of *Drosophila* muscle satellite cell research is still in its infancy, the molecular and cellular events that give rise DLM repair are presently poorly characterized. The sole example of a factor required for *Drosophila* muscle regeneration is the well conserved protein RACK1, without which wound healing was significantly impaired. In a mouse injury model, RACK1 was upregulated in regenerating muscle fibres, pointing towards a conserved mechanism between the two systems (Catalani *et al.* 2022). These data highlight the potential usefulness of using *Drosophila* to identify important, relevant, gene products that are involved in the process of muscle regeneration.

1.3 Mef2 expression and function

My PhD research largely focuses on the transcription factor Mef2, a key player involved in the differentiation and maintenance of a number of systems, including muscle, the nervous system and the immune system (Clark *et al.* 2013; Taylor and Hughes 2017; Crittenden *et al.* 2018; Assali *et al.* 2019). This protein is well conserved in terms of both sequence and function amongst a variety of taxa. Mef2 family members are implicated in a number of key signaling pathways, including MAPK, Wnt, PI3K/Akt and Ca^{2+}. Furthermore, a growing number of reports show an association of Mef2 and the development of a variety of human diseases (Chen et al., 2017). Thus, fully determining the roles of Mef2 protein, and how its activity is regulated in time and space, is directly relevant to human health and biology.

Mef2 belongs to the MADS-box family of transcription factors, which are characterized by a highly conserved DNA-binding MADS (MCM1, Agamous, Deficiens and SRF) domain in eukaryotic organisms (Messenguy & Dubois, 2003). Mef2 proteins bind the consensus DNA sequence $YTA(A/T)_4TAR$ (Andres *et al.* 1995; Fickett 1996), and can act as both an activator or repressor of gene expression, depending upon other co-factor interactions (Potthoff *et al.* 2007; Taylor and Hughes 2017). The N-terminus of Mef2, comprising the MADS and Mef2 domains (Figure 1.5), is particularly well conserved amongst family members, being implicated in some of Mef2's most important activities as a transcription factor, including DNA-binding, protein-protein interactions and nuclear localization. For example, *Drosophila* Mef2's MADS and MEF2 domains share 90% and 68% identity with Mef2A (Potthoff and Olson 2007).

The Mef2 family comprises four members in mammals; Mef2A-D, which have overlapping patterns of expression, and possible functional redundancy, between genes (Liu *et al.* 2014). Studying *Drosophila's* single *Mef2* orthologue serves to simplify this complexity by elucidating Mef2's most conserved functions.

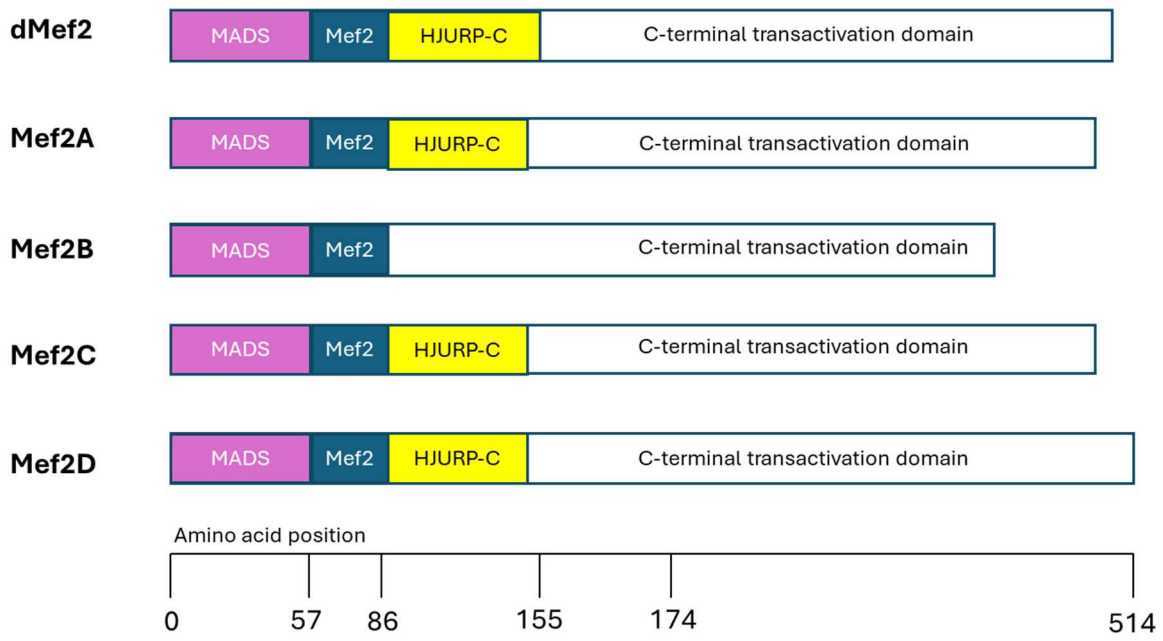

Figure 1.5 – *Drosophila* and mammalian Mef2 domain alignment.

A Mef2 alignment which shows the presence of the N-terminal MADS and Mef2 domains throughout the Mef2 family. An adjacent HJURP-C domain is also present in each of the displayed family members, with Mef2B being the exception. (Adapted from Spicer 2024).

1.31 Vertebrate Mef2 expression and function

Initially, mammalian Mef2 was first described in the context of mammalian cell culture (Gossett *et al.* 1989). It was then found that expression of Mef2 could enhance the rate at which the myogenic bHLH factor MyoD could convert fibroblasts into myoblasts, suggesting cooperativity between these factors in activating muscle gene expression (Molkentin *et al.* 1995). Consistent with a role in the regulation of muscle genes, a more recent study found that shRNA mediated knockdown of Mef2A in C2C12 cells impaired their intrinsic capacity to differentiate into myotubes (Snyder *et al.* 2013). Whilst cell culture studies such as these have proven a useful tool to unveil a general function of Mef2, it is critical to explore it in the context of an animal model, in order to get a more precise understanding of its role in normal development.

Mammalian Mef2 expression patterns are well characterized throughout development. Mef2A, Mef2B, Mef2C and Mef2D are seen in a broad range of tissues throughout development, but are particularly highly expressed in developing muscle.

Edmondson *et al.* 1994 were the first to study *Mef2* expression patterns during mouse embryonic muscle development, using *in situ* hybridization, finding *Mef2C* to be the first to appear in developing heart and somatic muscle lineages, shortly followed by *Mef2A* and *Mef2D*. The *Mef2B* expression pattern was defined slightly later, and found to largely overlap in time and space with the other Mef2 genes during myogenesis (Molkentin *et al.* 1996).

In vivo evidence of Mef2 function in vertebrate systems is lacking, as it is thought there is functional redundancy between Mef2 family members, rendering analysis of loss-of-function mutants of the individual genes unhelpful. Indeed, mice with a single knockout of *Mef2A* or *Mef2D* don't exhibit an obvious skeletal muscle phenotype at all, and Mef2C mutants die at E9.5 due to vascular defects (Lin *et al.* 1998; Potthoff *et al.* 2007). Conditional knockout of *Mef2C* specifically in skeletal muscle doesn't impact muscle development, but there is a rapid deterioration in fibre integrity after birth, pointing towards a potential Mef2C-specific role in muscle maintenance (Potthoff *et al.* 2007). *Mef2B*'s role in somatic muscle differentiation is less studied than its counterparts, perhaps due to it being the most divergent Mef2 family member or difficulties generating specific reagents.

Liu *et al.* 2014 provide evidence for Mef2 functional redundancy in the context of skeletal muscle regeneration; a separate, but related process to muscle differentiation. Whilst muscle satellite cell specific conditional knockout of *Mef2A*, *Mef2C* and *Mef2D* separately doesn't impact muscle injury response, a triple knockout approach blocked tissue regeneration. Furthermore, triple *Mef2(A,C,D)* knock-out in cultured satellite cell derived myoblasts, lack the capacity to differentiate, revealing redundant roles for *Mef2A*, *Mef2C* and *Mef2D* in satellite cell-derived muscle regeneration (Liu *et al.* 2014). Whilst these data don't describe a role for Mef2 in muscle development, it does provide a potential explanation for the lack of developmental phenotype observed with loss-of-function of individual *Mef2* genes.

1.32 *Drosophila* Mef2 function and expression

Studying *Drosophila's* single, conserved, *Mef2* gene, serves to simplify an analysis of Mef2 function in somatic muscle development, since functional redundancy is not an obstacle in this system. Its expression and function have been explored during

both waves of *Drosophila* myogenesis, with findings demonstrating that it is indispensable for formation of both the larval and adult musculature.

During embryogenesis, Mef2 protein is present in developing somatic, cardiac and visceral muscle lineages. Embryonic loss-of-function of *Mef2* causes a complete failure in somatic muscle differentiation, demonstrated by a lack of fibres and the absence of differentiated muscle markers such as Myosin heavy chain (Mhc). Similarly, core cardiac and visceral muscle gene expression is lost, thus Mef2 function is required for the development to all *Drosophila* muscle sub-types in the embryo (Bour *et al.* 1995; Lilly *et al.* 1995; Ranganayakulu *et al.* 1995; Taylor *et al.* 1995).

A ChIP-on-chip approach in the *Drosophila* identified more than 200 direct target genes and a total of 670 bound regions in the genome. This was complemented by an analysis on *Mef2* mutant gene expression profile, to identify which genes require Mef2 regulation for proper expression. Genes across all stages of embryonic myogenesis are dependent on Mef2 activity, such as early expressed muscle identity genes *nautilus* (*nau*) and *Kruppel* (*Kr*), and later terminal muscle differentiation markers such as *Mhc* and *Mlp84B* (Sandmann *et al.* 2006). These experiments were performed with a tiling array covering only 50% of the *Drosophila* genome, so there are likely many Mef2 targets that were not identified. A similar study that combined a ChIP-chip strategy with *in silico* based target predictions, identified many of the same Mef2 targets. Again, only a fraction of the genome was sampled, so a complete picture of embryonic Mef2 targets is still lacking (Junion *et al.* 2005).

Mef2 function is also crucial to *Drosophila's* second wave of myogenesis, which occurs during pupation to give rise to the adult specific muscles. Gal4/UAS mediated knockdown of *Mef2*, using the AMP specific driver *1151Gal4* in combination with *UAS-Mef2-RNAi*, inhibits the development of a variety of different muscle types, including the tubular TDT and leg muscles, as well as the fibrillar IFMs: the DLMs and DVMs. Using the temperature sensitive $Gal80^{ts}$ to further temporally restrict Gal4 expression, separate functions of Mef2 were identified in both the re-modelling of muscle during early development, and its maintenance later on (Soler *et al.* 2012). Whilst ChIP data for Mef2 during adult myogenesis does not yet exist, there have been case studies on known Mef2 targets. For example, transcription of the

myoblast fusion regulator *singles bar* (*sing*) is dependent on Mef2, and mutating Mef2's binding motif in the *sing* enhancer drastically reduces its transcription (Brunetti *et al.* 2015). The gene *vestigial* (v*g)* is another key regulator of adult muscle development, which itself is regulated in part by Mef2. Mef2 RNAi results in decreased activation of a *vg* enhancer construct *in vivo*, providing evidence that *vg* depends on Mef2 for proper expression (Bernard *et al.* 2009).

1.4 Regulation of Mef2 activity

Mef2 target genes have a wide array of functions throughout myogenesis, with expression patterns that vary in time and in space. In the *Drosophila* embryo, Mef2 is present in all muscle lineages from gastrulation onwards, but despite this its target genes are expressed at different times and in different places. Mef2's regulatory activity must therefore by under tight control to activate these genes in the correct spatiotemporal patterns for proper muscle development to occur. One mechanism by which this is achieved is the fact that different target genes have differential requirements for Mef2 activity levels, which correlates with how early they are expressed in myogenic differentiation. For example, *Act57B* which requires a relatively low level of Mef2 activity, is activated earlier in the myogenic program than *Mhc*, which requires a higher level of Mef2 activity. By manipulating Mef2 activity, such as by using a $Mef2^{113}$ hypomorph which has decreased transactivation compared to wild-type, delays in the activation of Mef2 targets were observed in the embryo. Conversely, overexpression of Mef2 causes premature target gene activation (Elgar *et al.* 2008).

A comparable scenario is plausible during *Drosophila* adult muscle development, whereby Mef2 is expressed in larval wing disc associated AMPs prior to the onset of muscle gene activation. Overexpression of Mef2 in these cells causes expression of a Mhc-GFP reporter, a marker of terminal muscle differentiation, demonstrating that once again, an increase in Mef2 activity can prematurely activate target genes (Soler and Taylor, 2009). Less is known about the temporal expression patterns of Mef2 target genes during adult muscle development, but we do know from an RNAseq dataset that *Mef2* RNA increases as adult muscle development proceeds (Spletter *et al.* 2018). It is therefore plausible that Mef2 targets are differentially responsive to

increasing levels of Mef2 activity, as they are in the embryo. This would, at least in part, explain why key sarcomeric components such as *Mhc* are expressed later in adult muscle differentiation than genes implicated in the earlier process of myoblast fusion, such as *sing.*

Whilst the responsiveness of Mef2's targets to varying levels of Mef2 activity is clear, there are many routes by which Mef2 itself is known to be regulated, at both the transcriptional and protein level. This includes the generation of structurally and functionally diverse splice variants (Figure 1.6), microRNA regulation of *Mef2* transcripts, post-translational modification of Mef2 residues to activate or repress the protein, and interaction with other co-factors that may have an inhibitory or positive impact on Mef2 function (Kato 1997; Gunthorpe *et al.* 1999; Zhao *et al.* 1999; Cox *et al.* 2003; Soler and Taylor 2009; Zhang *et al.* 2015; Chen *et al.* 2012; Taylor and Hughes; 2017)

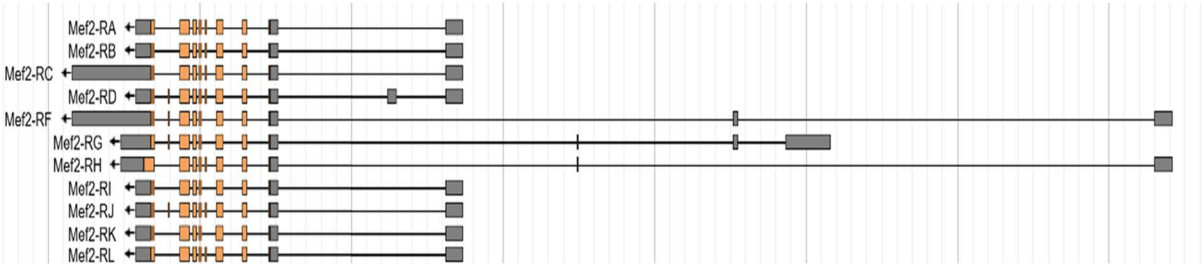

Figure 1.6 – *Drosophila Mef2* Isoforms.

A screenshot from JBrowse of a genomic map of the Mef2 locus, showing the different Mef2 isoform transcripts present in the Drosophila genome. Non-coding exons are grey, coding are peach. There are three alternative transcription start sites between the 11 isoforms.

1.41 Regulation of Mef2 activity by co-factor interaction

Transcription factors are regularly involved in a complex web of protein-protein interactions which determine their capacity to function correctly. These interactions can promote transcription, for example through binding to transcriptional co-activators and chromatin remodellers that facilitate formation of a pre-initiation complex, or, conversely, a transcription factor's activity can be inhibited via interactions with repressors that serve to restrain it from functioning until the correct time.

Soon after *Mef2*'s discovery, it quickly became apparent that protein-protein interactions are significant in modulating its activity. For example, rather than acting alone, mammalian Mef2 requires co-operation with bHLH proteins MyoD or myogenin in order to convert fibroblasts into muscle cells (Molkentin *et al.* 1995). Another known regulator of muscle gene expression, TEAD1, can physically interact with Mef2C through its N-terminal MADS domain in a mammalian two-hybrid experiment (Maeda *et al.* 2002). The *Drosophila* TEAD1 homolog, Scalloped (Sd), can also physically interact with Mef2, to cooperatively regulate expression of the Notch pathway component *delta* during adult muscle development, suggesting this interaction is functionally conserved (Caine *et al.* 2014). Other transcriptional co-activators that Mef2 is thought to cooperate with include P300, Klf5, MAML1, Desmin and Myoglobin, all of which are relevant to some aspect of muscle development (Li and Capetanaki 1994; Grayson *et al.* 1995; Shen *et al.* 2006; He *et al.* 2011; Hayashi *et al.* 2016).

Mef2-interacting repressors also play a role in its regulation by restraining its ability to activate target gene expression before the proper time. For example, HDAC4, which belongs to the Class IIa mammalian HDAC family, can bind to Mef2 in the nucleus and repress its activity (Miska *et al.* 1999). The crystal structure for this interaction has been resolved, and a HDAC-interaction domain has been mapped to the N-terminus of Mef2 (Han *et al.* 2005). The relevance of this interaction has not been explored during animal muscle development, but it is known that HDAC4 can inhibit the fibroblast to myoblast conversion (Lu *et al.* 2000).

The *Drosophila* gene *Him* is another known negative regulator of Mef2 activity, whose effects on muscle development have been well characterized. In the embryo,

Him is expressed broadly across the mesoderm at stage 9, but rapidly declines as muscle differentiation ensues (Liotta *et al.* 2007). Similarly, in the larval wing imaginal disc, Him is expressed in AMPs alongside Mef2 prior to the onset of adult muscle development, but is lost upon myoblast fusion (Soler *et al.* 2009). Overexpression of Him inhibits both embryonic and adult muscle development, consistent with the *Mef2* loss-of-function phenotype. Him overexpression is also able to rescue Mef2 overexpression induced phenotypes in both the embryo and the wing imaginal disc, indicating that Him has a negative effect on Mef2 activity (Liotta *et al.* 2007; Soler and Taylor, 2009). Whilst Him does not have a known mammalian homologue, a WRPW motif at its extreme C-terminus is thought to be implicated in an interaction with the conserved transcriptional co-repressor groucho (gro). In the embryo, gro function is required for Him mediated inhibition of muscle development. Moreover, overexpression of a HimΔWRPW mutant does not inhibit somatic muscle development (Liotta *et al.* 2007). These data strongly suggest that Him is acting through gro in order to repress myogenesis. gro function has not yet been explored during *Drosophila* adult muscle development.

These are examples of factors that can either co-operate with Mef2 to achieve gene expression, or inhibit its activity. This indicates that Mef2 activity *in vivo* is controlled by a balance of inputs, which can either tilt cells down the differentiation pathway, or retain them in an undifferentiated state. This is well illustrated by the *Drosophila* L3 wing disc associated AMPs, which express Mef2, but haven't yet begun to differentiate. This is thought to be because of the co-expression of inhibitors of Mef2 activity such as Him, Twi and Zfh1 at this stage (Soler and Taylor, 2009; Anant *et al.* 1998). As the level of these inhibitors decrease at the onset of adult muscle development, Mef2 activity subsequently increases and target gene activation can occur.

1.42 Transcriptional Regulation of *Mef2*

Whilst Mef2's role as a transcription factor is to regulate target gene expression, it itself is subject to transcriptional regulation through a variety of different mechanisms. In mammals, bHLH proteins not only co-operate with Mef2 protein to activate target muscle genes, they are also implicated in regulating *Mef2*'s own transcription through an E-box motif in its promoter region. Mutation to this regulatory element abolishes *Mef2C* reporter expression in a mouse model, demonstrating its

importance in conferring *Mef2* expression (Wang *et al.* 2001). This mechanism is also relevant to regulation of *Drosophila Mef2*, since the bHLH factor Twi binds to this evolutionarily conserved E-box to regulate its transcription during early embryonic muscle development (Cripps *et al.* 1998). During early mesoderm formation, 42% of Mef2 bound enhancers are co-occupied by Twi, echoing the collaboration between bHLH factors and Mef2 observed in vertebrate systems (Sandmann *et al.* 2007). Following mesoderm specification, Twi expression rapidly declines, but by this stage Mef2 autoregulates its own transcription through a conserved Mef2 binding motif in its promoter sequence (Cripps *et al.* 1998).

Twi represents an interesting case to study, as its role in early embryonic muscle development as a pro-myogenic factor is seemingly at odds with its function during adult muscle development. Whilst Twi also contributes to regulation of *Mef2* expression in the wing imaginal disc associated AMPs, paradoxically, it also acts as an anti-differentiation signal. Whilst embryonic somatic musculature can still develop even with Gal4/UAS induced Twi overexpression, the same scenario presented in the AMPs prevents them from differentiating (Baylies and Bate 1996; Cripps *et al.* 1997; Anant *et al.* 1998).

The *Drosophila* ZEB1 homolog, Zfh1, also binds to *Mef2*'s E-box, in this instance to repress expression of *Mef2* via recruitment of the general co-repressor CtBP (Postigo *et al.* 1999; Siles *et al.* 2013). In the embryo, Zfh1 is initially expressed throughout the mesoderm, but is downregulated after gastrulation in muscle (Lai *et al.* 1991). Transfection assays show Zfh1 binding blocks Twi from activating a *Mef2* promoter construct, demonstrating an interplay between these two factors in determining whether or not *Mef2* is expressed. Indeed, if Zfh1 expression is maintained during embryonic muscle development, *Mef2* expression is significantly downregulated, resulting in inhibition of somatic muscle differentiation (Postigo *et al.* 1999). This is dependent on Zfh1's CtBP binding domain, as the same effect is not observed with a *UAS-Zfh1ΔCtBP* mutant (Siles *et al.* 2013).

Zfh1 mediated repression of *Mef2* is also relevant to the process of adult muscle development. The AMPs, which are set aside embryonically, maintain Zfh1 expression right through until differentiation of the adult musculature begins during pupation. Even at this stage, a subset of AMPs maintain Zfh1 expression during

differentiation, forming the adult muscle satellite cells which contribute to repair and homeostasis of the developed adult muscles (Chaturvedi *et al.* 2017; Boukhatmi and Bray 2018; Leroux *et al.* 2023).

1.43 Regulation of Mef2 by Post-Translational Modification

Another route by which Mef2 function is modulated is via post-translational modification. The attachment of chemical moieties to a target substrate can profoundly affect its biochemical properties, influencing its stability, its DNA-binding properties or its ability interact with other proteins. This is particularly relevant to the biology of a transcription factor, as by modifying these properties its ability to activate target genes can be drastically altered.

A variety of Mef2 post-translational modifications have been documented, including phosphorylation, acetylation, sumoylation and methylation, each of which has varying consequences on its activity. The Mef2 residues implicated in post-translational modification are often well-conserved (Figure 1.7), even those within Mef2's relatively divergent C-terminus, suggestive of an important conserved function in regulation of Mef2 (Zhao, *et al.* 1999; Kang *et al.* 2006; Grégoire *et al.* 2006; Shalizi *et al.* 2007; Choi *et al.* 2014).

Largely, research on Mef2 post-translational modification has relied on a combination of *in vitro* and cell culture-based experiments to firstly determine whether Mef2 can be modified, and then the effects of specific modifications on its activity. For example, mutations to Mef2A's conserved Thr312 and Thr319 phosphorylation sites results in reduced transactivation of a luciferase reporter in embryonic kidney cell line 293, suggesting that phosphorylation of these residues has a net positive effect on Mef2A activity. The MAP-kinase p38 is thought to be responsible for this phosphorylation, although the mechanism by which Mef2 activity is enhanced is not yet clear (Zhao *et al.* 1999).

Vishal *et al.* 2023 recently published the first study to investigate the consequence of Mef2 post-translational modification on muscle development in an animal model. Mass-spectrometry detected that *Drosophila*'s conserved Ser98 residue was a phosphorylation target in embryonic muscle. A CRISPR/Cas9 approach was used to generate a S98A phosphorylation deficient Mef2 at its endogenous location within

the genome. Mutant larvae displayed a phenotype consistent with reduced Mef2 function, whereas in AMPs Mef2 activity is enhanced, demonstrating stage-specific effects of phosphorylation on Mef2 activity for the first time. In tissue culture cells, Mef2^{S98A}, a phospho-mimetic Mef2^{S98E} and wild-type Mef2 behave equivalently in their ability to activate reporter gene expression (Vishal *et al.* 2023), demonstrating that PTMs should be studied in their native environment in order to fully understand their *in vivo* function.

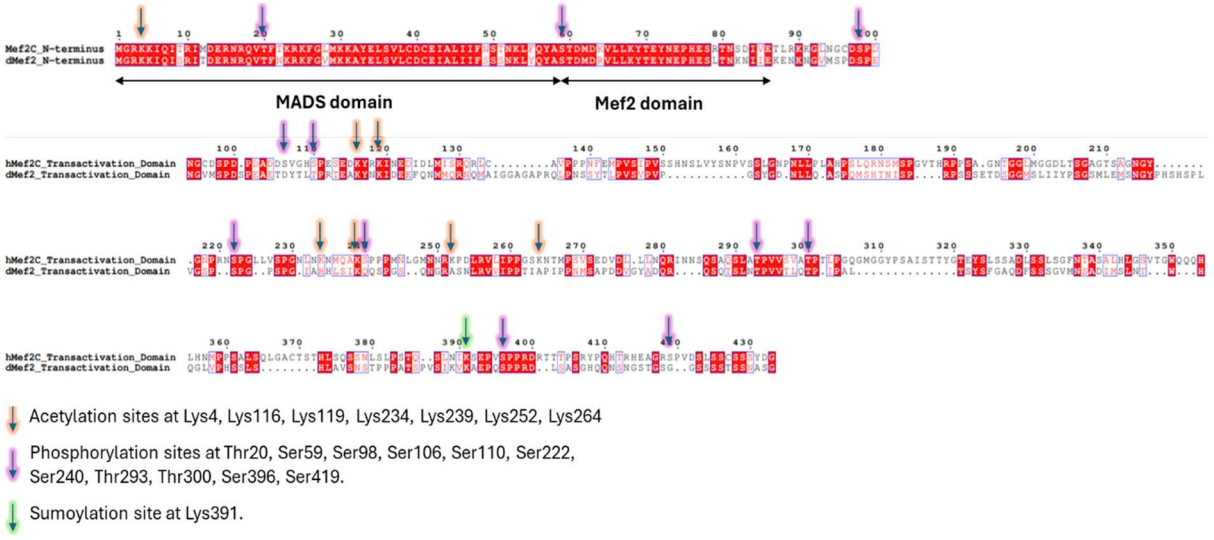

Figure 1.7 – dMef2 & Mef2C alignment with post-translational modification sites

An alignment showing the high degree of conservation of post-translationally modified sites on Mef2, including acetylation, phosphorylation and sumoylation sites. Red highlighting indicates fully conserved amino acids, whereas a black box shows amino acids that have similar biochemical properties. 15 out of 19 target residues are conserved between the two family members.

Mef2 acetylation has also been linked to regulating its function. Mef2C can be acetylated at multiple sites (K4, K116, K119, K234, K239, K252 and K264), each of which enhances its ability to bind to DNA i*n vitro* (Ma *et al.* 2005). The effect this was

explored in the context of cell culture, with differentiating C2C7 muscle cells demonstrating an increase in Mef2C DNA binding as development proceeds, thought to be a consequence of increased acetylation. Blocking acetylation dramatically decreases Mef2C's transcriptional activity and inhibits myogenic differentiation in these cells (Angelelli *et al.* 2008). Therefore, Mef2 acetylation, like phosphorylation, is associated with an increase in its activity, in this context.

1.44 Regulation of Mef2 Activity by the Sumoylation Pathway

The sumoylation pathway is responsible for the covalent attachment of a SUMO peptide to an acceptor Lys residue. Sumoylation can impair the activity of transcription factors by promoting recruitment of co-repressors, affecting subcellular localization, blocking transcription promoting PTMs or by affecting DNA-binding capability (Rosonina *et al.* 2017). Whilst sumoylation is generally considered a repressive modification, cases exist whereby this modification can actually increase transcriptional activity. One such example is HIF-1α, which has increased stability and transcriptional activity following sumoylation (Bae *et al.* 2004).

The sumoylation pathway is well conserved between vertebrates and *Drosophila*. It is a three-step enzymatic reaction, first involving SUMO activation by the E1 activating enzymes SAE1/SAE2 (AOS1/Uba2). These act as a heterodimer, forming a thioester bond between them and the sumo peptide. The sole E2 activating enzyme Ubc9 catalyzes the transfer of SUMO from the E1 enzymes to the target substrate via formation of an isopeptide bond, with co-operation from a SUMO E3 ligase. The E3 ligases are a much more diverse than the other enzymes in the pathway with over 25 described in the literature. It is thought they confer substrate specificity, ensuring that the correct target is modified (Gareau and Lima 2010; Shi *et al.* 2022).

Mef2 has a conserved sumoylation motif in its C-terminal transactivation domain (Grégoire *et al.* 2006; Kang *et al.* 2006). There are several documented variations to the core motif (ΨKxE), with Mef2's being a phosphorylation dependent sumoylation motif (PDSM, ΨKxExxSP). This is a bipartite sequence, consisting of a consensus SUMO site and a downstream proline directed phosphorylation site. In order for sumoylation of the target lysine to occur, downstream phosphorylation is first

required. This conserved motif is present in a number of other important transcriptional regulators, including heat-shock-factors, GATA1 & estrogen-related receptors (ERRs) (Hietakangas *et al.* 2006).

Mutation of Mef2C's sumoylation motif to generate a K391R mutant enhances its transcriptional activity in a luciferase reporter assay, suggesting that sumoylation negatively regulates Mef2 transactivation (Kang *et al.* 2006). The mechanism for this is unclear, since sumoylation of Mef2C does not affect its nuclear localization, stability, or DNA binding capabilities. Neither does it affect Mef2C's ability to bind to HDAC4 or HDAC5, characterized repressors of its activity (Kang *et al.* 2006). It is possible that sumoylation of Mef2C acts to recruit a different transcriptional repressor, which has not yet been identified.

A Mef2C mutant with the downstream phosphorylation site mutated, S396A, cannot be sumoylated *in vitro* or transfected HeLa cells, demonstrating that phosphorylation is indeed a pre-requisite for efficient Mef2C sumoylation. The kinase responsible for this *in vivo* has not yet been reported, although Cdk1 can enhance Mef2C phosphorylation *in vitro*, but not that of Mef2C-S396A. Since the phosphorylated serine residue is followed by a proline, it is likely that the relevant kinase is a proline-directed kinase such as a Cdk or MAP Kinase (Kang *et al.* 2006).

Shalizi *et al.* 2007 provide evidence that it is the PIAS family of SUMO E3 ligases that is responsible for Mef2 sumoylation in a phosphorylation-dependent process, although this particular study focuses on Mef2A in the context of dendritic morphogenesis. In this system, sumoylation mediated repression of Mef2A activity drives dendritic claw differentiation in the rat cerebellum, providing the first evidence that Mef2 sumoylation is relevant to development in an animal model. To further complicate the mechanism, the same Mef2 residue that is sumoylated can also be subject to acetylation. The switch from Mef2 sumoylation to acetylation is thought to be modulated by calcineurin, as a constitutively active calcineurin variant reduced Mef2 sumoylation and enhanced its acetylation state in 293T cells. Shalizi *et al.* propose that this change in modification state represents a switch from a repressed Mef2 to a more active variant, which is critical for proper synapse development.

The role that Mef2 sumoylation plays during animal muscle differentiation has not yet been explored, and it is still an open question as to the mechanism by which

sumoylation represses Mef2 activity. It is clear from Vishal *et al.* 2023, that the most reliable results come from studying Mef2 modifications in their native environment. Therefore, to generate more reliable results, studies on the role of Mef2 sumoylation during muscle development should be validated in an animal model.

1.5 Project Aims

Whilst the *Drosophila* system has already proven an excellent model for demonstrating the importance of Mef2 function to myogenesis, there is still a lot to learn about how Mef2 activity is regulated in order to ensure the correct developmental outcomes.

In this project, I largely focused on a model progenitor cell system: the wing imaginal disc and its associated adult muscle progenitors (AMPs), to explore several facets of Mef2 regulation to build on the current understanding of how its activity is modulated in time and space.

The first aim of the project was to establish the expression pattern of Mef2 in the wing imaginal disc AMPs using a newly generated CRISPR eGFP directly tagged allele (Hubbert 2023). This tissue could then be used to further characterize a previously observed Mef2-overexpression phenotype; the premature activation of target muscle differentiation genes (Soler and Taylor 2009). I aimed to establish if this is simply a case of premature reporter gene activation, or whether precocious muscle fibres are actually developing. To do so, I analyzed their structure, and their expression pattern of key sarcomeric proteins, hypothesizing that they would resemble developed muscle if premature fibre differentiation is indeed occurring.

A second goal of my project was to analyze the impact of *Him* during myogenesis, with specific reference to any potential regulation of Mef2 activity. I generated a CRISPR/Cas9 based *Him* allele using a specific variation of the technique that generates a null allele, reporter construct and directly-tagged protein all-in-one (Poernbacher *et al.* 2019). This, in combination with pre-existing tools, was used to analyze *Him* expression and function during *Drosophila* adult muscle development. If *Him* is functionally important for proper muscle differentiation, loss-of-function would

be expected to impact some aspect of muscle development. Therefore, muscle morphology of *Him* mutant animals was studied to establish developmental phenotypes. To determine any Mef2-regulatory aspect of Him function, I tested for a genetic interaction using the AMP premature differentiation assay as a readout for Mef2 activity, and for a physical protein-protein interaction between them both using Yeast-2-Hybrid.

Another aspect of Mef2 regulation of interest is its potential sumo-modification – a post-translational modification that is regularly implicated in repression of target substrates. A sumoylation motif in *Drosophila* Mef2's C-terminal transactivation domain strongly suggests that this modification is occurring, and its conservation amongst Mef2 family members points towards an important function. Because of this, I wanted to explore the importance of sumoylation on muscle development, and in particular the impact it has on Mef2 activity. Loss-of-function of sumoylation machinery was assayed, reasoning that if the pathway is important to myogenesis, an observable phenotype would be present. To determine Mef2-specific consequences of sumo-modification, a series of mutant constructs were generated to both block, and enhance Mef2 sumoylation state. I hypothesized that if sumoylation is important in regulating Mef2, then blocking the modification would impact its activity to some degree. To test this, mutant vs wild-type constructs were compared in i) a reporter-based assay to determine resultant Mef2 activity, and ii) the impact they have on adult muscle development when overexpressed.

A separate, but related aspect of *Mef2* gene function is its role in muscle post-development, in the maintenance of differentiated tissue. The discovery of Him protein expression in adult muscle satellite cells part-way through the project prompted a preliminary investigation into MuSC biology. A specific objective was to determine if Mef2 is implicated in the muscle satellite cell contribution to muscle homeostasis and repair upon injury. To investigate this, I assayed MuSC-specific Mef2-RNAi knockdown, to determine if muscle maintenance and repair was impacted, using flight behavior as a read-out for proper muscle function.

Chapter 2 – Methods

2.1 Fly Husbandry

2.11 *Drosophila* culture

Drosophila melanogaster cultures were maintained in plastic vials under standard conditions using a standard maize/dextrose/agar-based culture medium. For long term storage of stocks, flies were kept at 18°C and flipped into fresh food every 5 weeks. Flies used in ongoing experiments were maintained at 21°C and flipped every week to ensure a constant emergence of freshly eclosed adult flies. The stock genotypes used in this project are listed in Table 1.

2.12 Setting up crosses

Experimental crosses were performed in a 25°C incubator unless otherwise stated. To select flies of the relevant sex and genotype, flies were emptied onto a fly pad (SLS, FLY1032) and anaesthetized using CO_2. Flies were gently manipulated using a fine paintbrush to avoid damage to individuals. Female virgins for crosses were collected by emptying appropriately staged culture vials in the morning and selecting for a visible meconium. Further collections took place at midday, and then in the late afternoon, with all newly emerged females assumed to be virgin. Crosses were set up in a culture vial, using at least 15 female virgin flies per vial, at a female to male ratio of 3:1. These were turned into fresh food every 2-3 days to prevent overcrowding of developing larvae and to create a succession of F1 emergence.

2.13 Setting up laying pots

Laying pots were used to collect embryos for experimental analysis, comprised of a plastic cage attached to a yeast covered apple juice agar plate which acted as an egg laying substrate.

To make apple juice agar, 6 g sucrose was dissolved in 60 ml apple juice on a hot plate, whilst 6 g agarose was dissolved in 200 ml dH_2O in the microwave. Both solutions were mixed together and allowed to cool to approximately 70 °C. 3 ml 10% Tegosept (SLS, FLY1136) diluted in ethanol was added to the cooled solution and mixed by swirling, and then poured into 60 mm petri dishes (Fisher, 11758573).

To set up a laying pot, approximately 150 virgin females and 50 male flies were used. Standard baker's yeast was mixed with dH_2O to generate a paste, which was smeared onto the laying cap. Embryo collections usually were performed overnight to generate a large range of developmental stages. The same laying pot was used for up to a week when large numbers of embryos were required for an experiment.

2.2 Behavioral Assays

2.21 Jumping assay

Jumping ability was tested according to Chechenova *et al.* 2017 with minor modification. Young (<2 days) male flies were anaesthetized on a fly pad using CO_2, and had their wings removed using dissection scissors (Fine Science Tools, 15003-08). Flies were returned to a culture vial at 25°C overnight, to recover from being anesthetized. Individual flies were transferred onto a piece of lined paper for a jumping trial, which was filmed using a Samsung Galaxy S21 smart phone. A paintbrush was used as a looming stimulus to elicit a jump escape response, by moving the brush towards the posterior of the fly. The horizontal distance travelled by the jumping fly was calculated using Tracker software (physlets.org/tracker), with the lines on the paper providing scale. Each fly had 5 jumps recorded, with the mean of the longest 3 calculated and used for comparison. A minimum of 15 flies per genotype were assayed.

Table 1. List of project-relevant stock genotypes and their sources.

Genotype	Construct ID (if relevant)	Source
1151Gal4;;		Brand and Perrimon, 1993.
;;MhcGFP	FlyFos022462(pRedFlp-Hgr)(Mhc[14903]::2XTY1-SGFP-V5-preTEV-BLRP-3XFLAG)dFRT	VDRC318471 fTRG collection (Sarov et al. 2016).
1151Gal4;;MhcGFP		Transgenes combined for this study.
1151Gal4;Mhc-TauGFP		Soler et al. 2004
;;B3-TubulinGFP	FlyFos029115(pRedFlp-Hgr)(betaTub60D[32130]::2XTY1-SGFP-V5-preTEV-BLRP-3XFLAG)dFRT	VDRC318309 – fTRG collection (Sarov et al. 2016).
1151Gal4,,B3-TubulinGFP		Transgenes combined for this study.
w[1118];;Su(var)2-10-GFP	PBac{y[+mDint2] w[+mC]=Su(var)2-10-GFP.FPTB}VK00037	BL64795
w[1118];;Enh3Gal4-AttP2	P{y[+t7.7] w[+mC]=GMR35H09-GAL4}attP2	BL49924
w[*];UAS-mCherryNLS;MRKS/TM6B		BL38425
;UAS-mCherryNLS;Enh3Gal4-AttP2		Transgenes combined for this study.
w[*];UAS-mCherryCD8;		BL27391
w[*];If/CyO;HimGFP L2-2		Liotta et al. 2007
Mef2GFP		Sean Hubbert, unpublished Mef2 Direct Tag
Him_mNeongreen_reporter;;		This study
Him_mNeongreen_direct_tag;;		This study
Him_mNeongreen_reporter; Mef2GFP		Transgenes combined for this study.
Him52;;		Daniel Hancock, unpublished
Himφ;;		Richard Cripps, unpublished
Him52;;HimGFP L2-2		Transgenes combined for this study.
Himφ;;HimGFP L2-2		Transgenes combined for this study.
w[*];;UAS-Mef2-WT-AttP2		This study
w[*];UAS-Mef2-WT-AttP40;		This study
w[*];;UAS-Mef2-K352R-AttP2		This study
w[*];;UAS-Mef2-S352A-AttP2		This study
w[*];;UAS-Mef2-S352E-AttP2		This study
w[*];UAS-HDAC4-AttP40;		Sean Hubbert, unpublished
w[*];UAS-Him (J7); TM3/TM6		Liotta et al. 2007
w[*];UAS-mCherryCD8;UAS-Mef2-WT-AttP2		Transgenes combined for this study.
w[*];UAS-Him(J7);UAS-Mef2-WT-AttP2		Transgenes combined for this study.
w[*];UAS-HDAC4-AttP40;UAS-Mef2-K352R-AttP2		Transgenes combined for this study.
w[*];UAS-Him(J7);UAS-Mef2-K352R-AttP2		Transgenes combined for this study.
y[1]sc[*]v[1]sev[21];;Su(var)2-10 RNAi	P{y[+t7.7] v[+t1.8]=TRiP.HMS00750}attP2	BL32956 – TRiP collection (Perkins et al. 2015)
;UAS-Su(var)2-10 RNAi;	P{KK108790}VIE-260B	VDRC100813 – KK collection (Green et al. 2014)
;UAS-Ubc9-RNAi;	P{GD10017}v33685	VDRC33685 - GD Collection (Dietzl et al. 2007)
;;UAS-Mef2-RNAi	P{GD5039}v15550	VDRC15550 – GD collection (Dietzl et al. 2007)
;;UAS-mCherry-RNAi		Gift from Mary Baylies
w[*];UAS-Su(var)2-10-AttP40;		This study
w[*];;UAS-Su(var)2-10-AttP2		This study
y1 w[*]; UAS-Ubc9;		BL9324
UAS-ReddM		Antonello *et al.* 2015

2.22 Flight assay

Flight ability was measured essentially as described previously (Drummond *et al.* 1991). A flight arena consisted of a plastic container measuring approximately 20 cm x 20 cm x 40 cm, with a lamp positioned above to encourage upwards flight towards the light (Figure 2.1). Flies were sorted for the correct genotype upon eclosion on a CO_2 pad, and housed in batches of 5-10 within culture vials until the appropriate age. Only female flies were used, as males elicit aggressive behavior towards one another which can result in damage to the wings, and hence alter flight ability. To perform the assay, flies were introduced through an opening midway up the flight arena, and scored based on whether they flew upwards (U), horizontally (H), down (D) or did not fly at all – null (N). A maximum of 10 flies were introduced each time, as this is the maximum it was possible to score reliably by eye. From these data, a flight index was calculated, as described in Deaguero *et al.* 2019. Each fly received a score of 3,2,1 or 0 dependent on whether it registered an up, horizontal, down or null response.

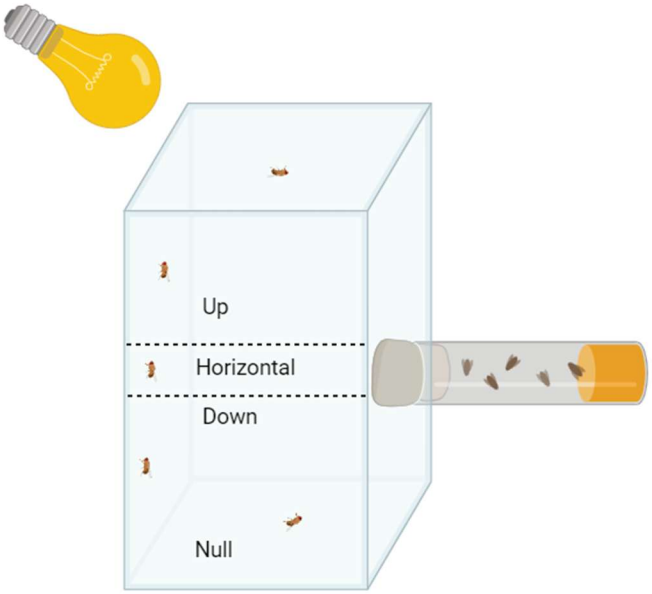

Figure 2.1 - Flight testing arena.

Flies were scored according to which of the four zones they landed in upon introduction midway up the flight arena: Up, Horizontal, Down or Null.

Table 2. Antibodies used in this study.

Primary Antibodies				
Antibody	**Host**	**Dilution**	**Source**	**Product Code**
Cut	Mouse	1/50	DSHB	2B10
Fas3	Mouse	1/100	DSHB	7G10
Sallimus	Rat	1/100	DSHB	BB2/17.9
Mhc	Mouse	1/100	DSHB	3E8-3D3
Integrin	Mouse	1/50	DSHB	CF.6G11
Eve	Rabbit	1/3,000	DSHB	Even-skipped
Zfh1	Rabbit	1/5,000	Ruth Lehmann	
RFP	Rat	1/1,000	Proteintech	5F8
Mef2	Rabbit	1/1,000	DSHB	Mef2
mNeongreen	Mouse	1/500	ProteinTech	32F6
GFP	Chicken	1/500	Abcam	ab13970
Secondary Antibodies				
Antibody	**Host**	**Dilution**		**Product Code**
Anti-Rabbit-488	Rabbit	1/500	Abcam	ab6556
Anti-Rabbit-555	Goat	1/500	Gift from SLQ	A-21428
Anti-Chicken-488	Donkey	1/500	Stratech	703-545-155
Anti-Mouse-488	Goat	1/500	ThermoFisher	A-11029
Anti-Mouse-555	Goat	1/500	Gift from HWC	A32727
Anti-Rat-555	Goat	1/500	Gift from SLQ	ab150158
Anti-Rat-594	Goat	1/500	ThermoFisher	A-11007
Anti-Rabbit-647	Goat	1/500	Gift from PW	A-21245
DAPI	NA	1/1,000	ThermoFisher	62248
Hoechst 33258	NA	1/3,000	ThermoFisher	H3569
ActiStain555	NA	1/140	Cytoskeleton Inc	PHDH1
ActiStain670	NA	1/140	Cytoskeleton Inc	PHDN1

2.3 Histology of *Drosophila* embryonic and adult musculature

Primary antibodies, secondary antibodies and additional stains used for immunofluorescent labelling of embryonic, larval and adult tissues are listed in Table 2, as well as the dilutions they were used at.

2.31 Embryo immunostaining

Fixation

Embryos were collected from apple juice plates using a fine paintbrush and dH_2O to transfer them into a wire mesh basket. Embryos were dechorionated within the basket using a 50% bleach solution diluted in dH_2O, taking approximately 2-3 min. Bleach was rinsed from the embryos using dH_2O, before they were dried by sitting

the basket on blue torque roll for 1 min. They were then transferred with a paintbrush, into a 2 ml Eppendorf containing 1 ml of n-Heptane, and 1 ml of fixative solution. Fixative solution was made fresh each time, using 200 µl 37% formaldehyde solution (Sigma, F8775), 80ul 10x PBS (Severn Biotech Ltd, 20-7400-10) and 720 µl dH2O. The embryos were fixed for 20 min, with agitation on a Luckman shaker (setting 4). The fixative solution was removed and replaced with 1 ml methanol. The embryos were devitellinized by vortexing vigorously for 30 sec, and then rinsed 3x with 1ml methanol. They were stored at -20°C in 500 µl methanol until required for antibody staining.

Fluorescent Antibody Staining

The methanol was removed from the fixed embryos, and they were rinsed three times with 1 ml 0.3% PBT, made by diluting triton-X100 (Sigma, X100) in 1X PBS. Three further washes with 1 ml 0.3% PBT were performed for 5 min each with agitation on a Luckman shaker. The embryos were incubated at room temperature in blocking solution (0.3% PBT containing 1% w/v BSA [Sigma, A7096-100G]) for 30 min with agitation, to reduce non-specific primary antibody binding. Embryos were incubated at 4°C overnight with primary antibody(s) diluted in blocking solution, with agitation on a rotary mixer. The following morning, the primary antibody was removed, and the embryos were rinsed three times with 1 ml 0.3% PBT. Three further 5 min washes with 1 ml 0.3% PBT were performed, before adding the appropriate secondary antibody diluted in blocking solution to the embryos. From this point onwards, samples were protected from light.

The embryos were incubated in the secondary solution at room temperature for 2 hr with agitation, followed by three final rinses and three 5 min washes with 1 ml 0.3% PBT. The PBT was removed, and the embryos stored in glycerol [Sigma, G5516-100ml] diluted to 80% with PBS at 4°C, until imaging. Embryos were mounted on glass microscope slides in 50 µl 80% glycerol, between two #1 thickness coverslips to act as a spacer. Embryos were rotated to the correct orientation during imaging by gently nudging the coverslip with a pair of forceps, taking care not to crush the samples.

2.32 Wing imaginal disc staining

Dissection of Late L3 Wing Imaginal Discs

Wing imaginal discs were isolated from third instar wandering larvae, which were gathered from the side of the culture vial using a damp paintbrush, and stored in PBS on ice for a maximum of 30 min until dissection. Larvae were dissected under a stereomicroscope in cold PBS on a dissection plate, constructed from a petri dish by trimming away its edge. Using sharp forceps (Agar Scientific, AGT502), each larva was grasped midway along the length of its body. The posterior end was pulled away from the anterior end and discarded. The anterior end of the larvae was inverted by holding the larval mouth parts with one pair of forceps, and rolling it up with the second, causing the internal organs to be displayed. Fat body tissue and the gut were discarded, leaving the brain and imaginal discs intact and attached. Inverted heads were collected in PBS and stored on ice for a maximum of 20 min prior to fixation.

Fixation and Immunostaining of Wing Imaginal Discs

Inverted heads were fixed in 500 µl 4% PFA (Sigma, 441244) diluted in PBS, for 20 min at room temperature on a nutating mixer. The PFA was removed, and the tissue rinsed three times with 1 ml cold 0.03% PBT. The tissue was washed three times with 1 ml 0.03% PBT for 15 min each time, with agitation at room temperature. The sample was blocked in 1 ml 2% normal donkey serum (NDS) [SLS, D9663]) diluted in 0.03% PBT for 30 min at room temperature. Primary antibodies were diluted in 2% NDS/0.03% PBT in a volume of 500 µl and applied to the sample overnight at 4°C on a rotary mixer. The following morning, the primary antibody was removed, and the tissue samples were rinsed and washed three times as before. Secondary antibodies were diluted in NDS, and staining was performed with agitation at room temperature for 2 hr. Hoechst 33258 and phalloidin (Cytoskeleton Inc, ActiStain555 or ActiStain670) were included with the secondary antibodies if required. This was followed by a final three rinses and washes with 1 ml 0.03% PBT. The wing imaginal discs were dissected away from inverted larval heads and mounted in 20 µl 80% glycerol on a standard glass microscope slide. Four larval brains were gathered during the wing imaginal disc dissection, and mounted alongside the discs to act as spacers when the coverslip was applied.

Exceptions to this protocol include when antibody staining for Cut, and Him-mNeongreen. The fixation period was reduced to 15 min, washes were performed in 0.1% PBT and the blocking step was with 10% normal goat serum (ThermoFisher, 16210064).

For some experiments, wing imaginal discs were fixed, and Hoechst stained in the absence of any antibody staining. Inverted larval heads were rinsed and washed three times with 0.03% PBT followed by a 30 min incubation at room temperature with Hoechst diluted in 0.03% PBT to a final concentration of 6 µM. The Hoechst solution was removed, and the sample was rinsed and washed three more times with 0.03% PBT. The imaginal discs were dissected and mounted as before.

Live imaging of Wing Imaginal Discs

To study live imaginal discs, larvae were dissected in sterile Schneider's insect medium (Merck, S0146). Wing discs were dissected in the absence of fixation and mounted in 20 µl Schneider's medium. Samples were imaged immediately after mounting.

Whenever sample size (n) is reported, I refer to the number of discs imaged, rather than the number of animals. An average yield is one disc per larva dissected.

2.33 Adult muscle dissections

Pharate DLM Transverse Cross-sectioning

Pharate pupae (~90-96hr APF) were selected on the basis of their dark coloration. A damp paintbrush was used to collect the pupae from the walls of the culture vial. Pupae were aligned on a strip of double-sided sticky tape and had their pupal cases removed gently using fine forceps. Dissection scissors were used to gently remove the head, leg and wings from the fly. Samples were gathered in PBS on ice for a maximum of 20 min prior to fixation. Fixation was performed in 500 µl 4% PFA for 20 min at room temperature on a nutating mixer. Transverse DLM sections were obtained using dissection scissors by cutting across the thorax, approximately between and 2nd and 3rd pairs of legs. Hemithoraces were washed twice for 10 min in 1 ml 0.3% PBT. Samples were stained using 100 nM phalloidin and 6 µM Hoechst diluted in 0.3% PBT, for 2 hr at room temperature on a nutating mixer. The samples were rinsed quickly twice, followed by two 10 min washes with 1 ml 0.3% PBT.

Transverse sections were mounted in 100 µl 80% glycerol on a glass microscope slide. Three layers of #1 coverslips (Menzel-Glaser) were attached to the slide using nail varnish, to act as a spacer, between which the samples were mounted.

Adult DLM Transverse Cross-sectioning

Adult IFM dissections were performed on young adult flies less than 3 days old. CO_2 was administered to render the flies unconscious to facilitate the removal of the head, wings and legs using dissection scissors. The rest of the protocol is identical to pharate DLM dissections.

DLM Satellite Cell Antibody Staining

DLM sagittal sections were prepared and stained for visualization of adult muscle satellite cells, essentially as described in Hunt and Demontis 2013. Female flies between 1 and 3 days old flies were immobilized using CO_2, and the head, wings, legs and abdomen were removed from the thorax using dissection scissors. During dissection, thoraces were pooled in an Eppendorf with PBS on ice for a maximum of 30 min. Samples were fixed at room temperature in 1 ml 4% PFA/1% PBT for 25 min on a nutating mixer. A strip of double-sided tape was attached to a microscope slide, along which the fixed thoraces were aligned. A scalpel (Swann-Morton, 0934) with a #23 blade was used to sagitally section each thorax along its midline. Hemithoraces were fixed for a further 30 min at room temperature. The fixative was removed, and the hemithoraces were washed twice for 10 min with 1 ml 0.3% PBT. Samples were blocked using 1ml 0.5% BSA diluted in 0.3% PBT for 30 min with agitation at room temperature. Primary antibodies were diluted in blocking solution and incubated with the samples overnight at 4°C on a rotary mixer. The following morning, samples were washed three times with 1 ml 0.3% PBT. Secondary antibodies were diluted in blocking solution, which included Hoechst and phalloidin when relevant. Samples were incubated in the secondary antibody solution for 2 hr at room temperature, before three final 10 min washes with 1 ml 0.3% PBT. Hemithoraces were mounted as described previously.

2.34 Cryosectioning of adult muscles

Cryosectioning was used to generate thoracic slices for antibody staining to visualize transverse views of TDT or DLMs, essentially as described in Morriss *et al.* 2012. For transverse TDT sections, whole flies were mounted dorsal side down on double sided sticky tape. For transverse DLM sections, flies had their heads, wings and abdomens removed and the remaining thoraces were mounted anterior side down on the tape. Samples were then submerged in OCT (CellPath, KMA-0100-00A), before being snap frozen in liquid nitrogen and stored at -80°C prior to sectioning. To section, samples were mounted on a chuck within the cryostat (Bright, OTF5000), which is maintained at approximately -30°C. To bond the sample to the chuck, OCT was applied to its surface and the frozen sample pressed into it using pre-chilled forceps. The sample was then left in the cryostat for 5 min whilst the fresh OCT set the sample to the chuck. Once set, excess OCT was trimmed away from around the sample using a razor blade. Approximately twenty 10-12 µm sections per fly thorax were then generated, which were gathered on an adhesive microscope slide (Epredia, J7800AMNZ), and stored at room temperature until antibody staining later the same day.

Slides were placed in a 100 ml slide holder in fixative solution (90 ml 1x PBS, 10 ml 37% formaldehyde) for 8 min on a shaker. The fixative was removed, and the slides washed with 0.1% PBT for 3 min on a shaker. An additional wash was performed with fresh 0.1% PBT for 30 min, followed by three further 5 min washes. 100ml blocking solution (3% BSA w/v diluted in 0.1% PBT) was added to the slide holder and incubated at room temperature for 30 min on a shaker. Primary antibodies were prepared by diluting in blocking solution, 120 µl per slide. Antibody was applied to each slide and a 60mm x 24mm #1 coverslip (Epredia) was gently applied. Slides were transferred to a humidity chamber (plastic box containing damp blue roll) and incubated overnight at room temperature in a dark cupboard. The following morning, the coverslips were removed, and the slides were washed for 5 min with 0.1% PBT. 120 µl secondary antibody diluted in blocking solution was applied to each slide, which were incubated in the humidity chamber for 2 hr at room temperature. A final 5 min wash with 0.1% PBT was performed. 75 µl 50% glycerol diluted in PBS was added to each slide, a coverslip was applied gently ensuring no bubbles and sealed with nail varnish.

2.35 Injury Assays

In order to investigate the injury response mechanisms in the DLMs, a standardized procedure was used to induce reproducible damage to the muscle fibres (Chakraborty *et al.* 2018). Young female flies between 1 and 3 days old were immobilized on a CO_2 pad. Flies were manipulated delicately with a fine paintbrush to avoid unwanted damage. To perform an injury, a fly was placed laterally under a dissection microscope and held in place by using the paintbrush on its abdomen. Injury was induced by inserting a 0.1 mm Minutien pin (FST, 26002-10) into the right-side lateral thorax just above the hinge region where the wing attaches the cuticle. The pin was inserted approximately 0.5 mm into the thorax, resulting in injury to only the right set of DLMs, leaving the left hemithorax DLMs to act as an internal control. After injury, flies were returned to their culture vials and aged at 25◦C for the desired period of time.

Immunohistochemical analysis of the injured fibre was performed essentially as described in section 2.33 '*DLM satellite cell antibody staining'* . DLM hemithoraces were stained with phalloidin to identify the injury site. Alternatively, the hemithorax was imaged using endogenously expressed fluorophores to visualize proteins of interest.

Live imaging of Hemithorax Preps

In order to undertake live imaging of dissected hemithorax preparations, a protocol was adapted from Bostock *et al.* 2020. Hemithoraces were bisected essentially as described in section 2.33 '*DLM satellite cell antibody staining'*, but without the fixation step. Hemithoraces were mounted in a 35 x 10 mm petri dish (Fisher, 11758573) in an agarose culture medium, which was prepared as follows.

A 2% low gelling agarose stock was prepared by diluting 0.2 g agarose (Merck, A9419-25g) in 10 ml sterile dH_2O using a microwave, which was poured into a gel casting tray to set. This was stored at 4◦C submerged in sterile dH_2O. Prior to mounting, 0.5 cm^3 cubes of the 2% gelling agarose were melted for 20 sec in the microwave and subsequently diluted to 0.4% in Schneider's insect medium (Merck, S0146), which had been preheated to 42◦C. The temperature of the solution was then lowered to 34◦C and added to the 35x10 mm petri dish to coat the bottom of it. Hemithoraces were transferred into the media, and oriented with the DLMs facing

downwards against the bottom of the dish. All movements and orientations of the tissue were achieved within 5 min of placing within the agarose, to avoid disrupting its setting. The agarose was left to solidify for 10 min, then cold Schneider's medium was added to cover the sample. Samples were imaged as soon as possible after mounting.

2.4 Imaging

Most immunofluorescent samples were imaged using conventional fluorescence microscopy, with the exception of satellite cells which can only be visualized using a confocal microscope.

2.41 Fluorescent Microscopy

Either an Olympus BX50 or an Olympus BX63 was used for visualizing fluorescent antibody stains in most experiments. An attached Hamamatsu camera (BX50 model no. 8484-05G02, BX63 model no. C11440-36U) was used for image acquisition using 4x, 10x or 20x objective lenses. For both microscopes, a pE300-lite LED light source in combination with Dapi, FITC, TRITC or CY5 (BX63 only) filter cubes to illuminate samples with fluorescently labelled probes. Imaging parameters such as gain, and exposure were kept consistent where relevant.

2.42 Confocal Microscopy

To obtain high resolution images, confocal microscopy was performed with assistance from Cardiff University, School of Bioscience's bioimaging hub. A Zeiss LSM880 confocal microscope was for image acquisition, at 10x, 20x, 40x or 63x magnification. Lasers lines used include 405 nm, 588 nm, 561 nm, 594 nm and 633 nm. Z-stacks were typically obtained with a 1 µm step at a pixel resolution of 1,024x1,024.

2.43 Image Processing

Raw images were processed and analyzed using FIJI software (Schindelin *et al.* 2019).

2.44 Quantification of Mef2 activity

Using a MhcGFP Reporter

1151Gal4;;MhcGFP females were used to drive overexpression of *UAS-Mef2* or *UAS-Mef2* mutants in wing imaginal disc AMPs at 25°C. Since the MhcGFP minigene is Mef2 responsive, it acts as a reporter of Mef2 activity level based on the amount of GFP present. Quantification of GFP allows the determination of how addition of other proteins of interest or mutations to the Mef2 coding sequence impact its activity. The quantification protocol below was standardized to allow comparisons between samples.

Late L3 larvae were dissected as previously described. Inverted larval heads were fixed for 20 min in 4% PFA at room temperature on a nutating mixer. Fixative was removed and the tissue rinsed 3x quickly with 500 µl cold 0.03% PBT. 500 µl Hoechst staining solution (6 µM Hoechst diluted in 0.03% PBT) was applied for 30 min with agitation at room temperature. Hoechst staining solution was removed, and the tissue rinsed 3x with 500 µl cold PBS. Wing discs were dissected away from the inverted heads, and mounted in 20 µl 80% glycerol on a microscope slide. At all steps exposure to light was minimized by covering samples with foil whenever possible.

Samples were imaged immediately after mounting to minimize loss of GFP signal, using the Olympus BX50 fluorescent microscope with the LED light source set to 10% brightness. Wing imaginal discs were imaged with both the 10x and 20x objectives using HC-Image software, at 16-bit image depth, 1.0 exposure and 0 gain.

To quantify the level of MhcGFP in each wing imaginal disc,10x images were first thresholded using FIJI to remove background signal. The auto-threshold tool was used to determine that the Triangle thresholding algorithm was most appropriate for these data (Zack *et al.* 1977). Thresholded area, mean grey value and integrated density metrics were recorded and compared amongst genotypes.

2.5 Molecular Biology Techniques

Molecular cloning was used to generate several of the fly stocks used during this project, including numerous overexpression lines and CRISPR mediated direct tagging of endogenous *Him*. This section describes the core molecular techniques employed to construct the required vectors for *Drosophila* transgenesis. Yeast2Hybrid assays to test for protein-protein interactions also required molecular cloning to generate bait and prey vectors including the insert sequences to be tested for interactions. The following techniques are also applicable to this.

2.51 gDNA extraction

To extract gDNA from *Drosophila*, Invitrogen's ChargeSwitch Kit (CS11203) was used. 3-5 young flies of the relevant genotype were selected for extraction which was performed essentially as described in the manufacturer's instructions. Following extraction, DNA was eluted in 50 µl buffer EB and stored at -20◦C.

2.52 PCR

DNA was typically PCR-amplified from a vector template or gDNA using Q5 high fidelity master mix (NB, M0492S). PCR Primers were ordered from Merck in dry powder format, reconstituted to 100 µM in molecular grade dH_2O upon receipt, and stored at -20◦C. 10 µM working stocks of each primer were made by diluting 10 µl 100 µM stock in 90 µl molecular grade dH_2O. PCR reactions were performed in a BioRad T100 thermocycler, using the cycling conditions recommended by the polymerase manufacturer. NEB's Tm calculator was used to determine the annealing temperature of the primers during the PCR reaction. 25 µl reactions with 25-30 PCR cycles generated a sufficient quantity of DNA for downstream applications. A typical 25 µl reaction is as follows:

- 0.1 ng plasmid DNA OR 5 ng gDNA
- 500 nM FWD Primer
- 500 nM REV Primer
- 12.5 µl Q5 2x Master Mix
- dH_2O to 25 µl

An example set of cycling conditions are as follows:

- 98°C for 30 sec.
- 25 cycles of [98°C for 10 sec, 60°C for 30 sec, 72°C for 1 min].
- 72°C for 2 min.
- Hold at 4°C.

Qiagen's QIAquick PCR purification kit was used to purify PCR products following the reaction, according to the manufacture kit instructions.

2.53 Agarose Gel Electrophoresis

Agarose gels were routinely performed for analysis and purification of insert and vector DNA. Gels of 0.7-1.2% w/v were made by dissolving the appropriate amount of agarose (Meridian Bioscience, BIO41025) in 30 ml 1X TBE (Crystal Buffers, 20-6000-10) by heating in the microwave. 1 µl SYBR Safe DNA stain (ThermoFisher, S33102) was added to the solution, which was then set for 30 min at room temperature in a gel casting tray. The gel was transferred to a gel dock and submerged with 1X TBE. 6x loading dye (NEB, B7024S) was added to the DNA samples, which were then loaded into the wells of the agarose gel alongside either a 100bp (NEB, N3231S) or 1kb (NEB, N3232S) DNA ladder. Gels were run at 75 V for approximately 1 hr, and either imaged using a UV transilluminator, or visualized on a blue light box if DNA was to be extracted for further downstream processing.

Qiagen's QIAquick gel extraction kit was used to purify DNA from agarose gels. DNA was excised from the agarose gel on a blue light box using a clean scalpel. The gel fragment was transferred to an Eppendorf ready for extraction according to the kit protocol. Purified DNA was eluted in 30 µl elution buffer and stored at -20°C.

2.54 Restriction Digests

Restriction digestion was routinely used to generate compatible sticky ends on vector and insert DNA to facilitate their ligation. Either 2 µg vector DNA, or an entire purified PCR reaction worth of product (~30 µl) was digested in a 50 µl reaction using enzymes from NEB's high-fidelity collection. The digestion reaction was incubated at 37°C for 3 hr, and heat inactivated at 65°C for 20 min. For vector DNA only, 1 µl QuickCIP (NEB) was added after the digestion reaction and incubated for a further 20 min at 37°C to dephosphorylate the 5' and 3' ends of the cut vector DNA.

QuickCIP was heat inactivated at 65◦C for 10 min. Digested vector and insert DNA was run on an agarose gel for analysis and purification into 30 µl Buffer EB. Purified DNA was stored at -20◦C until ligation.

2.55 Ligation Reaction

Ligations were performed in a 20 µl reaction using T4 DNA ligase (NEB, M0202). A 3:1 molar ratio of insert to vector was typically used, with a total of 20 ng vector DNA. Ligations were performed for 16 hr overnight at 16◦C, followed by heat inactivation of the DNA ligase at 65◦C for 10 min. Ligation reactions were stored at 4◦C until transformation.

2.56 Gibson Reaction

Gibson assembly master mix (NEB, E2611S) was used for assembly of multiple, overlapping DNA sequences, using the kit manufacturer's instructions. For fragment assembly, 0.02-0.5 pmol total DNA (with three-fold molar excess of insert to vector) was incubated with 10 µl Gibson assembly master mix. The reaction was made up to a 20 µl reaction using dH_2O and incubated at 50◦C for 60 min. Following incubation, samples were stored on ice or at -20◦C until transformation. 3 µl of the Gibson reaction was used in transformation reactions.

2.57 Preparation of Mix & Go DH5α competent cells for transformation

Transformation was into 'Mix & Go' DH5α competent cells (Zymo Research, T3001). To prepare more of these cells, the Mix & Go *E.coli* transformation kit was used, with minor deviation from the manufacturer's instructions:

The -80◦C DH5α glycerol stock was thawed and spread onto a LB agar plate which was incubated overnight at 37◦C. The following morning, a single colony was picked using a sterile pipette tip and grown in 50 ml LB broth for 4-6 hr at 37◦C. 5 µl of this starter culture was transferred to a 50 ml solution of LB-20mM glucose and incubated at 18◦C in a shaking incubator at 200 rpm. Cells were incubated for 2-3 days until an OD^{600} of ~0.5 was reached, measured using a spectrophotometer (BIO-RAD, SmartSpec Plus). Cells were cooled on ice and pelleted via centrifugation at

2000g for 10 min at 2°C. The supernatant was removed, and cells were resuspended in 5ml chilled Wash Buffer. Cells were pelleted again, as described previously, and the supernatant discarded. Cells were resuspended in 5 ml chilled Competency Buffer from which 50 µl aliquots were transferred into 1.5 ml Eppendorf tubes. These were flash frozen in liquid nitrogen and stored at -80°C until use.

2.58 Transformation of DH5α

To transform, a 50 µl aliquot of cells was thawed on ice for 10 min. 3 µl of each ligation reaction or 2 µl Gibson Assembly reaction was transformed into the 50 µl cell aliquot and gently mixed by tapping the side of the Eppendorf. The reaction was incubated on ice for 5 min. 25 µl of each transformation mix was applied using a glass spreader to LB-agar (ThermoFisher, BP9724) plates supplemented with the relevant antibiotic (ampicillin 100 µg/ml or tetracycline 10 µg/ml) and incubated overnight in a 37°C incubator. The equivalent mass of cut vector was also transformed, as a control to check for vector background, uncut vector or unwanted reannealing of the cut vector backbone.

2.59 Plasmid Purification

Following transformation, 3-5 individual bacterial colonies were picked from the agar plate using a sterile pipette tip and each transferred into a separate 3 ml aliquot of LB broth (ForMedium, LMM0102) containing the relevant antibiotic. After overnight incubation at 37°C in a shaking incubator at 200 rpm, the plasmid was isolated from the culture using the QIAprep Miniprep kit (27104) and eluted into 50 µl Buffer EB. Plasmid concentration was determined using a NanoDrop. A diagnostic double restriction digest was performed to release the insert and verified using gel agarose electrophoresis to check for successful ligation.

2.510 Mutagenesis

Mutations to plasmid constructs were made using Agilent's QuikChange II site-directed mutagenesis kit. Primers were designed using Agilent's QuikChange primer

design program (www.agilent.com/genomics/qcpd). The mutagenesis reaction was performed with 10 ng vector DNA, 125 ng of each oligonucleotide primer, 5 µl 10x reaction buffer and 1 µl *PfuUltra* DNA polymerase in a 50 µl reaction. Cycling parameters were determined using the kit protocol. Following the reaction, 1 µl DpnI enzyme was added to digest the parental vector DNA, whilst leaving the mutagenized fragment intact. 3 µl of each reaction mix was used for transformation. Following plasmid purification, the mutagenized insert was subcloned into a fresh vector prep to eliminate the chance of off-target mutations in the plasmid backbone.

2.511 Sequence Verification

Eurofin's TubeSeq service was used to verify the sequence of insert DNA. A plasmid concentration of 50-100 ng/µl in a total volume of 15 µl was required for sequencing. To reduce the concentration of DNA to this range, the DNA was diluted in an appropriate volume of molecular grade dH_2O. Sufficient sequencing reactions were performed to ensure at least 2x coverage of each sequence to be verified. SnapGene Viewer was used to visualize the generated Fasta files and chromatograms to determine the nucleotide sequence and its quality.

2.512 Transgenesis

The BestGene microinjection service (https://www.thebestgene.com) was used to generate transgenic flies from the constructs made in house. For UAS-overexpression lines, BestGene introduced the construct into embryos bearing either the AttP40 (chromosome II) or AttP2 (chromosome III) landing site, with transgenesis occurring via PhiC31-mediated recombination (Bischof *et al.* 2007). w+ transformants were shipped, and balanced over either CyO or Tm6b on receipt, depending on whether the transgene was inserted onto chromosome II or III. For CRISPR genome engineering, constructs were injected into nos-Cas9 expressing embryos (Kondo and Ueda, 2013).

Table 3. Primers used in this study with information on directionality and overhangs.

Primer	Direction	Sequence	Notes
Mef2 overexpression			
Mef2III_CDS-EcoRI	FWD	CTAC**GGAATT**CATGGGCCGCAAAAAAATTC	FWD primer for pUASt-Mef2-WT cloning, EcoRI site in bold
Mef2III_CDS-XhoI	REV	ATCT**ACTCGA**GCTATGTGCCCCATCCGCC	REV primer for pUASt-Mef2-WT cloning, XhoI site in bold
Su(var)2-10 overexpression			
Su(var)2-10_EcoRI	FWD	CTAC**GGAATT**CATGCGAAAGACCCGCTCT	FWD primer for pUASt-Su(var)2-10 cloning, EcoRI site in bold
Su(var)2-10_XhoI	REV	ATCTA**CTCGAG**TTAGCCGACGTTTGGGCG	REV primer for pUASt-Su(var)2-10 cloning, XhoI site in bold.
Mef2 overexpression mutants			
Mef2-K352R_a1055g	FWD	CCCGTCTCCATAAAGGTC**AGG**GCTGAGCCG	Mutagenesis primer for Mef2-K352R. Mutated codon in bold.
Mef2-K352R_a1055g	REV	CGGCTCAGC**CCT**GACCTTTATGGAGACGGG	Mutagenesis primer for Mef2-K352R. Mutated codon in bold.
Mef2-S357A_t1069g	FWD	CTGAGCCGCAG**GCG**CCGCCGAGA	Mutagenesis primer for Mef2-S357A. Mutated codon in bold.
Mef2-S357A_t1069g	REV	TCTCGGCGG**CGC**CTGCGGCTCAG	Mutagenesis primer for Mef2-S357A. Mutated codon in bold.
Mef2-S357E_t1069g_c1070a	FWD	GGCTGAGCCGCAG**GAG**CCGCCGAGAGAT	Mutagenesis primer for Mef2-S357E. Mutated codon in bold.
Mef2-S357E_t1069g_c1070a	REV	ATCTCTCGGCGG**CTC**CTGCGGCTCAGCC	Mutagenesis primer for Mef2-S357E. Mutated codon in bold.
mNeongreen vector design			
mNeongreen_XmaI	FWD	GCT**cccgggCTAACGCGAGACCTATGGTCTCT**gttt ccaaaggtgaagaaga	FWD primer for construction of mNeongreen direct tag vector. Lower case bold is XmaI site. Upper case bold is vector backbone sequence to be reconstituted.
mNeongreen_BamHI	REV	CGC**ggatccCAGGTACGATAACTTCGTATAGCATA CATTATACGAAGTTAT**cttgtagagttcatccatgc	REV primer for construction of mNeongreen direct tag vector. Lower case bold is BamHI site. Upper case bold is vector backbone sequence to be reconstituted.
Him CRISPR			
Him_HA1_FWD	FWD	GAAAGACTGGGCCTTTCGCCCGGGCTAACGCGA TCGCAGAGTACCCTGTACTCGAGTAGT	FWD primer for PCR amplification and gibson assembly of Him homlogy arm 1 into mNeongreen direct tag vector.
Him_HA1_REV	REV	AGCCATATTGTCTTCTTCACCTTTGGAAACCATC GAGGTTGGTGGCTCTGCGGCTC	REV primer for PCR amplification and gibson assembly of Him homlogy arm 1 into mNeongreen direct tag vector.
Him_HA2_FWD	FWD	AGTTCGGGGTCCAGCGGTTCTTCAGGCAGTGGC GTCATCTACAAGATACTGAAGC	FWD primer for PCR amplification and gibson assembly of Him homlogy arm 2 into mNeongreen direct tag vector.
Him_HA2_REV	REV	GCCCTTGAACTCGATTGACGCTCTTCGACAATCC GGCTACCAAGGTCGCCACA	REV primer for PCR amplification and gibson assembly of Him homlogy arm 2 into mNeongreen direct tag vector.
Him_gDNA_FWD	FWD	**GTCG**TAGATGACGCCCATCGAGGT	gDNA oligo for cloning into pCFD3 vector for Him CRISPR. BbsI site in bold.
Him_gDNA_REV	REV	**AAAC**ACCTCGATGGGCGTCATCTA	complementary gDNA oligo for cloning into pCFD3 vector for Him CRISPR. BbsI site in bold.
Yeast2Hybrid			
Him_BamHI_FWD	FWD	GCG**GGATCC**TTATGGGCGTCATCTACAAG	FWD primer for cloning full-length Him into PP6. BamHI site in bold. 2bp spacer italicized.
Him_XbaI_FWD	REV	ATC**TCTAGA**ACCAAGGTCGCCACACCAC	REV primer for cloning full-length Him into PP6. XbaI site in bold.
Su(var)2-10_FWD_BamHI	FWD	GCG**GGATCC**TTATGCGAAAGACCCGCTCT	FWD primer for cloning full-length Su(var)2-10 into PP6. BamHI site in bold. 2bp spacer italicized.
Su(var)2-10_REV_XbaI	REV	ATC**TCTAGA**AGCCGACGTTTGGGCGCCT	REV primer for cloning full-length Su(var)2-10 into PP6. XbaI site in bold.
Mef2_EcoRI_FWD	FWD	CTAC**GGAATT**CATGGGCCGCAAAAAAATTC	FWD primer for cloning Mef2[1-156] into PB27. EcoRI site in bold.
Mef2_NotI_REV	REV	ATAT**GCGGCC**GCCGGCACCGGAACAGAAAC	REV primer for cloning Mef2[1-156] into PB27. NotI site in bold.

2.6 Construct Generation

Primers used for the generation of DNA constructs for *Drosophila* transgenesis and Yeast2Hybrid can be found in Table 3. This includes information on overhangs where relevant.

2.61 *UAS-Mef2*

The *Mef2* insert used to generate landing site situated overexpression lines is the same sequence present in the published *UAS-Mef2-III*, originally made using P-element mediated transgenesis (Gunthorpe *et al.* 1999). The insert is approximately 3.3 kb in length, consisting of the entire coding sequence of *Mef2* isoform RC, as well as an additional ~500bp of 3'UTR and ~1200bp of 5'UTR.

The *Mef2* insert was isolated from the original pUASt-Mef2III vector (Gunthorpe *et al.* 1999) via double digestion with EcoRI & NotI restriction enzymes, before subcloning into double digested pUASt-AttB (Bischof *et al.* 2007). This *UAS-Mef2* construct was used to make three transgenic lines: inserted into the AttP18 X chromosome landing site, AttP40 chromosome II landing site and also the AttP2 chromosome III landing site.

2.62 *UAS-Mef2* SUMO motif mutants

UAS-Mef2 mutants were made via mutagenesis of the pUASt-Mef2-AttB construct, to generate the following mutants:

UAS-Mef2-K352R – sumoylation deficient Mef2 construct. Codon 352 mutated from AAG to AGG.

UAS-Mef2-S357A – phosphorylation deficient Mef2 construct. Codon 357 mutated from TCG to GCG.

UAS-Mef2-S357E – phosphomimetic Mef2 construct. Codon 357 mutated from TCG to GAG.

Following the mutagenesis reaction, the mutagenized Mef2 fragment was released from the pUASt-AttB vector using an EcoRI/NotI double digest, and subcloned into a fresh pUASt-AttB prep, to eliminate the chance of off-target mutations in the vector

back bone. The mutant Mef2 fragments were then sequenced to ensure the desired change was present, and that no off-target mutations elsewhere in the insert had occurred. Each mutant Mef2 overexpression construct was inserted into the AttP2 landing site on chromosome III, to facilitate direct comparison between mutant Mef2 and wild-type lines.

2.63 *UAS-Su(var)2-10*

The *Su(var)2-10* insert was inserted into the pUASt-AttB vector using a PCR based cloning approach. The entire 1806 bp coding sequence of *Su(var)2-10* isoform RD was PCR amplified from the clone RE73180, obtained from the DGRC collection of cDNAs. The PCR forward primer contained an overhang with an EcoRI restriction site, and the reverse an overhang with a XhoI site, for ligation into EcoRI/XhoI double digested pUASt-AttB. The *UAS-Su(var)2-10* construct was inserted into both the AttP40 chromosome II landing site, and the AttP2 chromosome III landing site.

2.64 CRISPR N-terminal mNeongreen tag vector design

To directly N-terminally tag genes with mNeongreen at their endogenous locus using CRISPR, a pre-existing mScarlet tagging vector (gift from Cyrille Alexandre, Figure 2.2A) was modified. The mScarlet vector was double digested with XmaI and BamHI which released the mScarlet insert, as well as an additional upstream 29 bp and downstream 48 bp either side of the insert. Primers were designed to amplify the entire mNeongreen coding sequence from Addgene vector 131137, with overhangs to reconstitute the missing upstream 29 bp and downstream 48 bp from the original digest (Table 3). The mNeongreen insert was double digested with XmaI and BamHI, but since a BamHI site is present in the middle of the mNeongreen sequence, it yielded two fragments. The N-terminal mNeongreen fragment was cloned in first and sequence verified. The partially constructed vector was then single digested with BamHI, and the C-terminal mNeongreen fragment was cloned in (Figure 2.2B). The construct was sequence verified again, to ensure that the C-terminal mNeongreen fragment was inserted in the correct orientation.

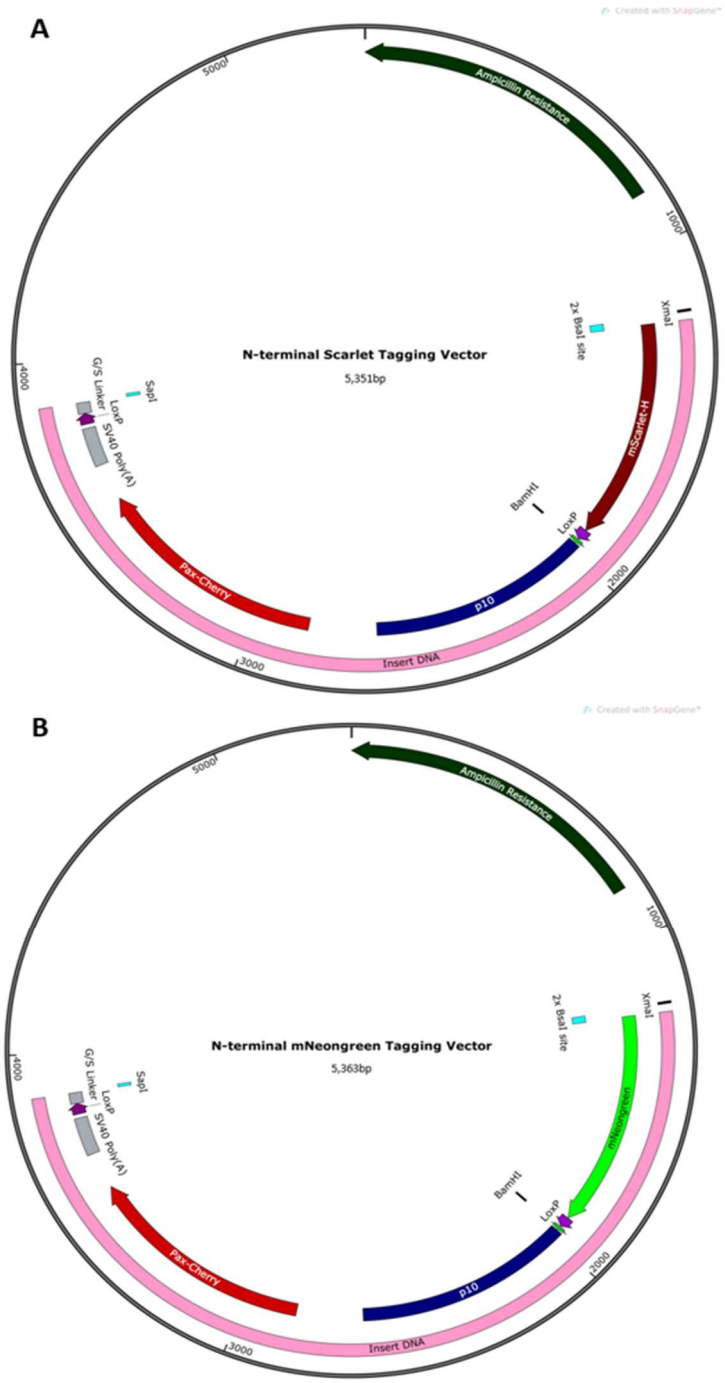

Figure 2.2 – CRISPR N-terminal mNeongreen tag vector design.

The vector required for N-terminally tagging genes at their endogenous locus with mNeongreen was constructed by adapting a pre-existing mScarlet-H tagging vector (Cyrille Alexandre) .Upon Cas9-induced DNA cleavage, the vector acts as a template for DNA repair, consequently incorporating the desired fluorophore to the target site.

A) The mScarlet-H vector map detailing the insert DNA sequence, including the mScarlet-H fluorophore, and LoxP flanked p10 transcriptional termination and Pax-Cherry transformation marker sequences. XmaI and BamHI restriction sites flank the mScarlet-H sequence, facilitating the subcloning of alternative fluorophore sequences such as mNeongreen, as depicted in B).

2.65 CRISPR N-terminal Tagging of Him

CRISPR N-terminal tagging of Him at its endogenous locus with mNeongreen required two plasmid constructs. Firstly, pCFD3 containing guideRNA to direct Cas9 to induce a double-stranded break at the desired edit site (Port *et al.* 2014). Secondly, the newly constructed mNeongreen Tagging vector which acts as a template for homology directed repair, causing the desired DNA sequence to be incorporated into the genome at the relevant site. The insert DNA consists of the mNeongreen fluorophore, as well as LoxP flanked sequences including a p10 terminator, a Pax-Cherry transformation marker, a SV40 poly(A) signal. The constructs were designed to insert this DNA fragment directly upstream of *Him*'s endogenous start codon. Initially, this results in a *Him* reporter with mNeongreen expression under control of *Him*'s native promoter (Figure 2.3A). This is also a *Him* null allele, since the rest of *Him*'s coding sequence is translocated downstream of the insert DNA and is theoretically not transcribed. The LoxP flanked sequences were subsequently removed by crossing the mNeongreen reporter line to flies expressing Cre-recombinase, to make the Him-mNeongreen direct tag linked via the short G/S linker (Figure 2.3B).

Figure 2.3 – CRISPR engineered Him allele before and after addition of Cre-Recombinase.

A) Initially, the insert DNA is incorporated into the *Him* locus, directly downstream from *Him*'s endogenous start codon. This results in a CRISPR allele that acts both as a null, and as a mNeongreen reporter construct under the control of *Him*'s native promoter. These flies express Pax-Cherry as a transformation marker. **B)** Upon exposure to Cre-recombinase, the LoxP flanked sequences are removed from the locus resulting in a Him-mNeongreen directly tagged protein. The resultant fly strain is now Pax-Cherry negative.

gRNA Design and pCFD3 Cloning

In order to generate the *Him* allele, an appropriate CRISPR target site in the vicinity of the *Him* start codon was required. 'CRISPR optimal target finder' under maximum stringency conditions was used to locate a target cut site with an appropriately located protospacer adjacent motif (PAM) for Cas9 dependent cleavage (Gratz *et al.* 2013). Several sites were identified, but a PAM 7bp upstream of *Him*'s start codon was selected, since any potential off-target events were low probability and limited to other chromosomes, so could be backcrossed out. Genomic DNA from the *Drosophila* strain to be microinjected was isolated and sequenced which verified that the target sequence was conserved (Figure 2.4).

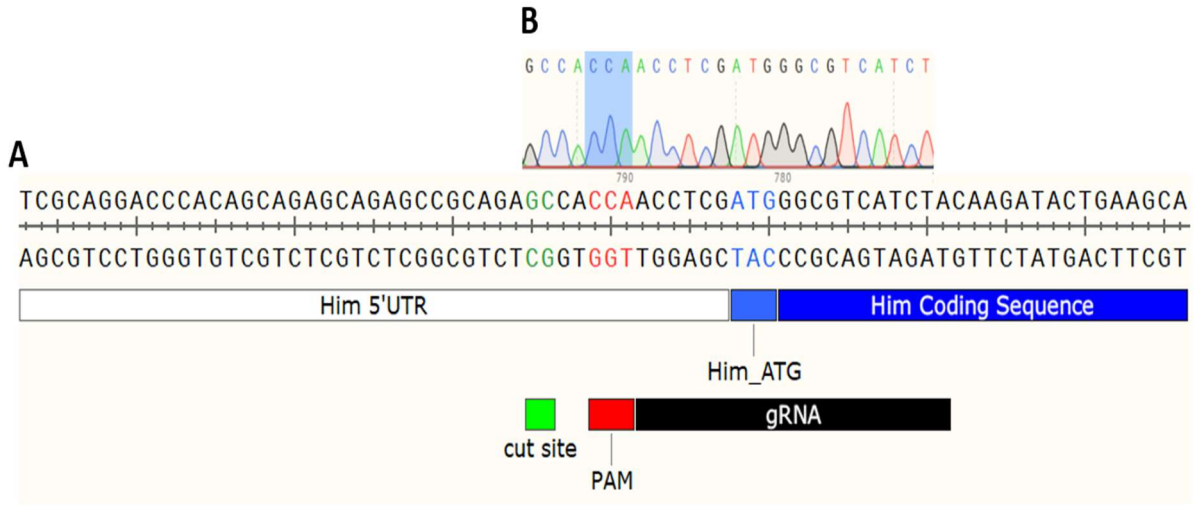

Figure 2.4 – Identification and sequencing of the Him target CRISPR site.

A) The identified PAM (red) and adjacent guideRNA target sequence (black), to result in a Cas9 cleavage at the cut site (green), just upstream of *Him*'s start codon. B) Sanger sequencing of the microinjection strain confirms that the target sequence is conserved with the 'CRISPR optimal target finder' reference genome sequence.

A 20bp gRNA oligo (Table 3) was designed for the sense and anti-sense of the target site, consisting of the identified PAM, as well as the adjacent 17bp of homologous *Him* sequence. To clone the gRNA into pCFD3, the following protocol from 'CRISPR fly design' was followed (www.crisprflydesign.org). The gRNA oligos

were annealed to one another using T4 PNK (NEB, M0201S) in a 10 µl reaction. The reaction was incubated at 37°C for 30 min, followed by 5 min at 95°C. The temperature was then ramped down by 5°C per min, from 95°C to 25°C. Meanwhile, 2 µg pCFD3 was single digested with BbsI. A 15 µl ligation reaction with 1 µl 1:200 dilution of the annealed oligos, 50 ng BbsI digested pCFD3, 1 µl T4 DNA ligase 1.5 µl T4 ligation buffer (NEB) and dH_2O was set up at room temperature for 30 min. DH5α were transformed with 3 µl of the ligation reaction and plated on ampicillin plates. Transformants were identified, the plasmid purified and then sequence verified to ensure the gRNA had cloned in correctly (Figure 2.5).

Figure 2.5 - Cloning and verification of him gRNA into pCFD3.

A) The pCFD3 vector was digested with BbsI to B) facilitate subcloning of the *Him* gRNA oligos (in black). C) Sanger sequencing of the pCFD3 vector across the insert confirms successful integration of the gRNA sequence into the plasmid.

mNeongreen N-terminal Tag Vector Cloning

Homology arms, consisting of DNA homologous to the *Him* locus either side of the double stranded break, were cloned into the N-terminal mNeongreen tagging vector, either side of the insert sequence. The endogenous DNA repair mechanisms use this as a template to repair the Cas9 induced damage, consequently incorporating the desired insert DNA into the genome.

Homology arms that were approximately 1 kb in length, were amplified by PCR from gDNA using primers with compatible overhangs (Table 3), to facilitate Gibson assembly based cloning into the tagging vector either side of the insert DNA sequence (Figure 2.6). The tagging vector was double digested with BsaI and SapI, to generate two vector fragments. 0.02 pmol total digested vector and 0.04 pmol each homology arm were assembled via Gibson Assembly.

The construct was transformed, purified, sequence verified, and sent to BestGene for microinjection alongside the pCFD3 vector *yw*;;*nos-Cas9* transgenic flies. The F1 progeny of the injected embryos were screened by BestGene for transformants expressing PaxCherry, which were subsequently balanced and the Cas9 containing chromosome removed.

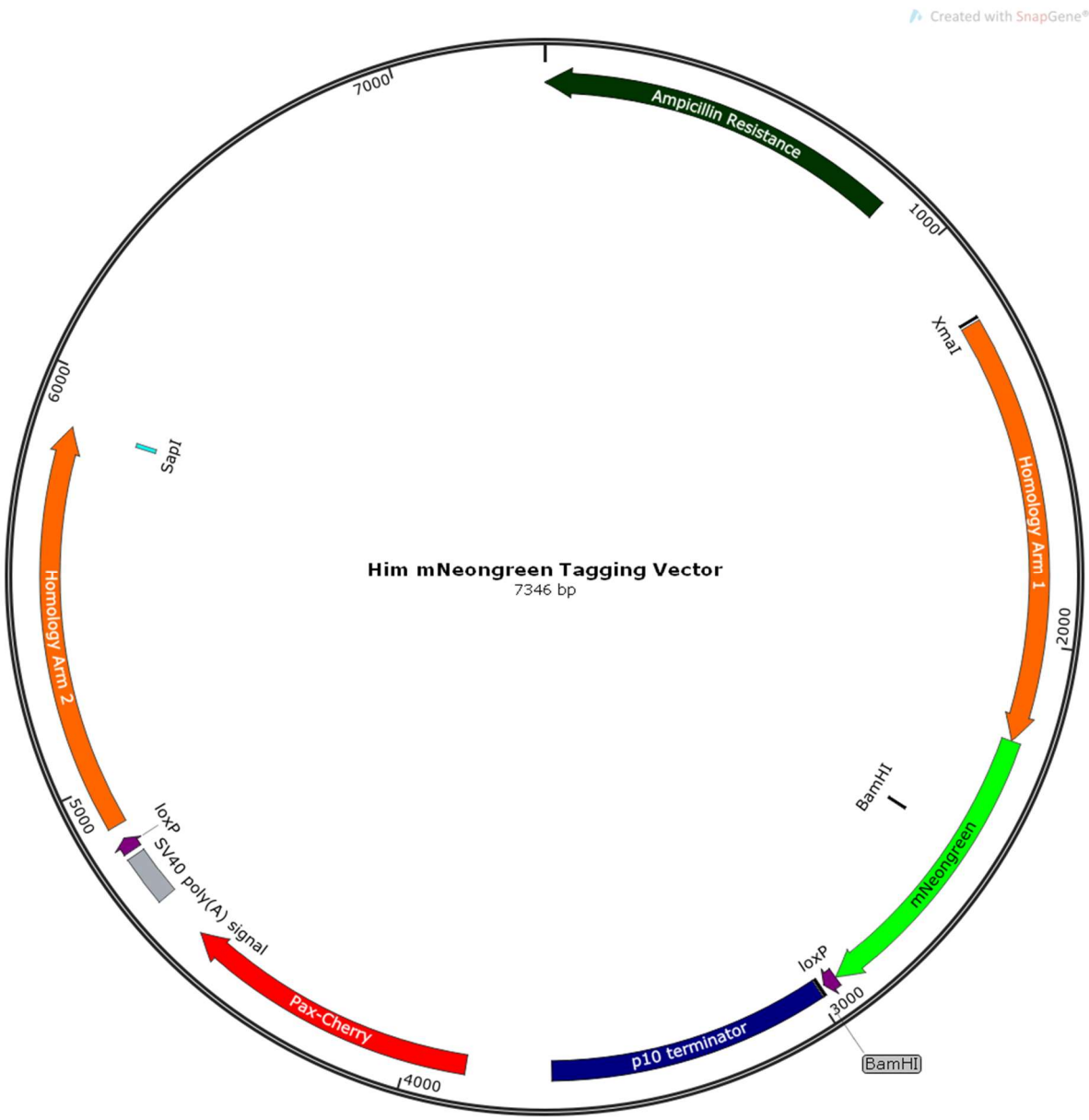

Figure 2.6 – Cloning of Him homology arms into the mNeongreen direct tag vector.
A vector map of the N-terminal mNeongreen *Him* direct tag vector following Gibson Assembly of the digested plasmid and *Him* homology arms. Homology arm 1 consists of ~1kb homologous DNA sequence upstream of the Cas9 cut site at the *Him* locus. Homology arm 2 consists of ~1kb homologous DNA sequence downstream of the Cas9 cut site.

Cre-Recombinase Crossing Scheme

A crossing scheme was designed and implemented to convert the *Him_mNeongreen* null/reporter line into a *Him_mNeongreen* directly tagged allele. This was mediated by a transgenic Cre-Recombinase source, to remove the LoxP flanked sequences between the mNeongreen insertion, and downstream *him* region. The following 3 generation crossing scheme was used to apply Cre-Lox recombination and subsequently remove the Cre-Recombinase transgene. Despite the Cre being under the control of the heat-shock (hs) promoter, I found that performing the crosses at 25 ˚C was sufficient for Cre transgene expression.

Parental *Him_mNeongreen_Null* / *Him_mNeongreen_Null*; + / +; + / + **x** *w[-]* / *Y*; *hs-Cre / CyO; TM2 / TM6*

F1 *Him_mNeongreen_DirectTag* / *Y* ; *hs-Cre* / + **x** *FM7* / *w[-]* ; *Cyo* / *Sco*

F2 *Him_mNeongreen_DirectTag* / *FM7*; *hs-Cre* / *CyO* **x** *FM7* / *Y* ; *hs-Cre* / *Sco*

F3 *Him_mNeongreen_DirectTag* / *FM7*; *CyO* / *Sco* **x** *Him_mNeongreen_DirectTag*/*Y* ; *Cyo* / *Sco*

Final Stock *Him_mNeongreen_DirectTag* ; *Cyo* / *Sco*

To confirm the crossing scheme was successful, flies were screened to check the PaxCherry marker had been excised.

2.7 Yeast2Hybrid

Yeast2Hybrid was used to test whether two proteins of interest were capable of physical interaction.

2.71 Experimental Workflow

The protein fragments to be tested for interaction had their corresponding DNA sequences cloned into either a PB27-LexA (bait) or PP6-Gal4AD (prey) vector. Sequence verified PB27 bait and PP6 prey plasmids were then sequentially transformed into yeast strain L40ΔGal4, using auxotrophic markers to select for positive transformants at each stage. PB27-LexA transformed yeast were grown on

YPD agar, drop-out 1 (-TRP) and drop-out 2 (-LEU/-TRP) for 2-3 days at 30°C. Since PB27-LexA encodes TRP1, successful transformants should grow on drop-out 1 (-TRP), but not on drop-out 2 (-LEU/-TRP). YPD agar acted as a positive control to check the yeast cells survived transformation.

Next, a PB27-LexA positive yeast colony was isolated and transformed with pP6-Gal4-AD and grown on YPD agar, drop-out 1 (-TRP), drop-out 1 (-LEU), drop-out 2 (-LEU/-TRP) and drop-out 3 (-HIS/-LEU/-TRP) for 2-3 days at 30°C. Since PP6 contains a LEU1 auxotrophic marker gene, a double yeast transformant with both the bait and prey plasmids should grow on media lacking both Leucine and Tryptophan. Growth on drop-out 3 indicates a direct physical interaction between the proteins cloned into PB27 and PP6. In the case of a protein-protein interaction, the LexA DNA binding domain and Gal4 activation domain are reconstituted into an acting transcription factor, which drives expression of a LexaOP_His3 auxotrophic reporter gene, allowing the yeast to grow on media lacking Histidine. Yeast growth was imaged using the camera of a Samsung Galaxy S21 mobile phone.

2.72 Y2H Reagents

YPD plates – 35 g YPD agar powder (Formedium, CCM0105) was suspended in 500 ml dH_2O and autoclaved at 121°C for 15 min before pouring into 90 mm petri dishes (Sarstedt, 82.1473) in a laminar flow hood. Media was allowed to set for 20 min and stored in the refrigerator at 4°C.

Drop-out Plates – 6.9 g yeast nitrogen base (Formedium, CYN0401), 20 g agar and either 740 mg drop-out 1 -TRP (Formedium, DCS0141), 590 mg drop-out 1 -LEU (Formedium, DCS0091), 1546 mg drop-out 2 -TRP/-LEU (Formedium, DSCK172) or 1470 mg drop-out 3 -TRP/-LEU/-HIS (Formedium, DSCK424) were suspended in 1 L dH_2O and then autoclaved. Once cool enough to touch, filter sterilized 60% w/v glucose solution (Formedium, GLU02) was added to give a final concentration of 2% w/v glucose. Plates were poured in a laminar flow hood and stored at 4°C.

YPAD Broth – 50 g YPAD powder (Formedium, CCM1002) was suspended in 1 L dH_2O and autoclaved. YPAD broth was stored at 4°C for up to 1 month.

1 M Lithium Acetate (LiOAc) – 5.1 g LiOAc (Sigma, L4158-100G) was dissolved in 50 ml dH_2O and pH adjusted to pH 7.5 using glacial acetic acid (Sigma, A623-100ml). The solution was autoclaved and stored at room temperature.

Polyethylene Glycol (PEG) 3350, 50% w/v – 50 g PEG 3350 (Sigma, 2022444-250G) was dissolved in 30 ml dH_2O on a hot plate with magnetic stirrer. Once dissolved, the volume was made up to 100 ml with dH_2O. The solution was autoclaved and stored at room temperature.

LA solution (10 ml) – 1 ml 1M LiOAc, 1 ml 10x TE (100 mM tris, 10 mM EDTA) pH7.6 (Fisher, BP2475-100 ml) and 8 ml dH_2O was mixed by vortexing, then filter sterilized and stored at room temperature.

LAP solution (30 ml) – 3 ml 10x TE, 24 ml 50% PEG 3350 and 3 ml 1 M LiOAc was mixed by vortexing, filter sterilized and stored at room temperature.

5x TE/LA solution – 1 ml of 10x TE and 1 ml LiOAc was mixed by vortexing, filter sterilized and stored at room temperature.

Glassware – 250 ml glass flasks were thoroughly washed by submerging in 5% v/v DECON 90 in dH_2O for 2 min. DECON was removed by rinsing the flasks 5x with tap water, followed by 3 rinses with dH_2O. 100 ml dH_2O was added to the flask and autoclaved.

2.73 Cloning into bait and prey plasmids

Bait and prey fragments were cloned into the MCS of pB27-LexA and pP6-Gal4-AD (Hybrigenics) respectively, resulting in a LexA-Bait or Gal4_AD-prey fusion construct. pB27-LexA contains tetracycline resistance, and pP6-Gal4-AD ampicillin resistance, for selection of bacterial transformants. The following constructs were made:

- Mef2[1-350]-pB27-LexA
- Mef2[1-156]-pB27-LexA
- Him[1-192]-pP6-Gal4-AD
- Su(var)2-10[1-601]-pP6-Gal4-AD

Mef2[1-350]-pB27-LexA was cloned by Hybrigenics for an original library screen (Michael Taylor, unpublished). The Mef2[1-156]-pB27-LexA fragment was generated by PCR using Mef2[1-350]-pB27-LexA as a template. The primer sequences contained EcoRI and NotI overhangs to facilitate ligation into double digested pB27-LexA. In some cases, a 2-nt spacer was incorporated into the primer to ensure the cloned fragment remained in-frame with the Gal4-AD or LexA sequence (Table 3).

The full-length fragment for Him[1-192]-pP6-Gal4-AD was PCR amplified from a Him cDNA in pBluescript II KS (Liotta *et al.* 2007) with BamHI and XbaI overhangs for ligation into pP6-Gal4-AD.

The full-length fragment for Su(var)2-10[1-601]-pP6-Gal4-AD was PCR amplified from RE73180 (DGRC) with BamHI and XbaI overhangs for ligation into pP6-Gal4-AD. All constructs were sequenced to verify the correct insert was present.

2.74 Yeast transformation protocol

Yeast strain L40ΔGal4 (gift from Hybrigenics) was revived from a 30% glycerol stock stored at -80°C, by streaking onto YPD agar with an inoculation loop, and grown at 30°C for 3 days. A single colony was transferred to 10ml of YPAD broth and incubated for 16 hr overnight at 200 rpm at 30°C. OD600 was measured using a spectrophotometer, to calculate yeast cell concentration. Yeast were diluted to $2.5x10^6$ cells/ml in a total volume of 50 ml YPAD within a sterile glass flask. The subculture was incubated at 30°C/200 rpm for a further 4 hr. Final yeast cell concentration was then calculated by measuring OD600 as previously.

Yeast cells were pelted by centrifugation at 2500 g for 5 min. The YPAD was discarded, and the pellet washed twice with 1X TE (1 ml 10x TE diluted in 9 ml dH_2O). Cells were resuspended in LA to a concentration of $2x10^9$ cells/ml. For each transformation, the following solution was prepared in a 2 ml Eppendorf, by adding in order:

- 200 µl yeast cells in LA ($2x10^9$ cells/ml).
- 20 µl 10 mg/ml salmon sperm DNA (Invitrogen, 15632-011).
- 4 µl 5x TE/LA.
- 2.2 µg of bait or prey plasmid DNA.

- 1.2 ml LAP.

Negative control mock transformations were run for each experiment, by omitting the plasmid DNA from the transformation solution. The transformation solution was mixed by inverting the Eppendorf multiple times, and then incubated at 30°C and 150 rpm in a shaker for 30 min. 140 µl DMSO (Sigma, D8418-50ml) was added to each tube, and incubated at 42°C for 15 min to heat-shock the yeast and facilitate transformation. Immediately afterwards, the tubes were incubated on ice for 2 min. Yeast cells were pelleted via centrifugation 10,000 rpm for 30 sec. The transformation solution was removed, and the pellet resuspended in 200 µl 1x TE. 50 µl cells were spread per plate using a sterile glass rod, which were incubated at 30° C for 2-3 days.

2.8 Data Analysis

2.81 Statistical Analysis

R software (R Core Team 2021) was used for statistical analysis. For normally distributed, continuous data, ANOVA was used to test for differences between multiple groups, with a Post-hoc Tukey HSD to determine where differences lie. For non-normally distributed or ordinal data, the Kruskal-Wallis test was used for multiple group comparisons, followed by a post-hoc Dunn's test.

2.82 Graph generation

MATLAB software was used for the generation of graphs. The sigstar plug-in was used to add asterisks to plots, to denote significant differences (https://github.com/raacampbell/sigstar).

Chapter 3 – Mef2 overexpression induces premature muscle fibre formation

3.1 Introduction

The wing imaginal disc is home to the adult muscle progenitors (AMPs) that give rise to the indirect flight muscles (IFMs) and direct flight muscles (DFMs) during pupation (Sudarsan *et al.* 2001; Bernard *et al.* 2009). This process is dependent on the pro-myogenic activity of the transcription factor Mef2, which is known to regulate gene expression throughout *Drosophila* adult muscle development (Bryantsev *et al.* 2012; Soler *et al.* 2012). Indeed, knockdown of *Mef2* in AMPs, using *1151Gal4* driven *Mef2*-RNAi, has drastic consequences for the development of the adult musculature, including the DLMs, DVMs, TDT and leg muscles (Soler and Taylor, 2012).

Mef2 is expressed in the AMP population, but its transcription factor activity at this stage is restrained, as it co-exists with its characterized repressors: Him and Zfh1 (Soler and Taylor 2009; Siles *et al.* 2019). Overexpression of a *Mef2* construct within the AMPs allows it to overcome its repression and trigger premature activation of a MhcGFP reporter construct, a Mef2 regulated marker of terminal muscle differentiation not usually upregulated until 30 hr after pupal formation (APF) (Soler and Taylor, 2009; Spletter *et al.* 2018).

Since Mef2's initial characterization in the wing imaginal disc AMPs (Ranganayakulu *et al.* 1995; Baker *et al.* 2005; Soler and Taylor 2009), our understanding of this cell type has dramatically increased, and we now know that several distinct clusters of AMPs exist across a spectrum of differentiation states (Gunage *et al.* 2014; Zappia *et al.* 2020). Here, I describe the Mef2 protein expression pattern throughout the late L3 wing imaginal disc AMP population using a CRISPR directly tag Mef2GFP transgene (Hubbert 2023), at much higher resolution than previous work. I also further characterize the Mef2 overexpression phenotype to demonstrate that not only is premature reporter gene activation observed, but actual muscle fibre differentiation is occurring precociously. I describe a system based on this result that allows Mef2 activity level to be quantified. This allows the impact of regulators of Mef2 activity to be determined, as well as the functional consequences of point mutations to important, conserved regions of the Mef2 protein to be assayed, discussed in later chapters.

3.2 Mef2 is expressed prior to the onset of adult muscle development

Mef2 protein has typically been visualized in the wing imaginal disc AMPs through the use of a Mef2 primary antibody in an immunofluorescence-based approach (Cripps *et al.* 1998; Soler and Taylor 2009; Zappia and Frolov 2016). Recently, a C-terminal directly tagged *Mef2GFP* CRISPR construct was generated in-house by homology directed repair (Hubbert 2023). To determine if directly tagged Mef2 protein can be detected without antibody staining, wandering L3 larval imaginal discs, and bisected adult thoraces were mounted directly in Schneider's insect medium and imaged live without fixation. Mef2GFP positive cells were detected in both the larval wing imaginal disc, and the differentiated DLM nuclei (Figure 3.1). This allele is therefore compatible with live imaging-based approaches.

To further characterize Mef2 protein expression in the wing imaginal disc, late L3 Mef2GFP larval discs were stained with both anti-GFP, and anti-Cut (Ct), a canonical marker for the entire AMP population (Sudarsen *et al.* 2001; Zappia *et al.* 2020). Mef2GFP and Ct were expressed in an entirely overlapping pattern across the AMPs, confirming that Mef2GFP is ubiquitous throughout this population of cells.

The AMPs can be subdivided into two populations: those progenitors that will give rise to the DFMs, and those the IFMs. The DFM progenitors reside close to the presumptive wing hinge, and the IFM progenitors atop the presumptive notum. DFM progenitors are also known to express a higher level of Ct than IFM progenitors (Sudarsen *et al.* 2001). In agreement with this, I observed the highest level of cut staining in the DFM progenitors (Figure 3.2A). Conversely, Mef2GFP staining intensity appears relatively uniform throughout both AMP sub-types (Figure 3.2B).

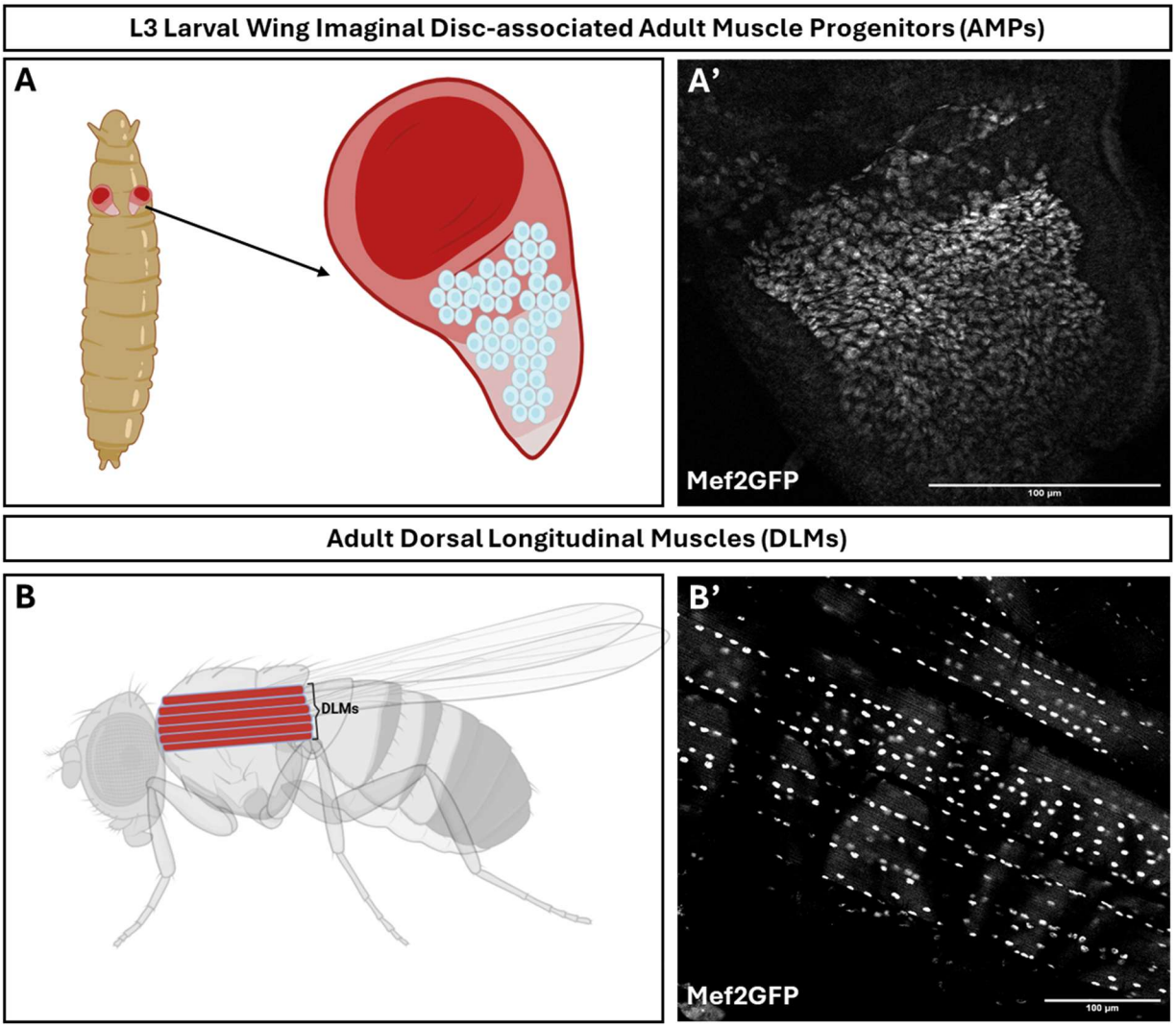

Figure 3.1 – CRISPR directly tagged Mef2-GFP live in the wing imaginal disc and DLMs

(A) Schematic of the larval wing imaginal disc (red) with the associated adult muscle progenitors (cyan). (A') These cells can be visualized live and unfixed using the Mef2GFP CRISPR knock-in. Image shows a single confocal Z-slice of a late 3rd instar wing imaginal disc (n=10 discs).

(B) Schematic showing the positioning of the dorsal longitudinal muscles (DLMs) in the adult fly thorax, which develop from wing disc-associated muscle progenitors. (B') Maximum intensity projection of live Mef2GFP in a sagittal cross-section of the adult thorax, which shows strong expression of the protein (n=8 hemithoraces).

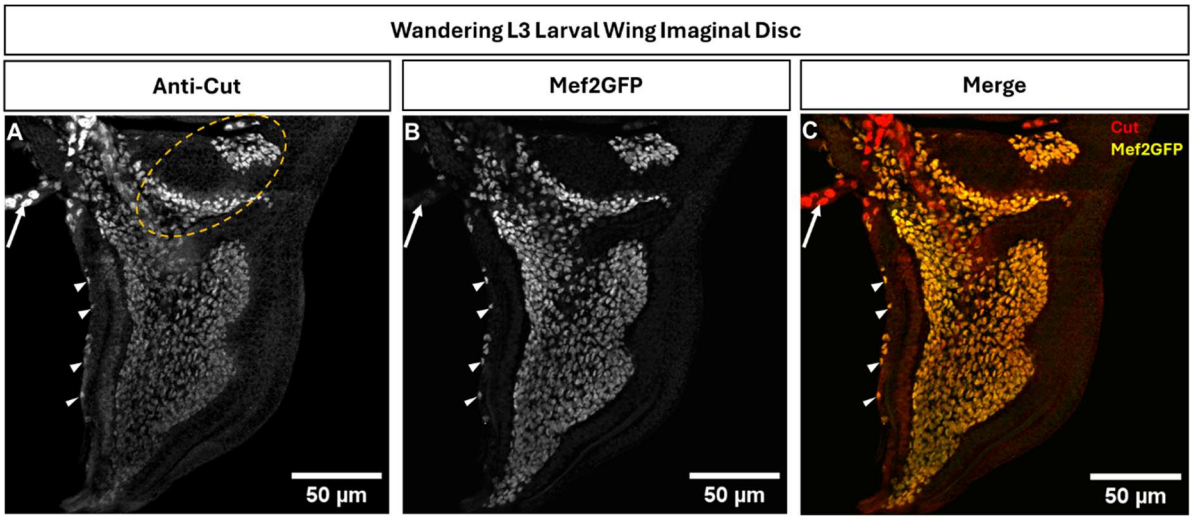

Figure 3.2 – Mef2GFP co-localizes with the canonical AMP marker Cut in the late 3rd instar larval wing imaginal disc

Representative maximum intensity projections of confocally imaged Mef2GFP expressing wing imaginal discs (n=7 discs) showing A) anti-Cut, B) anti-GFP, and C) a merge of both channels. Mef2GFP and Cut co-localize across the entire AMP population, as well as in the tracheoblasts (white arrowheads). Differentiated trachea nuclei are Cut positive but are not labelled by Mef2GFP (white arrow). DFM progenitors (orange dashed oval) express a relatively high level of Cut compared to IFM progenitors.

Cut is also known to label tracheoblasts associated with the spiracular branches of the wing imaginal disc tracheal network (Pitsouli and Perrimon 2010). Interestingly, Mef2GFP can also be detected alongside Cut in this cell type (Figure 3.2B), a novel finding suggesting that Mef2 could have a role in the developing adult tracheal system. Cut also labels differentiated trachea nuclei, which is not the case with Mef2GFP (Figure 3.2A).

A second method to visualize the wing disc AMP population is to co-stain for Mef2GFP alongside Fascilin 3 (Fas3), a well-characterized marker of the wing disc epithelium (Bate and Martinez Arias 1991). Sc-RNAseq data shows that *Fas3* is expressed in every compartment of the disc, except from the AMPs (Zappia *et al.* 2020). Consistent with this, Mef2GFP and Fas3 did not overlap in their expression in late L3 antibody stained wing imaginal discs (Figure 3.3). The ortho-slice merge neatly demonstrates the multi-layered AMP population positioned atop the basal surface of the wing disc epithelium.

These data demonstrate that robust Mef2GFP protein expression is detectable throughout the entire late L3 AMP population, prior to the onset of adult muscle development. Therefore, Mef2 can be used as a reliable marker for the AMPs, since its expression pattern closely mimics that of the well-defined marker Cut. Unlike Cut, which is more highly expressed in DFM than DLM progenitors, Mef2GFP expression appears to be more consistent throughout the entire AMP population.

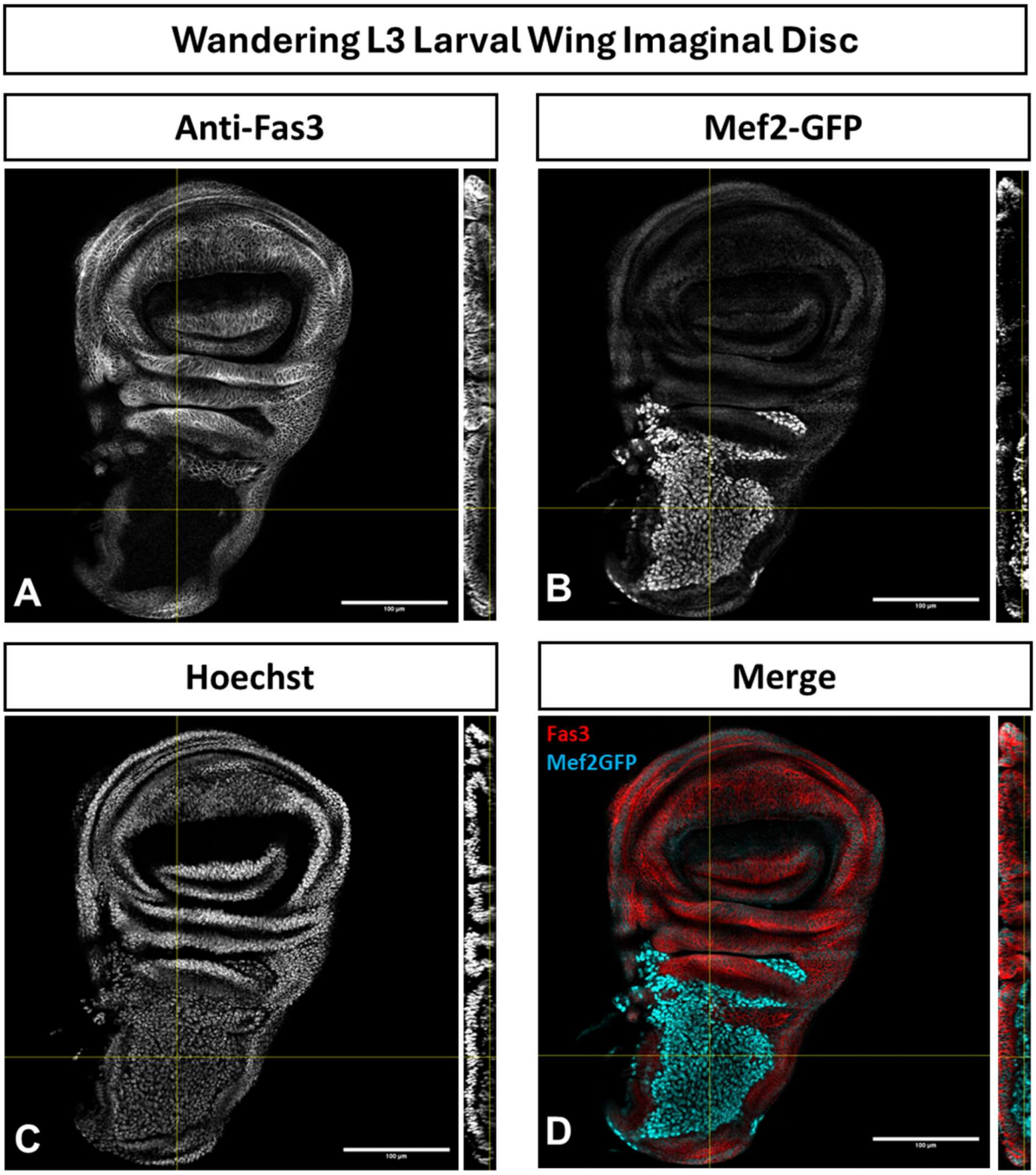

Figure 3.3 – Mef2GFP and Fas3 label distinct cells of the late third instar wing imaginal disc

Single confocal slices with orthogonal views of representative late third instar larval wing imaginal discs of the Mef2GFP line labelled with A) anti-Fas3, B) anti-GFP and C) Hoechst. In D) Fas3 (red) and Mef2GFP (cyan) channels are merged, demonstrating that the Mef2GFP positive AMPs sit in a multi-stratified arrangement atop the Fas3+ wing disc epithelium (n=8 discs).

3.3 Mef2 overexpression in AMPs can induce premature reporter gene expression

I generated a *UAS-Mef2* landing site construct which was inserted into multiple well characterized AttP landing sites using PhiC31-mediated recombination (Bischof *et al.* 2007). These lines consist of *Mef2* isoform III (Flybase nomenclature – RC, introduction Figure 1.6) under UAS control, containing the same cDNA sequence as a previously published overexpression line termed *UAS-Mef2-III-low* (Gunthorpe *et al.* 1999). Fly lines were generated with the construct inserted into AttP18 (chromosome X), AttP40 (chromosome II) and AttP2 landing sites (chromosome III), to facilitate making combination stocks with other transgenes on other chromosomes. The use of AttP sites negates genomic position effect, a drawback to the P-element transgenesis technology that existed at the time when the original *UAS-Mef2* line was made.

UAS-Mef2-III-low has previously been shown to induce premature Mhc-TauGFP reporter expression in L3 larvae, when overexpressed in the wing imaginal disc using the *1151Gal4* driver (Soler and Taylor 2009). This Gal4 driver is active in the wing imaginal disc-associated AMPs and developing muscles until about 40hr APF (Anant *et al.* 1998; Schönbauer *et al.* 2011). *Mhc* has three-Mef2 binding motifs in its promoter sequence, and its expression is known to be directly regulated by Mef2 (Hess *et al.* 2007). Since Mhc is a marker of terminal muscle differentiation, representing a core component of the sarcomere, it is not expected to be expressed in muscle progenitors prior to their differentiation. Indeed, a flight muscle transcriptomics dataset suggests that *Mhc* expression is upregulated from 30hr APF, after myoblast fusion is complete and sarcomeres begin to self-organize (Spletter *et al.* 2018).

My new *UAS-Mef2-AttP2* stock can also trigger premature expression of Mhc-TauGFP when driven by *1151Gal4* at 25°C, in 100% discs imaged (n=10 discs). This demonstrates that the updated stock retains the capacity to trigger reporter gene activation, despite the different genomic landing site of the transgene (Figure 3.4). Since the tauGFP is a reporter expressed under the control of Mhc's promoter sequence, conclusions cannot be drawn about the localization of Mhc protein itself in this assay. Premature MhcTauGFP expression is not observed in any of the wing imaginal discs imaged from *1151Gal4;;MhcTauGFP* control flies (n=10).

This experiment demonstrates that Mef2 overexpression can trigger target gene activation in AMPs, yet in wild-type discs it does not, despite the fact that robust Mef2 protein expression can be detected at this stage (Figure 3.3B). This suggests that at this step of development, endogenous Mef2 activity is not high enough to trigger significant gene expression.

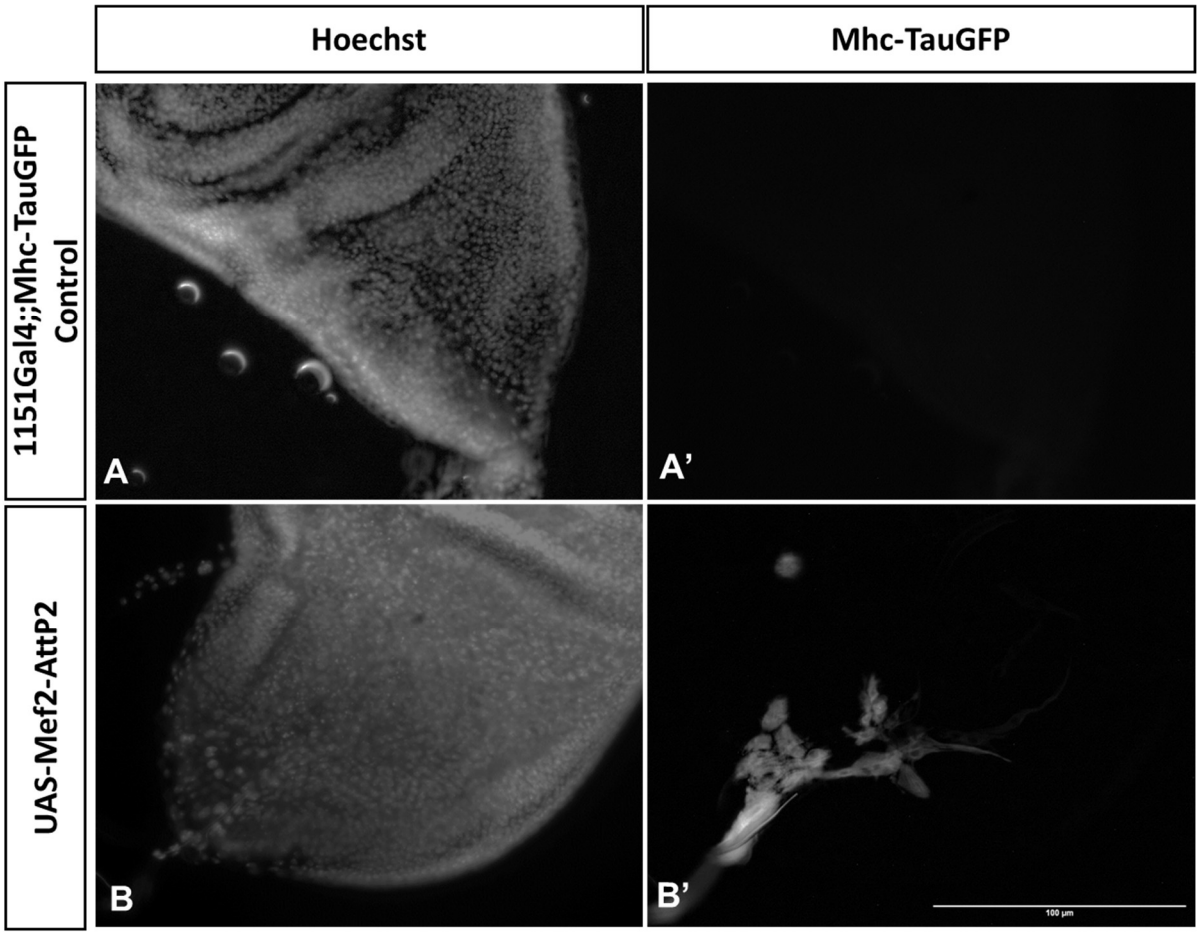

Figure 3.4 – Mef2 overexpression in the wing imaginal disc can induce premature Mhc-TauGFP reporter expression

A') Representative fluorescent microscopy image of a *1151Gal4;;Mhc-TauGFP* control larval wing imaginal disc demonstrating an absence of Mhc-TauGFP reporter expression B') *1151Gal4;;Mhc-TauGFP* driven overexpression of *UAS-Mef2-AttP2* at 25◦C induces activation of the Mhc-TauGFP reporter. Hoechst counterstaining allows visualization of the morphology of A) the control disc and B) the Mef2 overexpression disc. (n=10 discs per genotype).

3.4 Mef2 overexpression in AMPs can induce premature muscle differentiation

In order to determine whether Mef2 overexpression induced premature Mhc-TauGFP expression is simply a case of reporter gene activation in AMPs, or whether precocious muscle fibre differentiation is occurring, I tested to see if expression of a panel of differentiated muscle markers were induced in an organized, sarcomeric pattern.

Mef2 overexpression in the wing imaginal disc caused premature activation of an fTRG-MhcGFP transgene. This construct consists of an N-terminal GFP tag of Mhc protein (isoforms K,L,M), in addition to several kb of upstream and downstream regulatory sequences (Sarov *et al.* 2016). Thus, unlike the Mhc-TauGFP reporter, Mhc-GFP is a directly tagged protein. *1151Gal4;;MhcGFP* driven *UAS-Mef2-AttP2* at 25◦C induces premature expression of fTRG-MhcGFP in 100% discs imaged (n=46 discs). This was not seen in any *1151Gal4;;MhcGFP* control discs (n=23) (Figure 3.5). It is important to note that the wing imaginal disc is attached to the leg and haltere imaginal discs by differentiated muscle (Dambly-Chaudière *et al.* 1986), sometimes observed on the posterior region of the disc hinge in dissected discs. This was omitted from analyses based on its localization, which is distinct from that observed in prematurely differentiating AMPs on the disc's notum.

Premature MhcGFP was typically expressed in a striated pattern that resembles an array of sarcomeres, suggesting the differentiation of precocious myofibres in the imaginal disc, rather than just upregulation and translation of a Mef2-responsive gene. Since the minigene contains *Mhc*'s upstream and downstream regulatory sequences, it likely recapitulates the localization of endogenous Mhc protein in the thick filament of the sarcomere (Sarov *et al.* 2016).

Other sarcomeric markers including Sallimus (Sls), the *Drosophila* homolog of Titin, and actin, were also expressed in the prematurely differentiated myofibres (Figure 3.6). Although Sls is an extremely large protein that stretches a considerable length along the sarcomere, the antibody used (Kig16) recognizes an antigen near where it anchors the Z-disc. Consequently, MhcGFP and Sls can be observed as alternating stripes in the premature myofibres, since they label different components of the sarcomere (Figure 3.6E). Expression of actin, the major thin filament protein, overlaps with MhcGFP and Sls. Since phalloidin labels all F-actin variants, it is not

possible from this experiment to determine which particular actin protein is upregulated in response to Mef2 overexpression.

These data demonstrate that not only can Mef2 overexpression induce premature muscle gene activation, but organized myofibres precociously differentiate in the wing imaginal disc. Markers for several distinct sarcomeric components can be detected with striated patterning, resemblant of their arrangement in differentiated muscle fibres such as the DLMs. This highlights how significant the role of Mef2 is in the development of AMP into adult muscle, since overexpression of this factor alone is sufficient to induce the expression of all the genes required to form organized myofibre-like structures from muscle progenitors.

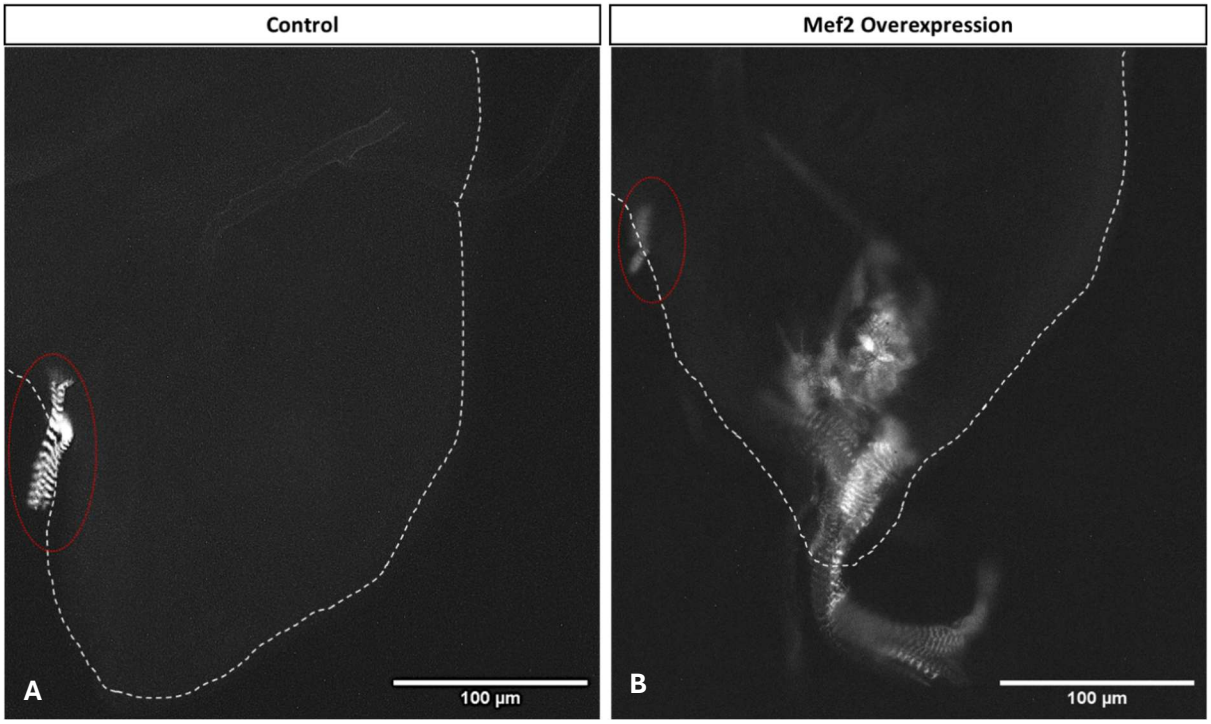

Figure 3.5 - Mef2 overexpression in the wing imaginal disc can induce premature expression of MhcGFP in a striated pattern

A) A representative fluorescent microscopy image of a *1151Gal;;MhcGFP* control larval wing imaginal disc demonstrating an absence of MhcGFP minigene expression in the wing disc notum (n=23 discs). Differentiated muscle can occasionally be detected on the periphery of the wing imaginal disc (red circle). This serves as an attachment point for the haltere and T3 leg imaginal discs which exist as a complex. B) *1151Gal4;;MhcGFP* driven overexpression of *UAS-Mef2-AttP2* at 25°C induces premature MhcGFP minigene expression in a striated pattern in the notum of the wing disc (n=46 discs). Imaginal disc outlines are sketched with a white dashed line.

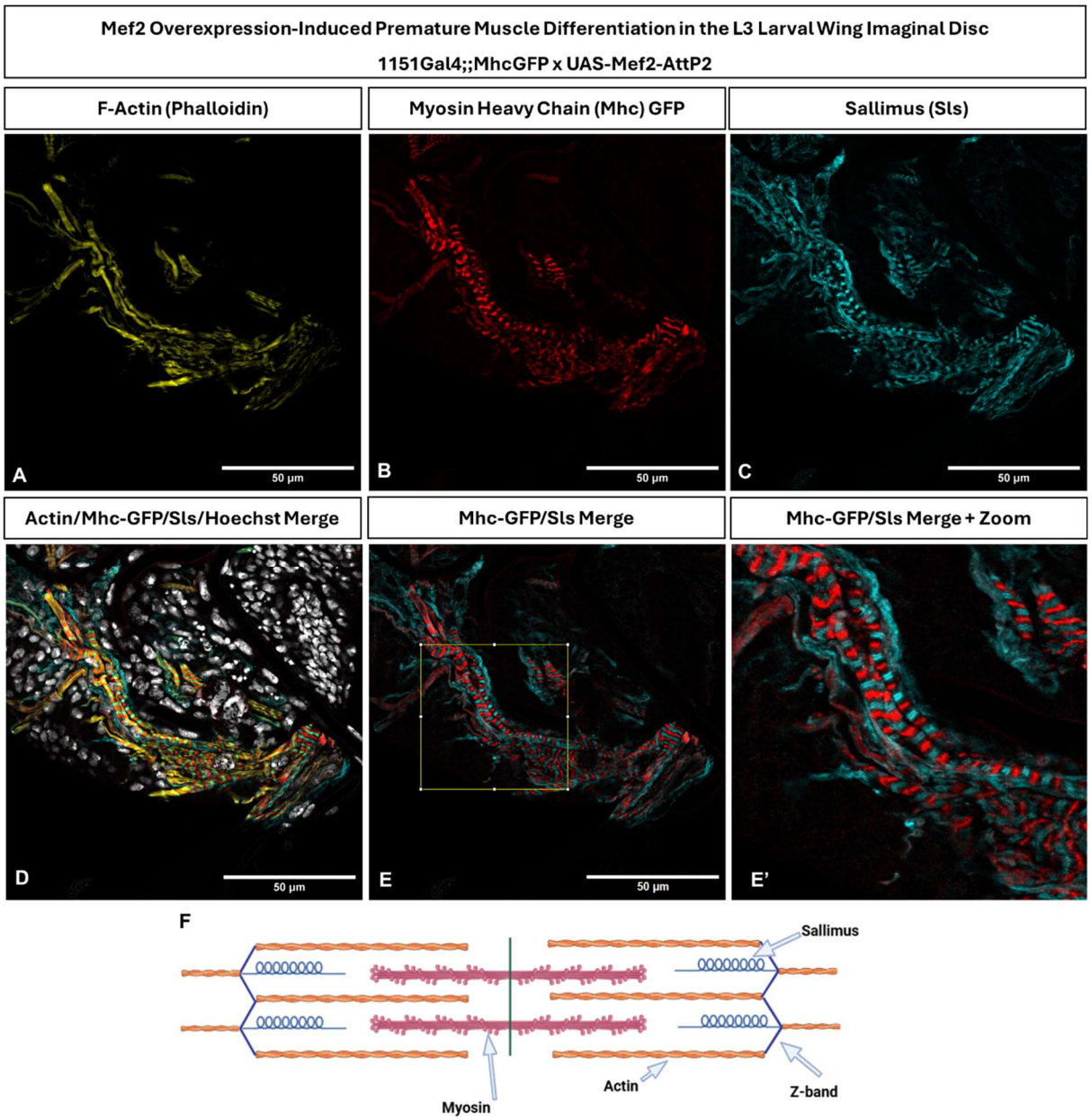

Figure 3.6 – Premature myofibres express a panel of sarcomeric proteins

Single confocal slice of *1151Gal4;;MhcGFP* driven Mef2 overexpression in the third instar larval wing imaginal disc. Single channel images of (A) F-Actin phalloidin staining (yellow), (B) anti-GFP labelling of MhcGFP (red), (C) Anti-Sls (cyan) and (D) a multi-channel merge including Hoechst nuclear label (grey). (E-E') Alternating striations are evident with staining for Mhc and Sls, which label distinct components of the sarcomere in differentiated muscle. (F) A schematic of a sarcomere showing the myosin thick filament, actin thin filament and Z-band, which defines the boundary between sarcomeres (n=6 discs).

3.5 Mef2 overexpression induced premature myofibres are multinucleated, localize to the dorsal notum and are closely associated with the tracheal network

To explore whether premature myofibres are multinucleated, and thus arise from fusion of multiple AMPs, the *1151Gal;;MhcGFP* driver was used in combination with *UAS-mCherryCD8;UAS-Mef2-AttP2* at 25°C. mCherryCD8 localizes to the cell membrane, to allow the boundaries of premature myofibres to be distinguished. Late L3 wing discs were co-stained with anti-GFP and anti-RFP to enhance the MhcGFP and *UAS-mCherryCD8* signal respectively. High resolution confocal imaging of these discs demonstrate that multiple nuclei are indeed associated with a single myofibre, suggesting that myoblast fusion is part of the induced precocious differentiation (Figure 3.7).

Premature MhcGFP is largely localized to the dorsal end of the notal region of the wing imaginal disc (Figure 3.8), despite *1151Gal4* driving *UAS-Mef2* expression throughout the AMP population, which spans the entire notum. This suggests that a subset of AMPs is more prone to differentiate in response to Mef2 activity, otherwise the MhcGFP pattern observed would be more uniform throughout the notum.

The premature myofibres are usually seen in close proximity to the disc associated tracheal branch (Figure 3.7F, Figure 3.8), which enters the wing imaginal disc at the dorsal notum where the highest concentration of MhcGFP is typically observed. Whether this is because the trachea is acting as a scaffold for the myofibres to attach to and grow from, or because the oxygen supply provided by the trachea is a requirement for muscle differentiation, is impossible to distinguish from these experiments. It is also plausible that pro-myogenic signals arise from the trachea which are required for this premature myogenesis to occur. Or that the premature muscle formation is influenced by the same signaling that dictated the original patterning of the trachea, causing them to occupy the same space.

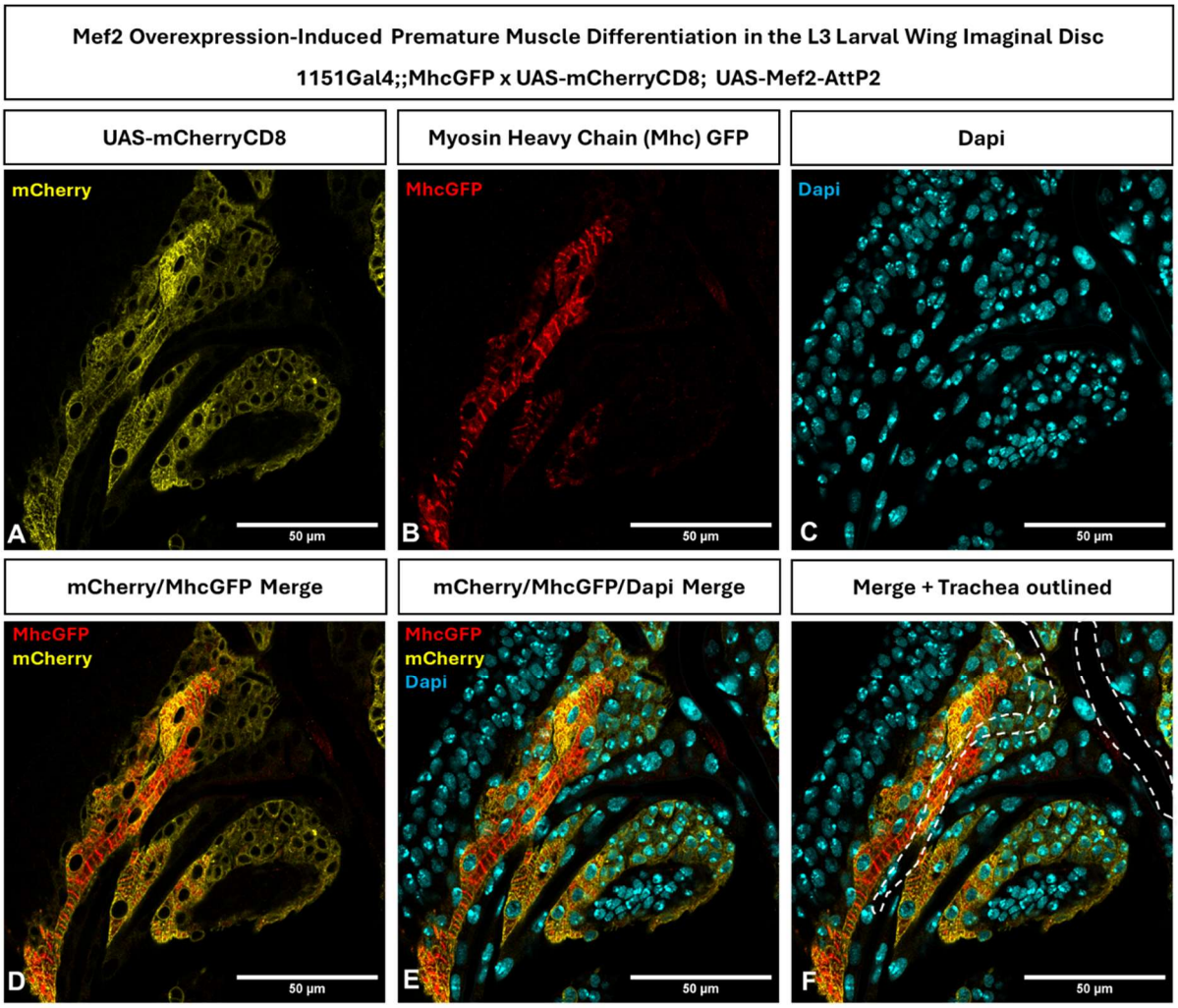

Figure 3.7 – Premature myofibres are multinucleated, and closely associate with the wing disc tracheal network.

A high resolution 63x confocal image of *1151Gal4;;MhcGFP* driven *UAS-mcherryCD8;UAS-Mef2-AttP2* induced premature differentiation in the dorsal wing imaginal disc. This is a single Z-slice of 0.5 µm thickness, showing multiple nuclei associated with the same myofibre. Single channel images for A) mCherryCD8 (yellow), (B) MhcGFP (red) and (C) DAPI. D) MhcGFP (red) and mCherryCD8 (yellow) merge shows the outlines of multiple nuclei associated with a single bundle of myofibres. E) MhcGFP (red), mCherryCD8 (yellow) and DAPI (cyan) merge. F) The trachea is outlined with a white dashed line to show the close association of the myofibre with the trachea. (n=5 discs).

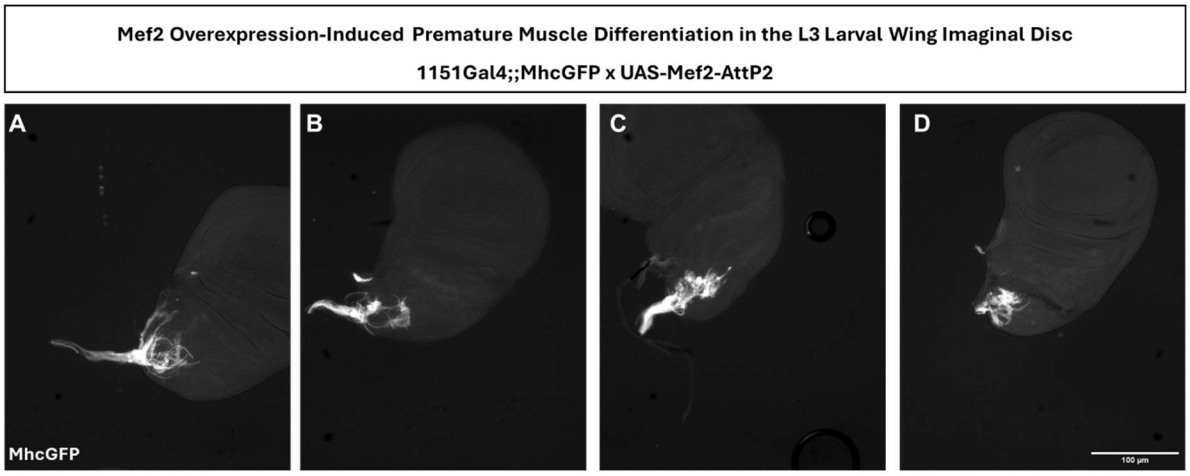

Figure 3.8 -Mef2 overexpression induced premature differentiation in the late L3 wing imaginal disc is localized to the dorsal notum.

(A-D) Representative low resolution fluorescent microscopy images of wing imaginal discs to show the dorsal localization of Mef2 overexpression induced premature MhcGFP expression. (n=19 discs).

3.6 AMPs undergo morphological changes with Mef2 overexpression

B3-Tubulin is a marker that can be used to label wing imaginal disc-associated AMPs (Boukhatmi and Bray, 2018). A *B3-Tubulin:GFP* minigene in control discs uniformly labels the AMP population. B3-Tubulin localization appears largely cytoplasmic, giving an indication of the shape of the cell (Figure 3.9A). When Mef2 is overexpressed with *1151Gal4* at 25◦C, AMPs undergo changes in cell shape which can be visualized using the B3-Tubulin:GFP minigene (Figure 3.9B). Many cells appear elongated, extending lengthy projections which are not observed with B3-tubulin:GFP in control discs.

This phenotype is also observed with Mhc antibody staining, which seemingly provides a more sensitive readout for total Mhc protein than the isoform K,L,M specific MhcGFP minigene. The minigene, even in combination with anti-GFP staining, seems to label only sarcomeric structures associated with precocious myofibres (Figure 3.6B), whereas the Mhc antibody seems to also label individual cells when Mef2 is overexpressed (Figure 3.9B'). Whilst sarcomeres can be

observed with the Mhc antibody in some regions of the disc, elsewhere the expression pattern overlaps broadly with B3-Tubulin:GFP. Control discs express only a very low level of Mhc protein throughout the structure, with a higher level observed within tracheal cell nuclei (Figure 3.9A').

These results demonstrate that Mef2 overexpression induces phenotypes in addition to precocious myofibre differentiation. As discussed previously, these myofibres largely localize to the dorsal region of the imaginal disc. B3-Tubulin:GFP and Mhc antibody staining show that other subsets of AMPs, including those located ventrally, appear to have undergone morphological changes, which plausibly represents an intermediate step in their differentiation.

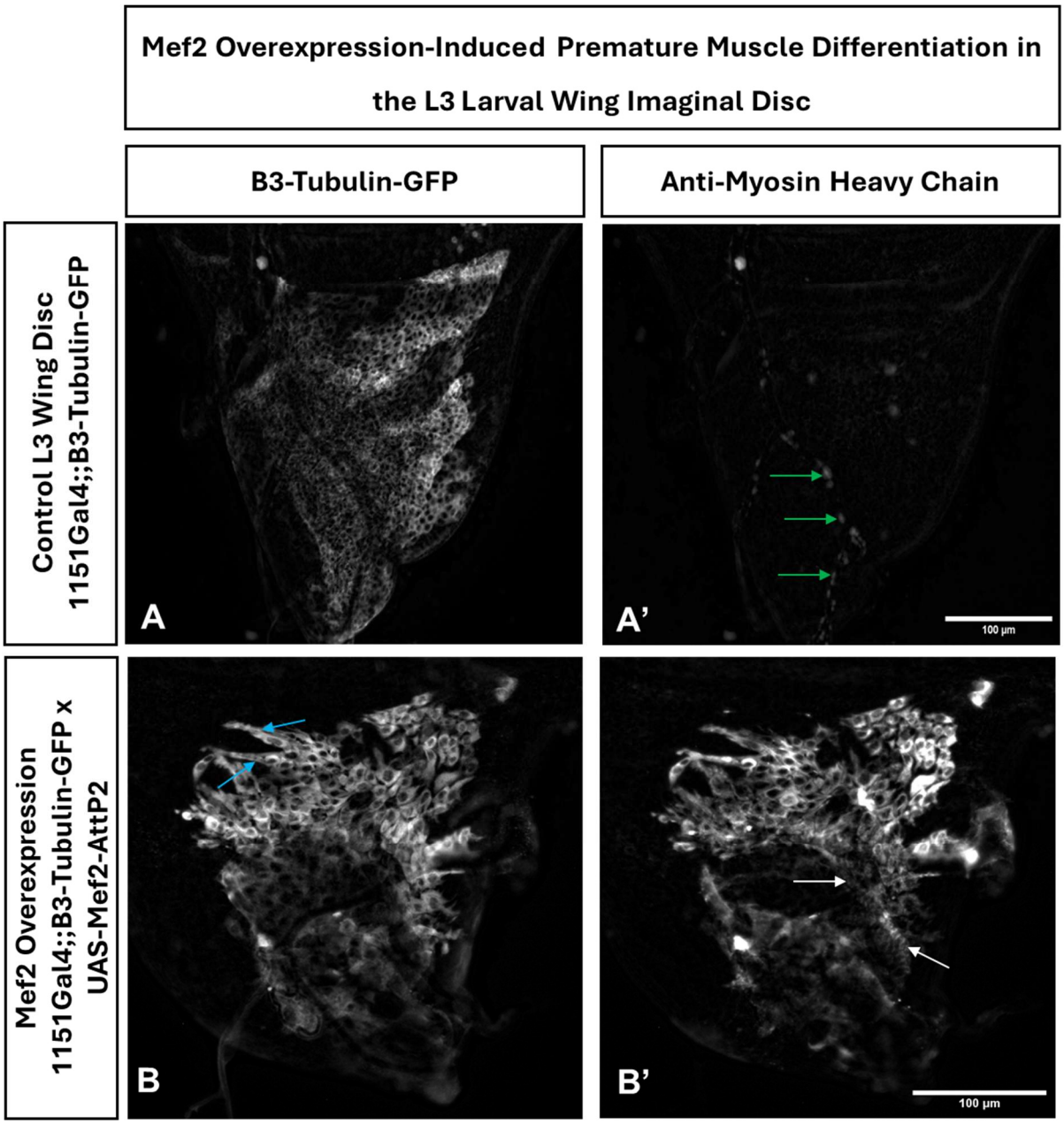

Figure 3.9 AMPs undergo morphological changes in response to Mef2 overexpression

(A) B3-Tubulin:GFP anti-GFP staining labels the AMP population in control wing imaginal discs. (A') Anti-Mhc staining (red) does not label the AMPs in the control sample, but a low level of signal is detected in tracheal cells (green arrows). (B) With Mef2 overexpression, B3-Tubulin:GFP reveals changes in cellular morphology, with large cellular projections visible (blue arrows) that are not seen in control AMPs. (B') Mef2 overexpression causes a significant upregulation of Mhc protein which now labels the AMP population. Precocious muscle fibre striations are visible (white arrows). (n=6-8 discs per genotype).

3.7 MhcGFP can be used as a readout to quantify Mef2 activity

To demonstrate that the MhcGFP line can be used as a tool to quantify Mef2 activity, I performed a proof-of-concept experiment by manipulating the level of Mef2 protein overexpression in the wing imaginal disc to show a dose dependent response in MhcGFP activation (Figure 3.10). Since the Gal4-UAS system is temperature dependent (Brand *et al.* 1994), *UAS-Mef2-AttP2* expression level was modulated by performing the cross with *1151Gal4;;MhcGFP* at 18°C, 25°C or 29°C. Wandering late L3 larval wing imaginal discs from each temperature treatment were dissected, processed and imaged in tandem to allow direct comparison between the samples. ImageJ's 'Triangle' algorithm was used to threshold each image to remove background. Of the 17 different algorithms available on ImageJ's software, Triangle consistently performed best at removing background signal without compromising the observable premature differentiation, across a range of imaginal discs with variable levels of MhcGFP. *1151Gal4;;MhcGFP* larvae were used as a control for this experiment. An exposure value was selected than ensured no pixels were saturated during imaging.

Increasing the temperature at which crosses were performed from 18°C (n=23 discs) to 25°C (n=19) or 29°C (n=23), resulted in a significant increase in the area of premature MhcGFP observed in late L3 wing imaginal discs. Control larval discs did not express MhcGFP at a detectable level (n=15). The area of MhcGFP observed was not significantly different between the crosses performed at 25°C and 29°C.

"Integrated density" was calculated for each group, by multiplying the observed thresholded area of MhcGFP by mean pixel value over this area. Since discs were imaged at 16-bit depth, each pixel value could range from 1-65,536 depending on its brightness. The integrated density metric therefore captures information on brightness of MhcGFP, so is indicative of the total amount of GFP present, whereas the area measurement alone is not. Integrated density of MhcGFP significantly increased between 18°C and 25°C, and again between 25°C and 29°C, demonstrating that as the level of *UAS-Mef2* induced expression increases, so does the quantity of MhcGFP protein. Therefore, MhcGFP can be used as a robust read-out of Mef2 activity, to determine how addition of co-factors or mutation of Mef2 residues of interest can impact upon its transcription factor activity.

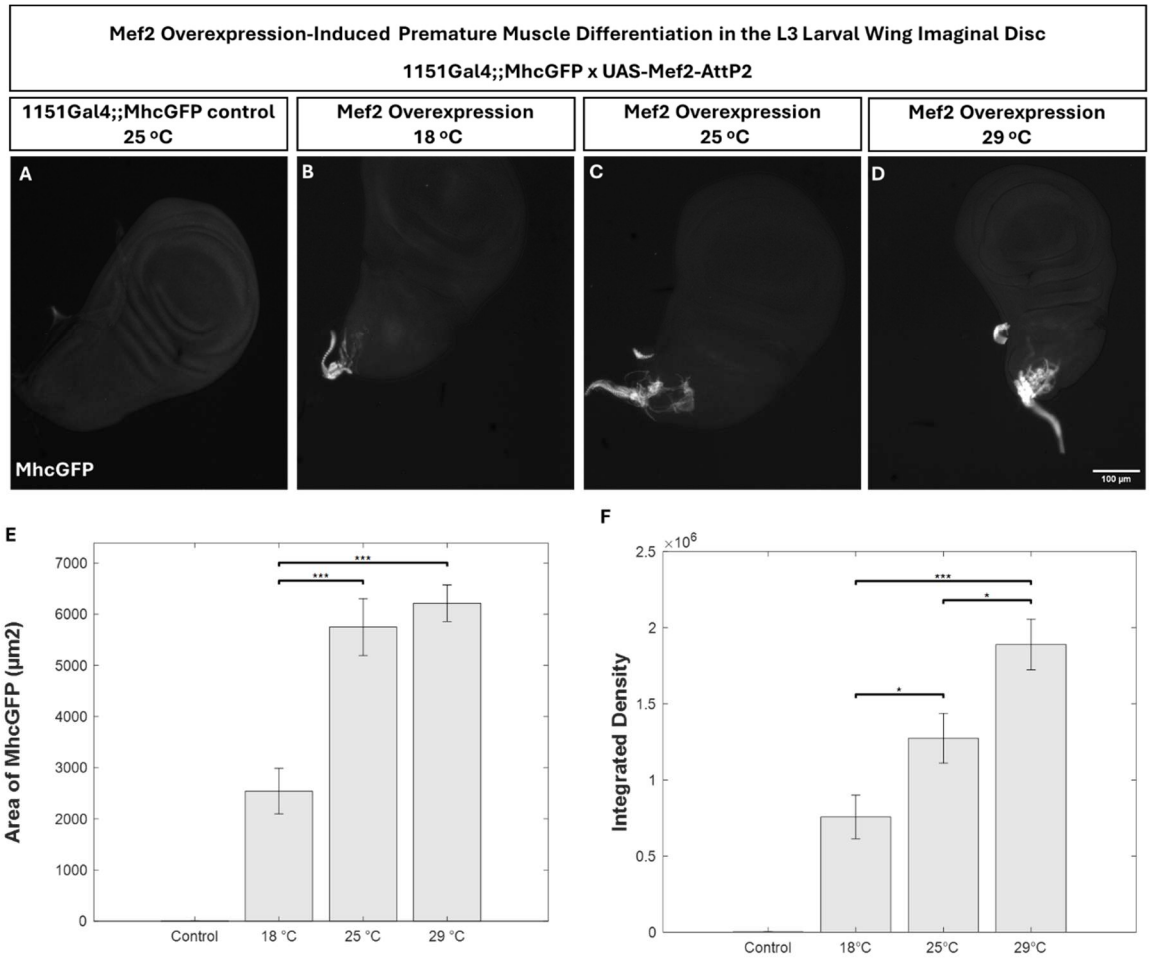

Figure 3.10 – MhcGFP can be used as a readout to quantify *1151Gal4* driven Mef2 activity

Representative 10x fluorescent microscopy images showing wing imaginal disc MhcGFP expression in A) *1151Gal4;;MhcGFP* controls (n=15 discs), B) Mef2 overexpression at 18◦C (n=23 discs), C) Mef2 overexpression at 25◦C (n=19 discs) and D) Mef2 overexpression at 29◦C (n=23 discs). E) Bar graph showing quantification of area (μm^2) of MhcGFP. Bars denote mean value per sample ± SEM. (Kruskal Wallis followed by Post-Hoc Dunns test: 18◦C vs 25◦C ***p=0.0002, 18◦C vs 29◦C ***p<0.0001). F) Bar graph showing quantification of MhcGFP integrated density. Bars denote mean value per sample ± SEM. (Kruskal Wallis followed by Post-Hoc Dunns test: 18◦C vs 25◦C *p=0.027, 18◦C vs 29◦C ***p<0.0001, 25◦C vs 29◦C *p= 0.042).

3.8 Discussion

In this chapter, I have further characterized Mef2 protein expression in the late L3 wing imaginal disc with an in-house generated CRISPR direct-tag *Mef2GFP* transgene (Hubbert 2023), in combination with other known wing disc markers, Ct and Fas3. Whilst Ct is a well-characterized marker of the entire AMP population, the level of Ct protein is known to be higher in the distal AMPs that will give rise to the DFMs, than in those that will give rise to the IFMs (Sudarsen *et al.* 2001). This is consistent with scRNAseq data from the wing imaginal disc which shows that a similar pattern is observed between *cut* RNA and Cut protein (Zappia *et al.* 2020). Contrastively, I observed Mef2 protein to have a relatively constant expression level throughout the entire late L3 AMP population. This is in agreement with published immunostainings using a Mef2 antibody, and the scRNAseq dataset (Zappia *et al.* 2019; Vishal *et al.* 2020).

Recent work suggests that the DFM and IFM AMP populations can be further subdivided into cells that are more naïve, versus those that are beginning down the differentiation pathway (Zappia *et al.* 2020). These differentiating cells display markers such as the muscle morphogenesis regulator *hoi-polloi* (*hoip*), and *hairy* (*h*) which is expressed in the embryonic musculature (San Martin *et al.* 2001; Johnson *et al.* 2013). Since my analysis demonstrates Mef2GFP protein expression is relatively consistent throughout these subclusters, this might suggest that the expression level of Mef2 inhibitors instead varies to facilitate the developmental gradient of cell types that exist. Indeed, the scRNAseq data for known repressors of myogenesis, Him and Twist, show their upregulation in the subclusters that represent undifferentiated cells, but much lower expression in “differentiating” myoblasts. Therefore, AMP differentiation state is plausibly a consequence of Mef2 activity, since its repression is diminished in cells that are beginning to differentiate.

Using the Mef2GFP construct to visualize Mef2 protein is advantageous for several reasons. I’ve shown that it can be imaged ‘live’ and unfixed, without need for antibody staining, which will facilitate future time-lapse based experiments. For example, assaying Mef2 protein expression as adult muscle development proceeds might reveal dynamic changes in Mef2 protein expression at specific stages. Fluorescently tagged proteins are also compatible with analyses such as

fluorescence resonance energy transfer (FRET), to demonstrate physical protein interactions between FRET donors and acceptors (Miyawaki 2011). Since Mef2 is known to be co-expressed with several of its regulators throughout muscle development, FRET is a viable option to explore where and when specific Mef2 interactions occur. Mef2GFP is also a superior tool for immunofluorescent studies, because commercially sourced anti-GFPs provide much cleaner, lower background images than the currently available Mef2 antibodies.

Whilst it is clear that Mef2 protein is already expressed in late L3 wing imaginal disc AMPs, by inducing overexpression of *UAS-Mef2* using the Gal4/UAS system, I've shown that these cells can be nudged considerably further down the differentiation pathway. In response to elevated Mef2, these AMPs seemingly prematurely differentiate, based on the observation of precocious myofibres with organized sarcomeres within the wing imaginal disc. In wild-type flies, sarcomeric assembly doesn't even begin until 30hr APF, and well-organized sarcomeres are not observed until about 48h APF (Spletter *et al.* 2018). It is remarkable that with the addition of just one protein, Mef2, naïve AMPs can give rise to organized, differentiated muscle tissue, highlighting just how important Mef2 function is to muscle differentiation as a whole. Since *ex vivo* culture of imaginal discs is possible, this system can be used in combination with time-lapse imaging to study muscle differentiation live in future experiments (Tsao *et al.* 2016; Sohr *et al.* 2019). For example, the processes of myoblast fusion and sarcomerogenesis which usually occur during pupation, and are extremely difficult to study live, can be induced prematurely in an *ex vivo* wing imaginal disc prep and imaged over a number of hours.

Mef2 overexpression induced premature myofibres seemingly show a bias towards the dorsal region of the notum. This suggests that a certain subset of AMPs are more prone to differentiate in response to Mef2 activity, as precocious fibres have not been observed in the more ventrally located AMPs, such as those that give rise to the DFMs. The observation that myofibres closely associate with the disc-associated tracheal network suggests that it might play some role in their differentiation, perhaps through delivery of oxygen. However, in both a mouse satellite cell model, and in human primary myoblasts, muscle-specific gene expression is actually stimulated by hypoxic conditions (Koning *et al.* 2011; Urbani *et al.* 2012). Another possible

explanation is that signals emanating from the trachea influence the differentiation process. A role for trachea acting as a signaling hub has already been described in the *Drosophila* gut, where tracheal FGF signaling drives intestinal stem cell proliferation in response to damage (Perochon *et al.* 2021). To investigate whether a similar mechanism is required for Mef2 induced differentiation, future studies could perform a tracheal specific knockdown of the FGF ligand *branchless* (*bnl*) to see if this affects the process.

The finding that Mef2 overexpression induces cellular phenotypes in addition to precocious fibre differentiation, provides new opportunities for assaying Mef2 gain-of-function. I have shown that antibody staining against Mhc gives a much more sensitive read-out of Mef2 activity than Mhc-GFP, showing upregulation in the majority of the AMP population when Mef2 is overexpressed. On the other hand, Mef2 induced Mhc-GFP expression is largely localized to the precocious myofibres. Whilst Mhc antibody staining will label all Mhc isoforms, the strategy to generate the Mhc-GFP minigene resulted in the tagging of only three out of the eleven *Mhc* isoforms (K, L, M), which might explain the differences in expression observed (Sarov *et al.* 2016). Indeed, the different Mhc isoforms are known to be expressed at different developmental stages (Zhao and Swank 2013), and in different muscle types (Sarov *et al.* 2016), and it is plausible that isoforms K, L, M do not represent the whole spectrum of Mhc splice variants induced by Mef2 overexpression. A more sensitive read-out of Mef2 activity, such as Mhc antibody staining, will permit more subtle changes in Mef2 activity to be detected. For example, whilst loss-of-function of Him, a negative regulator of Mef2 activity, does not induce premature MhcGFP expression (Cedric Soler, unpublished), antibody staining against Mhc might reveal a phenotype.

In addition to further describing Mef2 induced premature differentiation, I have also shown that this system can be used as a readout for quantifying Mef2 activity level. Since *Mhc* is known to be directly regulated by Mef2's transcription factor activity (Sandmann *et al.* 2006), it stands to reason that if the amount of Mef2 protein is increased, a downstream consequence of this would be increased Mhc transcription. This seems to be the case when I quantified the amount of MhcGFP to varying quantities of Mef2 protein, achieved by using temperature to manipulate Gal4/UAS-

Mef2 overexpression. An alternative biochemical approach to quantify Mef2 activity would be to use a beta-galactosidase assay in combination with a Mef2 sensitive reporter, such as *Mhc-LacZ*. Here, the amount of reporter protein produced can be quantified in a colorimetric reaction using a spectrophotometer. A similar approach has already been applied to the *Drosophila* jump muscle, where *TpnC41C* promoter fragments were tested for LacZ activity (Chechenova *et al.* 2015).

Now that a system to quantify Mef2 activity has been developed, downstream applications of this include co-expressing co-factors of Mef2, or its inhibitors, to determine the net impact this has on its activity. Additionally, this assay would facilitate the impact of Mef2 mutations to conserved regions of interest to be assayed, to give insight into functions of specific residues. Examples of both of these scenarios are presented later in this thesis.

Chapter 4. *Him* is required for the correct patterning of the jump muscle and pericardial cells

4.1 Introduction

Him is a known negative regulator of Mef2 activity, during both embryonic and adult muscle development (Liotta *et al.* 2007; Soler and Taylor 2009). During early embryonic development, Him has a broad mesodermal expression pattern. As muscle differentiation proceeds, Him expression declines, becoming restricted to the pericardial cells of the developing heart, and the adult muscle progenitors (AMPs), which are set aside and remain undifferentiated until adult myogenesis (Liotta *et al.* 2007; Panta *et al.* 2020). In the embryo, the onset of Mef2-dependent gene expression correlates with the observed decline in Him protein, consistent with a repressive role for Him in Mef2 regulation (Liotta *et al.* 2007). Similarly, prior to adult myogenesis, Him is expressed in L3 larval wing imaginal disc-associated AMPs alongside Mef2, where it is thought it could prevent Mef2 dependent gene expression until the proper time (Soler *et al.* 2009).

Genetic evidence also supports a role for Him as a Mef2 repressor, as Him overexpression can repress Mef2-induced phenotypes (Liotta *et al.* 2007; Soler and Taylor, 2009). Mechanistically, it is currently unknown whether Him mediated repression of Mef2 is via a genetic interaction or physical protein-protein interaction. During embryonic muscle development, Him mediated repression of Mef2 is dependent on its WRPW motif, a well characterized protein-protein interaction domain required for association with the general transcriptional repressor Groucho (Gro) (Liotta *et al.* 2007).

In this chapter, I describe several previously uncharacterized *Him* mutant phenotypes using three distinct *Him* mutant alleles. I have generated a directly tagged *Him-mNeongreen* line using CRISPR, which can act as a mutant, reporter and directly tagged protein, to further our understanding of Him expression, regulation and function. This fast maturing fluorophore can be visualized without the need for antibody staining, so is suited to live imaging based approaches, unlike the *HimGFP* minigene used in previous analyses of Him expression (Liotta *et al.* 2007; Soler and Taylor, 2009). Furthermore, I've used a Yeast2Hybrid (Y2H) based

approach to demonstrate that Him mediated repression of Mef2 is via a direct interaction, mapped to the N-terminus of the Mef2 protein.

4.2 Genomic structure of the *Him* alleles

Three distinct *Him* mutant alleles were used to phenotype *Him* loss-of-function. *Him52* was previously generated in-house using recombination between two pBac elements, resulting in a 90kb deletion including *Him* and five other genes; *Hesr*, *CG33649*, *Frq2*, *andorra* and *Frq1* (Figure 4.1A, Daniel Hancock, PhD thesis, Cardiff University). Despite the six gene deletion, the fly line is homozygous viable. *Himφ* was generated by Richard Cripps' lab, using a CRISPR based approach to induce a two nucleotide deletion in *Him's* endogenous locus. This results in a premature stop codon at codon 14, and consequently a null allele (Mitchell-Gee *et al.* 2024).

I generated *Him_mNeongreen* using CRISPR to insert the fast-maturing fluorophore mNeongreen directly downstream of *Him's* endogenous promoter. Additional LoxP flanked sequences were also inserted adjacent to the fluorophore, including a pax-Cherry transgenesis marker and transcription termination signals (Figure 4.1B). Initially, this construct acts as both a *Him* null mutant and reporter, as the rest of the *Him* coding sequence, which has been translocated downstream, is not transcribed. A transgenic cre-recombinase source was used to excise the LoxP flanked sequences, resulting in a directly tagged protein with a short linker fragment between Him and the mNeongreen fluorophore (Figure 4.1C). Confirmation of successful recombination is demonstrated by the excision of the Pax-Cherry marker, which is usually expressed in the larval brain complex and the adult eyes. I refer to the null reporter allele as *Him_mNeongreen_NR*, and the directly-tagged allele as *Him_mNeongreen_DT*.

A previously published HimGFP minigene (chromosome III) was also used to determine Him protein localization, as well as in rescue experiments (Liotta *et al.* 2007). The construct consists of approximately 3.8kb upstream *Him* sequence, followed by N-terminally eGFP tagged *Him* coding sequence and its 3'UTR (Liotta *et al.* 2007).

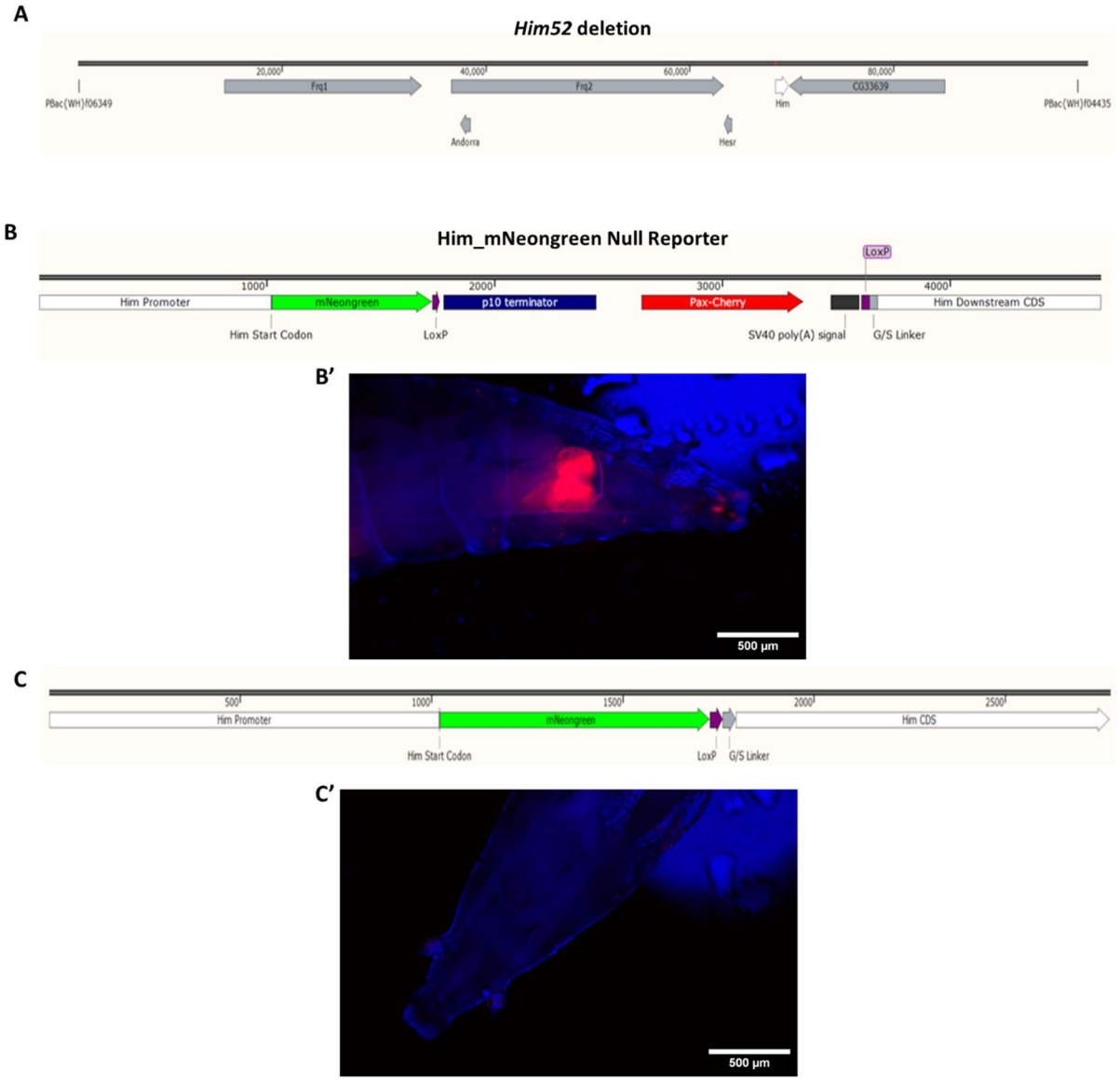

Figure 4.1 - The genomic structure of the Him alleles.

(A) The previously generated *Him52* allele showing the deleted fragment between the two PBac elements, resulting in an approximately 90kb deletion including Him (white arrow) and 5 other genes (grey arrows). (B) The *Him_mNeongreen_NR* line following CRISPR homology directed repair. The resulting allele provides a readout of him promoter activity based on mNeongreen expression. Adjacent to the fluorophore, is a LoxP flanked cassette, including a p10 terminator sequence, Pax-Cherry transgenesis marker and SV40 poly(A) signal, which should disrupt him gene expression. Pax-Cherry expression can be detected in (B') the larval brain complex to confirm successful transgenesis. (C) Following Cre-mediated recombination, the LoxP flanked cassette is excised to generate a directly tagged him allele, with mNeongreen fused to Him via a short G/S linker. Flies no longer express Pax-Cherry (C').

4.3 Analysis of Him protein expression pattern in late L3 wing imaginal disc associated AMPs reveals spatial heterogeneity

Wing imaginal disc associated AMPs are known to express Him, based on both scRNAseq data and anti-GFP staining of the HimGFP minigene (Zappia *et al.* 2020; Soler and Taylor 2009). However, the amount of *Him* transcript present doesn't necessarily correlate with the amount of protein, nor does the HimGFP minigene inform on levels of endogenous Him protein, as its insertion is elsewhere in the genome and is therefore subject to genomic position effect. Furthermore, the minigene cannot be observed 'live', requiring anti-GFP staining to visualize, potentially because Him protein's half-life is shorter than the maturation time of its GFP tag. The CRISPR engineered Him_mNeongreen insertion was designed with the aim of overcoming these issues, allowing endogenous Him to be visualized without the need for antibody staining, as well as providing a more accurate readout of endogenous gene and protein expression. mNeongreen was selected as it is a rapidly maturing and bright fluorophore, thus is a useful tag for proteins that have a fast turnover (Shaner *et al.* 2013).

Wing imaginal discs from late L3 wandering larvae were studied to determine the Him protein expression pattern at this stage just prior to pupation and the onset of adult muscle development (Figure 4.2). Anti-GFP staining of the HimGFP minigene reveals a uniform staining pattern throughout the AMP population on the notum of the wing imaginal disc (Figure 4.2A). Him_mNeongreen_NR and Him_mNeongreen_DT can be visualized live and unfixed, without the need for antibody staining, with both lines reassuringly in agreement over where Him is expressed (Figure 4.2B and 4.2C). A localized cluster of AMPs in the wing imaginal discs anterior presumptive lateral hemi-notum appear to display an increased level of Him compared to AMPs elsewhere in the imaginal disc. This is the same region of the disc identified by Zappia *et al.* 2020 as being home to the most developmentally naïve IFM-AMP clusters 1-2. Antibody staining of Him_mNeongreen_NR masks this specific localization of Him, demonstrating the importance of 'live' imaging where possible (Figure 4.2D).

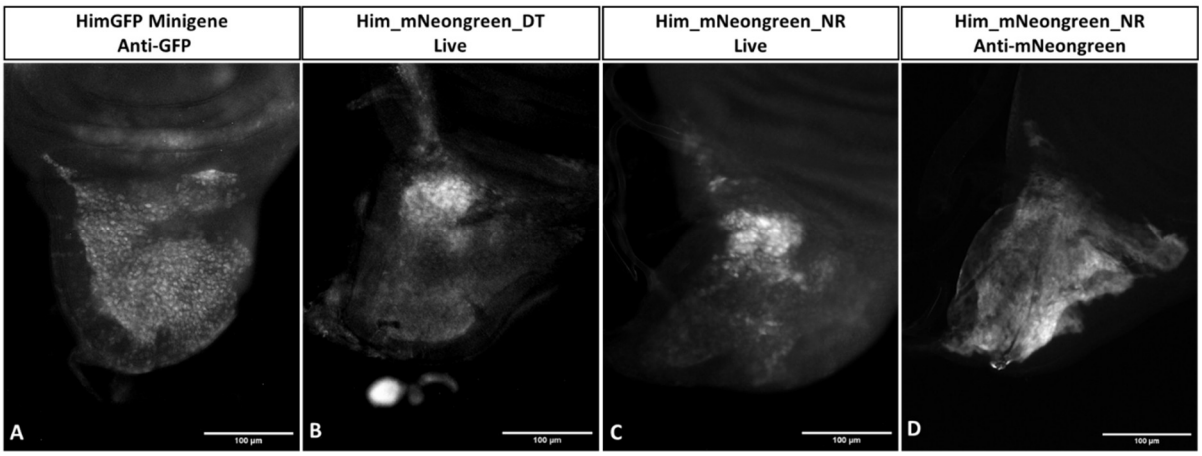

Figure 4.2 - Him expression pattern in the late L3 larval wing imaginal disc.

(A) The HimGFP minigene (Liotta *et al*. 2007) in combination with anti-GFP staining, shows that Him is expressed uniformly throughout the AMP population. Both (B) The Him_mNeongreen_DT and (C) Him_mNeongreen_NR lines, when imaged live, show a highly localized expression pattern atop the presumptive lateral heminotum of the disc. (D) Anti-mNeongreen staining of the Him_mNeongreen_NR line masks the highly localized pattern seen in live preps. (n=6-10 discs per sample).

4.4 Him can negatively regulate Mef2 activity in the wing imaginal disc

I generated a *Him_mNeongreen_DT*; *Mef2GFP* stock to visualize the co-localization of endogenous Him and Mef2 protein in the wing imaginal disc. Since the attached fluorophores have similar excitation and emission spectra, antibody staining against mNeongreen and GFP was required to distinguish between them using secondary antibodies conjugated to distinct fluorophores. The traditional immunofluorescent staining protocol was unsuccessful for Him_mNeongreen_DT, so the protocol was adapted to include a shorter fixation period, a stronger concentration of triton to increase permeabilization of the tissue, and blocking was performed in Normal Goat Serum (NGS) rather than Normal Donkey Serum (NDS) (see methods for further details).

In the late L3 wing imaginal disc, Mef2GFP and Him_mNeongreen_DT expression can be detected in AMP nuclei. As previously described (Figure 3.2), Mef2GFP expression can be detected throughout the AMP population, whereas Him_mNeongreen_DT expression is highest in a particular subset of the cells, which was reflected in the co-stain (Figure 4.3). The mNeongreen signal is diffuse, so it is

difficult to draw conclusions about subcellular localization of endogenous Him in this tissue.

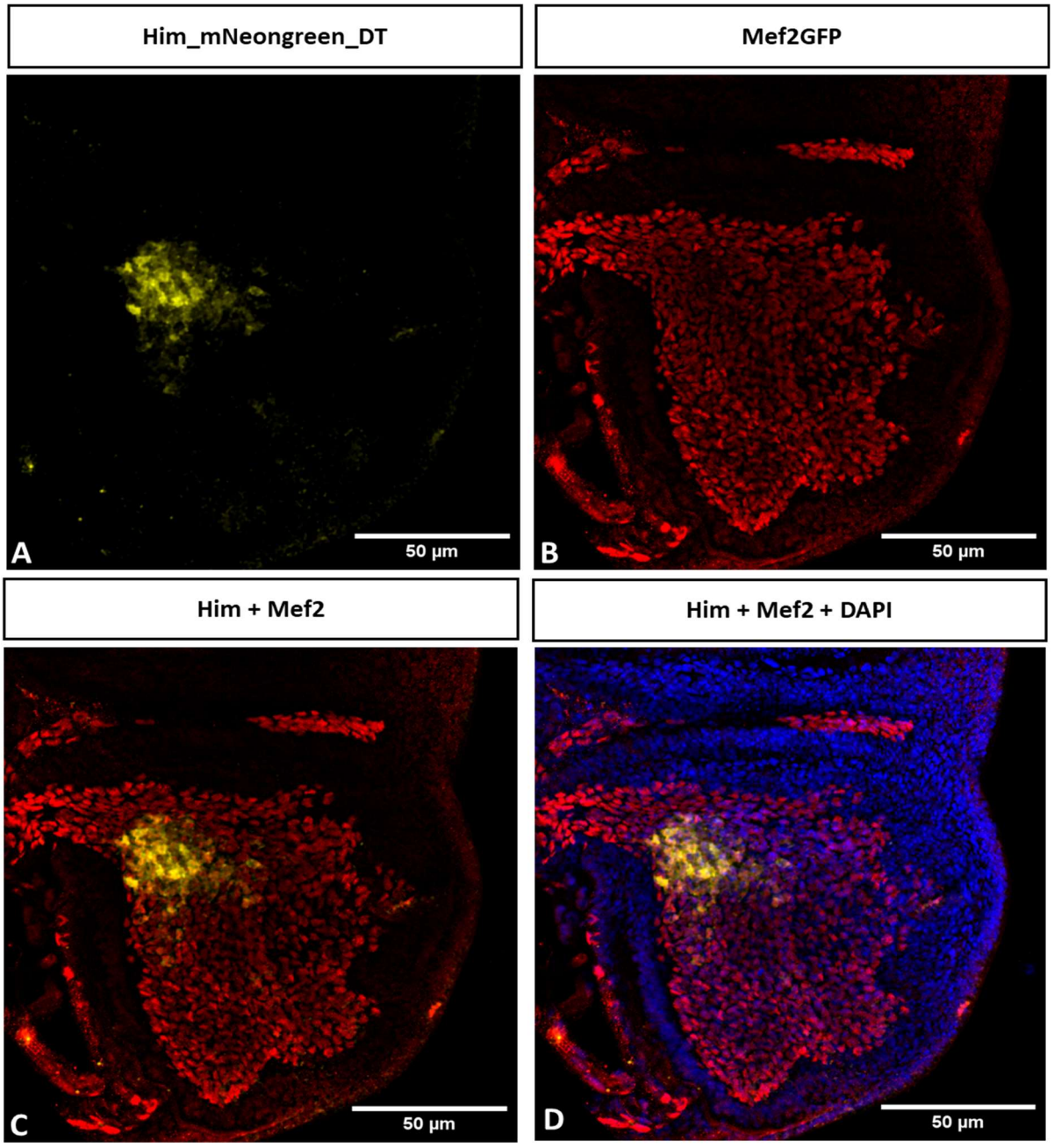

Figure 4.3 - Him_mNeongreen_DT and Mef2GFP co-localize in a subset of AMPs of the late L3 larval wing imaginal disc.

Maximum intensity projections of confocally imaged *Him_mNeongreen_DT*; *Mef2GFP* wing imaginal disc-associated AMPs, in single channel for (A) anti_mNeongreen staining (yellow) and (B) anti-GFP staining (red). (C) The merge shows co-localization of Him_mNeongreen_DT (yellow) and Mef2GFP (red) in the subset of AMPs that express Him. (D) Counter-staining with DAPI labels all wing imaginal disc nuclei. (n=5 discs).

The “premature differentiation” assay in the L3 larval wing imaginal disc was used to determine the net effect that Him protein has on Mef2 activity, using the MhcGFP fTRG line as a readout of Mef2 activity (Figure 4.4). Used in the previous chapter, this transgene is a directly tagged allele inserted into a third chromosome landing site, which recapitulates endogenous Mhc expression in the DLMs (Sarov *et al.* 2016). *1151Gal4* was used at 25°C to drive *UAS-Mef2* overexpression alone, or alongside *UAS-Him*, specifically in the AMPs. To exclude the possibility that any suppression of the *UAS-Mef2* phenotype is due to Gal4 dilution, rather than the effect of *UAS-Him*, a *UAS-mCherryCD8; UAS-Mef2* control was performed. Wing discs from the three genotypes were processed concurrently to allow direct comparison of amount of MhcGFP activation between them. Both the area of MhcGFP and integrated density were calculated for each genotype to act as a readout of Mef2 activity, as discussed in the previous chapter.

Mef2 overexpression alone resulted in premature MhcGFP expression in 100% of wing imaginal disc imaged (n=23 discs). When co-overexpressed alongside Him, Mef2 could no longer induce any detectable premature MhcGFP in 100% discs analyzed (n=15). Co-overexpression of a *UAS-mCherry-CD8* construct alongside Mef2 yielded equivalent MhcGFP activation to *UAS-Mef2* alone (Figure 4.4D-E). These data demonstrate that the repression of the Mef2 induced phenotype isn’t due to Gal4 dilution, but rather due to the presence of Him.

This assay determines that Him is a negative regulator of Mef2 activity, although it doesn’t discriminate between a physical protein-protein interaction and a genetic interaction. Since Him and Mef2 are co-expressed in adult muscle progenitor cells, these data provide compelling evidence that Him’s role in this cell-type is a repressor of Mef2 activity. Him’s localization pattern, being upregulated in a specific subset of AMPs, suggests that the extent to which it represses Mef2 depends on location within the AMP population. This provides further evidence to the idea that AMPs exist in a spectrum of differentiation state (Gunage *et al.* 2014; Zappia *et al.* 2019), with Him expression declining and net Mef2 activity subsequently increasing in differentiating cells.

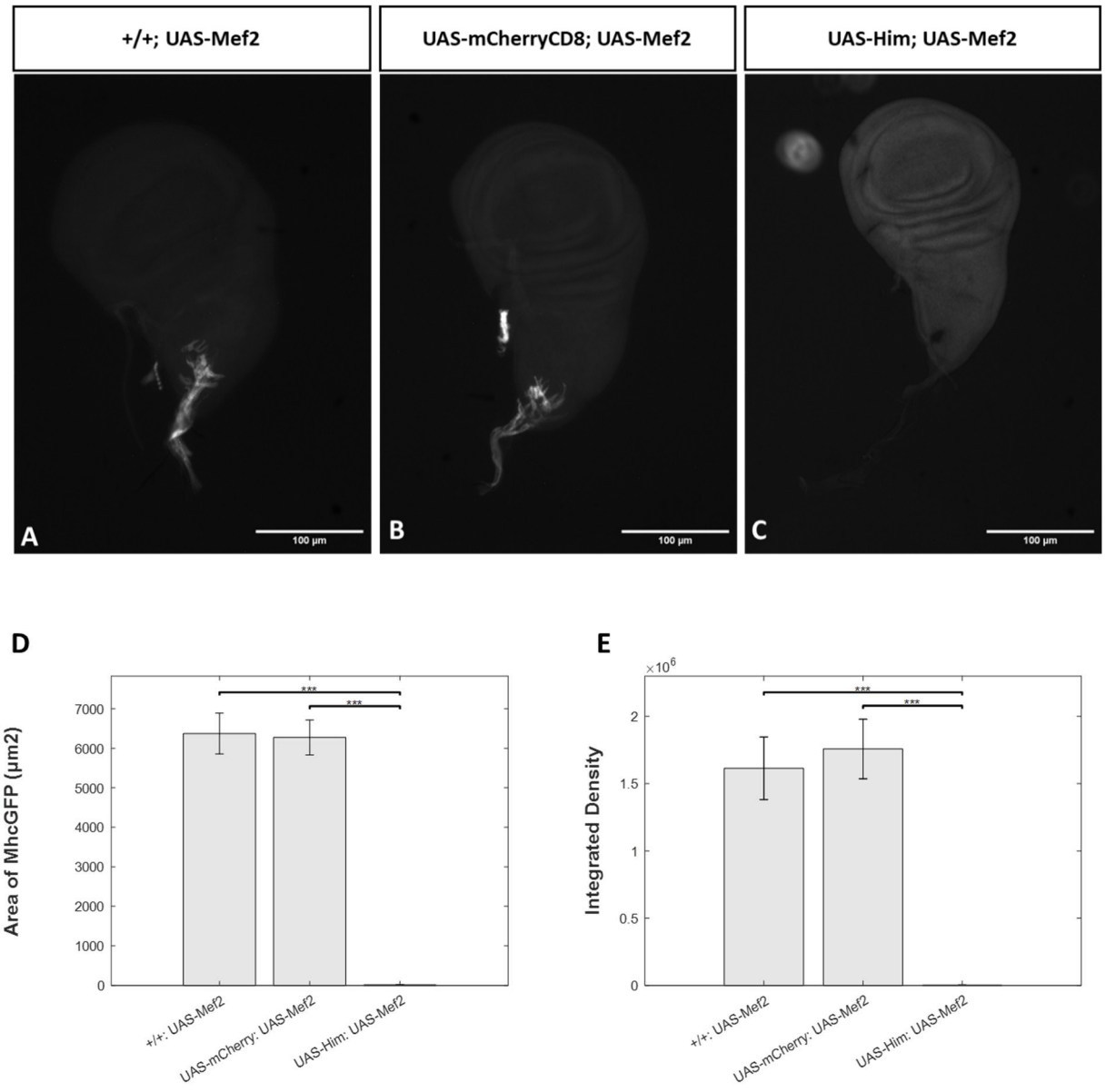

Figure 4.4 – Him negatively regulates Mef2 activity in the premature differentiation assay. Representative fluorescent microscopy images of *1151Gal4;;MhcGFP* driving (A) *UAS-Mef2* alone, (B) both *UAS-mCherryCD8* and *UAS-Mef2* and (C) both *UAS-Him* and *UAS-Mef2*. Mef2 induced premature differentiation is entirely repressed by overexpression of Him. (D) Bar graph showing quantification of area (μm^2) of MhcGFP per genotype. Bars denote mean value per sample ± SEM. (Kruskal Wallis followed by Post-Hoc Dunns test *UAS-Mef2* vs *UAS-Him; UAS-Mef2* ***p<0.0001, *UAS-mCherryCD8; UAS-Mef2* vs *UAS-Him; UAS-Mef2* ***p<0.0001). E) Bar graph showing quantification of MhcGFP integrated density. Bars denote mean value per sample ± SEM. (Kruskal Wallis followed by Post-Hoc Dunns test: *UAS-Mef2* vs *UAS-Him; UAS-Mef2* ***p<0.0001, *UAS-mCherryCD8; UAS-Mef2* vs *UAS-Him; UAS-Mef2* ***p<0.0001). (n=15-23 discs per genotype).

4.5 Him and Mef2 can physically interact with one another in a Yeast-2-Hybrid assay

To identify whether Mef2 repression by Him is dependent on a physical protein-protein interaction, Yeast-2-Hybrid (Y2H) was performed to test whether both proteins are indeed capable of this, using an auxotrophic marker based reporter system. Mef2 fragments were cloned into bait vector PB27, resulting in a Mef2/Gal4-activation domain (AD) fusion protein. Full length Him was cloned into prey vector PP6, resulting in a Him/LexA-DNA binding domain (DBD) fusion. Both vectors were sequentially transformed into yeast strain L40ΔGal4, which cannot biosynthesize histidine due to the presence of a *his3Δ200* mutation. In the presence of a physical interaction between bait and prey proteins, the Gal4-AD & LexA-DBD are reconstituted to form an active transcription factor, which can drive expression of a (*lexAop*)*4-His3* reporter to allow yeast to grow on media lacking this component (drop-out 3).

An N-terminal 1-350 Mef2 fragment was used to test for protein-protein interactions, as during an initial Hybrigenics screen (2010, unpublished), it was found that the full length Mef2 protein could auto-activate the *His*3 reporter in the absence of any protein-protein interaction. The vast majority of Mef2 interacting partners are mapped to its conserved N-terminus (Mef2C interactants reviewed by Dong *et al.* 2017), so the missing C-terminal portion of the protein is unlikely to hinder a potential Him interaction.

The Mef2 (1-350) fragment could physically interact with a full-length Him construct (1-192), based on activation of the *His3* reporter and growth on DO3 (Figure 4.5). A shorter Mef2 fragment (1-156) comprising the MADS, Mef2 and HJURP-C domains could also physically interact with full length Him, so this interaction can be mapped to Mef2's N-terminus. A negative control consisting of Mef2 (1-350), and empty PP6 vector did not grow on DO3, showing that the Mef2 (1-350) fragment could not auto-activate the *His3* reporter. Assays were performed in duplicate to ensure consistent results.

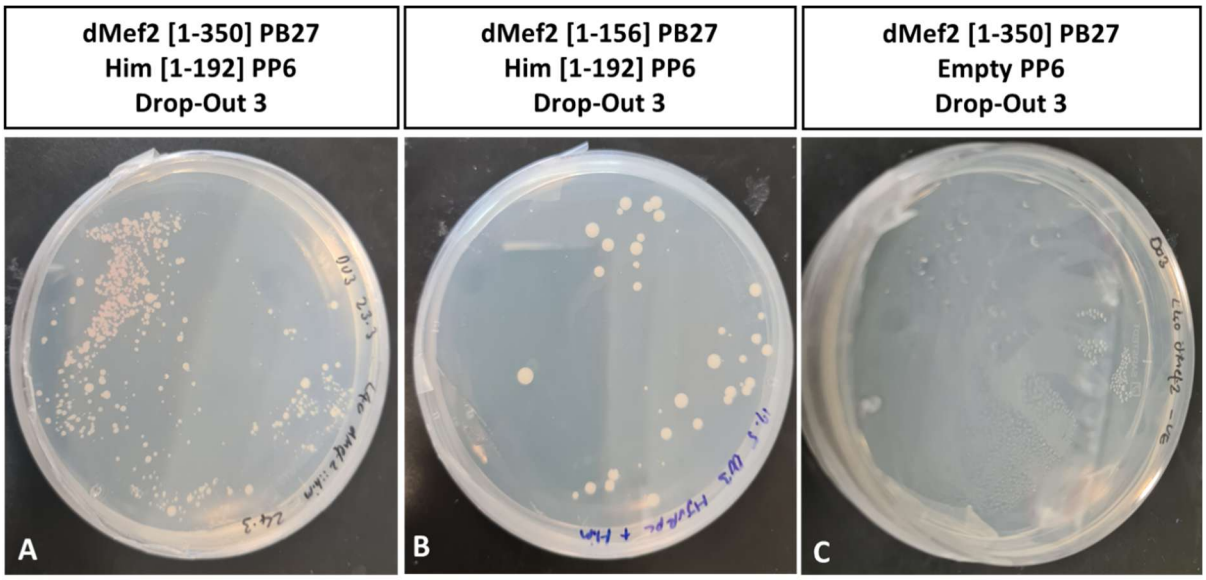

Figure 4.5 – Him and Mef2 can physically interact in a Y2H assay.

Yeast transformed with both the PB27 bait plasmid (+TRP), and PP6 prey plasmid (+LEU) were grown on Drop-out 3 Media (-LEU/-TRP/-HIS) and evaluated for growth, to indicate a protein-protein interaction based on His3 reporter activation. Photographs of the resultant plates after 3 days growth of yeast transformed with (A) PB27-Mef2[1-350] and PP6-Him[1-192], (B) PB27-Mef2[1-156] and PP6-Him[1-192] and (C) an autoactivation control consisting of PB27-Mef2[1-350] and empty PP6 vector.

4.6 A mild DLM phenotype observed with *Him* loss-of-function may be attributable to genetic background

In order to determine whether *Him* loss-of-function affects some aspect of adult muscle development, I began by studying the DLMs, the most extensively studied *Drosophila* muscle group. Phalloidin stained transverse cross-sections of young adult male flies (< 3 days) were assessed to see if muscle fibre number was reduced in the *Him* mutant condition compared to wild-type controls. Male flies were selected, as in the subsequent rescue experiment only F1 males were the appropriate genotype. Wild-type flies normally have six DLM fibres running from the anterior to the posterior end of the thorax, on either side of the hemithorax midline (Figure 4.6A). In transverse section, you can observe the cross-sectional face of each of the DLMs when stained with phalloidin (Figure 4.6B).

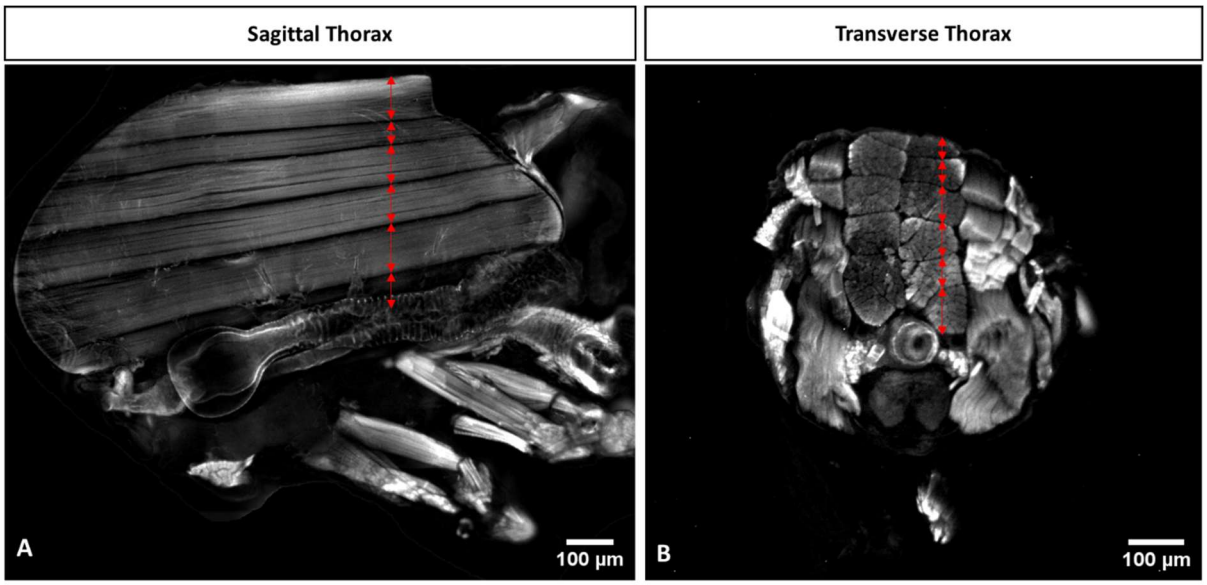

Figure 4.6 – Wild-type control thoraces in sagittal and transverse section.

Phalloidin stained control thoraces. (A) A sagittal section allows the entire length of the DLM to be viewed laterally. (B) A transverse preparation shows the cross-sectional face of each DLM. Red arrows mark the boundaries between each of the six muscles.

The wild-type strain Oregon R was used as a control (n=32 hemithoraces). Whilst the majority of control hemithoraces analyzed had a wild-type number of DLMs, a few individuals had only 5 per hemisegment. This is likely a consequence of a failed template splitting during pupation, which is known to occur occasionally even in wild-type *Drosophila* strains (Chaturvedi *et al.* 2019).

Analysis of the *Him* mutant hemithoraces revealed a mild, but significant, reduction in the number of DLMs, for both the *Him52* and *Him_mNeongreen_NR* alleles compared to Oregon R (Figure 4.7). Mean DLM counts for *Him52* mutants, *Him_mNeongreen_NR* mutants and Oregon R controls were 5.47 (n=30 hemithoraces), 5.38 (n=32) and 5.91 (n=32) respectively. In both of these mutant conditions, the frequency of hemithoraces with only 4 or 5 fibres is increased compared to wild-type, likely a result of increased failure rates in template splitting. For the *Himφ* mutant line, the reduction in DLM number to 5.74 (n=38) was not significantly different from the control.

To confirm that the *Him52* phenotype was due to loss of *Him*, rather than one of the other genes in the deleted region, homozygous mutant females were crossed to males expressing the HimGFP minigene on chromosome III. The F1

Him52/Y;;*HimGFP*/+ flies DLM count was rescued significantly towards wild-type, with a mean of 5.93 per hemithorax (n=30).

In contrast to this, the *Him_mNeongreen_NR* phenotype is not significantly rescued by Lox-Cre-ing, based on observation of the DLMs of the *Him_mNeongreen_DT* line (n=34 hemithoraces). Due to the considered design of Him_mNeongreen, a complete rescue would be expected if the mild phenotype observed is due to loss of *Him*, unless the fluorescent tag is impacting Him function somehow. Taken together, these data are therefore not compelling that *Him* loss-of-function has a significant impact on DLM number, with genetic background a plausible explanation for the differences seen between strains. This argument is strengthened by the *Himφ* mutant data, which doesn't display a significant reduction in DLM number when compared to wild-type.

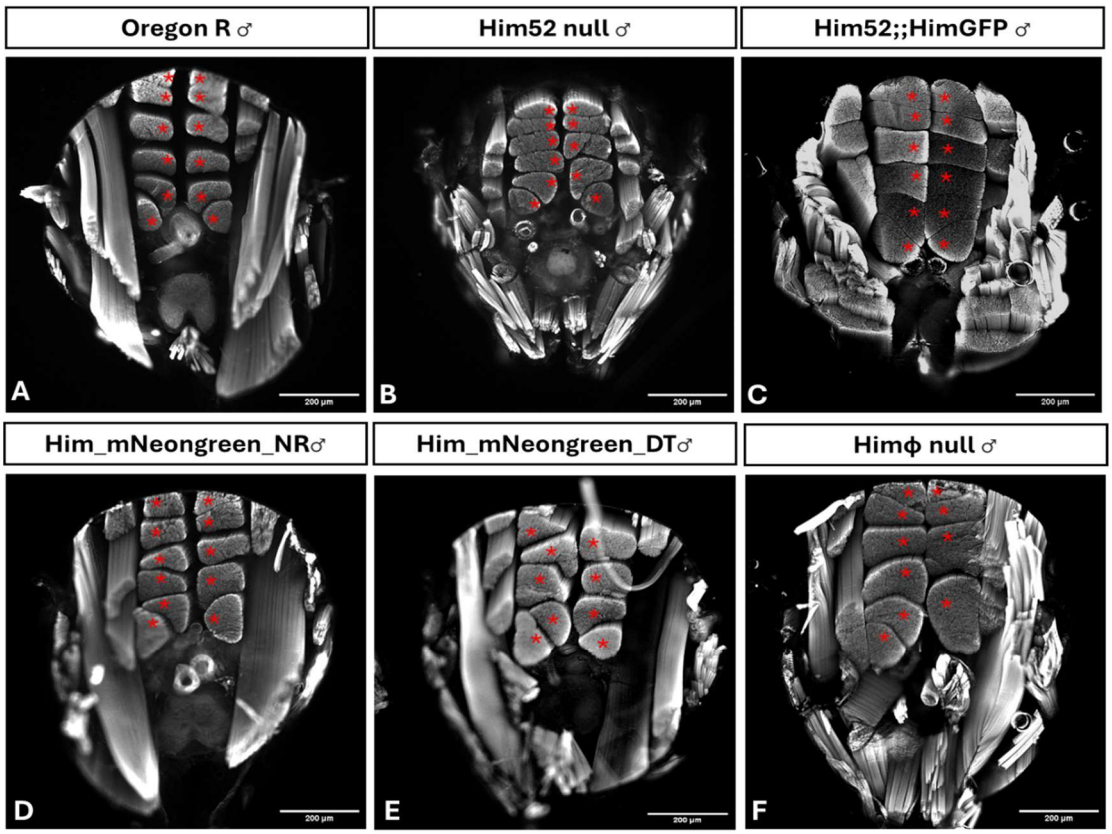

G

Genotype	N hemithoraces	% WT hemithoraces
Oregon R	30	90%
Himφ/Y	36	75%
Him52/Y	30	60%
Him52;;HimGFP/+	30	93%
Him_mNeongreen_NR/Y	32	53%
Him_mNeongreen_DT/Y	34	65%

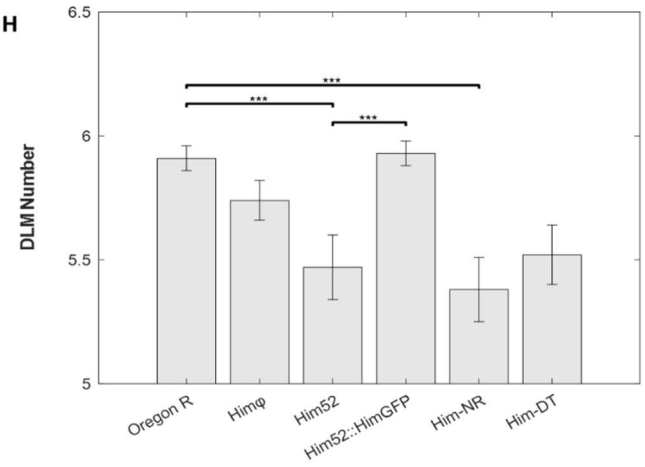

Figure 4.7 – Analysis of DLM counts in Him loss-of-function and rescue conditions.

Representative examples of phalloidin stained transverse cross-sections of young adult male DLMs, imaged by standard fluorescent microscopy. Red asterisks label each DLM counted per image. (A) Oregon R control, (B) *Him52*/Y null, (C) *Him52*/Y;;*HimGFP*/+rescue, (D) *Him_mNeongreen_NR*/Y, (E) *Him_mNeongreen_DT*/Y and (F) *Himφ*/Y. (G) Table of results showing number of hemithoraces quantified, and the percentage that had wild-type numbers of DLMs. (H) Bar graph showing mean DLM count ± SEM. *Him52* and *Him_mNeongreen_NR* possessed significantly fewer DLMs than Oregon R controls. HimGFP was able to rescue the *Him52* DLM number towards wild-type. (Kruskal Wallis followed by Post-Hoc Dunns test: Oregon R vs *Him52*/Y ***p=0.0002, Oregon R vs *Him_mNeongreen_NR*/Y ***p=0.0007, *Him52* vs *Him52*/Y;;HimGFP/+ ***P<0.0001).

4.7 *Him* loss-of-function causes a fully penetrant TDT patterning phenotype

The TDT is a tubular muscle found in the adult thorax, comprising two columns of neatly organized muscle fibres in an ovoid pattern around a structured mid-line. These stretch from the mesothoracic leg (T2) to the dorsal notum of the thorax, contracting to power the force required for the insect to jump prior to take-off (Trimarchi and Schneiderman 1995). The number of fibres that make up this muscle varies between 20 to 30, depending on the wild-type strain studied, but the pattern of their arrangement is stereotypical (Jaramillo *et al.* 2009). A Mef2^{S98A} mutant displays a TDT, but not a DLM phenotype, suggesting this muscle type is more sensitive to subtle changes in Mef2 activity and thus represents a sensible place to look for a *Him* mutant somatic muscle phenotype (Vishal *et al.* 2023).

In collaboration with Professor Richard Cripps' lab, we assessed the impact that *Him* loss-of-function has on the TDT structure of adult flies. 10-12µm transverse cryosections of the TDT were stained with an antibody against βPS-integrin to visualize the outline of each of the fibres that comprise the muscle. Young male flies <2 days old were analyzed, since the subsequent rescue experiment could only be performed with F1 males.

There were structural abnormalities in the TDT of *Himφ* (n=7 TDT from 7 flies), *Him52* (n=8) and *Him_mNeongreen_NR* (n=6) mutants when compared to *yw* control flies (n=6). Although the TDT still developed, the stereotypical arrangement of the muscle fibres was disrupted in the mutant condition (Figure 4.8). Instead of two neat columns of muscle fibres, the muscle had a fractured, disorganized appearance. This phenotype was fully penetrant in all three mutants analyzed, with 100% mutant flies sectioned displaying dysmorphic TDT structure. A heteroallelic combination of *Himφ*/*Him52* (♀ n=8) yielded the same result, suggesting that the phenotype is due to *Him* loss-of-function rather than an off-target in either mutant allele.

To rescue the phenotype, the HimGFP minigene was used (Liotta *et al.* 2007). Homozygous *Him* mutant females were crossed to HimGFP expressing males, and the result F1 *Him* mutant males had their TDT sectioned and analyzed. This fulfils the dual purposes of testing whether the HimGFP minigene can substitute for

endogenous *Him* during tubular muscle development, as well as increasing certainty that the TDT phenotypes observed are due to *Him* loss-of-function rather than an off-target. This is particularly important for the *Him52* line which is a six gene deletion.

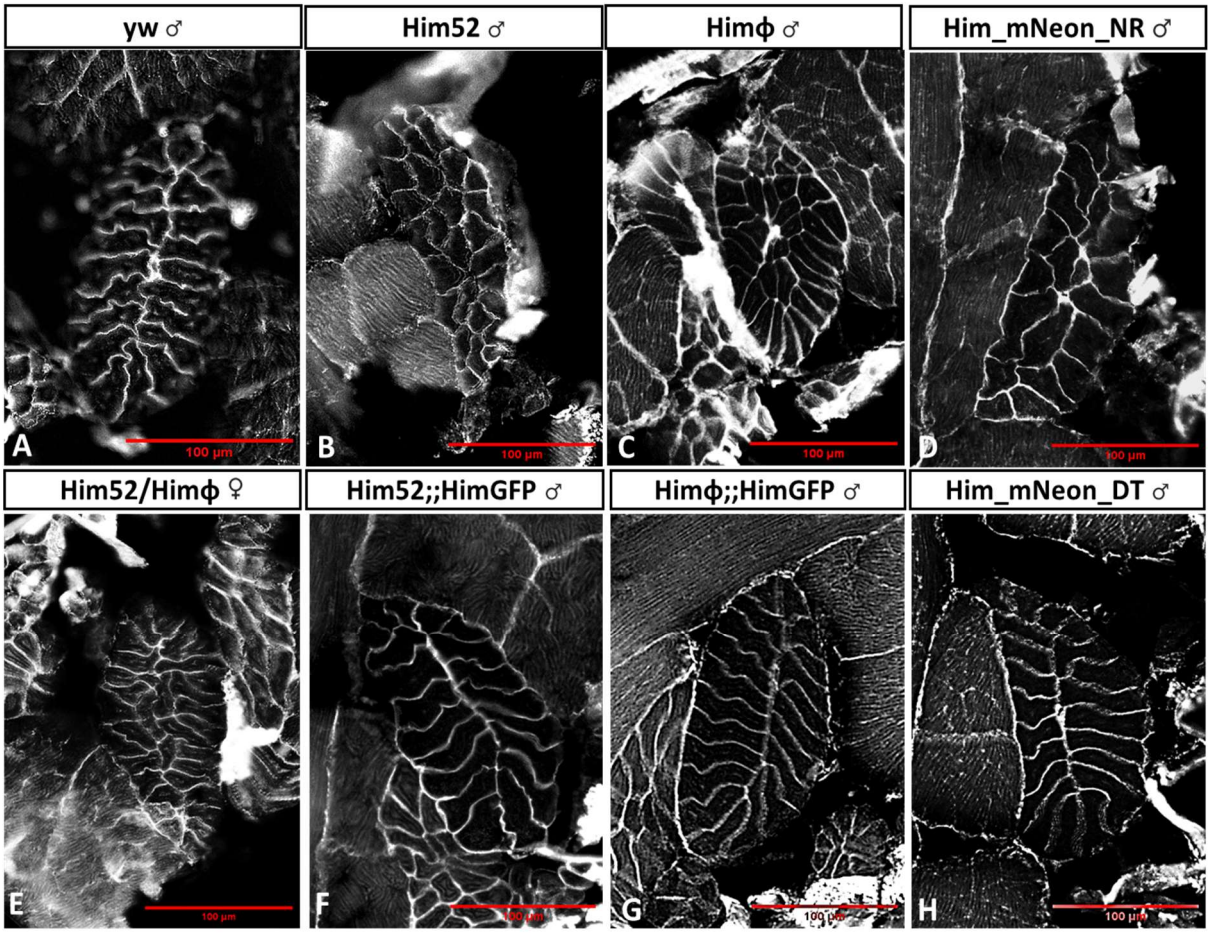

Figure 4.8 – Him Loss-of-Function results in a full penetrant TDT morphological phenotype. Representative fluorescent microscopy images of transverse TDT cryosections from young adult male flies, labelled with anti-integrin to outline the fibres that form the muscle. (A) *yw*/Y control muscles. Morphology is disrupted with loss of *Him*, observed in (B) *Him52*/Y, (C) *Himφ*/Y and (D) *Him_mNeongreen_NR*/Y alleles. (E) A heteroallelic *Him52*/*Himφ* combination also has affected TDT. The phenotype is rescued with the HimGFP minigene (F and G), as well as in (H) the *Him_mNeongreen_DT* allele. (n=6-10 flies per genotype).

The HimGFP minigene is able to rescue the TDT phenotype present in *Himφ* and *Him52* mutant flies. *HimΦ*/Y;;*HimGFP*/+ (n=7) and *Him52*/Y;; *HimGFP*/+ (n=7) flies have TDT resemblant of wild-type Oregon R control fly lines in 100% of the samples analyzed (Figure 4.8). From this, I can conclude that the HimGFP minigene is

functional in developing TDT, and that the phenotypes observed are due to *Him* loss-of-function. Similarly, the *Him_mNeongreen_NR* phenotype is also rescued when compared to the lox-cre'd version of the line, *Him_mNeongreen_DT* (n=6). Taken together, these results provide extremely compelling evidence that the TDT phenotype is caused by loss of *Him*, since with three different mutant alleles, and two different rescue strategies, the results are equivalent.

To complement the morphological phenotyping, I performed a jumping assay on young adult male flies (<3 days) to determine whether the disrupted TDT in *Him* mutants impacts upon jump muscle function (Figure 4.9). *Drosophila* are known to jump both as an escape response from a looming stimulus, or to "take-off" to initiate flight (Zumstein *et al.* 2004; Card and Dickinson 2008). Flies were de-winged under CO_2 anaesthetic, and allowed to recover overnight before being subjected to jump testing the next day.

Jumping ability was defined as the horizontal displacement observed in response to a looming stimulus, averaged over the best 3 of 5 total jumps. Both *Himφ* (n=15 flies) and *Him52* (n=18) mutant flies had a mild, but significant reduction in jumping ability compared to *yw;;nos-cas9* control flies (n=19), demonstrating a functional consequence to the disrupted muscle morphology observed. Similarly to the morphological data, the presence of one copy of the *HimGFP* minigene was able to rescue the behavioral phenotype to wild-type. *HimΦ*/Y;;*HimGFP*/+ (n=18) and *Him52*/Y;;*HimGFP*/+ (n=20) were both able to jump significantly further than the respective mutants, and were indistinguishable from wild-type.

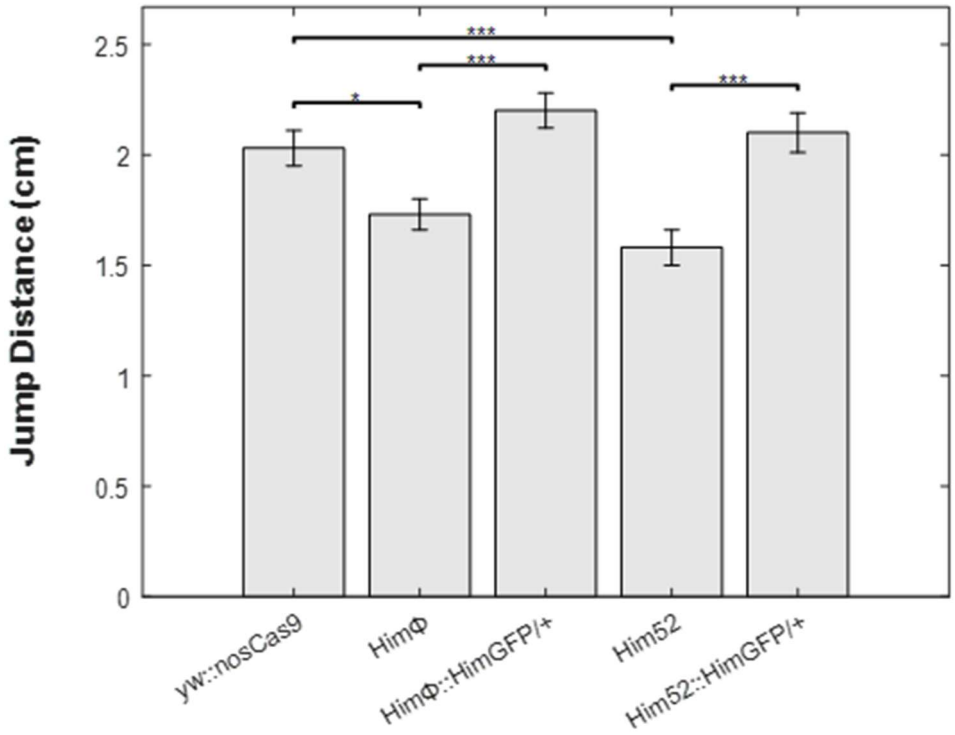

Figure 4.9 – Compromised jump muscle morphology impairs jumping ability.

A bar graph showing mean horizontal displacement jumped ± SEM, in response to a looming stimulus. *Himφ*/Y and *Him52*/Y jump significantly less distance than *yw*/Y;;*nosCas9* controls. (ANOVA followed by Post-Hoc Tukey HSD test: *yw*;;*nosCas9* vs *Himφ*/Y *p=0.033, *yw*;;*nosCas9* vs *Him52*/Y ***p=0.0003). HimGFP rescued the *Him* mutant phenotypes to wild-type (ANOVA followed by Post-Hoc Tukey HSD test: *Himφ*/Y vs *Himφ*/Y;;*HimGFP*/+ ***p=0.002, *Him52*/Y vs *Him52*/Y;;*HimGFP*/+ ***p=0.0002). (n=15-20 flies per genotype).

Him expression in the developing TDT has not yet been characterized. The TDT develops from myoblasts originating from the notal region of the T2 mesothoracic leg disc (Jaramillo *et al.* 2009). To this end, I antibody stained for Him and Mef2 in late L3 larval T2 leg discs to see if Him could be detected alongside Mef2 in leg disc associated myoblasts, as in the wing disc AMPs. Two different approaches were utilized to visualize Him and Mef2 protein in this tissue. Firstly, *Him_mNeongreen_DT*; *Mef2GFP* larval discs were stained with anti-mNeongreen

and anti-GFP to visualize the endogenous direct tags (Figure 4.10A). Secondly, the *HimGFP* mini-gene line was used in conjunction with anti-GFP and anti-Mef2 staining (Figure 4.10B).

I found that Him_mNeongreen_DT was expressed in a subset of Mef2GFP expressing leg disc cells, which likely represent the myoblasts that will give rise to the mesothoracic leg and jump muscle based on their position at the proximal region of the disc (Jaramillo *et al.* 2009). Although Mef2GFP could be detected in Him negative cells, it is possible these represent neuronal progenitors rather than myoblasts, which are thought to give rise to the neurons of the adult leg (Tse *et al.* 2022).

The HimGFP line was imaged at much higher resolution, showing subcellular co-localization of Him and Mef2 protein within the nucleus. Expression of both proteins overlap outside of the bright foci observed in the DAPI channel within the nucleus, which represent densely packed DNA in the form of heterochromatin (Kourmouli *et al.* 2004).

In summary, these data point towards a role for *Him* in the development of the tubular TDT, since *Him* loss-of-function causes an organizational phenotype in the structure of the muscle, which has functional behavioral consequences. The rescue data confirms that the phenotypes observed are down to loss of *Him* rather than an off-target, and that the tagged Him variants can substitute for endogenous Him during normal development. Since Him can be detected alongside Mef2 in the T2 leg imaginal disc myoblasts, it is plausible that the phenotypes observed are due to mis-regulation of Mef2 activity during TDT development. Indeed, Mef2 activity has previously been shown to be important to proper TDT development (Soler and Taylor, 2012, Vishal *et al.* 2023), so loss of a Mef2 regulator causing a phenotype is not unexpected.

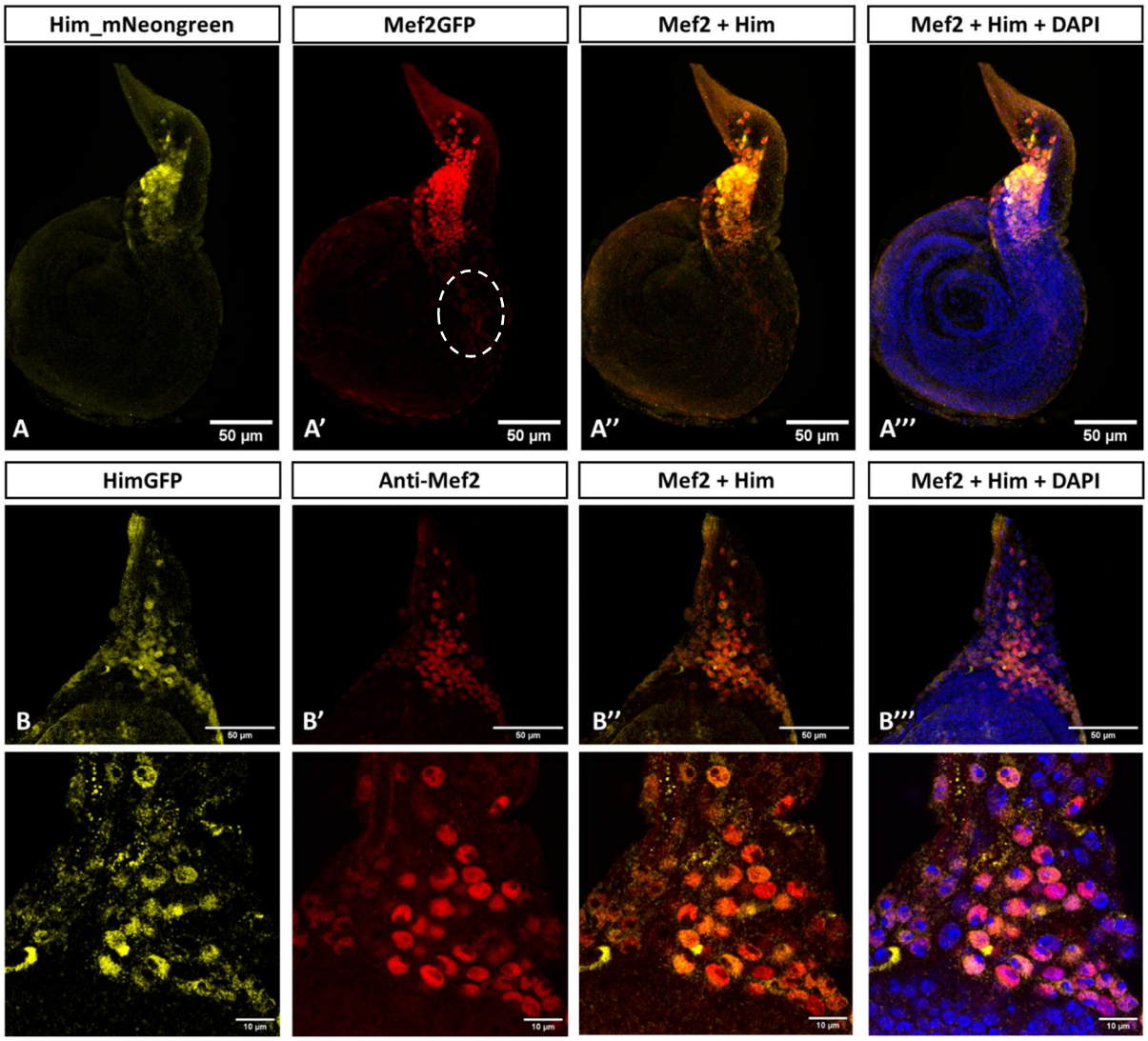

Figure 4.10 - Him and Mef2 co-localize in the T2 mesothoracic leg imaginal disc.

Maximum intensity projections of confocally imaged leg discs showing co-localization of Him and Mef2 in A) *Him_mNeongreen_DT*; *Mef2GFP* and B) *HimGFP* lines.

(A) Anti-mNeongreen labelled Him_mNeongreen_DT (yellow) co-localizes with (A') Anti-GFP labelled Mef2GFP (red) in the TDT progenitors situated in the notum of the leg disc, shown in the merge (A''). (A''') Counter-staining with DAPI labels all the nuclei of the imaginal disc. A subset of cells express a low level of Mef2, but no Him (white dashed circle). (n=5 discs).

(B) High magnification (20x and 63x) projections show that Anti-GFP labelled HimGFP (yellow) co-localizes with (B') anti-Mef2 labelled cells (red), demonstrated in the merge (B''). (B''') DAPI labelled foci do not overlap with Mef2 and Him expression in the nucleus. (n=4 discs).

4.8 *Him* loss-of-function causes a reduction in the number of Eve+ pericardial cells in the embryo

Pericardial cells represent the only non-myogenic cell type that are known to express Him (Elwell *et al.* 2015; Panta *et al.* 2020). They can be found next to the cardiomyocytes that make up the embryonic heart tube, acting to filter the hemolymph on its journey into the heart proper (Choma *et al.* 2011). Since pericardial cells share a lineage with a subset of the larval somatic muscles, they represent a viable model to explore how particular factors can influence their correct specification and development.

Here, I characterize a *Him* loss-of-function phenotype that affects the number of pericardial cells present in the late embryonic heart. Embryos were antibody stained against the pericardial cell marker Eve, which labels two pericardial cells per abdominal hemi-segment A2-A7, and one cell in hemi-segments A1 and A8 (Ward and Skeath, 2000). Only abdominal segments were analyzed, since Eve labels a cluster of overlapping pericardial cells in the thoracic segments that are difficult to quantify (Figure 4.11).

A significant reduction in abdominal Eve+ pericardial cell number was detected in both the *Himφ* (n=18 embryos) and *Him52* (n=19) mutants when compared to Oregon R control embryos (n=20) (Figure 4.11). In both mutants, there were hemi-segments that were missing either just 1, or both, Eve+ pericardial cells. No bias for particular abdominal segments being disproportionately affected was observed.

The HimGFP minigene was able to rescue both the *HimΦ* and *Him52* mutant pericardial cell counts towards wild-type. Since only male F1 embryos retained a Him mutant background, an antibody against Sxl was used to select against female embryos. Both mutants, when rescued, were indistinguishable from control embryos in the arrangement and number of Eve+ pericardial cells.

These data demonstrate a role for Him in the development of the correct patterning of the pericardial cell network, and provide further evidence that the HimGFP minigene can substitute for endogenous Him. However, it remains unknown whether the reduction in pericardial cells is due to original mis-specification of their progenitors, or something later in development is going awry.

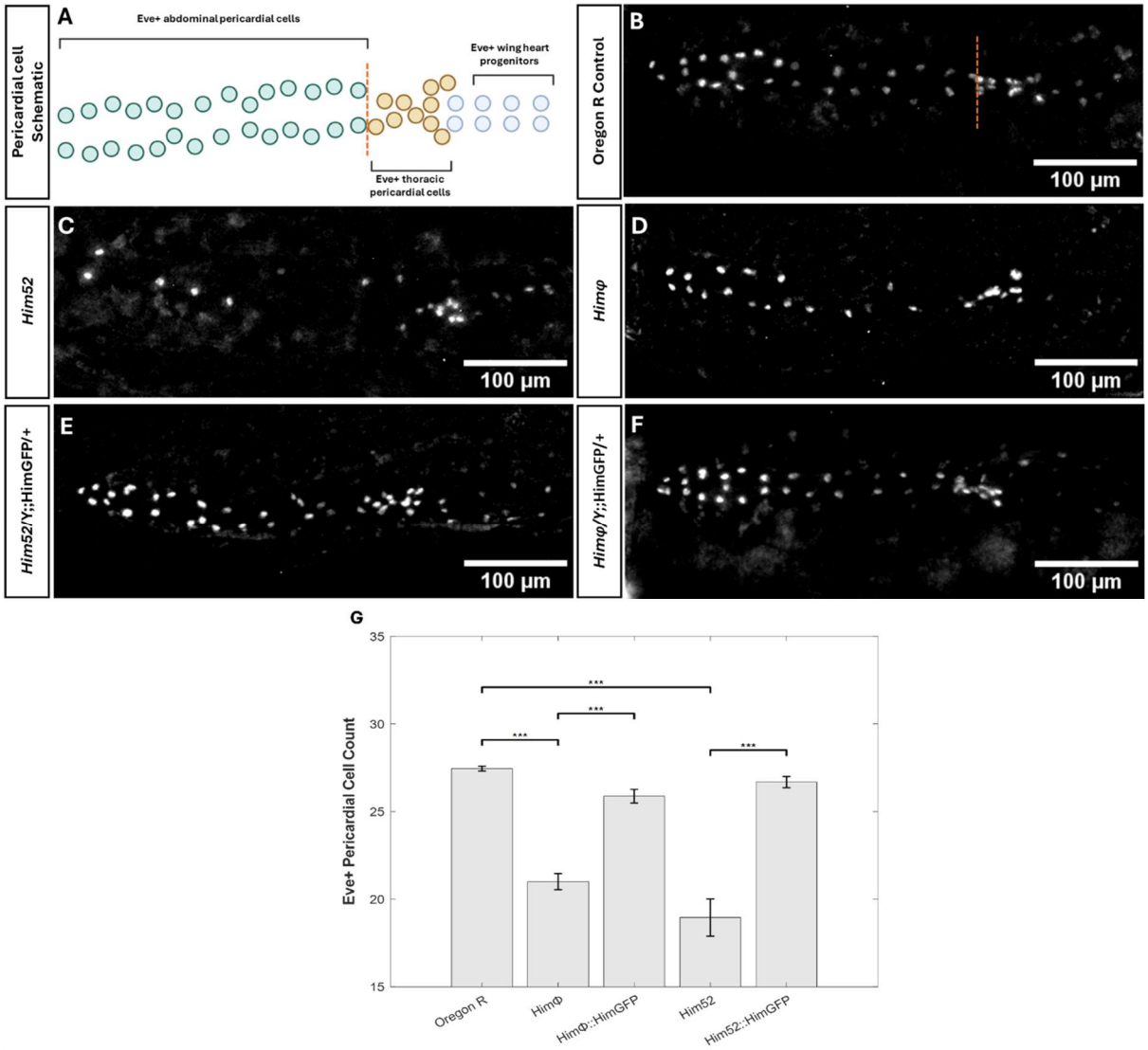

Figure 4.11 - *Him* loss-of-function results in a reduction in the number of Eve+ pericardial cells.

(A) A schematic showing the Eve+ abdominal pericardial cells (green), Eve+ thoracic pericardial cells (yellow) and Eve+ wing heart progenitors (blue) of the late stage *Drosophila* embryo when viewed from the dorsal side. The orange dotted line denotes the boundary between the abdominal pericardial cells which were counted in this analysis, and the thoracic pericardial cells which were not.

(B-F) Dorsal views of late-stage embryos stained with anti-Eve imaged using standard fluorescent microscopy. Representative examples of (B) Oregon R controls, (C) *Him52* mutants, (D) *Himφ* mutants, (E) *Him52*/Y;;*HimGFP*/+ rescue and (F) *Himφ*/*Y*;;*HimGFP*/+ rescue embryos. (G) A bar graph showing mean pericardial cell count per genotype ± SEM. *Him* mutants have significantly fewer abdominal Eve+ pericardial cells than Oregon R controls (Kruskal Wallis followed by Post-Hoc Dunns test: Oregon R vs *Himφ*/Y ***p<0.0001, Oregon R vs *Him52*/Y ***p<0.0001). The *HimGFP* minigene rescued the phenotype towards wild-type (Kruskal Wallis followed by Post-Hoc Dunns test: *Himφ*/Y vs *Himφ*/Y;;*HimGFP*/+ ***p=0.0006, *Him52*/Y vs *Him52*/Y;;*HimGFP*/+ ***p<0.0001). (n=18-20 embryos per genotype).

4.9 Discussion

To date, Him function has largely been characterized through overexpression experiments, which have demonstrated an inhibitory effect on both embryonic and adult muscle development. Overexpression of Him during embryonic myogenesis results in a severe muscle phenotype, with a substantial reduction in myosin expression observed. Similarly, when Him is overexpressed during adult muscle development, formation of the DLMs is considerably inhibited (Liotta *et al.* 2007; Soler and Taylor 2009).

In this chapter, I have built on the published knowledge of *Him*, using a combination of pre-existing and newly developed tools. Traditionally, Him has been visualized using a HimGFP minigene in combination with an anti-GFP antibody. In both the embryo and the wing imaginal disc, its expression is seen to decline as muscle development proceeds, supporting the view that Him represses myogenesis (Liotta *et al.* 2007; Soler and Taylor 2009).

The generation of the Him_mNeongreen tool allows us to study Him expression with much more precision than the pre-existing HimGFP tool. This CRISPR strategy to generate N-terminal directly tagged proteins is extremely powerful for genetic analysis. The incorporation of the fluorophore upstream of *Him*'s endogenous start codon initially results in a null allele for phenotyping loss-of-function, as well as providing a readout of *Him* promoter activity, as in the *Him_mNeongreen_NR* line. Following exposure to Cre-recombinase and generation of the directly tagged protein, Him protein dynamics can be visualized live. This strategy is adaptable for any protein, and the fluorophore in the N-terminal direct tag vector can be swapped out for any other with basic cloning methodologies. In the case of *Him*, we chose mNeongreen for its fast maturation time (10 minutes), and its high relative brightness compared to eGFP (Shaner *et al.* 2013).

Studying Him_mNeongreen expression in the late L3 larval wing imaginal disc demonstrates that Him protein expression is not uniform throughout the AMP population as previously suggested, but instead largely localizes to a particular group of cells in the discs' anterior presumptive lateral hemi-notum. A potential explanation for the discrepancy between the HimGFP expression pattern and the tagged CRISPR alleles is that the minigene doesn't accurately recapitulate endogenous Him

expression, due to genomic position effect of the transgene. Alternatively, antibody staining may mask the true expression pattern of mature Him protein due to amplification of the signal in cells expressing a low level of Him. Indeed, this seems true of *Him_mNeongreen_NR*, where the localized reporter gene expression seen live is no longer observed when antibody stained. This result highlights the need to study protein expression live at its endogenous level, wherever possible.

Interestingly, the same region of the disc where relatively high Him expression is detected, is also home to AMPs that express high levels of several *E(spl)* genes, known targets of the Notch signaling pathway including *E(spl)m6-BFM*, *E(spl)m7-HLH*, *E(spl)m3-GLG* and *E(splt)mbeta-HLH* (Zappia *et al.* 2019). Similarly, the *Him* promoter contains several Su(H) binding sites, suggesting that Notch signaling may play a role in ensuring this localized pattern of *Him* expression (Panta *et al.* 2020). From their scRNAseq profile, these cells represent clusters that are considered to be developmentally naïve, expressing high levels of myogenic repressors, such as Him and Twist, unlike the rest of the AMP population which has begun its journey down the developmental pathway.

Evidence to date suggests that Him is acting through Mef2 to inhibit myogenesis until the correct developmental time-point. For example, Him overexpression induced phenotypes in both the embryo and pupa are rescued towards wild-type with Mef2 overexpression (Liotta *et al.* 2007; Soler and Taylor 2009). Similarly, I have shown that overexpression of Him can repress Mef2 overexpression induced premature muscle differentiation in the wing imaginal disc. Mechanistically, Him mediated Mef2 repression is likely through a direct protein-protein interaction, which I've shown is theoretically possible using the Y2H assay. An in-house Mef2-mScarlet3 directly tagged allele is currently being generated, which will permit future FRET based analysis of Him and Mef2's interaction in live preparations of our tissue of interest; a gold-standard approach for studying protein-protein interactions.

Him's N-terminal WRPW motif is suggestive of an interaction with the conserved transcriptional repressor Groucho (Gro), which is known to interact with other proteins through this domain (Fisher *et al.* 1996). Whilst Gro is not known to bind DNA itself, it is regularly implicated within transcriptional repressor complexes (Mannervik, 2014). For example, during early embryogenesis, the well characterized

transcription factor Dorsal is converted from a transcriptional activator, to a repressor based on its interaction with Gro (Chambers *et al.* 2017). It is possible that Him is acting as an adapter protein to permit a Gro-Mef2 interaction, which would function to inhibit Mef2-dependent gene transcription until the correct time. Indeed, co-staining of Him_mNeongreen_DT and Mef2_GFP in the wing imaginal disc demonstrates an overlap in expression profile specifically within the naïve subclusters of AMPs, which do not yet have the hallmarks of a differentiating myoblast (Zappia *et al.* 2019). A Chip-Seq omics-based approach to compare Mef2-Gro DNA binding dynamics through developmental time would shed light on this potential interaction.

Previous to this work, detecting a penetrant *Him* loss-of-function phenotype has proven difficult. Driving *UAS-Him-RNAi* during embryonic or adult muscle development results in mild, low penetrance disruption to muscle morphology (Liotta *et al.* 2007; Soler and Taylor 2009). Since loss of *Him* function is homozygous viable, this suggests that some major muscle defect is not present, else flies would not complete development. Nonetheless, I explored *Him* loss-of-function with three mutant alleles, *Him52*, *HimΦ* and *Him_mNeongreen_NR*. The DLM dataset I have presented does not provide compelling evidence that loss of Him function significantly affects development of this major muscle subset. As a repressor of Mef2 activity, *Him* loss-of-function would be expected to phenocopy Mef2 overexpression. Since overexpression of Mef2 during adult myogenesis only results in a mild DLM phenotype, it is not surprising that *Him* loss-of-function doesn't majorly affect DLM formation (Chapter 5, Figure 5.6). Another Notch-regulated repressor of Mef2 activity, Zfh1, is also expressed in adult muscle progenitor cells alongside Him (Siles *et al.* 2013; Zappia *et al.* 2019). It is possible that Zfh1 can compensate for loss of Him, so double knockdown analysis might be required to see a substantial effect in these muscles.

In collaboration with Professor Richard Cripps lab, we've identified and characterized a 100% penetrant phenotype in the tubular TDT, or jump muscle (Mitchell-Gee *et al.* 2024). Immunostainings for Him shows co-localization with Mef2 in the T2 mesothoracic leg disc, which contains the myoblasts that will later give rise to the TDT. Therefore, it is possible that Him is fulfilling a similar role in the leg disc as the wing disc, as a repressor of Mef2 activity until development proceeds. With loss of

Him, we observe structural abnormalities in the organization of this muscle. Consequently, affected flies cannot jump as far as wild-type controls, demonstrating a functional consequence to the impaired morphology. Both the morphological and functional phenotypes could be rescued with the HimGFP minigene. This provides reassurance that the phenotypes observed were due to loss of *Him*, rather than some off-target effect, and that the HimGFP minigene can behave like wild-type Him in the context of TDT development.

It is possible that development of the TDT is more sensitive to subtle changes in Mef2 activity than the development of the DLMs. This would explain why loss of *Him* causes a fully penetrant phenotype specifically in the TDT. Indeed, a Mef2-S98A point mutant, which is hypothesized to have increased transcription factor activity compared to wild-type, results in a mild TDT organizational phenotype, whilst DLMs develop normally (Vishal *et al.* 2023). Plausibly, TDT development requires a lower level of Mef2 activity than the development of the fibrillar DLMs. This would mean that loss of Mef2 inhibition by *Him* would have a greater net impact during TDT development compared to DLM development. In this scenario, the subsequent increase in Mef2 activity, whilst not catastrophic to DLM formation, has significant implications for the TDT. Some evidence for this is provided by Mef2-RNAi experiments, which when performed specifically at 25^{o}C with a myoblast specific driver, results in a complete absence of DLMs, whereas the TDT and leg muscles are less drastically affected (Soler *et al.* 2012). Conversely, Mef2 overexpression results in a strong TDT phenotype, which morphologically resembles the loss of *Him* I have presented here (Vishal *et al.* 2023).

Future research could build on these data using a Mef2_mScarlet3 allele currently being generated in house. FRET-based analysis of *Him_mNeongreen*; *Mef2_mScarlet* during TDT development could confirm the ideas discussed here; that Him is acting as a repressor of Mef2 activity, and that the loss-of-function phenotype observed is due to Mef2 dysregulation.

In addition to the TDT dataset, I have begun characterization of an additional *Him* mutant phenotype; loss-of-function results in a reduction in the number of Eve positive pericardial cells. These non-myogenic cells share a lineage with the DA1 somatic muscles which develop during embryogenesis (Frasch and Levine 1987). A

previous in-house dataset shows that the DA1 muscles are frequently duplicated in *Him52* mutant embryos, suggesting that loss of *Him* function could result in initial mis-specification of the founder cells that give rise to the pericardial cells and DA1 muscles (Dan Hancock, PhD Thesis, Cardiff University). A role for Mef2 in founder cell specification during embryogenesis has not been thoroughly explored, but these preliminary data suggests the level of Mef2 activity at this stage might matter, so warrants further investigation. Another interesting aspect of pericardial cell biology is that these cells express a high level of both Zfh1 and Him, repressors of myogenesis that are known to act through Mef2 (Panta *et al.* 2020). Therefore, this system represents a viable model to not only study a role for Mef2 in founder cell specification, but also to explore the action of Mef2 inhibitors in ensuring the correct developmental outcome.

Chapter 5. Mef2 activity is regulated by its sumoylation motif

5.1 Introduction

A previous in-house dataset identified a potential interaction between mouse Mef2C and PIAS1, a member of the PIAS family of SUMO E3 ligases. These enzymes contribute to the SUMO modification of target substrates; the covalent attachment of an ~100 amino acid peptide via an isopeptide bond, typically to a lysine acceptor on the modified protein (Matunis *et al.* 1996; Mahajan *et al.* 1997). There are numerous examples of PIAS family members interacting with transcription factors in the literature, including AIRE, SOX9, NFκB and PITX2, all of which have some aspect of their biology altered as a consequence of the resultant sumoylation (Liu *et al.* 2005; Hyun *et al.* 2007; Ilmarinen *et al.* 2008; Wang *et al.* 2013). Sumoylation is usually considered a repressive modification, reducing the transcriptional activity of target transcription factors. Mechanistically, this repression can be achieved through a variety of routes - by altering sub-cellular localization, affecting DNA binding capability or protein stability, or by enhancing co-repressor interaction (Rosonina *et al.* 2017). Thus, SUMO-modification is particularly relevant to transcription factor regulation, as it can significantly impact upon transactivation potential.

Previous studies have already implicated sumoylation in the regulation of Mef2 activity (Grégoire *et al.* 2006; Kang *et al.* 2006; Riquelme *et al.* 2006; Shalizi *et al.* 2007), For example, a sumoylation deficient mouse Mef2C-K391R mutant is more active than wild-type Mef2C in cell culture, more efficiently converting fibroblasts into myoblasts. SUMO modification of Mef2 is dependent on prior phosphorylation of the downstream serine residue, S396, as a Mef2C-S396A phosphorylation deficient mutant is less sumoylated *in vitro* and *in vivo*. Consequently, this mutant is significantly more active than wild-type Mef2 in a luciferase reporter assay, phenocopying Mef2C-K391R (Kang *et al.* 2006). It remains an open question as to the mechanism by which SUMO modification of Mef2 reduces its activity. Sumoylation does not appear to alter Mef2's DNA binding capability, its stability, its sub-cellular localization, nor enhance its interaction with HDACs, which are characterized repressors of Mef2 activity (Gocke *et al.* 2005; Kang *et al.* 2006).

The sumoylation pathway is well conserved, but simplified, in *Drosophila melanogaster*. The pathway consists of the sequential activities of an E1 activating enzyme, E2 conjugating enzyme and E3 ligase. The E1 and E2 enzyme families consist of only a few, extremely well conserved proteins (Table 4). The E3 ligases are far more diverse in their membership comprising several families of enzymes, which are thought to confer substrate specificity and enhance reaction catalysis (Gareau and Lima 2010).

The E1 activating enzymes form a bipartite complex consisting of SAE1 and SAE2 subunits (Aos1/Uba2 in *Drosophila*), whose function is to catalyze the formation of an Adenosine Monophosphate (AMP)-SUMO intermediary. This is then passed onto the sole E2 conjugating enzyme, Ubc9, which either alone, or in collaboration with an E3 ligase, covalently attaches the SUMO peptide to an ε-amino group of the target lysine residue (Lomelí and Vázquez 2011). Since the in-house Y2H screen identified PIAS1 as a mouse Mef2C interactor, this indicates that the PIAS family is the relevant enzymatic group implicated in Mef2 regulation. Su(var)2-10 is the only PIAS family member in the *Drosophila* system, so it represents the sole E3 ligase candidate for promoting *Drosophila* Mef2 sumoylation.

Acting in the opposite direction of the sumoylation pathway are the SUMO deconjugating enzymes: a family of cysteine proteases that act to cleave the isopeptide bond between the SUMO peptide and modified protein. There are at present three characterized groups of these enzymes the Ulp/SENP, Desi and USPL1 families (Nayak and Müller 2014). In an overexpression model, SENP2 significantly decreased Mef2A sumoylation in 293T cells, suggesting that this is the relevant enzyme to Mef2A SUMO-deconjugation. In agreement with this, SENP2-/- mouse embryos accumulate the sumoylated form of MEF2A (Lu *et al.* 2013). *Drosophila* only has two characterized Ulp/SENP family members, *Ulp1* and *Ulp2*. Of these, *Ulp1* is the SENP2 orthologue, and thus the more likely to be implicated in Mef2 regulation if the interaction is conserved (Nayak and Müller 2014).

Sumoylation has not yet been explored in the context of muscle development, so this chapter represents a first exploration into this field, using *Drosophila* adult myogenesis as a model system. I characterize the effect that both loss- and gain-of-function of sumoylation machinery has on muscle differentiation as a whole, by

studying the DLMs post-development after genetic manipulation of pathway components . To determine Mef2-specific effects of sumoylation, I have generated a series of mutant Mef2 constructs. This includes a sumoylation deficient K352R, a phosphorylation deficient S357A and a phosphomimetic S357E mutant, each of which is predicted to alter the net sumoylation status of Mef2.

Table 4. Overview of genes encoding sumoylation and SUMO-deconjugating pathway components in vertebrate and *Drosophila* systems.

Enzymatic Role	Vertebrate Genes	*Drosophila* Genes
SUMO Peptide	*SUMO1, SUMO2, SUMO3*	*smt3*
E1 Activating Enzyme	*SAEI/SAE2* heterodimer	*Aos1/Uba2* heterodimer
E2 Conjugating Enzyme	*Ubc9*	*Ubc9* (AKA *lwr*)
E3 SUMO Ligases – PIAS family	*PIAS1, PIAS3, PIASx, PIASy*	*Su(var)2-10*
Other E3 SUMO Ligases	*RanBP2, Pc2, Mms21, Trim24, TRIM33, TRIM28, TRIM19, TRIM27, TRIM11, TRIM22, SLX4, ZNF451*	*Tonalli, Nup358*
SUMO deconjugating Enzymes	*SENP1, SENP2, SENP3, SENP5, SENP6, SENP7, DESI1, DESI2, USPL1*	*Ulp1, Ulp2*

5.2 Loss-of-function of *Drosophila* sumoylation machinery inhibits adult myogenesis

In order to determine if the sumoylation pathway is relevant to *Drosophila* adult muscle development, the sole E2 conjugating enzyme Ubc9, and E3 ligase PIAS1 homolog, Su(var)2-10, were knocked down separately using *1151Gal4* driven UAS-RNAi lines to determine if DLM development was affected. When the crosses were performed at 25°C, *Ubc9* RNAi and *Su(var)2-10* RNAi were both late pupal lethal, presumably due to defects in the musculature required to eclose from the pupal

case. Consequently, DLM transverse cross-sections were analyzed in pharate flies, to determine the extent that loss of sumoylation pathway function impacts upon muscle development, by analyzing the number of DLMs that form (Figure 5.1).

Whilst 88% of *1151Gal4* control pharate hemithoraces possessed a wild-type number of 6 DLMs, a few individuals had only 4 or 5 DLMs in a hemithorax, likely due to a failure in template splitting, resulting in a mean DLM count of 5.9 (n=50 hemithoraces). RNAi against the SUMO E3 ligase *Su(var)2-10* at 25◦C was performed with two separate RNAi lines, BL32956 from the TRiP collection (TRiP[HMS00750]) (n=44) and VDRC100813 from the KK collection (KK100813) (n=28). Both lines resulted in a significant decrease in the number of DLMs compared to *1151Gal4* controls. BL32956 resulted in significantly more severe phenotype than KK100813, with a mean of 1 DLM per hemithorax vs 4.3 DLMs per hemithorax respectively. This could be due to differing knockdown efficiencies between the short hairpin TRiP RNAi line, and the long hairpin KK line. Short hairpin RNAi is widely considered a more effective strategy in maximizing RNA knockdown in *Drosophila*, so the stronger phenotype elicited by the TRiP line is not surprising (Dietzl *et al.* 2007; Bartoletti *et al.* 2017). When the cross was performed at 18◦C (n=32), the BL32956 phenotype was less severe than at 25◦C, consistent with the temperature dependent nature of the Gal4/UAS system (Brand *et al.* 1994). RNAi knockdown of *Ubc9* RNAi (GD33685) at 25◦C also resulted in a significant reduction in mean DLM count compared with control, to 3.11 per hemithorax (n=36).

These data indicate that the sumoylation pathway is relevant to *Drosophila* adult myogenesis, as DLM formation is perturbed with pathway loss-of-function in developing muscle. Since the Ubc9 E2 enzyme acts before the E3 Su(var)2-10 in the sumoylation pathway, it would be expected that loss-of-function of *Ubc9* would phenocopy loss-of-function of *Su(var)2-10*. The observed difference in phenotype severity could be attributed to RNAi knockdown efficiency, which can be extremely variable between lines (Dietzl *et al.* 2007; Schnorrer *et al.* 2010). These data cannot be tied to a Mef2-specific effect at this stage, since RNAi against *Ubc9* and *Su(var)2-10* during muscle development will affect the sumoylation state of more proteins than just Mef2.

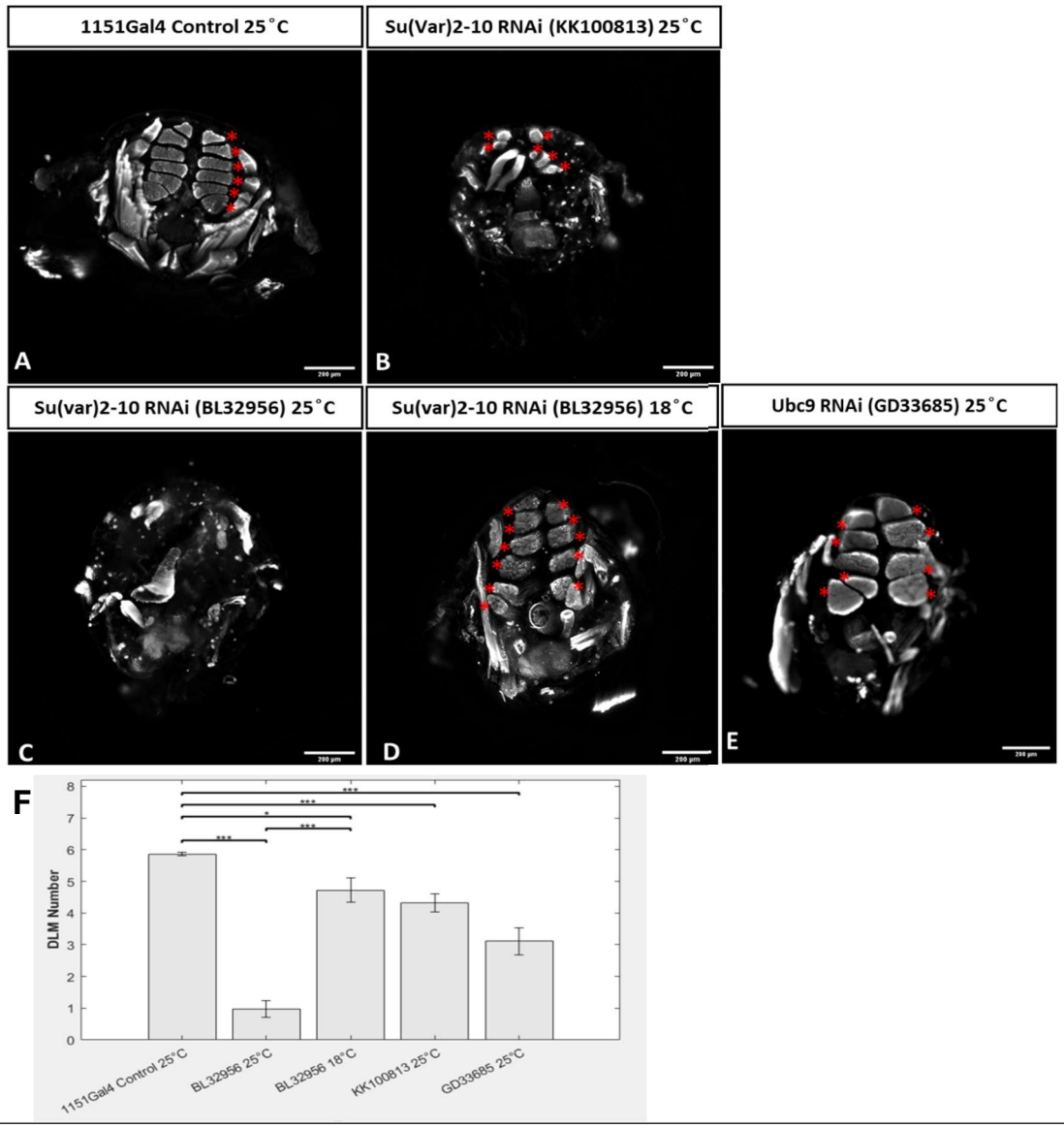

Figure 5.1 - Muscle-specific knockdown of sumoylation machinery inhibits myogenesis.

Representative fluorescent microscopy images of phalloidin stained transverse cross-sections to visualize pharate pupal DLMs in *1151Gal4* controls, *1151Gal4>Ubc9-RNAi* or *1151Gal4>Su(var)2-10-RNAi* flies. Flies were reared at either 25◦C or 18◦C as indicated. (A) *1151Gal4* control hemithorax [25◦C], (B) *1151Gal4>Su(var)2-10-RNAi* [KK100813] [25◦C], (C) *1151Gal4>Su(var)2-10-RNAi* [BL32956] [25◦C], (D) *1151Gal4>Su(var)2-10-RNAi* [BL32956] [18◦C] and (E) *1151Gal4>Ubc-RNAi* [GD33685] [25◦C]. Red asterisks denote each DLM fibre. (F) Bar graph showing mean DLM count ± SEM per genotype. Knockdown of *Su(var)2-10* with both independent RNAi lines results in a significant decrease in DLM number, as does *Ubc9* RNAi. *Su(var)2-10-RNAi* with the TRiP BL32956 line is rescued towards wild-type when the cross is performed at 18◦C rather than 25◦C (Kruskal Wallis followed by Post-Hoc Dunns test: *1151Gal4* control 25◦C vs BL32956 25◦C ***p<0.0001=, BL32956 25◦C vs BL32956 18◦C ***p<0.0001, *1151Gal4* control 25◦C vs BL32956 18◦C *p=0.034 , *1151Gal4* control 25◦C vs KK100813 25◦C ***p<0.0001, *1151Gal4* control 25◦C vs GD33685 ***p<0.0001). (n=28-50 hemithoraces per sample).

5.3 Overexpression of *Drosophila* sumoylation machinery inhibits adult myogenesis

To assess whether overexpression of sumoylation machinery affects DLM development, I first had to construct a *UAS-Su(var)2-10* line, since there was no commercially available option. I cloned the Su(var)2-10 isoform RD CDS into pUASt-AttB in-house, and inserted this into the AttP2 landing site via PhiC31 mediated recombination.

UAS-Ubc9 (Apionishev *et al.* 2001) and *UAS-Su(var)2-10* were overexpressed separately in developing muscle using the *1151Gal4* driver at 25°C and 29°C. Overexpression of *UAS-Su(var)2-10-AttP2* was pupal lethal, so pharate pupal thorax sections were analyzed and compared amongst genotypes (Figure 5.2).

Overexpression of *UAS-Su(var)2-10* has an inhibitory effect on DLM development, when the cross is performed at either 25°C (n=30 hemithoraces) or 29°C (n=88) (Figure 5.2). The mean DLM count observed is significantly reduced from 5.86 DLMs per hemithorax in *1151Gal4* controls, to 4.82 with Su(var)2-10 overexpression at 25°C, or 3.6 at 29°C. Conversely, *UAS-Ubc9* (BL9324) does not cause an observable DLM phenotype, even when the cross is performed at 29°C (n=36). Unlike Su(var)2-10 overexpression, *UAS-Ubc9* is not pupal lethal, and F1 progeny retain the ability to fly, indicating that DLMs develop and function correctly. The lack of phenotype with *UAS-Ubc9* suggests that the amount of endogenous Su(var)2-10 is rate limiting in this scenario, otherwise you would expect overexpression of these proteins to phenocopy one another. Moreover, these data provide evidence that Ubc9 requires E3 ligase co-operation to sumoylate target proteins in *Drosophila* muscle, as a phenotype would be expected if it were acting alone.

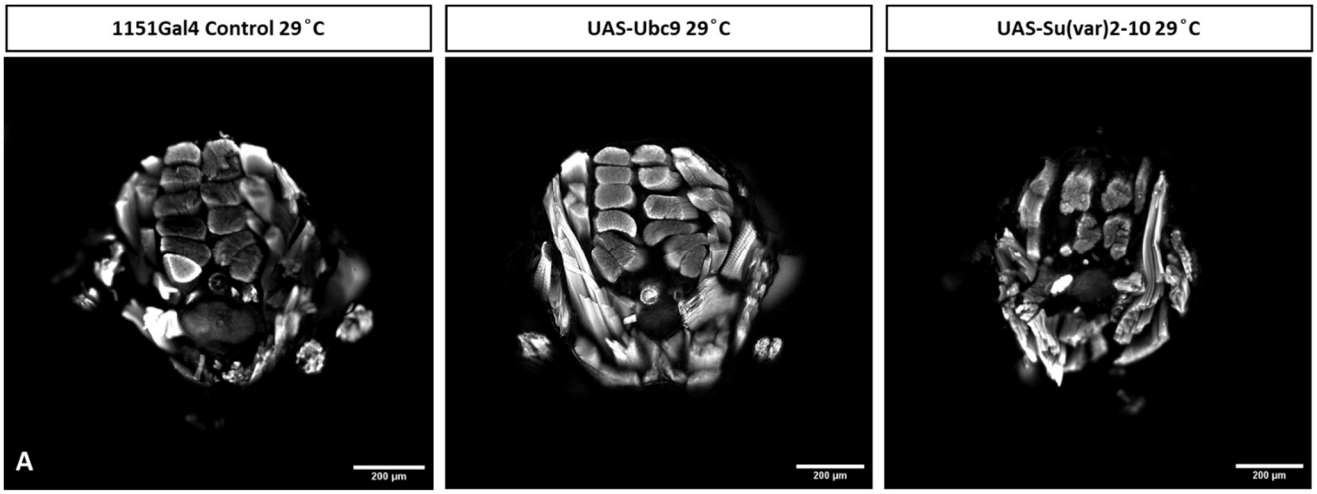

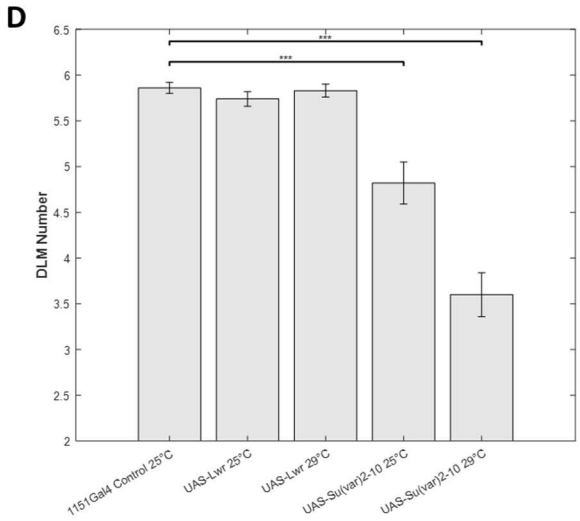

Figure 5.2 - Overexpression of Su(var)2-10, but not Ubc9, inhibits myogenesis.

Representative fluorescent microscopy images of phalloidin stained transverse cross-sections to visualize pharate pupal DLMs in *1151Gal4* controls, *1151Gal4>UAS-Ubc9* or *1151Gal4>UAS-Su(var)2-10*, each reared at 29◦C. (A) *1151Gal4* control hemithorax (n=50), (B) *1151Gal4>UAS-Ubc9* [BL9324] (n=36) and (C) *1151Gal4>UAS-Su(var)2-10-AttP2 (n=88)*. (D) Bar graph showing mean DLM count ± SEM per genotype. *1151Gal4* driven Su(var)2-10 overexpression at 25◦C and 29◦C causes a significant reduction in DLM number compared to wild-type, whereas Ubc9 overexpression does not. (Kruskal Wallis followed by Post-Hoc Dunns test: *1151Gal4* control 25◦C vs *UAS-Su(var)2-10* 25◦C ***p=0.0002, *1151Gal4* control vs *UAS-Su(var)2-10* 29◦C ***p<0.0001).

5.4 *Drosophila* Mef2 has a conserved phosphorylation dependent sumoylation motif (PDSM)

A multiple sequence alignment of Mef2 family members shows a high degree of conservation of a phosphorylation dependent sumoylation motif (PDSM) across a variety of taxa, suggesting an important, evolutionarily conserved function of this amino acid sequence.

The classical sumoylation consensus is ψKxE, in which the lysine is the target residue for SUMO modification. Ψ represents any bulky hydrophobic amino acid, such as isoleucine, leucine or valine. A PSDM consists of this core motif, in addition to a proline directed phosphorylation motif, three amino acids downstream. The multiple sequence alignment demonstrates that both the lysine target residue, and the proline directed phosphorylation site, are entirely conserved amongst diverse taxa including mammals, fish, insects and nematodes (Figure 5.3). Intriguingly, this conserved domain exists in an otherwise relatively unconserved stretch of Mef2's C-terminal transactivation domain, so is likely an important sequence in regulating proper Mef2 function that warrants further investigation.

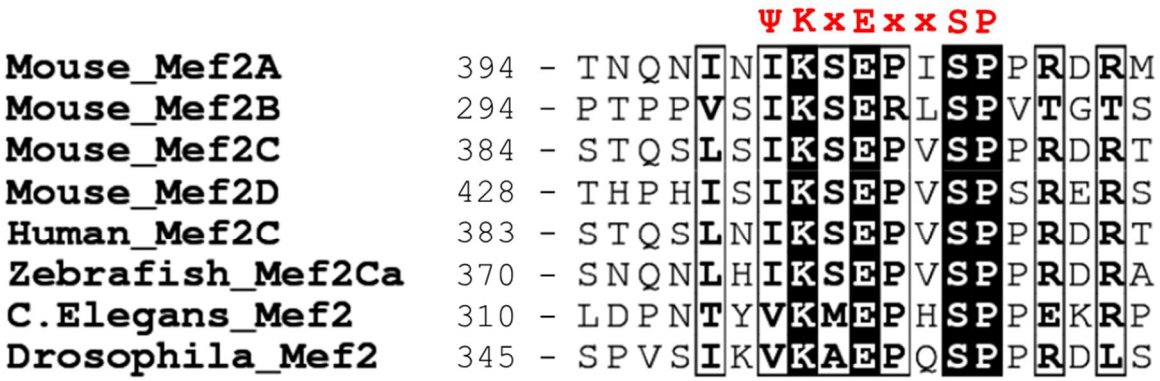

Figure 5.3 - *Drosophila* Mef2 has a conserved phosphorylation-dependent sumoylation motif (PDSM).

A multiple sequence alignment of the PDSM of Mef2 family members shows a high degree of conservation of key residues. The consensus PDSM (red text) is present in each of the Mef2 family members shown. Amino acids with similar biochemical properties are framed, identical amino acids are highlighted in black.

5.5 Su(var)2-10 can physically interact with *Drosophila* Mef2 in a Y2H assay

Whilst the loss- and gain-of-function experiments point towards important roles of sumoylation in muscle development as a whole, they do not inform on any specific effect on Mef2 regulation. The conservation of the PDSM strongly suggests that *Drosophila* Mef2 is subject to sumoylation, so I used a Y2H approach to determine if Mef2 can physically interact with sumoylation machinery.

A previous Y2H screen performed in the lab identified that the mammalian Su(var)2-10 homolog PIAS1 can interact with mMef2C (1-349). The PIAS1 fragment consisted of the protein's N-terminus (1-217), which contains a conserved SAP domain and approximately half of a conserved PINIT domain (Duval *et al.* 2003). Su(var)2-10 is the only PIAS family member in *Drosophila*, so is the likely E3 ligase candidate implicated in Mef2 regulation, if the interaction is conserved.

To determine whether this interaction is conserved with the conserved *Drosophila* homologs, I initially tested a Mef2 bait construct (1-350) against a full length Su(var)2-10 (1-601) prey construct. Yeast transformed with both plasmids could grow on plates lacking *His3*, indicating that the two proteins can indeed physically interact with one another in this system (Figure 5.4). Since *Drosophila* Mef2's sumoylation motif spans residues 352-357, outside of the tested fragment, this indicates that the two proteins interact through an alternative domain. A control consisting of empty bait vector PB27 and Su(var)2-10 (1-601) demonstrated that Su(var)2-10 does not auto-activate the His3 reporter. I have shown that Mef2 (1-350) cannot auto-activate this reporter previously (Figure 4.5).

A shorter N-terminal Mef2 fragment (1-156) could no longer interact with full length Su(var)2-10, suggesting that the Su(var)2-10 interacting domain resides somewhere between residues 157-350 within Mef2's N-terminal transactivation domain.

Whilst these data provides evidence that *Drosophila* Mef2 and Su(var)2-10 are capable of direct physical interaction within yeast, it provides no indication that they do within our *Drosophila* tissue of interest. Additionally, further mapping is required to define a more precise interaction domain.

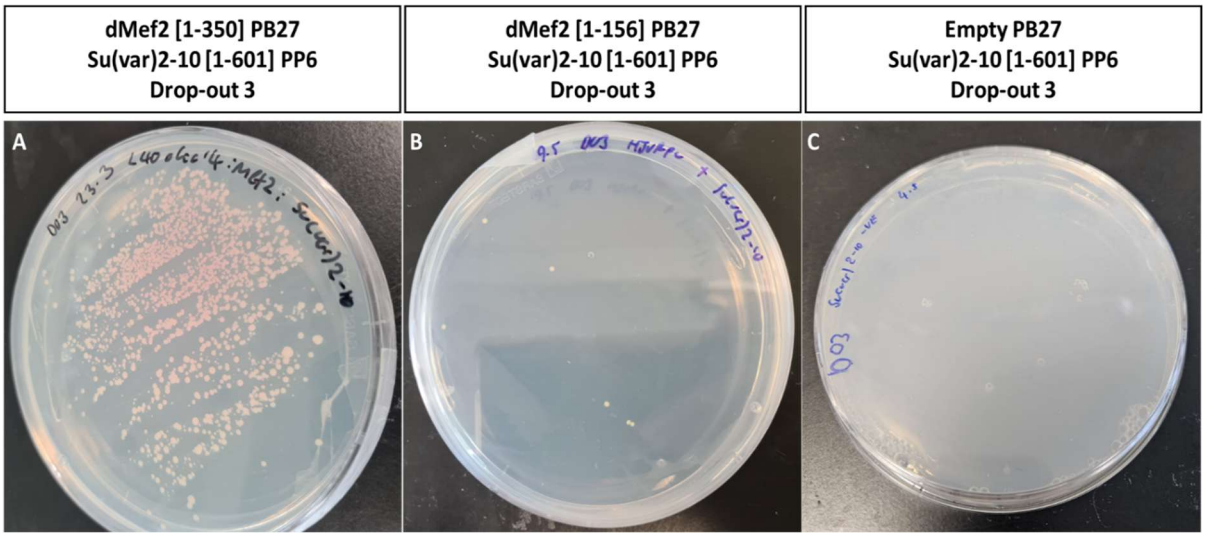

Figure 5.4 – Su(var)2-10 and Mef2 can physically interact in a Y2H assay.

Yeast transformed with both the PB27 bait plasmid (+TRP), and PP6 prey plasmid (+LEU) were grown on Drop-out 3 Media (-LEU/-TRP/-HIS) and evaluated for growth, to indicate a protein-protein interaction based on His3 reporter activation. Photographs of the resultant plates after 3 days growth of yeast transformed with (A) PB27-Mef2[1-350] and PP6-Su(var)2-10[1-601], (B) PB27-Mef2[1-156] and PP6-Su(var)2-10[1-601] and (C) an autoactivation control consisting of PP6-Su(var)2-10[1-601] and empty PB27 vector.

5.6 Su(var)2-10 is co-expressed with Mef2 in AMPs

To resolve whether Su(var)2-10 and Mef2 are co-expressed in the third instar larval wing imaginal disc associated AMPs, I used a tagged Su(var)2-10::GFP construct (VK00037), which was generated by the modERN project, in combination with anti-GFP and anti-Mef2 staining (Kudron *et al.* 2018). Confocally imaged immunostainings of wing imaginal discs isolated from late L3 wandering larvae show that Su(var)2-10::GFP and Mef2 are co-expressed in the nucleus of AMPs (Figure 5.5). Whilst Mef2 protein expression is limited to the AMP population, Su(var)2-10::GFP can be detected throughout the entire wing disc, consistent with the scRNAseq dataset which shows expression in every cell-type of the tissue (Zappia *et al.* 2019). These data, in combination with the Y2H result, is a strong indication that a Su(var)2-10 and Mef2 interaction exists and likely within the context of *Drosophila* adult muscle development.

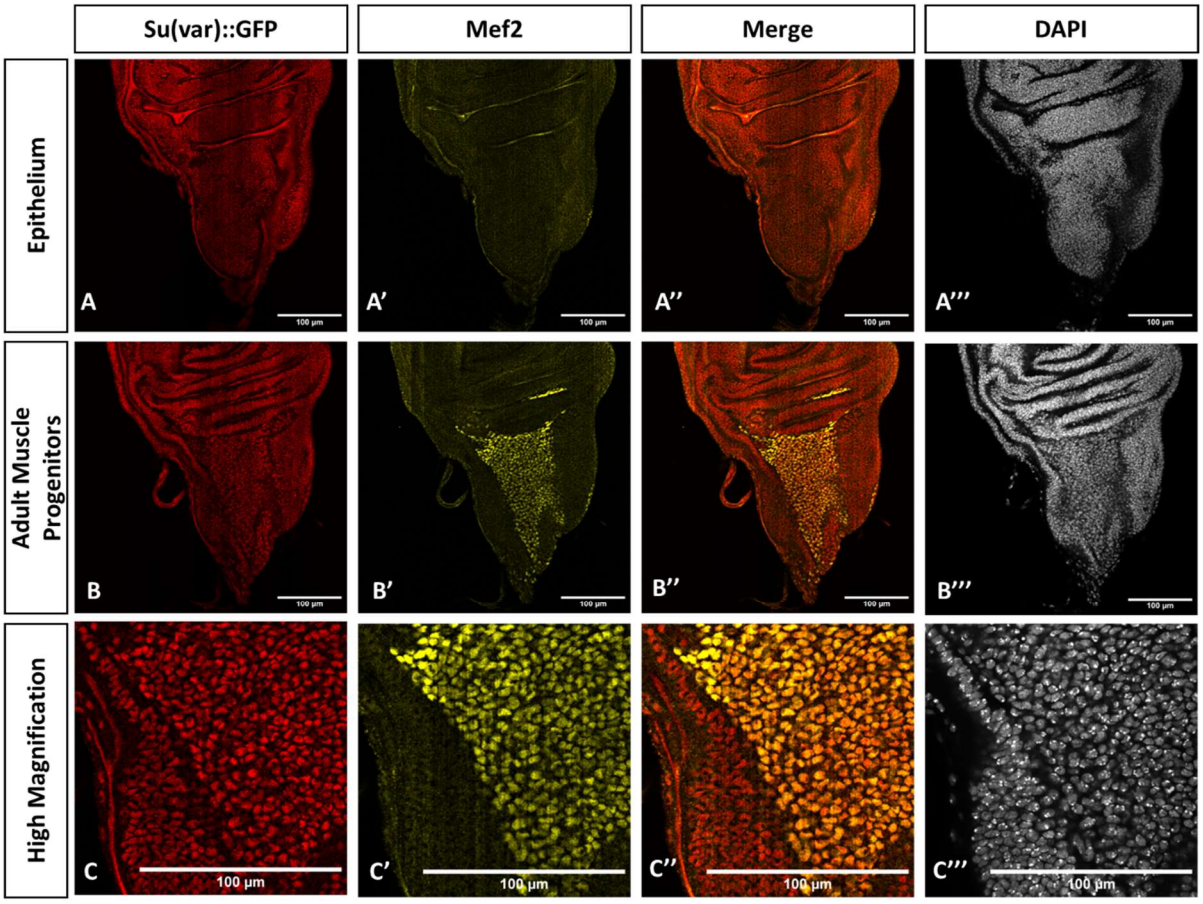

Figure 5.5 - Drosophila Mef2 and Su(var)2-10::GFP are co-expressed in adult muscle progenitors.

Single confocal slices of a representative wing imaginal disc isolated from late L3 Su(var)::GFP larvae stained with anti-GFP, anti-Mef2 and DAPI. (A-A''') An epithelial layer of the wing imaginal disc expresses Su(var)::GFP (red) but not Mef2 (yellow). (B-B''') The population of AMPS express both Su(var)::GFP and Mef2. (C-C''') 63x magnification showing Su(var)2-10::GFP and Mef2 localization in nuclei of AMPs, but not epithelial cells. (n=3 discs).

5.7 Overexpression of Mef2 sumoylation motif mutants form an allelic series of DLM Phenotypes

I constructed a series of Mef2 overexpression lines with the sumoylation motif mutated to assay how this domain impacts upon Mef2 activity. I generated a sumoylation deficient *UAS-Mef2[K352R]*, by mutating the hypothesized sumoylation target lysine residue to an arginine. Additionally, I constructed phosphorylation deficient *UAS-Mef2[S357A]* and phosphomimetic *UAS-Mef2[S357E]* lines, which are hypothesized to have opposite effects on determining Mef2's sumoylation state, if phosphorylation is indeed a pre-requisite, as presence of the motif suggests. Since

each construct is inserted into the same AttP2 landing site, the expression level of each transgene can be considered equivalent and therefore the results from their overexpression directly comparable. Initially, I overexpressed each of the constructs using *1151Gal4* at 25◦C, using quantification of pharate DLM phenotypes as an indirect readout of Mef2 activity, to determine whether Mef2 mutants enhance or repress the developmental phenotypes seen compared to the wild-type construct.

The different Mef2 overexpression constructs give rise to an allelic series of DLM phenotypes when overexpressed using *1151Gal4* at 25◦C (Figure 5.6). *UAS-Mef2[S357E]* overexpression results in a mean number of 5.76 DLMs per hemithorax (n=34 hemithoraces), *UAS-Mef2[WT]* 5.44 DLMs per hemithorax (n=32), *UAS-Mef2[S357A]* 5.08 DLMs per hemithorax (n=36) and *UAS-Mef2[K352R]* 4.03 DLMs per hemithorax (n=30). This allelic series reflects the predicted sumoylation state of each overexpression construct, with sumoylation susceptible Mef2 proteins causing less severe muscle phenotypes than sumoylation deficient Mef2s. Interestingly, *UAS-Mef2[WT]* and the phosphomimetic *UAS-Mef2[S357E]* phenocopy one another, both causing only a mild DLM phenotype when overexpressed with *1151Gal4*. It is plausible that *UAS-Mef2[WT]* exists in a largely sumoylated form, since in this assay it behaves similarly to the S357E mutant which mimics constitutive phosphorylation, and should therefore also be constitutively sumoylated. Similarly, the phospho-mutant and sumoylation deficient Mef2's have a significantly greater impact on the DLM phenotype than the other constructs. This is consistent with a model whereby phosphorylation-dependent sumoylation acts to repress Mef2 activity, since in its absence a greater impact on muscle development is observed. These data provide compelling evidence that Mef2's PDSM is indeed relevant to its function, since point mutations in the motif significantly alter phenotype severity with Mef2 overexpression.

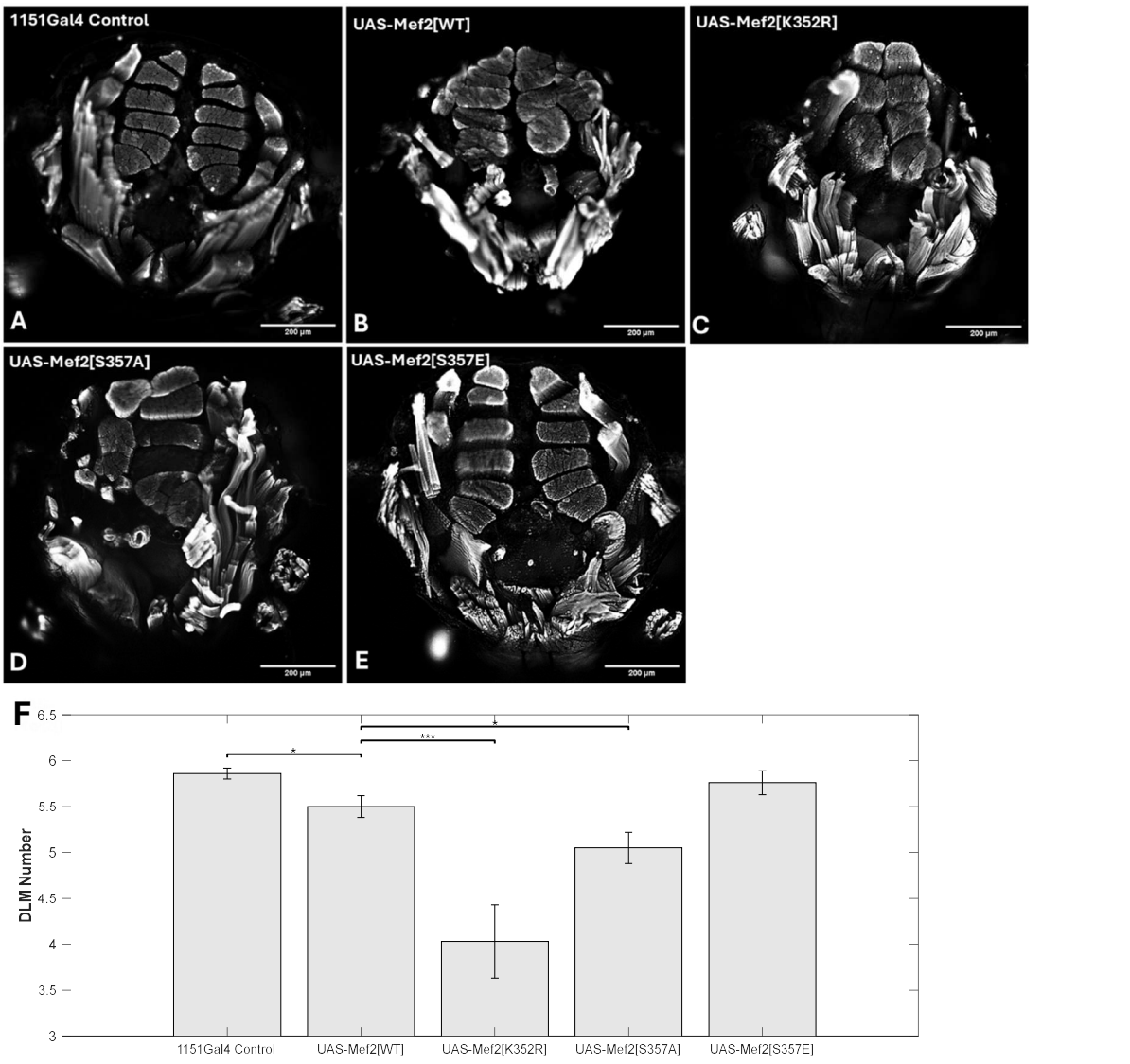

Figure 5.6 - Overexpression of Mef2 sumoylation motif mutants form an allelic series of DLM phenotypes.

Fluorescent microscopy images of phalloidin stained transverse cross-sections to visualize pharate pupal DLMs in *1151Gal4* controls, overexpression of wild-type Mef2 or overexpression of the mutant Mef2 constructs, each raised at 25°C. Representative examples of (A) a *1151Gal4* control hemithorax, (B) overexpression of wild-type Mef2, (C) overexpression of sumoylation deficient Mef2[K352R], (D) overexpression of phosphorylation deficient Mef2[S357A] and (E) overexpression of phosphomimetic Mef2 [S357E]. (F) Bar graph showing mean DLM count ± SEM per genotype. Overexpression of sumoylation deficient Mef2 and phosphorylation deficient Mef2 both result in a significantly worse DLM phenotype than overexpression of wild-type Mef2 (Kruskal Wallis followed by Post-Hoc Dunns test: *1151Gal4* control vs *UAS-Mef2[WT]* *p=0.0283 , *UAS-Mef2[WT]* vs *UAS-Mef2[K352R]* ***p=0.0003, *UAS-Mef2[WT]* vs *UAS-Mef2[S357A]* *p=0.03411). (n=30-36 hemithoraces per genotype).

5.8 Mef2 mutants cause higher activation of MhcGFP in the premature differentiation assay

As opposed to DLM quantification, the MhcGFP premature differentiation assay in the wing imaginal disc provides a more direct readout of Mef2 activity. I used this assay to compare how the transactivation potential of Mef2 mutants compared to wild-type Mef2 in the context of the wing imaginal disc. Mef2 UAS-constructs were overexpressed using *1151Gal4* at 25°C, and the resulting MhcGFP response quantified in the late L3 larval wing discs. Each sample was processed concurrently using the standardised protocol (see Methods 2.44), so that results could be directly compared between genotypes.

Each of *UAS-Mef2[K352R]* (n=15 discs), *UAS-Mef2[S357A]* (n=15) and *UAS-Mef2[S357E]* (n=23) resulted in enhanced activation of MhcGFP when compared to *UAS-Mef2[WT]* (n=23). MhcGFP quantification showed that each of the three Mef2 mutants induced significantly more MhcGFP than wild-type Mef2 in terms of both the area and integrated density of GFP observed (Figure 5.7). Each of the mutant Mef2 constructs behaved equivalently with one another in this assay. Whilst *UAS-Mef2[K352R]* and *UAS-Mef2[S357A]* were predicted to enhance Mef2 activity since SUMO-modification is blocked, enhanced activation by *UAS-Mef2[S357E]* is difficult to interpret as the phosphomimetic was designed to enhance Mef2 sumoylation state. Nonetheless, these data support the hypothesis that sumoylation-deficient Mef2 has a higher activity level than wild-type, therefore Mef2 sumoylation is an inhibitory modification in this context.

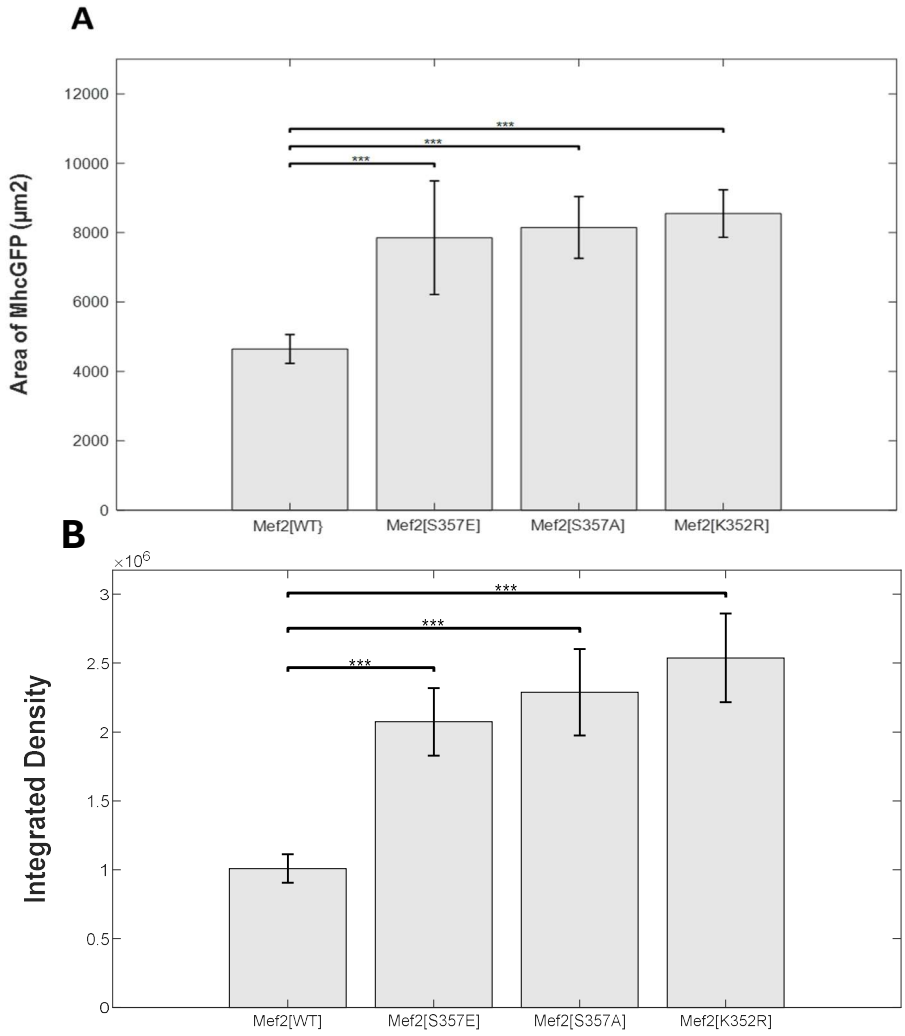

Figure 5.7 - Sumoylation motif mutant overexpression constructs are more active than wild-type in the wing imaginal disc premature differentiation assay.

1151Gal4;;MhcGFP driving overexpression of wild-type Mef2 or mutant Mef2 in the wing imaginal disc results in quantifiable genotype differences in MhcGFP activation in late L3 larvae raised at 25°C. (A) Bar graph showing mean area ± SEM of Mef2 overexpression induced MhcGFP. Phosphomimetic Mef2, phosphorylation deficient Mef2 and sumoylation deficient Mef2 all significantly enhance the area of MhcGFP observed compared to wild-type. (Kruskal Wallis followed by Post-Hoc Dunns test: *UAS-Mef2[WT]* vs *UAS-Mef2[S357E]* ***p=0.0006, *UAS-Mef2[WT]* vs *UAS-Mef2[S357A]* ***p=0.0010, *UAS-Mef2[WT]* vs *UAS-Mef2[K352R]*****p=0.0001).

(B) Bar graph showing mean integrated density ± SEM of Mef2 overexpression induced MhcGFP. Phosphomimetic Mef2, phosphorylation deficient Mef2 and sumoylation deficient Mef2 all significantly enhance the MhcGFP integrated density compared to wild-type. (Kruskal Wallis followed by Post-Hoc Dunns test: *UAS-Mef2[WT]* vs *UAS-Mef2[S357E]* ***p=0.0005, *UAS-Mef2[WT]* vs *UAS-Mef2[S357A]* ***p=0.0006, *UAS-Mef2[WT]* vs *UAS-Mef2[K352R]*****p<0.0001). (n= 15-23 discs per genotype).

5.9 Him's ability to repress Mef2 activity is diminished in the sumoylation deficient Mef2 mutant

Mechanistically, one route by which sumoylation can repress a target protein's activity is by enhancing its association with a repressor. To this end, I tested using the premature differentiation assay whether sumoylation deficient *UAS-Mef2[K352R]* activity could be repressed by Him, a known inhibitor of Mef2 activity (Figure 4.4, Soler and Taylor 2009). I applied a qualitive approach to the analysis, recording presence or absence of premature MhcGFP in each of the genotypes analyzed.

1151Gal4 driven *UAS-Mef2[WT]* (n=23 discs) and *UAS-Mef2[K352R]* (n=15) induced premature MhcGFP in 100% of L3 larval wing imaginal discs imaged at 25◦C (Figure 5.8). Whilst *UAS-Him* is able to completely repress *UAS-Mef2[WT]* induced premature MhcGFP in 100% of discs (n=15), this is reduced to 30% of discs with the *UAS-Mef2[K352R]* line (n=10). An alternative repressor of Mef2 activity, HDAC4 (Hubbert 2023) is still able to repress the activity of *UAS-Mef2[K352R]* in 100% of discs (n=18). These data demonstrate that Him's ability to repress Mef2 activity is diminished in the absence of Mef2 sumoylation, suggesting the interaction between Him and Mef2 may be enhanced based on Mef2's sumoylation state. This observation is specific to Him, as the rescue potential of an alternative Mef2 repressor, HDAC4, is unaffected by Mef2's sumoylation state in this assay.

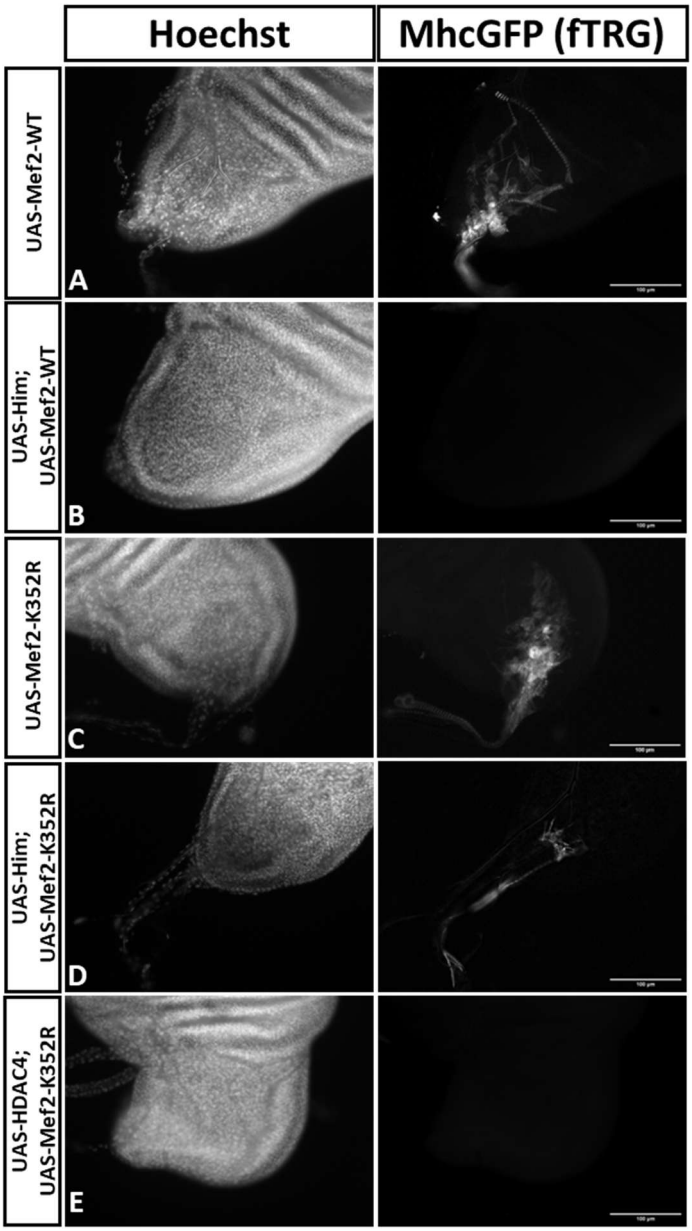

Figure 5.8 - Sumoylation-deficient Mef2 is more resistant to Him mediated repression.
Fluorescent microscopy images of MhcGFP counterstained with Hoechst, in the late L3 larval wing imaginal disc. (A) Overexpression of Mef2[WT] induces premature MhcGFP expression. (B) Co-overexpression of Him fully represses Mef2[WT] induced premature differentiation. (C) Overexpression of Mef2[K352R] induces premature MhcGFP expression. (D) Co-overexpression of Him can only partially repress Mef2[K352R] induced premature differentiation. (E) Co-overexpression of HDAC4 can fully repress Mef2[K352R] induced premature differentiation. (F) Bar graph showing percentage of imaginal discs imaged with observable premature MhcGFP expression. (n=10-23 discs per genotype).

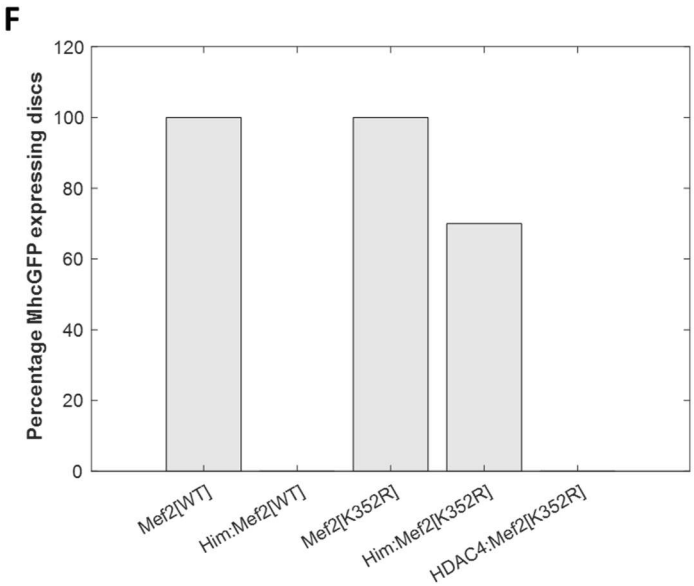

5.91 Discussion

This study is the first to explore sumoylation in the context of *Drosophila* muscle development. RNAi knockdown of the conserved PIAS family member *Su(var)2-10* using *1151Gal4* results in a severe developmental DLM phenotype, as does RNAi against the sole E2 conjugating enzyme *Ubc9*. Although other *Drosophila* E3 ligases exist, Su(var)2-10 is the only described member of the PIAS family, which is thought to be the relevant E3 ligase group to Mef2 sumoylation (Kang *et al.* 2006; Riquelme *et al.* 2006; Shalizi *et al.* 2007). It is possible that important muscle factors other than Mef2 will be impacted by knockdown of sumoylation machinery, so this RNAi knockdown data cannot be tied to a Mef2 specific effect. For example, Erect Wing (Ewg) and Cut are two additional transcription factors expressed during adult muscle development have putative sumoylation motifs (GPS-SUMO, motif finder), (DeSimone and White 1993; Sudarsan *et al.* 2001).

Similar to *Su(var)2-10* knockdown, overexpression of this component of the sumoylation pathway during adult muscle development inhibits DLM formation considerably. Ubc9 overexpression does not cause such an effect, with DLMs appearing and functioning as wild-type. Two potential explanations for this are:

1) The level of Su(var)2-10 is rate limiting in this system, so no matter how highly Ubc9 is expressed, muscle development will not be affected.

2) The *UAS-Su(var)2-10* transgene drives a much higher level of protein expression than the *UAS-Ubc9* line, due to different genomic landing sites of the transgenes. For example, a low level of Ubc9 overexpression might not be expected to perturb DLM formation as significantly as a high level of Su(var)2-10 overexpression. However, performing the Ubc9 overexpression experiment at 29°C instead of 25°C to boost Gal4 dependent gene expression did not increase phenotype severity, suggesting that the level of Ubc9 is not the reason for a lack of phenotype observed.

To show that Su(var)2-10 is relevant to Mef2 regulation, I have demonstrated that the two proteins can physically interact using a Y2H approach. This interaction can be mapped to Mef2[157-350], since a Mef2[1-156] construct cannot interact with a full length Su(var)2-10[1-601] construct. This is unusual, since most documented Mef2 interactions occur through its well conserved N-terminus, although there are

examples interacting outside of this region including MAML1 and P38 (McKinsey *et al.* 2002; Shen *et al.* 2006).

The original in-house library screen dataset identified that PIAS1's Mef2C interaction domain can be mapped to [1-217], which includes a conserved SAP domain, and approximately half of a conserved PINIT domain. The SAP domain contains an LXXLL (NR box) motif, which is implicated in a variety of protein-protein interactions (Plevin *et al.* 2005). Future interaction domain mapping work should therefore target Su(var)2-10's well conserved SAP domain as a likely target for mediating a *Drosophila* Mef2 interaction.

Since Su(var)2-10 and Mef2 protein are co-expressed in the nucleus of AMPs, and are capable of direct physical interaction, this is strong evidence that Su(var)2-10 is implicated in Mef2 regulation at this stage. To build on this aspect of the project, future experiments should focus on co-immunoprecipitation assays, to explore protein-protein interactions in the context of *Drosophila* muscle development. For example, demonstrating that Su(var)2-10:GFP can co-IP with Mef2 would confirm the hypothesis that these proteins physically interact within the wing imaginal disc-associated AMPs.

The mutant Mef2 overexpression constructs highlight the relevance of sumoylation to Mef2 regulation *in vivo,* in the relevant developmental context. Although previous studies on Mef2 sumoylation have largely focused on its effects within cell culture, these results largely align with those presented here, with; sumoylation-deficient Mef2 being more transcriptionally active than wild-type Mef2 (Grégoire *et al.* 2006; Kang *et al.* 2006; Riquelme *et al.* 2006). Overexpression of the mutant Mef2 constructs during adult muscle development leads to an allelic series of DLM morphological phenotypes. The hypothesized sumoylation-deficient Mef2 variants, K352R and S357A, induce a worse developmental phenotype than the wild-type and theorized constitutively sumoylated S357E construct. This is consistent with the view that sumoylated Mef2 is less transcriptionally active, since a more active Mef2 variant would be expected to result in a higher level of target gene misregulation and a stronger phenotype. A similar scenario has been observed in the embryo, where a highly expressing *UAS-Mef2* construct triggers a substantial somatic muscle

phenotype, whereas embryos with only low-level overexpression appear wild-type (Gunthorpe *et al.* 1999).

Wild-type Mef2 overexpression phenocopies the extremely mild effect of the S357E phosphomimetic, suggesting that at the early stages of muscle development when the *1151Gal4* driver is active, wild-type Mef2 largely exists in its sumoylated form. To study this with higher precision, future studies should focus on the detection of SUMO modified endogenous Mef2, pulled down from our tissue of interest. A developmental time-series of Mef2's sumoylation status as muscle differentiation proceeds would shed light on the modification's relevance to endogenous Mef2 regulation. SUMO modifications can be preserved in these protein assays via addition of N-ethylmaleimide (NEM) to buffers, an inhibitor of the SUMO deconjugating enzymes that would otherwise cleave the modification during lysate preparation (Suzuki *et al.* 1999).

Interpretation of the results from the premature differentiation assay in the wing imaginal disc is more complex. In this scenario, all three mutants are significantly more active than wild-type Mef2 in triggering this more direct read-out of Mef2-dependent gene expression. The Mef2-S357E phosphomimetic mutant is hypothesized to be constitutively sumoylated, if prior phosphorylation of S357 is indeed a requirement for K352 sumoylation as the motif would suggest. Consequently, Mef2-S357E is expected to be less active than the other two mutants, which is not the case in this assay. A reason for this might lie in the experimental design. The serine to glutamic acid substitution is the most commonly employed strategy to mimic phosphorylation in the literature, since the switch to a negatively charged amino acid is thought to closely resemble that of a phosphorylated serine. However, it has been argued that the resultant charge from this change is not negative enough, and that the loss of bulkiness of the phosphate group is not accounted for, so this is not a true mimic of phosphorylation (Paleologou *et al.* 2008; Otto and Potter 2022). It is therefore possible that the *UAS-S357E* phosphomimetic does not actively promote sumoylation as initially predicted, since the glutamic acid switch isn't fully equivalent to a phosphorylated serine. This would explain why the construct is more active than wild-type Mef2 in this assay. A comparable result has been published previously; Mef2C-S396E is less efficiently sumoylated than wild-

type in 10T1/2 cells and is consequently more transcriptionally active than predicted (Kang *et al.* 2006).

Although this explanation is plausible, it is puzzling that Mef2-S357E and Mef2-WT overexpression phenocopy one another in the extent to which they inhibit DLM development. The DLM phenotype is a net result of all genes misregulated during the differentiation process, unlike the premature MhcGFP quantification assay which is a direct readout of just one gene. The complex web of interactions between the kinases, phosphatases and SUMO proteases that determine Mef2 sumoylation status throughout DLM development are likely not comparable to the far simpler wing imaginal disc readout of Mef2 activity. Nonetheless, both datasets concur that sumoylation deficient Mef2 exhibits markedly greater activity than wild-type, thereby indicating a negative regulatory role of sumoylation on Mef2 activity.

Mechanistically, it is unclear by which route sumoylation of Mef2 represses its transcription factor activity. Previous studies have shown that DNA-binding, subcellular localization and protein stability are unaffected by SUMO modification of Mef2 within the context of cell culture (Gocke *et al.* 2005; Kang *et al.* 2006). Enhancing co-repressor recruitment is another potential mechanism by which sumoylation reduces a targets activity. For example, the transcription factors p300 and Elk-1 are sumoylated, and this promotes an inhibitory interaction with HDAC2 or HDAC6 respectively (Girdwood *et al.* 2003; Yang and Sharrocks 2004; Uchimura *et al.* 2006). Since HDAC4 is a characterized repressor of Mef2 activity, it seems the obvious candidate for sumoylation mediated recruitment (Miska *et al.* 1999). However, here I have shown that overexpression of HDAC can still repress the activity of sumoylation-deficient Mef2 in the wing imaginal disc system, suggesting this is not the relevant mechanism here. Similarly, Mef2C's sumoylation status doesn't affect its interaction with mammalian HDAC4, as Mef2C-K391R and Mef2C-WT both bind HDAC4 equally well in a Co-IP experiment (Kang *et al.* 2006).

Conversely, Him can no longer fully repress Mef2-K352R activity, indicating that Him's interaction with Mef2 might be influenced by Mef2 sumoylation. Although *Him* does not have a known mammalian homolog, it is thought to repress Mef2 activity through recruitment of the conserved co-repressor Gro (Liotta *et al.* 2007). Previously, it has been shown that conserved Groucho family member Grg4's

interaction with the transcription factor SoxE is significantly enhanced by SoxE sumoylation, whilst simultaneously displacing the co-activator p300 (Lee *et al.* 2012). It is possible a similar scenario regulates *Drosophila* Mef2: sumoylation of Mef2 enhances Him-dependent recruitment of Gro, which diminishes Mef2's transactivation potential. Incidentally, *Drosophila* Mef2 is also known to interact with p300, thus future work could focus on the interplay between Mef2 sumoylation state and recruitment of co-activators & repressors such as P300 and Gro (Lin and Baines 2019). A Co-IP approach to determine the relative level of P300 or Him bound Mef2-WT and Mef2-K352R would shed further light on this facet of Mef2 regulation.

Whilst the overexpression data provides compelling evidence that Mef2 sumoylation is an inhibitory mechanism within the context of *Drosophila* muscle, there is no substitute for studying gene function and regulation at the endogenous level. The 'gold standard' experiment is to assess the consequence of blocking endogenous Mef2 sumoylation during normal development. Our lab has generated an in-house generated Mef2 CRISPR null allele, whilst simultaneously inserting an AttP landing site into the locus (Hubbert 2023). Crucially, wild-type *Mef2* cDNA insertion into this landing site rescues the null phenotype and lethality. Future experiments could utilise this tool in combination with SUMO motif mutant cDNA to determine the importance of the Mef2 SUMO modification to muscle development, and further probe how this modification might act to repress Mef2 activity.

Chapter 6. Further characterization of the recently discovered *Drosophila* MuSC population

6.1 Introduction

There is a resident stem cell population in skeletal muscle called “satellite cells”. Mouse and Zebrafish models have established that these cells play key roles in muscle homeostasis and repair, and understanding their biology is relevant to understanding muscle deterioration in both disease and ageing. However, there are still major gaps in understanding the genetic mechanisms that control their activation and function.

Vertebrate skeletal muscle is able to regenerate, a response that depends on the activity on the usually quiescent muscle satellite cells (MuSCs). These cells are situated on the periphery of the muscle fibre underneath the basal laminar, and in their quiescent state are marked by expression of the transcription factor Pax7 (Seale *et al.* 2000; Oustanina *et al.* 2004; Relaix *et al.* 2006). Upon injury, satellite cells become activated, as a programme of proliferation and myogenic differentiation begins (Figure 6.1- adapted from Romagnoli *et al.* 2021).

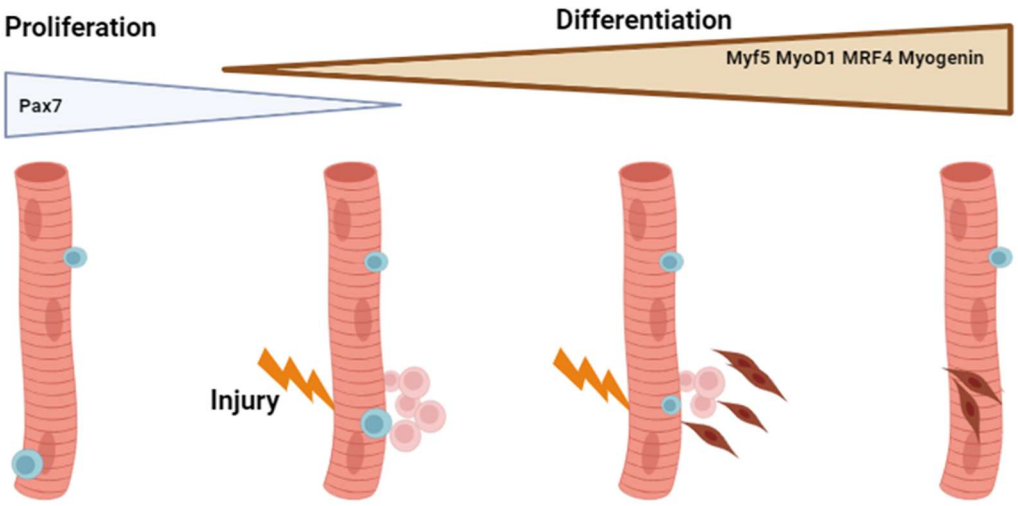

Figure 6.1 - MuSC dynamics in skeletal muscle repair.

Pax7 expressing quiescent muscle satellite cells (MuSCs) are activated upon injury, undergoing extensive proliferation. Activated MuSCs can either retain Pax7 expression and return to a quiescent state for future muscle repair or differentiate into myoblasts which undergo fusion to repair damaged muscle. MuSC derived myoblasts are characterized by expression of the myogenic regulatory factors (MRFs), including Myf5, MyoD1, MRF4 and Myogenin.

Proliferating cells maintain Pax7 expression, and either return to a quiescent state to maintain the MuSC pool for future repair, or commit to myoblast differentiation (Seale *et al.* 2000; Seale *et al.* 2004). Early hallmarks of differentiation include the MRFs Myf5 and MyoD1, whose expression temporally overlaps with Pax7 expression during the proliferative phase of the injury response. Myogenin is not expressed until terminal muscle differentiation, at which stage these myoblasts either fuse with one another to give rise to new myofibres, or fuse directly with the injured fibre to effectuate its repair (Smith *et al.* 1993; Lindon *et al.* 1998; Nicolas *et al.* 1996).

A MuSC population has recently been discovered in *Drosophila*, associated with the dorsal longitudinal muscles (DLMs) of the adult fly thorax (Chaturvedi *et al.* 2017; Boukhatmi and Bray 2018)]. These MuSCs derive from a subpopulation of wing imaginal disc associated AMPs that escape differentiation during pupation, and instead are found embedded on the periphery of the differentiated DLM fibre. Upon injury, these MuSCs proliferate and fuse to the damaged fibre to instigate repair, a process seemingly analogous with vertebrate skeletal muscle regeneration (Chaturvedi *et al.* 2017). The ablation of MuSCs during the adulthood of the fly results in defects of the flight musculature, attributable to a loss of homeostatic maintenance of these fibres (Boukhatmi and Bray 2018).

Drosophila MuSCs are characterized by expression of the ZEB1 homolog, Zfh1, an anti-differentiation signal already described in other myogenic precursor populations (Postigo *et al.* 1999; Siles *et al.* 2013; Chaturvedi *et al.* 2017; Boukhatmi and Bray 2018). Upon injury, these Zfh1+ cells undergo Notch-Delta signalling dependent proliferation and subsequently fuse to the injured fibre. Similarly, vertebrate MuSCs express ZEB1, which contributes to maintaining MuSC quiescence and preventing premature differentiation upon injury. At this stage, ZEB1 collaborates with the Notch signalling pathway to inhibit MRF expression until the correct time (Bjornson *et al.* 2012; Philippos *et al.* 2012; Siles *et al.* 2019).

Mef2 function has also been implicated in vertebrate skeletal muscle regeneration (Liu *et al.* 2014). In a mouse injury model, a triple conditional knockout of *Mef2A*, *Mef2C* and *Mef2D* (*Mef2-TKO*) in MuSCs completely inhibits the muscle repair process. MuSCs isolated from *Mef2-TKO* mice proliferate normally in culture, but fail to differentiate into myotubes. Whilst *Mef2* loss-of-function does not affect

expression of genes implicated in the early proliferative response to injury, including Pax7, MyoD and Myf5, cells fail to upregulate Mrf4, a key driver of MuSC differentiation (Liu *et al.* 2014). Conversely, Mef2C overexpression in a mouse injury model results in enhanced regeneration, due to an increase in protein synthesis and myoblast fusion (Baruffaldi *et al.* 2016).

Whilst a comparable function of Mef2 has not yet been described in *Drosophila* muscle repair, Mef2 function is essential for the closely related process of adult flight muscle development, during which the adult muscle progenitors (AMPs), a muscle stem cell population, differentiate and fuse to form the adult DLMs (Soler *et al.* 2012). Moreover, Zfh1 is a characterized repressor of *Mef2* expression and consequently myogenesis, so within MuSCs likely acts to counteract Mef2 dependent gene expression (Siles *et al.* 2013). Consistent with this, only a low level of Mef2 is detectable in quiescent MuSCs (Boukhatmi and Bray 2018).

This chapter provides further characterization of this recently discovered cell type in *Drosophila*. In particular, I present preliminary data on Mef2 expression dynamics in response to injury, and explore the consequences of *Mef2* loss-of-function in MuSCs. I've also detected expression of the Mef2-repressor, Him, as a new marker of MuSCs, as well as identifying a novel leg muscle associated MuSC population which is far more accessible than the DLM-MuSCs.

6.2 Identification of Him as a new marker of *Drosophila* MuSCs

To date, Zfh1 is the only published *Drosophila* MuSC marker (Chaturvedi *et al.* 2017; Boukhatmi and Bray 2018). Its expression in other cell types, particularly immune cells implicated in wound inflammatory response, highlights the need to discover additional, specific, markers of MuSCs (Frandsen *et al.* 2008; Boukhatmi and Bray 2018).

Like *zfh1, e*xpression of *Him* is regulated by the Notch signalling pathway. Both proteins are implicated in repression of Mef2, and both are co-expressed in a number of mesodermal derivatives, including pericardial cells and wing imaginal disc associated AMPs (Soler and Taylor 2009; Zappia *et al.* 2019; Panta *et al.* 2020). To this end, I studied Him expression post development to determine if it co-labels DLM-associated MuSCs alongside Zfh1.

Sagittal sections of the adult *Drosophila* thorax display the length of the six DLMs, which span from the anterior to posterior end of the thorax. MuSCs can be identified based on expression of Zfh1, and their location on the periphery of the muscle fibre (Chaturvedi *et al.* 2017; Boukhatmi and Bray 2018). To determine if Him is expressed in MuSCs, the *HimGFP* line was analysed in combination with Zfh1 antibody staining. Female flies were dissected, since their slightly larger size permits easier sample preparation.

HimGFP was found to be co-expressed with Zfh1 in MuSCs, which were typically situated on the periphery of the DLMs, thus confirming identification of a second marker for this cell type (Figure 6.2). Expression of both proteins overlapped with Hoechst staining, suggesting nuclear localization. Both Him and Zfh1 act to counteract the myogenic muscle differentiation program, through repression of Mef2 (Soler and Taylor 2009; Siles *et al.* 2013). This suggests that MuSCs expressing both of these markers are in a quiescent state and not actively undergoing differentiation to promote muscle repair.

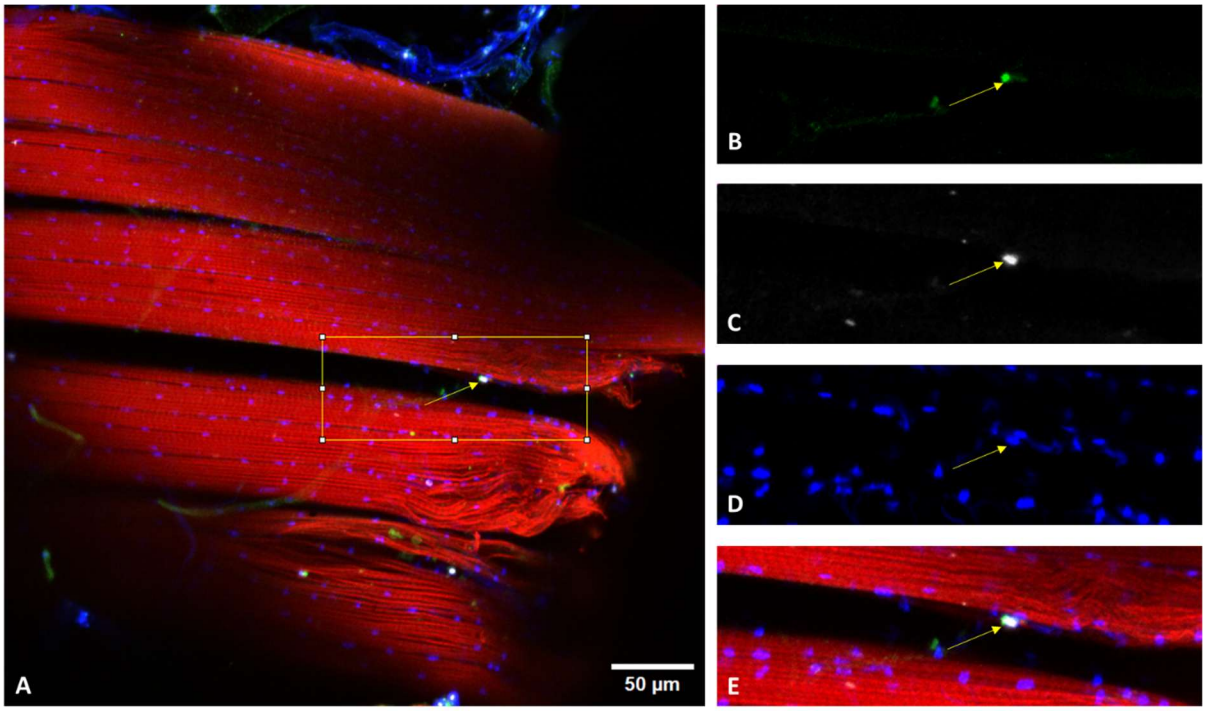

Figure 6.2 - Him is co-expressed with Zfh1 in *Drosophila* MuSCs.

Confocal Z-stack maximum intensity projection of a sagittal DLM cross-section from a *HimGFP* fly showing co-localization of Zfh1 and Him (n=6 hemithoraces). (A) Low magnification image showing a boxed region of interest on the periphery of a DLM fibre showing a MuSC (yellow arrow). (B-E) Higher magnification of the boxed region in (A), with single channel images of (B) anti-GFP (green) (C) anti-Zfh1 (white) and (D) Hoechst (blue) nuclear labelling. (E) A merge of HimGFP, Zfh1, Hoechst and phalloidin, showing overlap of Him and Zfh1 expression in the nucleus of a MuSC, on the periphery of the muscle fibre.

6.3 Mef2 expression dynamics upon injury

Mef2 is highly expressed throughout the DLM nuclei, but only a low level is detectable in the associated quiescent MuSCs (Boukhatmi and Bray 2018; Boukhatmi 2021). Since Mef2 expression is a requirement for vertebrate MuSC differentiation and repair, I performed an injury assay to study Mef2 expression dynamics upon Drosophila muscle injury to provide insight into a potential conserved function for Mef2.

The directly tagged Mef2GFP line was used in these analyses, in combination with anti-GFP staining to enhance the signal. Young female flies less than 3 days old were subjected to puncture wounds administered by a fine pin, which was sterilised with 70% ethanol approximately every 10 injuries. DLMs were then studied at several points after injury to develop a time-course of Mef2 expression. These data have been collected in collaboration with Dr Hadi Boukhatmi lab, who have been performing equivalent experiments alongside with a Mef2 antibody.

I found that upon injury, Mef2GFP expression rapidly declined within the injured fibre. Initially, this was in close proximity to the wound site, but by 24 hours post-injury the entire fibre was no longer expressing Mef2 (Figure 6.3). These results are consistent with what has been observed with Mef2 antibody (Dr Hadi Boukhatmi, personal communication).

In order to determine if Mef2 protein later returns to the muscle fibre, I performed dissections two weeks post injury, by which point stab-induced wounds have largely regenerated (Chaturvedi *et al.* 2017; Catalani *et al.* 2022). Of the six flies assayed, I observed three separate scenarios (Figure 6.4). The majority of individuals, four of the six, had fibres that once again resembled wild-type, based on Mef2 expression and lack of an observable wound with phalloidin staining (Figure 6.4C). In one individual, Mef2GFP had not returned, but a wound scar could still be seen within the fibre, so it is possible regeneration was still ongoing (Figure 6.4B). The final fly completely lacked phalloidin staining, suggesting that the initial wound was catastrophic and the muscle fibre entirely deteriorated (Figure 6.4A).

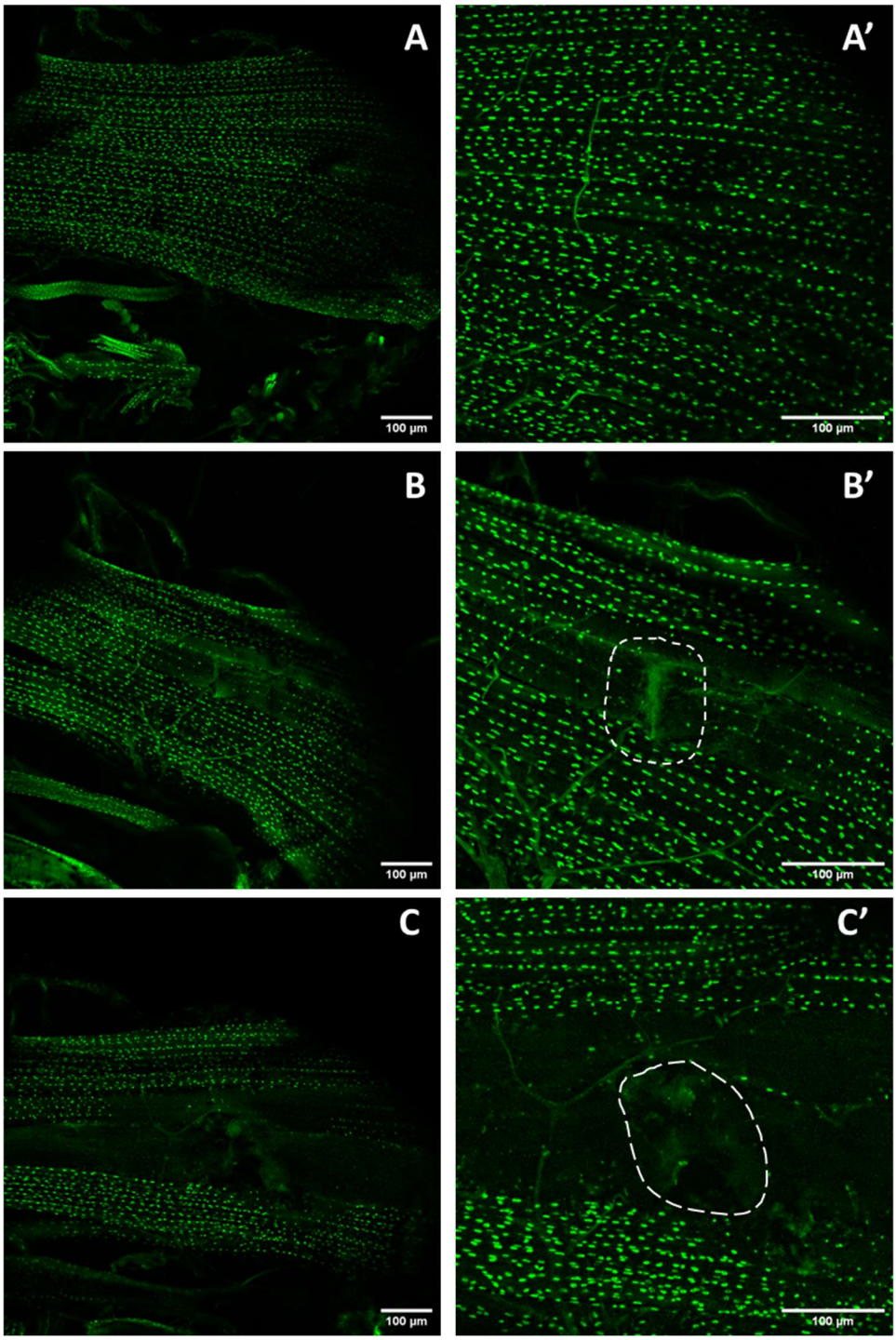

Figure 6.3 - Mef2GFP expression in the fibre is lost upon injury.

Confocal Z-stack maximum intensity projections of Mef2GFP expression in controls, 4 hours after injury and 24 hours after injury at 10x and 20x magnification. The wound sites are indicated by a dashed circle. (A-A') Control hemithoraces express Mef2GFP throughout each of the DLM fibres (n=10). (B-B') By 4 hours after injury, Mef2GFP is decreased in the muscle fibre close to the site of the injury (n=6). (C-C'') By 24 hours after injury, Mef2GFP has been lost throughout the entire fibre (n=6 hemithoraces per timepoint).

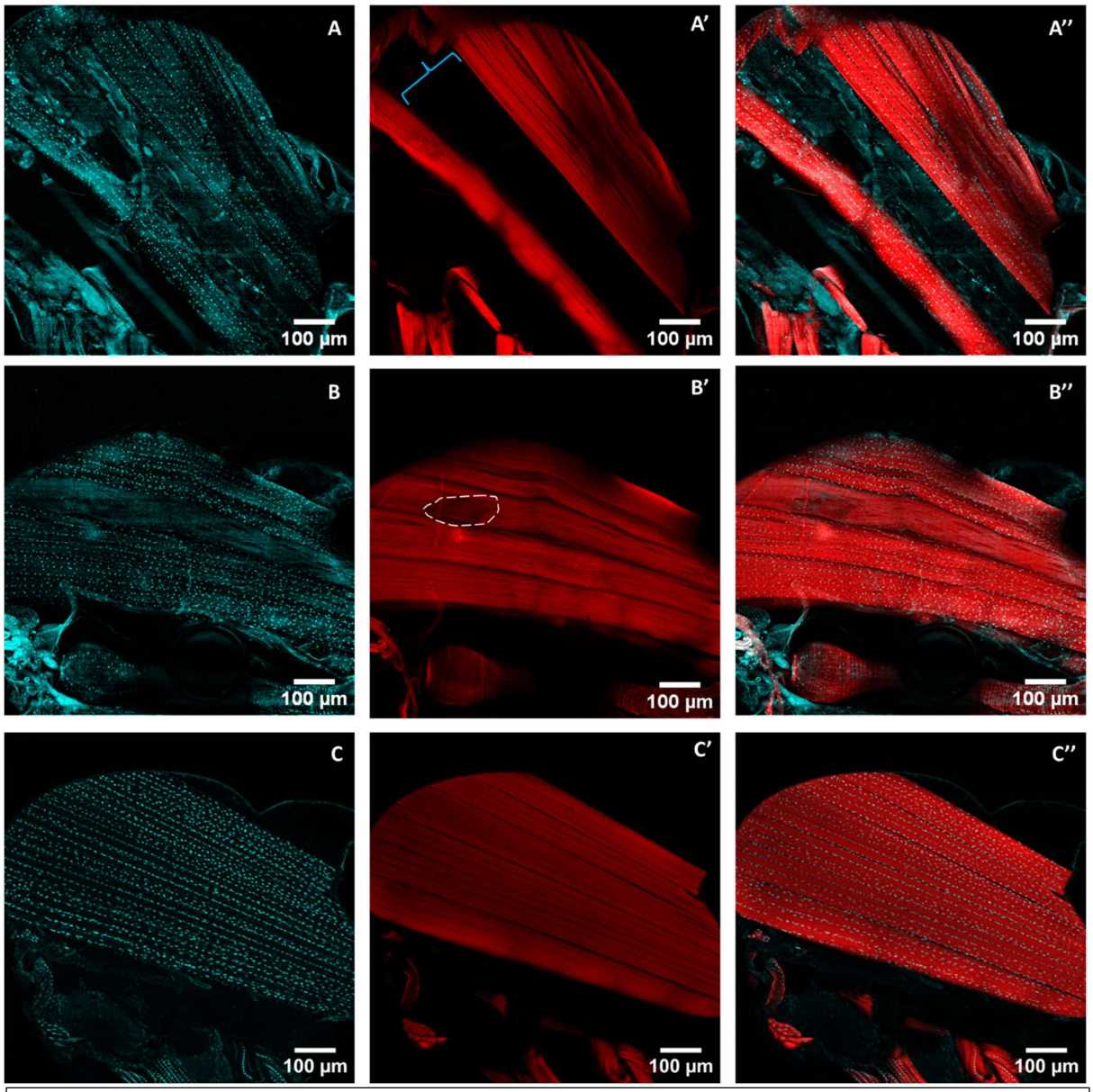

Figure 6.4 - Mef2GFP Expression 2-weeks post-injury.

Examples of sagitally sectioned *Mef2GFP* flies 2-weeks after a stab induced wound, stained with anti-GFP and phalloidin to label F-actin (n= 6 hemithoraces). Confocal microscopy Z-stack maximum intensity projections. (A-A'') A catastrophic wound in which the muscle fibre has completely deteriorated, demonstrated by a complete absence of Mef2 (cyan) and F-actin staining (red). (B-B'') A fibre which lacks Mef2GFP expression but still expresses F-actin. An observable scar in the injured DLM is circled with a dashed white line. (C-C'') A fully repaired example, which appears wild-type based on Mef2GFP and F-actin staining.

Whilst quiescent MuSCs are known to express a low level of Mef2 protein, Mef2 expression in active MuSCs in an injury model has not yet been characterized (Boukhatmi and Bray 2018).

To further explore this aspect of MuSC biology, I studied expression of Mef2 within the satellite cells using the directly tagged Mef2GFP line, in combination with Zfh1 antibody staining to identify the relevant cells. Initially, I imaged young uninjured female flies to determine if a low level of Mef2GFP could be detected in MuSCs, as has been reported in the literature with Mef2 antibody (Boukhatmi and Bray 2018). Indeed, a Mef2GFP signal was detectable, at a much lower level than in the surrounding muscle fibre nuclei (Figure 6.5).

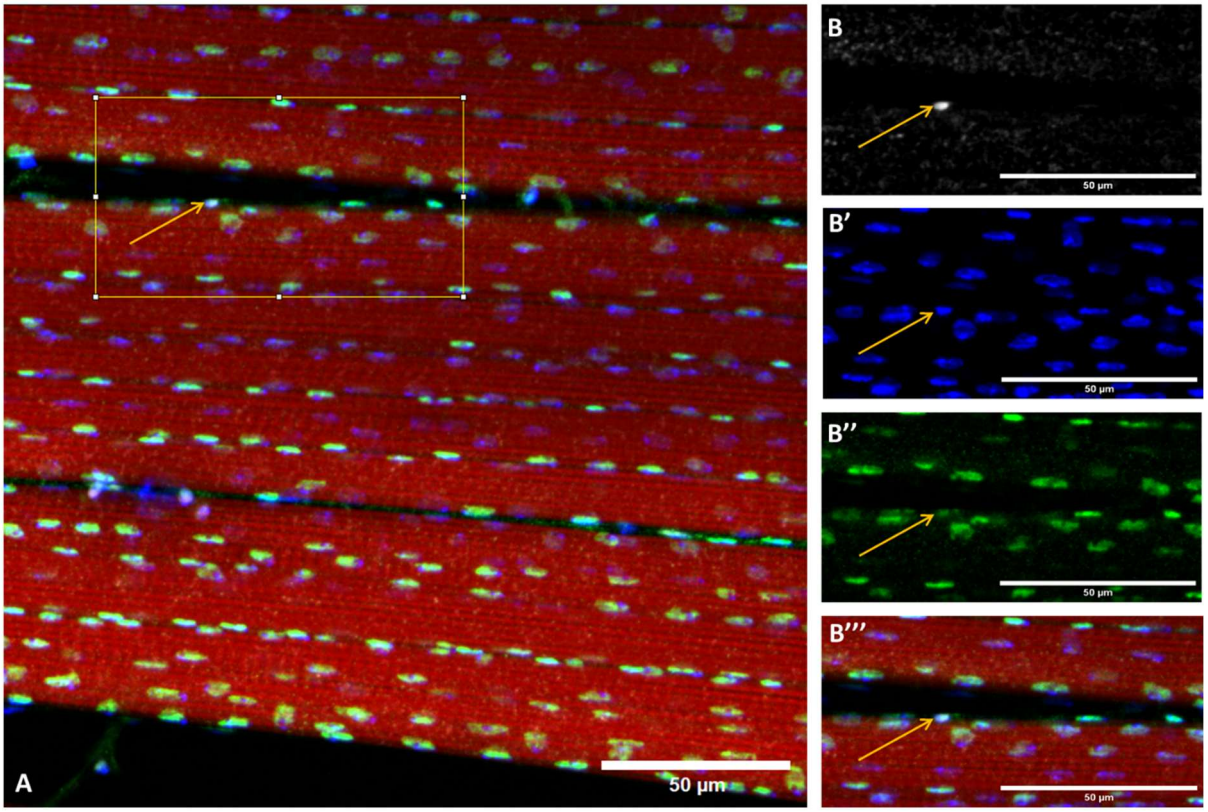

Figure 6.5 - Zfh1 positive MuSCs co-express a low level of Mef2 protein.

(A) Confocal Z-stack maximum intensity projection of a sagittal DLM cross-section of a young, uninjured Mef2GFP fly. Stained with anti-GFP (green), Hoechst (blue), anti-Zfh1 (white) and phalloidin (red), showing a MuSC on the periphery of the muscle fibre (orange arrow). (B-B''') Close-up of the area indicated in (A), with single channel images of (B) Anti-Zfh1, (B') Hoechst nuclear staining, (B'') anti-GFP and (B''') a merge of each in addition to F-actin phalloidin staining. The indicated Zfh1+ MuSC expresses a low level of Mef2GFP relative to the nearby muscle fibre nuclei. (n=8 hemithoraces).

I also studied expression of Mef2GFP within MuSCs 24 hours post-injury, as by this time point Zfh1+ MuSCs are known to surround the injury site (Chaturvedi *et al.* 2017). Zfh1 antibody staining was used to identify the relevant cell-type, in combination with anti-GFP staining. I identified two separate sub-populations of MuSCs near the wound – the previously described high Zfh1/low Mef2 cells, but also a group of high-Mef2 cells which contain an extremely low level of Zfh1 (Figure 6.6). I propose that the population with a high level of Mef2 are activated MuSCs that are actively promoting muscle repair. This is inferred from their close proximity to the site of the wound, and an equivalent role for Mef2 existing in vertebrate models (Liu *et al.* 2014).

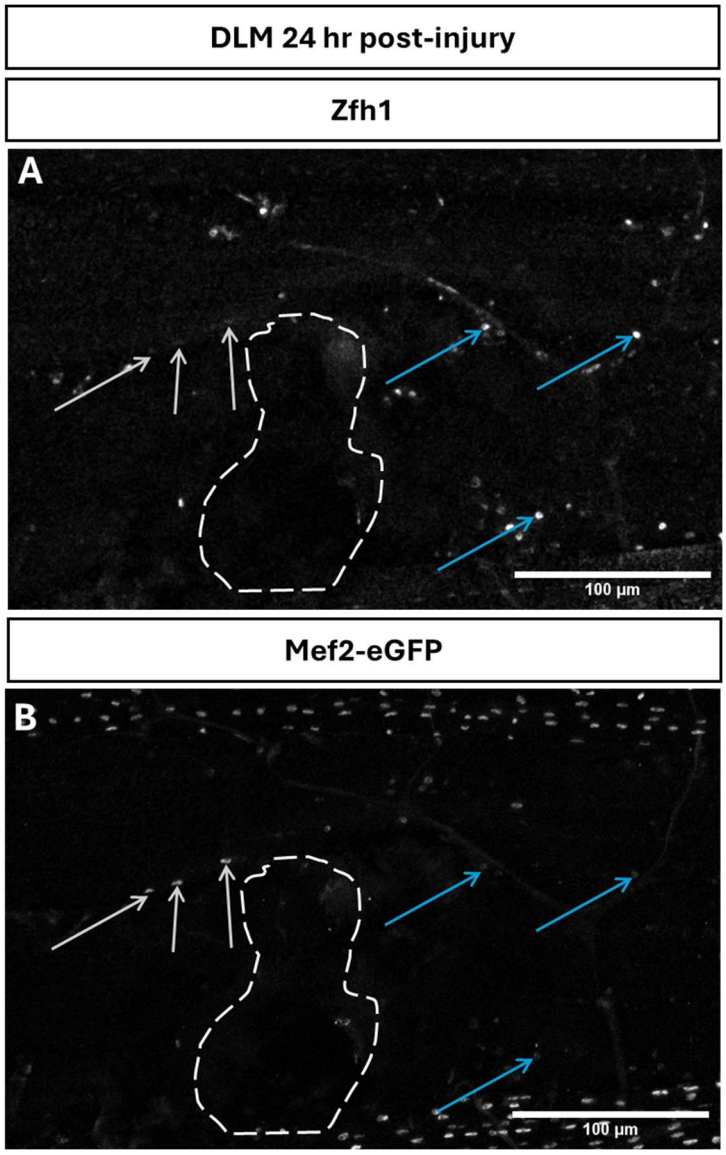

Figure 6.6 - Cells expressing a high level of Mef2 localize to the site of an injury.

Confocal Z-stack maximum intensity projection of the site of a wound (white dashed snowman) administered to the DLMs of a Mef2GFP expressing fly, 24-hours post-injury. (A) Single-channel image of anti-Zfh1 and (B) Mef2-eGFP. White arrows indicate cells which express a high level of Mef2 and a barely detectible level of Zfh1. Orange arrows indicate cells with a low level of Mef2 and a high level of Zfh1. (n=3 hemithoraces).

6.4 Exploring Mef2 function in muscle maintenance and repair

The expression of an increased level of Mef2 in cells on the periphery of the site of a wound, suggests some role for Mef2 activity in the repair response. To explore potential functions for Mef2 in MuSCs, a RNAi knockdown approach was adopted. The Gal4/UAS system was used to drive *UAS-Mef2-RNAi* (VDRC 15550) expression in MuSCs using the *Enh3-Gal4* driver. Enh3 is a specific Zfh1 enhancer that drives expression in a subset of wing disc associated AMPs, as well as in the adult MuSCs (Boukhatmi and Bray 2018). To restrict Gal4 expression to adulthood only, *TubGal80ts* was used in conjunction with the Gal4 driver. Crosses were performed at 18◦C at which temperature Gal80ts inhibits Gal4 activity. F1 progeny were transferred to 29◦C, to inactive Gal80ts and permit Gal4-mediated knockdown of *UAS-Mef2-RNAi* over a period of two weeks. An *UAS-mCherry-RNAi* transgene was used in place of the *UAS-Mef2-RNAi* as a control. Only female F1s were used, as male flies housed together can display aggressive behaviour, which can result in damage to the wings, and thus impair flight ability (Davis *et al.* 2018).

Initially, I explored whether loss of Mef2 in MuSCs impaired muscle homeostasis. Flight ability was used as a read-out of flight muscle function, reasoning that improperly maintained muscles would affect flight ability. A flight index was calculated for each genotype at each timepoint, to compare between experimental conditions (Deaguero *et al.* 2019). At day 1 after eclosion, *UAS-Mef2-RNAi* and control *UAS-mCherry-RNAi* flies could fly equivalently well, with a mean flight index of 2.78 (n=80 flies) and 2.80 (n=70) respectively (Figure 6.7). This result reassures that there is no developmental effect of *UAS-Mef2-RNAi* knockdown at this stage, as Gal80ts does not always entirely eliminate Gal4 activity (Eliason *et al.* 2018).

At day 14 of RNAi induction at 29◦C, both *UAS-mCherry-RNAi* controls and *UAS-Mef2-RNAi* flies displayed a significant reduction in flight ability compared to their day 1 counterparts, with a mean flight index of 2.55 (n=94) and 2.14 (n=72) respectively (Figure 6.7). Since the control flies' flight ability was significantly decreased over this period, this suggests that aging flies have reduced flight function, which may be exacerbated by the inhospitable conditions of raising them at 29◦C. Nonetheless, at day 14, the difference in flight index between controls and *UAS-Mef2-RNAi* is also significant, with Mef2 knockdown causing a significant reduction in flight muscle function at this timepoint. This indicates that loss of *Mef2*

function in *Enh3-Gal4* expressing cells impairs flight muscle function, pointing towards a role for Mef2 in satellite cell mediated muscle homeostasis.

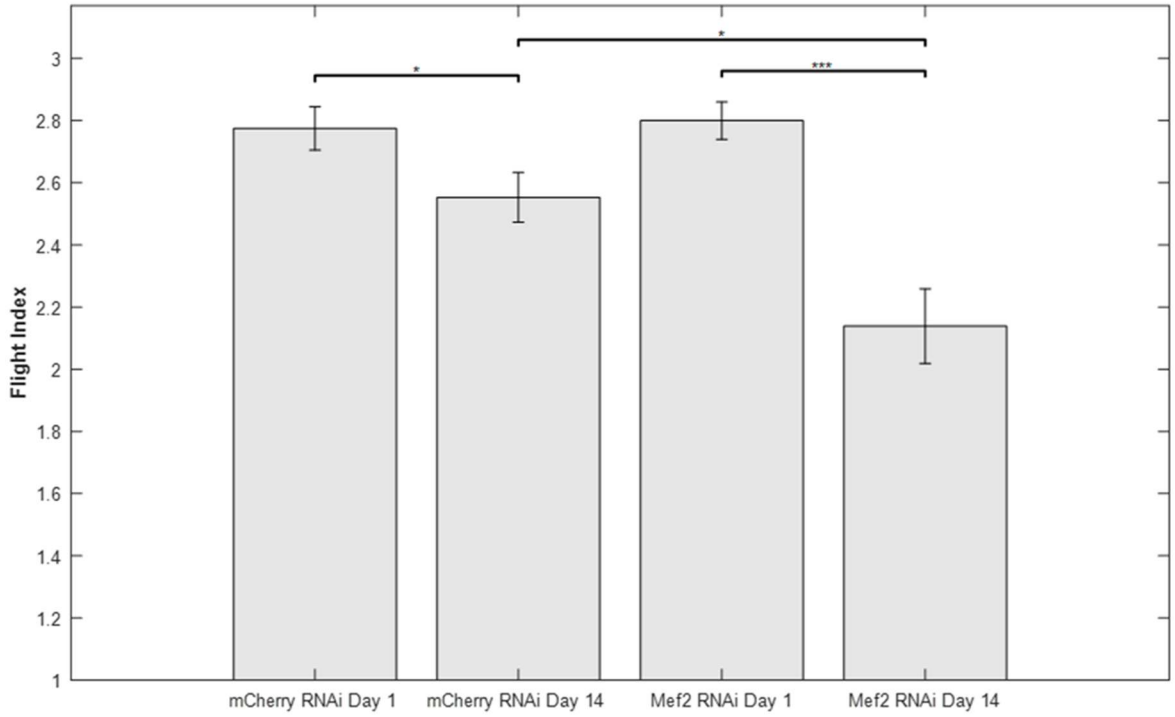

Figure 6.7 - *Mef2* loss-of-function in MuSCs affects flight ability.

Mean flight index ± SEM of flies expressing *TubGal80ts; Enh3-Gal4* driven *UAS-mCherry-RNAi* or *UAS-Mef2-RNAi* at day 1, and at day 14 after RNAi induction. Both controls, and *UAS-Mef2-RNAi* expressing flies have a significant decrease in flight ability at day 14 compared to day 1. At day 14, *UAS-Mef2-RNAi* flies are significantly worse at flying than controls. (Kruskal Wallis followed by Post-Hoc Dunns test mCherry RNAi day 1 vs mCherry RNAi day 14 *p=0.014, Mef2 RNAi day 1 vs Mef2 RNAi Day 14 ***p<0.0001, mCherry RNAi day 14 vs Mef2 RNAi Day 14 *p=0.011). (n=70-94 flies per sample).

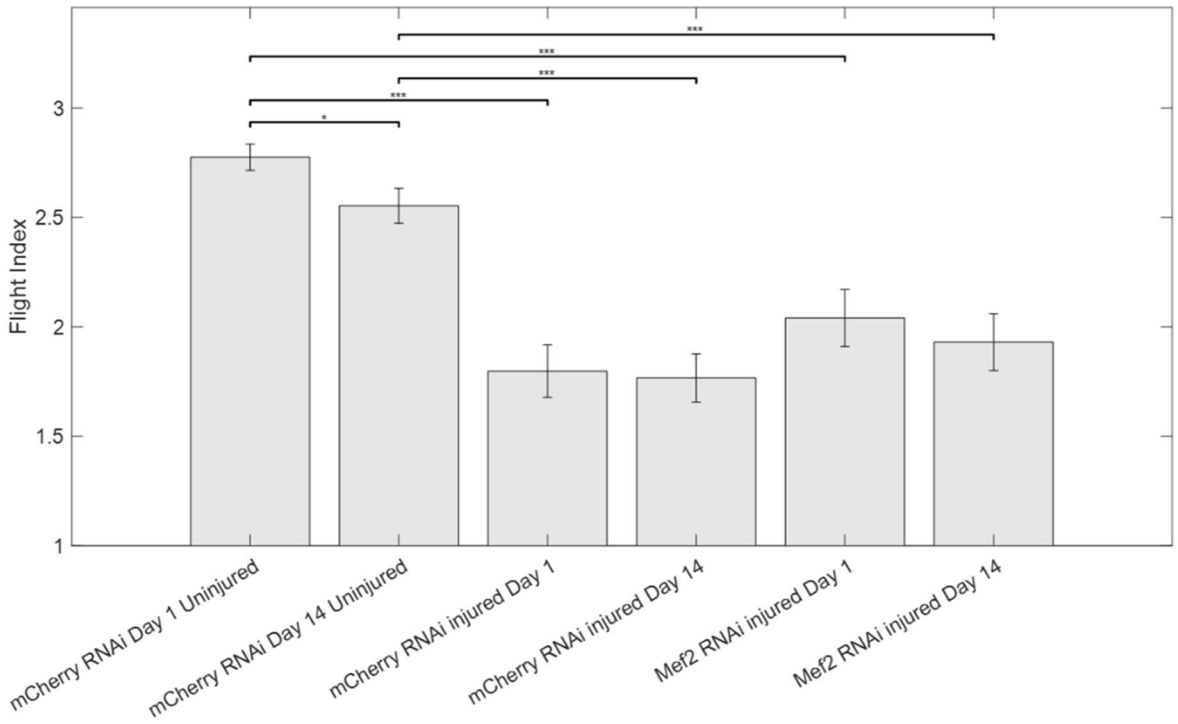

Figure 6.8 - Wounded flies have impaired flight ability, which does not improve over time. Mean flight index ± SEM of manually injured flies expressing *TubGal80ts; Enh3-Gal4* driven *UAS-mCherry-RNAi* or *UAS-Mef2-RNAi* at day 1, or at day 14 after RNAi induction. Uninjured *TubGal80ts; Enh3-Gal4* driven *UAS-mCherry-RNAi* was used to control for age. Injury significantly decreased flight ability by day 1, which was not rescued towards wild-type by day 14 in either controls or *UAS-Mef2-RNAi* expressing flies. (Kruskal Wallis followed by Post-Hoc Dunns test uninjured mCherry RNAi day 1 vs uninjured mCherry RNAi day 14 *p=0.046, uninjured mCherry RNAi day 1 vs injured mCherry RNAi day 1 ***p<0.0001, uninjured mCherry RNAi day 14 vs injured mCherry RNAi day 14 ***p<0.0001, uninjured mCherry RNAi day 1 vs injured Mef2 RNAi injured day 1 ***p<0.0001, uninjured mCherry RNAi day 14 vs injured Mef2 RNAi day 14 ***p<0.0001). (n=64-94 flies per sample).

To determine if Mef2 has a role in muscle repair post-injury, I combined the functional flight assay with an injury assay (Figure 6.8). Flies had their DLMs injured with a pin shortly after eclosion, and were either assayed for flight ability at day 1, or transferred to 29◦C and assayed after two-weeks, to provide a functional read-out of whether muscle repair had occurred over the time-period. Again, *Enh3-Gal4* in combination with Gal80ts was used to drive expression of either a *UAS-mCherry-*

RNAi control, or *UAS-Mef2-RNAi*, to see if loss of Mef2 affects the regenerative process.

As expected, day 1 after injury to the DLMs, I observed a significant reduction in flight index for injured *UAS-mCherry-RNAi* control flies (n=69 flies) and *UAS-Mef2-RNAi* expressing flies (n=71) compared to their uninjured counterparts (Figure 6.8). This shows that muscle injury has a direct consequence on flight ability. However, two-weeks after induction of the RNAi at 29◦C, flight muscle function had not been restored in either control (n=64) or *UAS-Mef2-RNAi* flies (n=67). Thus, this assay proved unsuitable for providing a functional read-out of muscle repair, since even control flies did not regain flight ability after two weeks of muscle regeneration.

6.5 Identification of a leg muscle associated MuSC population

Currently, DLMs are the only known *Drosophila* muscle type to have an associated MuSC population (Chaturvedi *et al.* 2017; Boukhatmi and Bray 2018). *Drosophila's* tubular leg muscles are more functionally and morphologically resemblant of vertebrate skeletal muscle than the DLMs, thus are arguably a more relevant model for exploring conserved aspects of MuSC biology. For this reason, I explored the *Drosophila* leg musculature for MuSCs, to establish a new model for studying satellite cell dynamics.

To study the ultrastructure of the leg musculature, cryosections of the leg of young adult Mef2GFP-expressing flies were analysed (Figure 6.9). I identified a population of Zfh1+ cells with the characteristic 'wedge' shaped appearance of a MuSC, which also express a low-level of Mef2GFP. Other Zfh1+ cells were also observed nearby, which were morphologically distinct from MuSCs. Based on their large, round nuclei, I hypothesise that these are hemocytes, which are also known to express Zfh1 (Boukhatmi and Bray 2018).

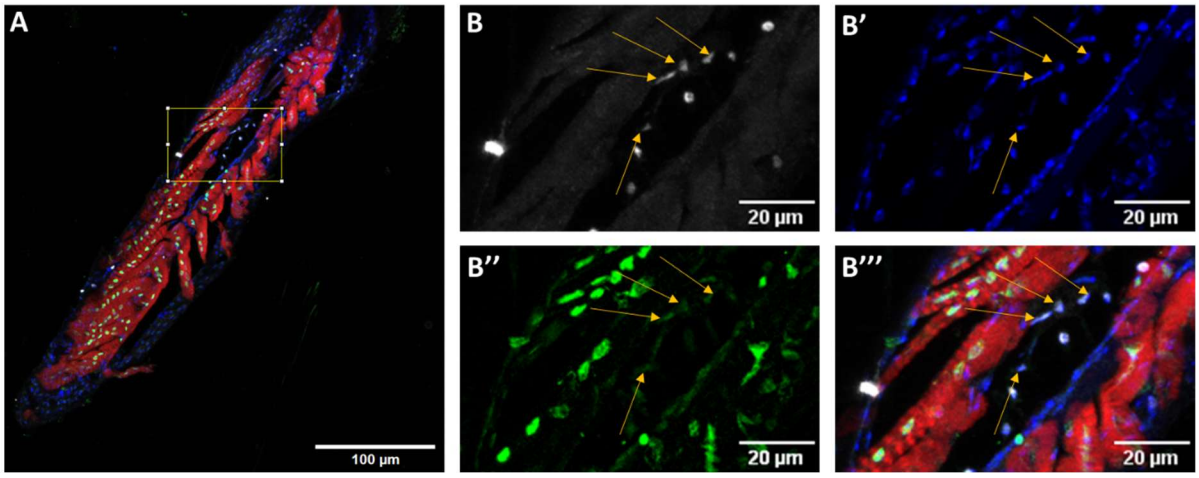

Figure 6.9 - Identification of a new leg associated MuSC population.

A confocally imaged cryosection of a *Drosophila* tibia from the Mef2GFP expressing line. The section is labelled with phalloidin (red), anti-Zfh1 (white), anti-GFP (green) and Hoechst (blue). (A) A multi-channel merge of the entire tibia structure showing the muscular arrangement. (B-B''') Single channel images showing a close-up of the region indicated in (A), of anti-Zfh1, Hoechst and anti-GFP staining, as well as a merge including phalloidin. Cells resemblant of MuSCs co-express Zfh1 and a low level of Mef2 (orange arrows). (n=1 leg per fly from 4 flies).

To confirm that these Zfh1+ cells are indeed MuSCs, a lineage tracing-method was adopted to determine if they contribute to muscle homeostasis. The 'repressible dual differential stability cell marker (ReddM)' system was utilised in combination with the *Enh3-Gal4* driver, which drives expression in adult MuSCs (Antonello *et al.* 2015; Boukhatmi and Bray 2018). This technique allows cells that are actively expressing Gal4 to be distinguished from differentiated progeny, based on expression of two different fluorophores with differing half-lives. Firstly, a *UAS-mCD8-GFP* that has a short half-life, marks cells where Gal4 is actively being expressed. Secondly, a long-lived *UAS-H2B-RFP*, labels progeny derived from Gal4 expressing cells for a period of at least 28 days. A Gal80ts has also been incorporated into the *UAS-ReddM* stock (Antonello *et al.* 2015), allowing the system to be switched on at a specific timepoint. Here, I raised the *Enh3-Gal4>UAS-ReddM* cross at 18◦C, and transferred progeny to 29◦C upon eclosion. Flies were reared at 29◦C for 10 days, before having their legs removed and imaged 'live' and unfixed in schneiders insect medium.

Live imaging of intact legs revealed that *Enh3-Gal4* positive cells could be seen through the cuticle, using a standard fluorescent microscope (Figure 6.10). The majority of cells observed were co-labelled with both *UAS-mCD8-GFP* and *UAS-H2B-RFP*, suggesting they are actively expressing *Enh3-Gal4*, and could represent MuSCs. A small subset of cells only expressed *UAS-H2B-RFP* (Figure 6.10E), indicating that they are progeny of *Enh3-Gal4* expressing cells, thus could represent MuSC-derived muscle fibre nuclei.

These data provide evidence of a novel MuSC population that exists in association with *Drosophila*'s tubular leg muscles. The immunostainings demonstrate several similarities with the previously characterised DLM-associated MuSC population, including the expression of Zfh1 alongside a low level of Mef2, a characteristic 'wedge-like' shape and close association with the muscle fibre. The ReddM data demonstrates that the characterized MuSC driver, *Enh3-Gal4*, contributes to a traceable lineage within the leg (Chaturvedi *et al.* 2017; Boukhatmi and Bray 2018). These cells can be imaged live through the cuticle of the leg using standard fluorescent microscopy, which represents a huge advantage to the system.

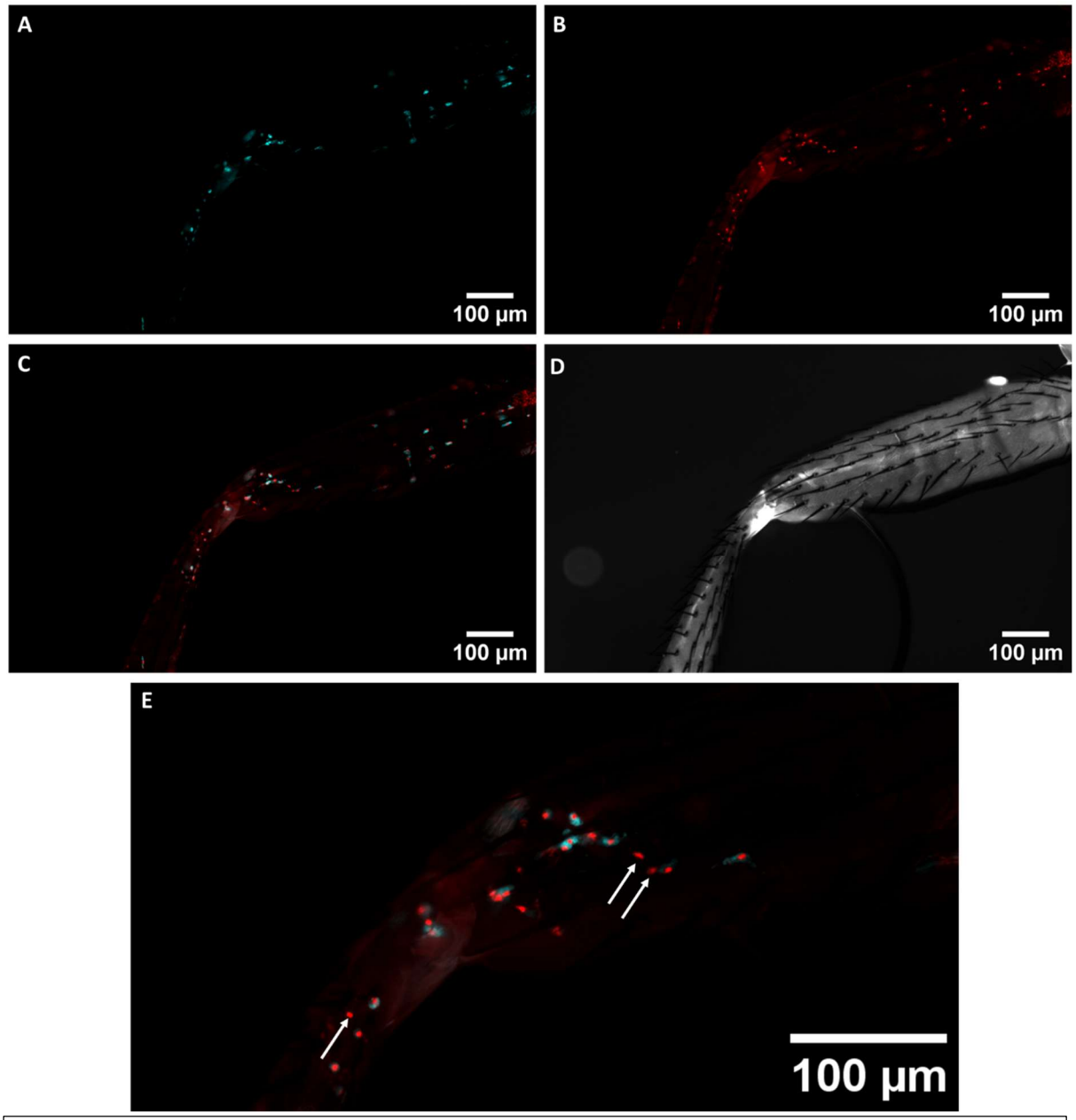

Figure 6.10 - *Enh3-Gal4>UAS-ReddM* lineage tracing can be observed live through *Drosophila's* leg cuticle.

Drosophila legs live imaged 10 days after induction of ReddM mediated lineage tracing. (A) *UAS-CD8:GFP* marks active expression of the Gal4 driver (cyan). (B) *UAS-H2B:RFP* labels cells actively expressing Gal4, in addition to committed progeny (red). (C) A merge of both channels shows co-localization of both markers in many cells, but also several examples of H2B:RFP positive cells which lack CD8:GFP expression. (D) Autofluorescence of the leg in the blue channel to aid visualization of the leg structure. (E) Close-up of (C), showing RFP positive cells which lack CD8:GFP co-localization (white arrows). (n=1 leg per fly from 5 flies).

6.6 Discussion

Whilst we recently celebrated the 60th anniversary of MuSC discovery, we are still lacking a thorough understanding of key mechanisms regarding their maintenance, activation and differentiation. The relatively recent discovery of a DLM-associated MuSC population in *Drosophila* opens new doors into studying conserved processes using this integrative model with its diverse genetic toolkit, to shed further light on the biology of these cells. Here, I have presented a new MuSC marker, identified a novel MuSC population and explored a potential conserved function for Mef2 in muscle maintenance and repair.

Previous to this work, Zfh1 was the only known specific marker of *Drosophila* MuSCs (Chaturvedi *et al.* 2017; Boukhatmi and Bray 2018). Here, I have shown that Him can also be detected in Zfh1+ MuSCs, which will facilitate the generation of further genetic tools, such as Gal4 drivers and reporter lines. As characterized repressors of myogenesis, (Liotta *et al.* 2007; Soler and Taylor 2009; Siles *et al.* 2013) which both act through repression of Mef2, it is likely that Him and Zfh1 are specific to quiescent MuSCs rather than cells that are actively differentiating to mediate repair. Whilst the vertebrate Zfh1 ortholog, ZEB1, has not been linked to repression of Mef2, it is known to be expressed in MuSCs, where it acts to prevent their premature differentiation following injury (Siles *et al.* 2019). This echoes the situation seen in the closely related muscle stem cells of the *Drosophila* wing imaginal disc, where Zfh1 and Him are thought to repress myogenesis until the correct time (Soler and Taylor 2009; Boukhatmi and Bray 2018).

Detection of cells expressing a high level of Mef2 around the periphery of an induced muscle injury strongly suggests that Mef2 function is implicated in the *Drosophila* repair response, as it is in the mouse model (Liu *et al.* 2014). As a crucial regulator of muscle gene expression during *Drosophila* development (Soler *et al.* 2012), its role in MuSCs could be to activate the myogenic program to drive muscle regeneration. To show this *in vivo*, a reporter that is sensitive to Mef2 would inform on its relative activity levels in quiescent vs activated MuSCs.

The finding that *Mef2* knockdown impairs flight ability after two weeks is consistent for a role of Mef2 in MuSCs. In this experiment, the previously characterized MuSC driver *Enh3-Gal4* was used to induce the *UAS-Mef2-RNAi*. It has not formally been

shown that Enh3 is expressed in activated MuSCs, although it is known to be expressed in quiescent MuSCs in control flies (Boukhatmi and Bray 2018). Since Enh3 is a *zfh1* enhancer, it is possible that the *Mef2* knockdown was only induced in quiescent MuSCs, thus a thorough examination of the expression pattern of the Gal4 driver will be required to fully characterize the phenotype. Nonetheless, this is the first functional evidence for Mef2 in promoting muscle homeostasis in *Drosophila*, providing a foundation for future studies exploring the role and regulation of Mef2 in this aspect of muscle biology.

An alternative, more powerful strategy to assay Mef2 loss-of-function in MuSC homeostasis and injury repair would be to use a CRISPR allele switch strategy, compatible with a Mef2-CRISPR null generated in house (Hubbert 2023). This null allele has an attP landing site into which *Mef2* cDNA has previously been inserted to rescue a null embryonic lethal muscle phenotype. In an allele switching strategy, a FRT flanked Mef2 rescue fragment can be flipped out in-place of another cDNA such as a fluorophore, using *UAS-FLP* driven in the cell-type of interest (Poernbacher *et al.* 2019). Using this powerful technique in combination with *Enh3-Gal4*, will ensure that all Gal4-expressing cells and their derived progeny entirely lack *Mef2* function, whilst simultaneously labelling the specific cells where the allele switch has occurred. This will permit a more thorough analysis of *Mef2* loss-of-function in MuSCs, to further characterize its role in MuSC-mediated muscle homeostasis and repair.

The discovery of a putative leg muscle associated MuSC population is a significant step forward for the field for several reasons. Firstly, the leg is an excellent system for live-imaging, which has proven a difficult barrier to overcome in other model systems. There is no substitute for observing MuSC activation and repair live as these events happen. Furthermore, leg muscles are more representative than the DLMs of the vertebrate skeletal system which we are trying to model. Like skeletal muscles, the tubular leg muscles possess laterally aligned sarcomeres and require fine motor input to control movement, thus using this system is arguably more relevant to vertebrate biology. The existence of leg-based assays in the *Drosophila* system, such as gait analysis or jump testing (Mendes *et al.* 2013; Chechenova *et al.* 2017), allows the functional performance of these muscles to be assessed to explore conserved factors implicated in correct muscle homeostasis. Then, findings can be extrapolated to more complex vertebrate models. The leg muscles are also far more

accessible for performing injury/repair assays than the DLMs, which are hidden within the thorax. Thus this system represents a promising new direction for future research into *Drosophila* muscle satellite cell biology.

The data presented in this chapter builds on several aspects of the recently characterized *Drosophila* MuSC system, demonstrating that this model can provide answers about conserved aspects of vertebrate satellite cell biology, such as Mef2 function. Future studies using *Drosophila*'s diverse genetic toolkit will further our understanding of conserved genetic mechanisms underlying muscle repair and homeostasis, in a live-imaging compatible system. Other conserved genes yet to be studied in *Drosophila* muscle repair/maintenance include the Pax7 homolog *gooseberry* (Seale *et al.* 2000b; Seale *et al.* 2004), and *nautilus*, the MyoD homolog which is already known to play an important role in muscle development (Wei *et al.* 2007).

Concluding Remarks

Exploring the function and regulation of Mef2 during muscle development in vertebrate models is proving extremely challenging. There are four *Mef2* genes, with overlapping patterns of expression, and functional redundancy, which makes teasing apart their relative contributions to muscle differentiation a nearly impossible task. Studying the single *Drosophila Mef2*, as I have done here, simplifies this complexity, whilst still informing on conserved aspects of its biology.

In this piece of work, I've studied several distinct, but related, aspects of Mef2 function and regulation. Firstly, I have established that Mef2 overexpression can cause the premature differentiation of adult muscle progenitors (AMPs) in the wing imaginal disc, and developed a method for quantifying Mef2 activity using this system. This will permit future analysis of how mutating conserved regions of interest affects Mef2's transcription factor activity, or how conserved interactions with co-repressors/factors can alter its behavior. Whilst it is possible to study such aspects of Mef2 biology using cell culture-based techniques, there is no substitute for studying a process in its *in vivo* setting, such as in the AMPs of the wing imaginal disc.

My work on *Him* demonstrates one route by which Mef2 activity can be modulated during muscle differentiation. The development of new tools to study Him expression and loss-of-function has unveiled key aspects of its biology, including its involvement in the development of the tubular TDT/ jump muscle, and its repression of Mef2 activity. Whilst there is no known vertebrate ortholog of *Him*, understanding how different factors can influence the myogenic program is of great importance. Specifically, understanding how a balance of signals permits a cell to initially maintain a progenitor-like state, but later can be triggered to differentiate, is essential. This has broad implications for understanding tissue development, and advancing stem cell biology applications.

An additional mechanism I have explored is the role of Mef2's conserved sumoylation motif, which I have demonstrated to be important to Mef2 function. In particular, blocking Mef2 sumoylation enhances its activity, consistent with a role for sumoylation in repressing Mef2 function. Since a sumoylation motif can be found in vertebrate Mef2 family members, my findings are of direct relevance to

understanding how Mef2 activity can be regulated in mammalian systems. Abnormal Mef2 function has already been implicated in cardiomyopathies, neurodevelopmental disorders and cancer (review: Chen *et al.* 2017), so uncovering conserved regulatory mechanisms can lead to advancements in understanding Mef2-related diseases and targeting potential therapies. More broadly, understanding the sumoylation pathway is crucial to both basic biology and health & disease, due to its widespread influence over the localization, stability and interactions of its target substrates.

My work on the newly discovered *Drosophila* muscle satellite cells (MuSCs) illustrates the promise of this emerging model for studying muscle maintenance and repair. Notably, Him is only the second marker identified in this cell type in *Drosophila*, and thus represents a useful tool for identification of these cells. My preliminary investigation into Mef2 function in these cells indicates that Mef2 may be implicated in muscle maintenance and repair, in addition to its role during initial muscle fibre development. This pioneering work further highlights how the adult *Drosophila* system can be used in the future for studying conserved aspects of MuSC biology. This model offers many experimental advances, including its diverse genetic toolkit for probing conserved gene function, and the suitability of the muscle for live imaging to reveal dynamic events such as MuSC activation, division and fusion.

.

Bibliography

Anant, S., Roy, S. and VijayRaghavan, K. (1998). Twist and Notch negatively regulate adult muscle differentiation in Drosophila. **125**(8):1361-1369. doi: 10.1242/dev.125.8.1361

Andres, V., Cervera, M. and Mahdavi, V. (1995). Determination of the consensus binding site for MEF2 expressed in muscle and brain reveals tissue-specific sequence constraints. *Journal of Biological Chemistry* **270**(40):23246–23249. doi: https://doi.org/10.1074/jbc.270.40.23246.

Angelelli, C., Magli, A., Ferrari, D., Ganassi, M., Matafora, V., Parise, F., … Molinari, S. (2008). Differentiation-dependent lysine 4 acetylation enhances MEF2C binding to DNA in skeletal muscle cells. *Nucleic Acids Research* **36**(3):915–928. doi: https://doi.org/10.1093/nar/gkm1114.

Antonello, Z.A., Reiff, T., Ballesta-Illan, E. and Dominguez, M. (2015). Robust intestinal homeostasis relies on cellular plasticity in enteroblasts mediated by miR-8–Escargot switch. *The EMBO Journal* **34**(15):2025. doi: https://doi.org/10.15252/EMBJ.201591517.

Artero, R.D., Castanon, I. and Baylies, M.K. (2001). The immunoglobulin-like protein Hibris functions as a dose-dependent regulator of myoblast fusion and is differentially controlled by Ras and Notch signaling. *Development (Cambridge, England)* **128**(21):4251–4264. doi: https://doi.org/10.1242/DEV.128.21.4251.

Assali, A., Harrington, A.J. and Cowan, C.W. (2019). Emerging Roles for MEF2 in Brain Development and Mental Disorders. *Current opinion in neurobiology* **59**:49. doi: https://doi.org/10.1016/J.CONB.2019.04.008.

Bae, S.H., Jeong, J.W., Park, J.A., Kim, S.H., Bae, M.K., Choi, S.J. and Kim, K.W. (2004). Sumoylation increases HIF-1α stability and its transcriptional activity. *Biochemical and Biophysical Research Communications* **324**(1):394–400. doi: https://doi.org/10.1016/J.BBRC.2004.09.068.

Baker, P.W., Tanaka, K.K.K., Klitgord, N. and Cripps, R.M. (2005). Adult Myogenesis in Drosophila melanogaster Can Proceed Independently of Myocyte Enhancer Factor-2. *Genetics* **170**(4):1747. doi: https://doi.org/10.1534/GENETICS.105.041749.

Bangi, E., Smibert, P., Uzilov, A. V., Teague, A.G., Gopinath, S., Antipin, Y., … Cagan, R.L. (2021). A Drosophila platform identifies a novel, personalized therapy for a patient with adenoid cystic carcinoma. *iScience* **24**(3):102212. doi: https://doi.org/10.1016/J.ISCI.2021.102212.

Bartoletti, R., Capozzoli, B., Moore, J., Moran, J., Shrawder, B. and Vivekanand, P. (2017). Short hairpin RNA is more effective than long hairpin RNA in eliciting pointed loss-of-function phenotypes in Drosophila. *Genesis (New York, N.Y. : 2000)* **55**(7). doi: https://doi.org/10.1002/DVG.23036.

Baruffaldi, F., Montarras, D., Basile, V., De Feo, L., Badodi, S., Ganassi, M., … Molinari, S. (2016). Dynamic Phosphorylation of the Myocyte Enhancer Factor 2C1 Splice Variant Promotes Skeletal Muscle Regeneration and Hypertrophy. *Stem cells*. doi: https://doi.org/10.1002/stem.2495.

Bate, M. and Martinez Arias, A. (1991). The embryonic origin of imaginal discs in Drosophila. *Development* **112**(3):755–761. doi: https://doi.org/10.1242/DEV.112.3.755.

Baylies, M.K. and Bate, M. (1996). twist: A myogenic switch in Drosophila. *Science* **272**(5267):1481–1484. doi: https://doi.org/10.1126/science.272.5267.1481.

Baylies, M.K., Bate, M. and Gomez, M.R. (1998). Myogenesis: A view from Drosophila. *Cell* **93**(6):921–927.

Bernard, F., Kasherov, P., Grenetier, S., Dutriaux, A., Zider, A., Silber, J. and Lalouette, A. (2009). Integration of differentiation signals during indirect flight muscle formation by a novel enhancer of Drosophila vestigial gene. *Developmental Biology* **332**(2):258–272. doi: https://doi.org/10.1016/J.YDBIO.2009.05.573.

Bernard, F., Krejci, A., Housden, B., Adryan, B. and Bray, S.J. (2010). Specificity of Notch pathway activation: Twist controls the transcriptional output in adult muscle progenitors. *Development* **137**(16):2633–2642. doi: https://doi.org/10.1242/dev.053181.

Bernard, F., Lalouette, A., Gullaud, M., Jeantet, A.Y., Cossard, R., Zider, A., … Silber, J. (2003). Control of apterous by vestigial drives indirect flight muscle development in Drosophila. *Developmental Biology* **260**(2):391–403. doi: https://doi.org/10.1016/S0012-1606(03)00255-0.

Bier, E. (2005). Drosophila, the golden bug, emerges as a tool for human genetics. *Nature Reviews Genetics 2005 6:1* **6**(1):9–23. doi: https://doi.org/10.1038/nrg1503.

Bischof, J., Maeda, R., Hediger, M., Karch, F. and Basler, K. (2007). An optimized transgenesis system for Drosophila using germ-line-specific phiC31 integrases. *Proceedings of the National Academy of Sciences of the United States of America* **104**(9):3312–3317. doi: https://doi.org/10.1073/PNAS.0611511104.

Bjornson, C.R.R., Cheung, T.H., Liu, L., Tripathi, P. V., Steeper, K.M. and Rando, T.A. (2012). Notch signaling is necessary to maintain quiescence in adult muscle stem cells. *Stem Cells* **30**(2):232–242. doi: https://doi.org/10.1002/stem.773.

Bodmer, R. (1993). The gene tinman is required for specification of the heart and visceral muscles in Drosophila. *Development (Cambridge, England)* **118**(3):719–729. doi: https://doi.org/10.1242/DEV.118.3.719.

Boukhatmi, H. (2021). Drosophila, an Integrative Model to Study the Features of Muscle Stem Cells in Development and Regeneration. *Cells 2021, Vol. 10, Page 2112* **10**(8):2112. doi: https://doi.org/10.3390/CELLS10082112.

Boukhatmi, H. and Bray, S. (2018). A population of adult satellite-like cells in Drosophila is maintained through a switch in RNA-isoforms. *eLife* **7**:1–24. doi: https://doi.org/10.7554/eLife.35954.

Boulay, J.L., Dennefeld, C. and Alberga, A. (1987). The Drosophila developmental gene snail encodes a protein with nucleic acid binding fingers. *Nature 1987 330:6146* **330**(6146):395–398. doi: https://doi.org/10.1038/330395a0.

Bour, B.A., Chakravarti, M., West, J.M. and Abmayr, S.M. (2000). Drosophila SNS, a member of the immunoglobulin superfamily that is essential for myoblast fusion. *Genes & Development* **14**(12):1498–1511. doi:

https://doi.org/10.1101/GAD.14.12.1498.

Bour, B.A., O'Brien, M.A., Lockwood, W.L., Goldstein, E.S., Bodmer, R., Taghert, P.H., … Nguyen, H.T. (1995). Drosophila MEF2, a transcription factor that is essential for myogenesis. *Genes & development* **9**(6):730–741. doi: https://doi.org/10.1101/GAD.9.6.730.

Brand, A.H., Manoukian, A.S. and Perrimon, N. (1994). Chapter 33 Ectopic Expression in Drosophila. *Methods in Cell Biology* **44**(C):635–654. doi: https://doi.org/10.1016/S0091-679X(08)60936-X.

Brand, A.H. and Perrimon, N. (1993). Targeted gene expression as a means of altering cell fates and generating dominant phenotypes. *Development* **118**(2):401–415. doi: https://doi.org/10.1242/DEV.118.2.401.

Brunetti, T.M., Fremin, B.J. and Cripps, R.M. (2015). Identification of singles bar as a direct transcriptional target of Drosophila Myocyte enhancer factor-2 and a regulator of adult myoblast fusion. *Developmental Biology* **401**(2):299–309. doi: https://doi.org/10.1016/J.YDBIO.2015.02.026.

Bryantsev, A.L., Baker, P.W., Lovato, T.A.L., Jaramillo, M.A.S. and Cripps, R.M. (2012). Differential requirements for Myocyte Enhancer Factor-2 during adult myogenesis in Drosophila. *Developmental Biology* **361**(2):191–207. doi: https://doi.org/10.1016/j.ydbio.2011.09.031.

Caine, C., Kasherov, P., Silber, J. and Lalouette, A. (2014). Mef2 interacts with the notch pathway during adult muscle development in Drosophila melanogaster. *PLoS ONE* **9**(9). doi: https://doi.org/10.1371/journal.pone.0108149.

Campbell, K.B. and Chandra, M. (2006). Functions of Stretch Activation in Heart Muscle. *The Journal of General Physiology J. Gen. Physiol. © The* **127**(2):89–94. doi: https://doi.org/10.1085/jgp.200509483.

Card, G. and Dickinson, M.H. (2008). Visually mediated motor planning in the escape response of Drosophila. *Current biology : CB* **18**(17):1300–1307. doi: https://doi.org/10.1016/J.CUB.2008.07.094.

Carmena, A., Bate, M. and Jimenez, F. (1995). lethal of scute, a proneural gene, participates m the specification of muscle progenitors during Drosophila embryogenesis. *Genes and Development* **9**(19):2373–2383. doi: https://doi.org/10.1101/gad.9.19.2373.

Carmena, A., Gisselbrecht, S., Harrison, J., Jiménez, F. and Michelson, A.M. (1998). Combinatorial signaling codes for the progressive determination of cell fates in the Drosophila embryonic mesoderm. *Genes & Development* **12**(24):3910. doi: https://doi.org/10.1101/GAD.12.24.3910.

Carmena, A., Murugasu-Oei, B., Menon, D., Jiménez, F. and Chia, W. (1998). inscuteable and numb mediate asymmetric muscle progenitor cell divisions during Drosophila myogenesis. *Genes & Development* **12**(3):304. doi: https://doi.org/10.1101/GAD.12.3.304.

Catalani, E., Zecchini, S., Giovarelli, M., Cherubini, A., Del Quondam, S., Brunetti, K., … Cervia, D. (2022). RACK1 is evolutionary conserved in satellite stem cell activation and adult skeletal muscle regeneration. *Cell Death Discovery 2022 8:1*

8(1):1–14. doi: https://doi.org/10.1038/s41420-022-01250-8.

Chakraborty, K., VijayRaghavan, K. and Gunage, R.D. (2018). A Method to Injure, Dissect and Image Indirect Flight Muscle of Drosophila. *BIO-PROTOCOL* **8**(10). doi: https://doi.org/10.21769/BIOPROTOC.2860.

Chambers, M., Turki-Judeh, W., Kim, M.W., Chen, K., Gallaher, S.D. and Courey, A.J. (2017). Mechanisms of Groucho-mediated repression revealed by genome-wide analysis of Groucho binding and activity. *BMC Genomics* **18**(1):1–17. doi: https://doi.org/10.1186/S12864-017-3589-6/FIGURES/7.

Chaturvedi, D., Reichert, H., Gunage, R.D. and VijayRaghavan, K. (2017). Identification and functional characterization of muscle satellite cells in Drosophila. *eLife* **6**. doi: https://doi.org/10.7554/ELIFE.30107.

Chechenova, M.B., Maes, S. and Cripps, R.M. (2015). Expression of the Troponin C at 41C Gene in Adult Drosophila Tubular Muscles Depends upon Both Positive and Negative Regulatory Inputs. *PLOS ONE* **10**(12):e0144615. doi: https://doi.org/10.1371/JOURNAL.PONE.0144615.

Chechenova, M.B., Maes, S., Oas, S.T., Nelson, C., Kiani, K.G., Bryantsev, A.L. and Cripps, R.M. (2017). Functional redundancy and nonredundancy between two Troponin C isoforms in Drosophila adult muscles. *Molecular Biology of the Cell* **28**(6):760. doi: https://doi.org/10.1091/MBC.E16-07-0498.

Chen, X., Gao, B., Ponnusamy, M., Lin, Z. and Liu, J. (2017). MEF2 signaling and human diseases. *Oncotarget* **8**(67):112152–112165.

Choi, J., Jang, H., Kim, H., Lee, J.-H., Kim, S.-T., Cho, E.-J. and Youn, H.-D. (2014). Modulation of lysine methylation in myocyte enhancer factor 2 during skeletal muscle cell differentiation. *Nucleic Acids Research* **42**(1):224–234. doi: https://doi.org/10.1093/NAR/GKT873.

Choma, M.A., Suter, M.J., Vakoc, B.J., Bouma, B.E. and Tearney, G.J. (2011). Physiological homology between Drosophila melanogaster and vertebrate cardiovascular systems. *DMM Disease Models and Mechanisms* **4**(3):411–420. doi: https://doi.org/10.1242/DMM.005231/-/DC1.

Clark, R.I., Tan, S.W.S., Péan, C.B., Roostalu, U., Vivancos, V., Bronda, K., … Dionne, M.S. (2013). MEF2 Is an In Vivo Immune-Metabolic Switch. *Cell* **155**(2):435. doi: https://doi.org/10.1016/J.CELL.2013.09.007.

Cox, D.M., Du, M., Marback, M., Yang, E.C.C., Chan, J., Siu, K.W.M. and McDermott, J.C. (2003). Phosphorylation motifs regulating the stability and function of myocyte enhancer factor 2A. *Journal of Biological Chemistry* **278**(17):15297–15303. doi: https://doi.org/10.1074/jbc.M211312200.

Cripps, R. (1997). The myogenic regulatory gene Mef2 is a direct target for transcriptional activation by Twist during Drosophila myogenesis. *Genes Dev* **12**.

Cripps, Richard M, Black, B.L., Zhao, B., Lien, C.-L., Schulz, R.A. and Olson, E.N. (1998). The myogenic regulatory gene Mef2 is a direct target for transcriptional activation by Twist during Drosophila myogenesis.

Cripps, Richard M., Black, B.L., Zhao, B., Lien, C.L., Schulz, R.A. and Olson, E.N. (1998). The myogenic regulatory gene Mef2 is a direct target for transcriptional

activation by Twist during Drosophila myogenesis. *Genes and Development* **12**(3):422–434. doi: https://doi.org/10.1101/gad.12.3.422.

Crittenden, J.R., Skoulakis, E.M.C., Goldstein, E.S. and Davis, R.L. (2018). Drosophila mef2 is essential for normal mushroom body and wing development. *Biology Open* **7**(9). doi: https://doi.org/10.1242/BIO.035618.

Cunha, P.M.F., Sandmann, T., Hilary Gustafson, E., Ciglar, L., Eichenlaub, M.P. and Furlong, E.E.M. (2010). Combinatorial Binding Leads to Diverse Regulatory Responses: Lmd Is a Tissue-Specific Modulator of Mef2 Activity. *PLOS Genetics* **6**(7):e1001014. doi: https://doi.org/10.1371/JOURNAL.PGEN.1001014.

Dambly-Chaudière, C., Ghysen, A., Jan, Y.N. and Jan, L.Y. (1986). Muscle connections between imaginal discs in Drosophila. *Developmental Biology* **113**(2):288–294. doi: https://doi.org/10.1016/0012-1606(86)90164-8.

Das, D., Aradhya, R., Ashoka, D. and Inamdar, M. (2008). Post-embryonic pericardial cells of Drosophila are required for overcoming toxic stress but not for cardiac function or adult development. *Cell and Tissue Research* **331**(2):565–570. doi: https://doi.org/10.1007/S00441-007-0518-Z/FIGURES/3.

Davis, S.M., Thomas, A.L., Liu, L., Campbell, I.M. and Dierick, H.A. (2018). Isolation of aggressive behavior mutants in drosophila using a screen for wing damage. *Genetics* **208**(1):273–282. doi: https://doi.org/10.1534/GENETICS.117.300292/-/DC1.

Deaguero, A.A., Castillo, L., Oas, S.T., Kiani, K., Bryantsev, A.L. and Cripps, R.M. (2019). Regulation of fiber-specific actin expression by the Drosophila SRF ortholog Blistered. *Development (Cambridge, England)* **146**(7). doi: https://doi.org/10.1242/DEV.164129.

DeSimone, S.M. and White, K. (1993). The Drosophila erect wing gene, which is important for both neuronal and muscle development, encodes a protein which is similar to the sea urchin P3A2 DNA binding protein. *Molecular and cellular biology* **13**(6):3641–3649. doi: https://doi.org/10.1128/MCB.13.6.3641-3649.1993.

Dietzl, G., Chen, D., Schnorrer, F., Su, K.C., Barinova, Y., Fellner, M., … Dickson, B.J. (2007). A genome-wide transgenic RNAi library for conditional gene inactivation in Drosophila. *Nature 2007 448:7150* **448**(7150):151–156. doi: https://doi.org/10.1038/nature05954.

Dobi, K.C., Schulman, V.K. and Baylies, M.K. (2015). Specification of the somatic musculature in Drosophila †. doi: https://doi.org/10.1002/wdev.182.

Drummond, D.R., Hennessey, E.S. and Sparrow, J.C. (1991). Characterisation of missense mutations in the Act88F gene of Drosophila melanogaster. *MGG Molecular & General Genetics* **226**(1–2):70–80. doi: https://doi.org/10.1007/BF00273589.

Duan, H., Skeath, J.B. and Nguyen, H.T. (2001). Drosophila Lame duck, a novel member of the Gli superfamily, acts as a key regulator of myogenesis by controlling fusion-competent myoblast development. *Development* **128**(22):4489–4500. doi: https://doi.org/10.1242/DEV.128.22.4489.

Dutta, D., Shaw, S., Maqbool, T., Pandya, H. and Vijayraghavan, K. Drosophila Heartless Acts with Heartbroken/Dof in Muscle Founder Differentiation. doi:

https://doi.org/10.1371/journal.pbio.0030337.

Duval, D., Duval, G., Kedinger, C., Poch, O. and Boeuf, H. (2003). The 'PINIT' motif, of a newly identified conserved domain of the PIAS protein family, is essential for nuclear retention of PIAS3L. *FEBS Letters* **554**(1–2):111–118. doi: https://doi.org/10.1016/S0014-5793(03)01116-5.

Edmondson, D.G., Lyons, G.E., Martin, J.F. and Olson, E.N. (1994). Mef2 gene expression marks the cardiac and skeletal muscle lineages during mouse embryogenesis. *Development* **120**(5):1251–1263.

Elgar, S.J., Han, J. and Taylor, M. V. (2008). mef2 activity levels differentially affect gene expression during Drosophila muscle development. *Proceedings of the National Academy of Sciences of the United States of America* **105**(3):918–923. doi: https://doi.org/10.1073/pnas.0711255105.

Eliason, J., Afify, A., Potter, C. and Matsumura, I. (2018). A GAL80 Collection To Inhibit GAL4 Transgenes in Drosophila Olfactory Sensory Neurons. *G3: Genes|Genomes|Genetics* **8**(11):3661. doi: https://doi.org/10.1534/G3.118.200569.

Fernandes, J., Bate, M. and Vijayraghavan, K. (1991). *Development of the Indirect Flight Muscles of Drosophila*. *Development* **133**(1):67-77. doi: https://doi.org/10.1242/dev.113.1.67

Fickett, J.W. (1996). Quantitative discrimination of MEF2 sites. *Molecular and Cellular Biology* **16**(1):437–441. doi: https://doi.org/10.1128/mcb.16.1.437.

Fisher, A.L., Ohsako, S. and Caudy, M. (1996). The WRPW Motif of the Hairy-Related Basic Helix-Loop-Helix Repressor Proteins Acts as a 4-Amino-Acid Transcription Repression and Protein-Protein Interaction Domain. *Molecular and Cellular Biology* **16**(6):2670–2677. doi: https://doi.org/10.1128/MCB.16.6.2670.

Frandsen, J.L., Gunn, B., Muratoglu, S., Fossett, N. and Newfeld, S.J. (2008). Salmonella pathogenesis reveals that BMP signaling regulates blood cell homeostasis and immune responses in Drosophila. *Proceedings of the National Academy of Sciences of the United States of America* **105**(39):14952–14957. doi: https://doi.org/10.1073/PNAS.0808208105/SUPPL_FILE/0808208105SI.PDF.

Frasch, M. (1995). Induction of visceral and cardiac mesoderm by ectodermal Dpp in the early Drosophila embryo. *Nature 1995 374:6521* **374**(6521):464–467. doi: https://doi.org/10.1038/374464a0.

Frasch, M. and Levine, M. (1987). Complementary patterns of even-skipped and fushi tarazu expression involve their differential regulation by a common set of segmentation genes in Drosophila. *Genes & development* **1**(9):981–995. doi: https://doi.org/10.1101/GAD.1.9.981.

Gajewski, K., Zhang, Q., Choi, C.Y., Fossett, N., Dang, A., Kim, Y.H., … Schulz, R.A. (2001). Pannier is a Transcriptional Target and Partner of Tinman during Drosophila Cardiogenesis. *Developmental Biology* **233**(2):425–436. doi: https://doi.org/10.1006/DBIO.2001.0220.

Gareau, J.R. and Lima, C.D. (2010). The SUMO pathway: emerging mechanisms that shape specificity, conjugation and recognition. *Nature Reviews Molecular Cell Biology 2010 11:12* **11**(12):861–871. doi: https://doi.org/10.1038/nrm3011.

Gildor, B., Schejter, E.D. and Shilo, B.Z. (2012). Bidirectional Notch activation represses fusion competence in swarming adult Drosophila myoblasts. *Development (Cambridge, England)* **139**(21):4040–4050. doi: https://doi.org/10.1242/DEV.077495.

Girdwood, D., Bumpass, D., Vaughan, O.A., Thain, A., Anderson, L.A., Snowden, A.W., … Hay, R.T. (2003). p300 transcriptional repression is mediated by SUMO modification. *Molecular Cell* **11**(4):1043–1054. doi: https://doi.org/10.1016/S1097-2765(03)00141-2.

Gocke, C.B., Yu, H. and Kang, J. (2005). Systematic Identification and Analysis of Mammalian Small Ubiquitin-like Modifier Substrates *. *Journal of Biological Chemistry* **280**(6):5004–5012. doi: https://doi.org/10.1074/JBC.M411718200.

Gómez, M.R. and Bate, M. (1997). Segregation of myogenic lineages in Drosophila requires Numb. *Development* **124**(23):4857–4866.

Gossett, L.A., Kelvin, D.J., Sternberg, E.A. and Olson, E.N. (1989). A new myocyte-specific enhancer-binding factor that recognizes a conserved element associated with multiple muscle-specific genes. *Molecular and cellular biology* **9**(11):5022–5033. doi: https://doi.org/10.1128/MCB.9.11.5022-5033.1989.

Gratz, S.J., Cummings, A.M., Nguyen, J.N., Hamm, D.C., Donohue, L.K., Harrison, M.M., … O'connor-Giles, K.M. (2013). Genome engineering of Drosophila with the CRISPR RNA-guided Cas9 nuclease. *Genetics* **194**(4):1029–1035. doi: https://doi.org/10.1534/GENETICS.113.152710/-/DC1/GENETICS.113.152710-2.PDF.

Grayson, J., Williams, R.S., Yu, Y.-T. and Bassel-Duby, R. (1995). Synergistic Interactions between Heterologous Upstream Activation Elements and Specific TATA Sequences in a Muscle-Specific Promoter. *Molecular and Cellular Biology* **15**(4):1870–1878. doi: https://doi.org/10.1128/MCB.15.4.1870.

Grégoire, S., Tremblay, A.M., Xiao, L., Yang, Q., Ma, K., Nie, J., … Yang, X.J. (2006). Control of MEF2 transcriptional activity by coordinated phosphorylation and sumoylation. *Journal of Biological Chemistry* **281**(7):4423–4433. doi: https://doi.org/10.1074/jbc.M509471200.

Gunage, R.D., Reichert, H. and VijayRaghavan, K. (2014). Identification of a new stem cell population that generates Drosophila flight muscles. *eLife* **3**(August2014):1–25. doi: https://doi.org/10.7554/eLife.03126.

Gunthorpe, D., Beatty, K.E. and Taylor, M. V (1999). Different Levels, but Not Different Isoforms, of the Drosophila transcription factor DMEF2 Affect Distinct Aspects of Muscle Differentiation. *Developmental Biology* **215**:130-145.

Han, A., He, J., Wu, Y., Liu, J.O. and Chen, L. (2005). Mechanism of recruitment of class II histone deacetylases by myocyte enhancer factor-2. *Journal of Molecular Biology* **345**(1):91–102. doi: https://doi.org/10.1016/j.jmb.2004.10.033.

Haralalka, S. and Abmayr, S.M. (2010). Myoblast Fusion in Drosophila. *Exp Cell Res* **316**(18):3007–3013. doi: https://doi.org/10.1016/j.yexcr.2010.05.018.

Hayashi, S., Manabe, I., Suzuki, Y., Relaix, F. and Oishi, Y. (2016). Klf5 regulates muscle differentiation by directly targeting muscle-specific genes in cooperation with MyoD in mice. *eLife* **5**(OCTOBER2016). doi: https://doi.org/10.7554/ELIFE.17462.

He, J., Ye, J., Cai, Y., Riquelme, C., Liu, J.O., Liu, X., … Chen, L. (2011). Structure of p300 bound to MEF2 on DNA reveals a mechanism of enhanceosome assembly. *Nucleic Acids Research* **39**(10):4464–4474. doi: https://doi.org/10.1093/nar/gkr030.

Hess, N.K., Singer, P.A., Trinh, K., Nikkhoy, M. and Bernstein, S.I. (2007). Transcriptional regulation of the Drosophila melanogaster muscle myosin heavy-chain gene. *Gene expression patterns : GEP* **7**(4):413. doi: https://doi.org/10.1016/J.MODGEP.2006.11.007.

Hietakangas, V., Anckar, J., Blomster, H.A., Fujimoto, M., Palvimo, J.J., Nakai, A. and Sistonen, L. (2006). PDSM, a motif for phosphorylation-dependent SUMO modification. *Proceedings of the National Academy of Sciences of the United States of America* **103**(1):45. doi: https://doi.org/10.1073/PNAS.0503698102.

Hubbert, S. (2023). Mef2 in muscle: A CRISPR-based approach to investigate the regulation of a master transcription factor. PhD Thesis, Cardiff University. https://orca.cardiff.ac.uk/id/eprint/171253

Hunt, L.C. and Demontis, F. (2013). Whole-mount immunostaining of Drosophila skeletal muscle. *Nature Protocols* **8**(12):2496–2501. doi: https://doi.org/10.1038/NPROT.2013.156.

Hyun, J.O., Kido, T. and Lau, Y.F.C. (2007). PIAS1 interacts with and represses SOX9 transactivation activity. *Molecular Reproduction and Development* **74**(11):1446–1455. doi: https://doi.org/10.1002/MRD.20737.

Ilmarinen, T., Kangas, H., Kytömaa, T., Eskelin, P., Saharinen, J., Seeler, J.S., … Ulmanen, I. (2008). Functional interaction of AIRE with PIAS1 in transcriptional regulation. *Molecular Immunology* **45**(7):1847–1862. doi: https://doi.org/10.1016/J.MOLIMM.2007.10.045.

Jaramillo, M.A.S., Lovato, C. V., Baca, E.M. and Cripps, R.M. (2009). Crossveinless and the TGFβ pathway regulate fiber number in the Drosophila adult jump muscle. *Development* **136**(7):1105–1113. doi: https://doi.org/10.1242/DEV.031567.

Johnson, A.N., Mokalled, M.H., Valera, J.M., Poss, K.D. and Olson, E.N. (2013). Post-transcriptional regulation of myotube elongation and myogenesis by Hoi Polloi. *Development* **140**(17):3645–3656. doi: https://doi.org/10.1242/DEV.095596.

Josephson, R.K., Malamud, J.G. and Stokes, D.R. (2000). Asynchronous Muscle: A Primer. *Journal of Experimental Biology* **203**(18):2713–2722. doi: https://doi.org/10.1242/JEB.203.18.2713.

Junion, G., Jagla, T., Duplant, S., Tapin, R., Da Ponte, J.P. and Jagla, K. (2005). Mapping Dmef2-binding regulatory modules by using a ChIP-enriched in silico targets approach. *Proceedings of the National Academy of Sciences of the United States of America* **102**(51):18479–18484. doi: https://doi.org/10.1073/PNAS.0507030102/SUPPL_FILE/07030FIG6.JPG.

Kang, J., Gocke, C.B. and Yu, H. (2006). Phosphorylation-facilitated sumoylation of MEF2C negatively regulates its transcriptional activity. *BMC Biochemistry* **7**:5. doi: https://doi.org/10.1186/1471-2091-7-5.

Kato, Y. (1997). BMK1/ERK5 regulates serum-induced early gene expression through transcription factor MEF2C. *The EMBO Journal* **16**(23):7054–7066. doi:

https://doi.org/10.1093/emboj/16.23.7054.

Komuro, I. and Izumo, S. (1993). Csx: a murine homeobox-containing gene specifically expressed in the developing heart. *Proceedings of the National Academy of Sciences of the United States of America* **90**(17):8145. doi: https://doi.org/10.1073/PNAS.90.17.8145.

Koning, M., Werker, P.M.N., Van Luyn, M.J.A. and Harmsen, M.C. (2011). Hypoxia promotes proliferation of human myogenic satellite cells: A potential benefactor in tissue engineering of skeletal muscle. *Tissue Engineering - Part A* **17**(13–14):1747–1758. doi: https://doi.org/10.1089/TEN.TEA.2010.0624.

Kosman, D., Ip, Y.T., Levine, M. and Arora, K. (1991). Establishment of the mesoderm-neuroectoderm boundary in the Drosophila embryo. *Science* **254**(5028):118–122. doi: https://doi.org/10.1126/SCIENCE.1925551.

Kourmouli, N., Jeppesen, P., Mahadevhaiah, S., Burgoyne, P., Wu, R., Gilbert, D.M., … Singh, P.B. (2004). Heterochromatin and tri-methylated lysine 20 of histone H4 in animals. *Journal of Cell Science* **117**(12):2491–2501. doi: https://doi.org/10.1242/JCS.01238.

Kudron, M.M., Victorsen, A., Gevirtzman, L., Hillier, L.W., Fisher, W.W., Vafeados, D., … Waterston, R.H. (2018). The ModERN Resource: Genome-Wide Binding Profiles for Hundreds of Drosophila and Caenorhabditis elegans Transcription Factors. *Genetics* **208**(3):937–949. doi: https://doi.org/10.1534/GENETICS.117.300657.

Lai, Z., Fortini, M.E. and Rubin, G.M. (1991). The embryonic expression patterns of zfh-1 and zfh-2, two Drosophila genes encoding novel zinc-finger homeodomain proteins. *Mechanisms of Development* **34**(2–3):123–134. doi: https://doi.org/10.1016/0925-4773(91)90049-C.

Lee, P.C., Taylor-Jaffe, K.M., Nordin, K.M., Prasad, M.S., Lander, R.M. and LaBonne, C. (2012). SUMOylated SoxE factors recruit Grg4 and function as transcriptional repressors in the neural crest. *The Journal of Cell Biology* **198**(5):799. doi: https://doi.org/10.1083/JCB.201204161.

Leptin, M. (1991). twist and snail as positive and negative regulators during Drosophila mesoderm development. *Genes and Development* **5**:1568-1576. doi: 10.1101/gad.5.9.1568

Leptin, M. and Grunewald, B. (1990). Cell shape changes during gastrulation in Drosophila. *Development* **110**(1):73–84. doi: https://doi.org/10.1242/DEV.110.1.73.

Leroux, E., Ammar, N., Moinet, S., Pecot, T. and Boukhatmi, H. (2023). Studying Muscle Transcriptional Dynamics at Singlemolecule Scales in Drosophila. *Journal of Visualized Experiments* **2023**(199). doi: https://doi.org/10.3791/65713.

Li, H. and Capetanaki, Y. (1994). An E box in the desmin promoter cooperates with the E box and MEF-2 sites of a distal enhancer to direct muscle-specific transcription. *EMBO Journal* **13**(15):3580–3589. doi: https://doi.org/10.1002/J.1460-2075.1994.TB06665.X.

Lilly, B., Zhao, B., Ranganayakulu, G., Paterson, B.M., Schulz, R.A. and Olson, E.N. (1995). Requirement of MADS Domain Transcription Factor D-MEF2 for Muscle

Formation in Drosophila. *Science* **267**(5198):688–693. doi: https://doi.org/10.1126/SCIENCE.7839146.

Lin, Q., Lu, J., Yanagisawa, H., Webb, R., Lyons, G.E., Richardson, J.A. and Olson, E.N. (1998). Requirement of the MADS-box transcription factor MEF2C for vascular development. *Development* **125**(22):4565–4574. doi: https://doi.org/10.1242/DEV.125.22.4565.

Lin, W.H. and Baines, R.A. (2019). Myocyte enhancer factor-2 and p300 interact to regulate the expression of homeostatic regulator Pumilio in Drosophila. *European Journal of Neuroscience* **50**(1):1727–1740. doi: https://doi.org/10.1111/ejn.14357.

Lindon, C., Montarras, D. and Pinset, C. (1998). Cell Cycle–regulated Expression of the Muscle Determination Factor Myf5 in Proliferating Myoblasts. *The Journal of Cell Biology* **140**(1):111. doi: https://doi.org/10.1083/JCB.140.1.111.

Lints, T.J., Parsons, L.M., Hartley, L., Lyons, I. and Harvey, R.P. (1993). Nkx-2.5: a novel murine homeobox gene expressed in early heart progenitor cells and their myogenic descendants. *Development* **119**(2):419–431. doi: https://doi.org/10.1242/DEV.119.2.419.

Liotta, D., Han, J., Elgar, S., Garvey, C., Han, Z. and Taylor, M. V. (2007). The Him Gene Reveals a Balance of Inputs Controlling Muscle Differentiation in Drosophila. *Current Biology* **17**(16):1409–1413. doi: https://doi.org/10.1016/j.cub.2007.07.039.

Liu, B., Yang, R., Wong, K.A., Getman, C., Stein, N., Teitell, M.A., … Shuai, K. (2005). Negative Regulation of NF-κB Signaling by PIAS1. *Molecular and Cellular Biology* **25**(3):1113. doi: https://doi.org/10.1128/MCB.25.3.1113-1123.2005.

Liu, N., Nelson, B.R., Bezprozvannaya, S., Shelton, J.M., Richardson, J.A., Bassel-Duby, R. and Olson, E.N. (2014). Requirement of MEF2A, C, and D for skeletal muscle regeneration. *Proceedings of the National Academy of Sciences of the United States of America* **111**(11):4109–4114. doi: https://doi.org/10.1073/PNAS.1401732111/-/DCSUPPLEMENTAL.

Lockwood, W.K. and Bodmer, R. (2002). The patterns of wingless, decapentaplegic, and tinman position the Drosophila heart. *Mechanisms of Development* **114**(1–2):13–26. doi: https://doi.org/10.1016/S0925-4773(02)00044-8.

Lomelí, H. and Vázquez, M. (2011). Emerging roles of the SUMO pathway in development. *Cellular and Molecular Life Sciences 2011 68:24* **68**(24):4045–4064. doi: https://doi.org/10.1007/S00018-011-0792-5.

Lu, H., Liu, B., You, S., Chen, L., Dongmei, Q., Gu, M., … Yu, B. (2013). SENP2 regulates MEF2A de-SUMOylation in an activity dependent manner. *Molecular Biology Reports* **40**(3):2485–2490. doi: https://doi.org/10.1007/s11033-012-2329-x.

Lu, J., McKinsey, T.A., Zhang, C.L. and Olson, E.N. (2000). Regulation of Skeletal Myogenesis by Association of the MEF2 Transcription Factor with Class II Histone Deacetylases. *Molecular Cell* **6**(2):233–244. doi: https://doi.org/10.1016/S1097-2765(00)00025-3.

Luan, H., Peabody, N.C., Vinson, C.R.R. and White, B.H. (2006). Refined Spatial Manipulation of Neuronal Function by Combinatorial Restriction of Transgene Expression. *Neuron* **52**(3):425–436. doi:

https://doi.org/10.1016/j.neuron.2006.08.028.

Ma, K., Chan, J.K.L., Zhu, G. and Wu, Z. (2005). Myocyte Enhancer Factor 2 Acetylation by p300 Enhances Its DNA Binding Activity, Transcriptional Activity, and Myogenic Differentiation. *Molecular and Cellular Biology* **25**(9):3575–3582. doi: https://doi.org/10.1128/mcb.25.9.3575-3582.2005.

Maeda, T., Gupta, M.P. and Stewart, A.F.R. (2002). TEF-1 and MEF2 transcription factors interact to regulate muscle-specific promoters. *Biochemical and Biophysical Research Communications* **294**(4):791–797. doi: https://doi.org/10.1016/S0006-291X(02)00556-9.

Maggert, K., Levine, M. and Frasch, M. (1995). The somatic-visceral subdivision of the embryonic mesoderm is initiated by dorsal gradient thresholds in Drosophila. *Development (Cambridge, England)* **121**(7):2107–2116. doi: https://doi.org/10.1242/DEV.121.7.2107.

Mahajan, R., Delphin, C., Guan, T., Gerace, L. and Melchior, F. (1997). A small ubiquitin-related polypeptide involved in targeting RanGAP1 to nuclear pore complex protein RanBP2. *Cell* **88**(1):97–107. doi: https://doi.org/10.1016/S0092-8674(00)81862-0.

Mannervik, M. (2014). Control of Drosophila embryo patterning by transcriptional co-regulators. *Experimental cell research* **321**(1):47–57. doi: https://doi.org/10.1016/J.YEXCR.2013.10.010.

Matunis, M.J., Coutavas, E. and Blobel, G. (1996). A novel ubiquitin-like modification modulates the partitioning of the Ran-GTPase-activating protein RanGAP1 between the cytosol and the nuclear pore complex. *Journal of Cell Biology* **135**(6):1457–1470. doi: https://doi.org/10.1083/JCB.135.6.1457.

McClure, C.D., Hassan, A., Aughey, G.N., Butt, K., Estacio-Gómez, A., Duggal, A., … Southall, T.D. (2022). An auxin-inducible, GAL4-compatible, gene expression system for Drosophila. *eLife* **11**. doi: https://doi.org/10.7554/ELIFE.67598.

McGuire, S.E., Le, P.T., Osborn, A.J., Matsumoto, K. and Davis, R.L. (2003). Spatiotemporal Rescue of Memory Dysfunction in Drosophila. *Science* **302**(5651):1765–1768. doi: https://doi.org/10.1126/SCIENCE.1089035/SUPPL_FILE/MCGUIRE.SOM.PDF.

McKinsey, T.A., Zhang, C.L. and Olson, E.N. (2002). MEF2: A calcium-dependent regulator of cell division, differentiation and death. *Trends in Biochemical Sciences* **27**(1):40–47. doi: https://doi.org/10.1016/S0968-0004(01)02031-X.

de Mena, L. and Rincon-Limas, D.E. (2020). PhotoGal4: A Versatile Light-Dependent Switch for Spatiotemporal Control of Gene Expression in Drosophila Explants. *iScience* **23**(7):101308. doi: https://doi.org/10.1016/j.isci.2020.101308.

Mendes, C.S., Bartos, I., Akay, T., Márka, S. and Mann, R.S. (2013). Quantification of gait parameters in freely walking wild type and sensory deprived Drosophila melanogaster. *eLife* **2013**(2). doi: https://doi.org/10.7554/ELIFE.00231.

Messenguy, F. and Dubois, E. (2003). Role of MADS box proteins and their cofactors in combinatorial control of gene expression and cell development. *Gene* **316**(1–2):1–21.

Mirzoyan, Z., Sollazzo, M., Allocca, M., Valenza, A.M., Grifoni, D. and Bellosta, P. (2019). Drosophila melanogaster: A model organism to study cancer. *Frontiers in Genetics* **10**:425859. doi: https://doi.org/10.3389/FGENE.2019.00051/BIBTEX.

Miska, E.A., Karlsson, C., Langley, E., Nielsen, S.J., Pines, J. and Kouzarides, T. (1999). HDAC4 deacetylase associates with and represses the MEF2 transcription factor. *The EMBO journal* **18**(18):5099–5107. doi: https://doi.org/10.1093/EMBOJ/18.18.5099.

Mitchell-Gee, R., Hoff, R., Vishal2, K., Hancock1, D., Mckitrick4, S., Newnes-Querejeta1, C., … Taylor1+, M. V (2024). The Drosophila myogenic inhibitor Him gene is essential for adult muscle function and muscle stem cell maintenance. *bioRxiv*:2024.09.06.611611. doi: https://doi.org/10.1101/2024.09.06.611611.

Miyawaki, A. (2011). Development of probes for cellular functions using fluorescent proteins and fluorescence resonance energy transfer. *Annual review of biochemistry* **80**:357–373. doi: https://doi.org/10.1146/ANNUREV-BIOCHEM-072909-094736.

Molkentin, J.D., Black, B.L., Martin, J.F. and Olson, E.N. (1995). Cooperative activation of muscle gene expression by MEF2 and myogenic bHLH proteins. *Cell* **83**(7):1125–1136. doi: https://doi.org/10.1016/0092-8674(95)90139-6.

Molkentin, J.D., Firulli, A.B., Black, B.L., Martin, J.F., Hustad, C.M., Copeland, N., … Olson, E.N. (1996). MEF2B is a potent transactivator expressed in early myogenic lineages. *Molecular and Cellular Biology* **16**(7):3814–3824. doi: https://doi.org/10.1128/mcb.16.7.3814.

Morriss, G.R., Bryantsev, A.L., Chechenova, M., Labeau, E.M., Lovato, T.L., Ryan, K.M. and Cripps, R.M. (2012). Analysis of Skeletal Muscle Development in Drosophila. *Methods in molecular biology (Clifton, N.J.)* **798**:127. doi: https://doi.org/10.1007/978-1-61779-343-1_8.

Muller, H.J. (1918). Genetic Variability, Twin Hybrids and Constant Hybrids, in a Case of Balanced Lethal Factors. *Genetics* **3**(5):422. doi: https://doi.org/10.1093/GENETICS/3.5.422.

Nayak, A. and Müller, S. (2014). SUMO-specific proteases/isopeptidases: SENPs and beyond. *Genome Biology* **15**(7):422. doi: https://doi.org/10.1186/S13059-014-0422-2/FIGURES/4.

Nicolas, N., Gallien, C.L. and Chanoine, C. Analysis of MyoD, Myogenin, and Muscle-Specific Gene mRNAs in Regenerating Xenopus Skeletal Muscle. *DEVELOPMENTAL DYNAMICS* **201**:6048–6049. doi: https://doi.org/10.1002/(SICI)1097-0177(199609)207:1.

Otto, N.M. and Potter, L.R. (2022). Vicinal glutamates are better phosphomimetics: Phosphorylation is required for allosteric activation of guanylyl cyclase-A. *Frontiers in Molecular Neuroscience* **15**:1012784. doi: https://doi.org/10.3389/FNMOL.2022.1012784/BIBTEX.

Oustanina, S., Hause, G. and Braun, T. (2004). Pax7 directs postnatal renewal and propagation of myogenic satellite cells but not their specification. *EMBO Journal* **23**(16):3430–3439. doi: https://doi.org/10.1038/SJ.EMBOJ.7600346.

Paleologou, K.E., Schmid, A.W., Rospigliosi, C.C., Kim, H.Y., Lamberto, G.R.,

Fredenburg, R.A., … Lashuel, H.A. (2008). Phosphorylation at Ser-129 but Not the Phosphomimics S129E/D Inhibits the Fibrillation of α-Synuclein. *Journal of Biological Chemistry* **283**(24):16895–16905. doi: https://doi.org/10.1074/JBC.M800747200.

Panta, M., Kump, A.J., Dalloul, J.M., Schwab, K.R. and Ahmad, S.M. (2020). Three distinct mechanisms, Notch instructive, permissive, and independent, regulate the expression of two different pericardial genes to specify cardiac cell subtypes. *PLOS ONE* **15**(10):e0241191. doi: https://doi.org/10.1371/JOURNAL.PONE.0241191.

Peckham, M., Molloy, J.E., Sparrow, J.C. and White, D.C.S. (1990). Physiological properties of the dorsal longitudinal flight muscle and the tergal depressor of the trochanter muscle of Drosophila melanogaster. *Journal of Muscle Research and Cell Motility* **11**(3):203–215. doi: https://doi.org/10.1007/BF01843574/METRICS.

Perochon, J., Yu, Y., Aughey, G.N., Medina, A.B., Southall, T.D. and Cordero, J.B. (2021). Dynamic adult tracheal plasticity drives stem cell adaptation to changes in intestinal homeostasis in Drosophila. *Nature cell biology* **23**(5):485. doi: https://doi.org/10.1038/S41556-021-00676-Z.

Philippos, M., Sambasivan, R., Castel, D., Rocheteau, P., Bizzarro, V. and Tajbakhsh, S. (2012). A critical requirement for notch signaling in maintenance of the quiescent skeletal muscle stem cell state. *Stem cells (Dayton, Ohio)* **30**(2):243–252. doi: https://doi.org/10.1002/STEM.775.

Pitsouli, C. and Perrimon, N. (2010). Embryonic multipotent progenitors remodel the Drosophila airways during metamorphosis. *Development* **137**(21):3615–3624. doi: https://doi.org/10.1242/DEV.056408.

Plevin, M.J., Mills, M.M. and Ikura, M. (2005). The LxxLL motif: a multifunctional binding sequence in transcriptional regulation. *Trends in biochemical sciences* **30**(2):66–69. doi: https://doi.org/10.1016/J.TIBS.2004.12.001.

Poernbacher, I., Crossman, S., Kurth, J., Nojima, H., Baena-Lopez, A., 3+, C.A. and Vincent, J.-P. (2019). Lessons in genome engineering: opportunities, tools and pitfalls. *bioRxiv*:710871. doi: https://doi.org/10.1101/710871.

Port, F., Chen, H.M., Lee, T. and Bullock, S.L. (2014). Optimized CRISPR/Cas tools for efficient germline and somatic genome engineering in Drosophila. *Proceedings of the National Academy of Sciences of the United States of America* **111**(29). doi: https://doi.org/10.1073/PNAS.1405500111/-/DCSUPPLEMENTAL/PNAS.201405500SI.PDF.

Postigo, A.A., Ward, E., Skeath, J.B. and Dean, D.C. (1999). zfh-1, the Drosophila Homologue of ZEB, Is a Transcriptional Repressor That Regulates Somatic Myogenesis. *Molecular and Cellular Biology* **19**(10):7255. doi: https://doi.org/10.1128/MCB.19.10.7255.

Potthoff, M.J., Arnold, M.A., McAnally, J., Richardson, J.A., Bassel-Duby, R. and Olson, E.N. (2007). Regulation of Skeletal Muscle Sarcomere Integrity and Postnatal Muscle Function by Mef2c. *Molecular and Cellular Biology* **27**(23):8143–8151. doi: https://doi.org/10.1128/mcb.01187-07.

Potthoff, M.J. and Olson, E.N. (2007). MEF2: A central regulator of diverse developmental programs. *Development* **134**(23):4131–4140. doi: https://doi.org/10.1242/dev.008367.

Ranganayakulu, G., Zhao, B., Dokidis, A., Molkentin, J.D., Olson, E.N. and Schulz, R.A. (1995). A Series of Mutations in the D-MEF2 Transcription Factor Reveal Multiple Functions in Larval and Adult Myogenesis in Drosophila. *Developmental Biology* **171**(1):169–181. doi: https://doi.org/10.1006/dbio.1995.1269.

Reim, I. and Frasch, M. (2005). The Dorsocross T-box genes are key components of the regulatory network controlling early cardiogenesis in Drosophila. *Development* **132**(22):4911–4925. doi: https://doi.org/10.1242/DEV.02077.

Relaix, F., Montarras, D., Zaffran, S., Gayraud-Morel, B., Rocancourt, D., Tajbakhsh, S., … Buckingham, M. (2006). Pax3 and Pax7 have distinct and overlapping functions in adult muscle progenitor cells. *Journal of Cell Biology* **172**(1):91–102. doi: https://doi.org/10.1083/JCB.200508044.

Riquelme, C., Barthel, K.K.B. and Liu, X. (2006). SUMO-1 modification of MEF2A regulates its transcriptional activity. *Journal of Cellular and Molecular Medicine* **10**(1):132–144. doi: https://doi.org/10.1111/J.1582-4934.2006.TB00295.X.

Romagnoli, C., Iantomasi, T. and Brandi, M.L. (2021). Available In Vitro Models for Human Satellite Cells from Skeletal Muscle. *International Journal of Molecular Sciences 2021, Vol. 22, Page 13221* **22**(24):13221. doi: https://doi.org/10.3390/IJMS222413221.

Rosonina, E., Akhter, A., Dou, Y., Babu, J. and Theivakadadcham, V.S.S. (2017). Regulation of transcription factors by sumoylation. *Transcription* **8**(4):220. doi: https://doi.org/10.1080/21541264.2017.1311829.

Roy, S. and VijayRaghavan, K. (1998). Patterning muscles using organizers: Larval muscle templates and adult myoblasts actively interact to pattern the dorsal longitudinal flight muscles of Drosophila. *Journal of Cell Biology* **141**(5):1135–1145. doi: https://doi.org/10.1083/jcb.141.5.1135.

Ruiz-Gómez, M., Coutts, N., Price, A., Taylor, M. V. and Bate, M. (2000). Drosophila dumbfounded: a myoblast attractant essential for fusion. *Cell* **102**(2):189–198. doi: https://doi.org/10.1016/S0092-8674(00)00024-6.

Ruiz-Gómez, M., Coutts, N., Suster, M.L., Landgraf, M. and Bate, M. (2002). myoblasts incompetent encodes a zinc finger transcription factor required to specify fusion-competent myoblasts in Drosophila. *Development* **129**(1):133–141. doi: https://doi.org/10.1242/DEV.129.1.133.

Rushton, E., Drysdale, R., Abmayr, S.M., Michelson, A.M. and Bate, M. (1995). Mutations in a novel gene, myoblast city, provide evidence in support of the founder cell hypothesis for Drosophila muscle development. *Development* **121**(7):1979–1988. doi: https://doi.org/10.1242/DEV.121.7.1979.

S Anant, S.R.K.V. (1998). Twist and Notch negatively regulate adult muscle differentiation in Drosophila. *Development* **125**:1361–1369.

San Martin, B., Ruiz-Gómez, M., Landgraf, M. and Bate, M. (2001). A distinct set of founders and fusion-competent myoblasts make visceral muscles in the Drosophila embryo. *Development* **128**(17):3331–3338. doi: https://doi.org/10.1242/DEV.128.17.3331.

Sandmann, T., Girardot, C., Brehme, M., Tongprasit, W., Stolc, V. and Furlong,

E.E.M. (2007). A core transcriptional network for early mesoderm development in Drosophila melanogaster. *Genes & Development* **21**(4):436. doi: https://doi.org/10.1101/GAD.1509007.

Sandmann, T., Jensen, L.J., Jakobsen, J.S., Karzynski, M.M., Eichenlaub, M.P., Bork, P. and Furlong, E.E.M. (2006). A Temporal Map of Transcription Factor Activity: Mef2 Directly Regulates Target Genes at All Stages of Muscle Development. *Developmental Cell* **10**(6):797–807. doi: https://doi.org/10.1016/j.devcel.2006.04.009.

Sarov, M., Barz, C., Jambor, H., Hein, M.Y., Schmied, C., Suchold, D., … Schnorrer, F. (2016). A genome-wide resource for the analysis of protein localisation in Drosophila. *eLife* **5**(FEBRUARY2016). doi: https://doi.org/10.7554/ELIFE.12068.

Schäfer, G., Weber, S., Holz, A., Bogdan, S., Schumacher, S., Müller, A., … Önel, S.F. (2007). The Wiskott-Aldrich syndrome protein (WASP) is essential for myoblast fusion in Drosophila. *Developmental biology* **304**(2):664–674. doi: https://doi.org/10.1016/J.YDBIO.2007.01.015.

Schnorrer, F., Schönbauer, C., Langer, C.C.H., Dietzl, G., Novatchkova, M., Schernhuber, K., … Dickson, B.J. (2010). Systematic genetic analysis of muscle morphogenesis and function in Drosophila. *Nature 2010 464:7286* **464**(7286):287–291. doi: https://doi.org/10.1038/nature08799.

Schönbauer, C., Distler, J., Jährling, N., Radolf, M., Dodt, H.U., Frasch, M. and Schnorrer, F. (2011). Spalt mediates an evolutionarily conserved switch to fibrillar muscle fate in insects. *Nature 2011 479:7373* **479**(7373):406–409. doi: https://doi.org/10.1038/nature10559.

Seale, P., Ishibashi, J., Holterman, C. and Rudnicki, M.A. (2004). Muscle satellite cell-specific genes identified by genetic profiling of MyoD-deficient myogenic cell. *Developmental biology* **275**(2):287–300. doi: https://doi.org/10.1016/J.YDBIO.2004.07.034.

Seale, P., Sabourin, L.A., Girgis-Gabardo, A., Mansouri, A., Gruss, P. and Rudnicki, M.A. (2000a). Pax7 is required for the specification of myogenic satellite cells. *Cell* **102**(6):777–786. doi: https://doi.org/10.1016/S0092-8674(00)00066-0.

Seale, P., Sabourin, L.A., Girgis-Gabardo, A., Mansouri, A., Gruss, P. and Rudnicki, M.A. (2000b). Pax7 is required for the specification of myogenic satellite cells. *Cell* **102**(6):777–786. doi: https://doi.org/10.1016/S0092-8674(00)00066-0.

Shalizi, A., Bilimoria, P.M., Stegmüller, J., Gaudillière, B., Yang, Y., Shuai, K. and Bonni, A. (2007). PIASx is a MEF2 SUMO E3 ligase that promotes postsynaptic dendritic morphogenesis. *Journal of Neuroscience* **27**(37):10037–10046. doi: https://doi.org/10.1523/JNEUROSCI.0361-07.2007.

Shaner, N.C., Lambert, G.G., Chammas, A., Ni, Y., Cranfill, P.J., Baird, M.A., … Wang, J. (2013). A bright monomeric green fluorescent protein derived from Branchiostoma lanceolatum. *Nature Methods 2013 10:5* **10**(5):407–409. doi: https://doi.org/10.1038/nmeth.2413.

Shen, H., McElhinny, A.S., Cao, Y., Gao, P., Liu, J., Bronson, R., … Wu, L. (2006). The Notch coactivator, MAML1, functions as a novel coactivator for MEF2C-mediated transcription and is required for normal myogenesis. *Genes and*

Development **20**(6):675–688. doi: https://doi.org/10.1101/GAD.1383706.

Shi, X., Du, Y., Li, S. and Wu, H. (2022). The Role of SUMO E3 Ligases in Signaling Pathway of Cancer Cells. *International Journal of Molecular Sciences* **23**(7):3639. doi: https://doi.org/10.3390/IJMS23073639/S1.

Siles, L., Ninfali, C., Cortés, M., Darling, D.S. and Postigo, A. (2019). ZEB1 protects skeletal muscle from damage and is required for its regeneration. *Nature Communications 2019 10:1* **10**(1):1–18. doi: https://doi.org/10.1038/s41467-019-08983-8.

Siles, L., Sánchez-Tilló, E., Lim, J.-W., Darling, Douglas S., Kroll, K.L. and Postigo, A. (2013). ZEB1 Imposes a Temporary Stage-Dependent Inhibition of Muscle Gene Expression and Differentiation via CtBP-Mediated Transcriptional Repression. *Molecular and Cellular Biology* **33**(7):1368–1382. doi: https://doi.org/10.1128/MCB.01259-12.

Simpson, P. (1983). Maternal-Zygotic Gene Interactions during Formation of the Dorsoventral Pattern in Drosophila embryos. **105**(3):615-632. 10.1093/genetics/105.3.615.

Smith, T.H., Block, N.E., Rhodes, S.J., Konieczny, S.F. and Miller, J.B. (1993). A unique pattern of expression of the four muscle regulatory factor proteins distinguishes somitic from embryonic, fetal and newborn mouse myogenic cells. *Development (Cambridge, England)* **117**(3):1125–1133. doi: https://doi.org/10.1242/DEV.117.3.1125.

Snodgrass, R.E. (1994). *Principles of Insect Morphology*. Cornell University Press, Cornell.

Snyder, C.M., Rice, A.L., Estrella, N.L., Held, A., Kandarian, S.C. and Naya, F.J. (2013). MEF2A regulates the Gtl2-Dio3 microRNA mega-cluster to modulate WNT signaling in skeletal muscle regeneration. *Development (Cambridge, England)* **140**(1):31–42. doi: https://doi.org/10.1242/DEV.081851.

Sohr, A., Du, L. and Roy, S. (2019). Ex vivo Drosophila Wing Imaginal Disc Culture and Furin Inhibitor Assay. *Bio-protocol* **9**(16). doi: https://doi.org/10.21769/BIOPROTOC.3336.

Soler, C., Daczewska, M., Da Ponte, J.P., Dastugue, B. and Jagla, K. (2004). Coordinated development of muscles and tendons of the Drosophila leg. *Development* **131**(24):6041–6051. doi: https://doi.org/10.1242/dev.01527.

Soler, C., Han, J. and Taylor, M. V. (2012). The conserved transcription factor Mef2 has multiple roles in adult Drosophila musculature formation. *Development* **139**(7):1270–1275. doi: https://doi.org/10.1242/dev.077875.

Soler, C. and Taylor, M. V. (2009). The Him gene inhibits the development of Drosophila flight muscles during metamorphosis. *Mechanisms of Development* **126**(7):595–603. doi: https://doi.org/10.1016/j.mod.2009.03.003.

Spicer, R. (2024). Analysis of genetic and protein interactions associated with mutant Huntingtin-induced degeneration. PhD Thesis, Cardiff University. https://orca.cardiff.ac.uk/id/eprint/174133

Spletter, M.L., Barz, C., Yeroslaviz, A., Zhang, X., Lemke, S.B., Bonnard, A., … Schnorrer, F. (2018). A transcriptomics resource reveals a transcriptional transition during ordered sarcomere morphogenesis in flight muscle. *eLife* **7**:1–34. doi: https://doi.org/10.7554/eLife.34058.

Spradling, A.C. and Rubin, G.M. (1982). Transposition of cloned P elements into Drosophila germ line chromosomes. *Science (New York, N.Y.)* **218**(4570):341–347. doi: https://doi.org/10.1126/SCIENCE.6289435.

Staehling-Hampton, K., Hoffmann, F.M., Baylies, M.K., Rushtont, E. and Bate, M. (1994). dpp induces mesodermal gene expression in Drosophila. *Nature* **372**(6508):783–786. doi: https://doi.org/10.1038/372783A0.

Strünkelnberg, M., Bonengel, B., Moda, L.M., Hertenstein, A., Gert de Couet, H., Ramos, R.G.P. and Fischbach, K.F. (2001). rst and its paralogue kirre act redundantly during embryonic muscle development in Drosophila. *Development (Cambridge, England)* **128**(21):4229–4239. doi: https://doi.org/10.1242/DEV.128.21.4229.

Sudarsan, V., Anant, S., Guptan, P., Vijayraghavan, K. and Skaer, H. (2001). Myoblast Diversification and Ectodermal Signaling in Drosophila. *Developmental Cell* **1**(6):829–839. doi: https://doi.org/10.1016/S1534-5807(01)00089-2.

Suzuki, T., Ichiyama, A., Saitoh, H., Kawakami, T., Omata, M., Chung, C.H., … Tanaka, K. (1999). A new 30-kDa ubiquitin-related SUMO-1 hydrolase from bovine brain. *Journal of Biological Chemistry* **274**(44):31131–31134. doi: https://doi.org/10.1074/jbc.274.44.31131.

Taylor, M. V., Beatty, K.E., Hunter, H.K. and Baylies, M.K. (1995). Drosophila MEF2 is regulated by twist and is expressed in both the primordia and differentiated cells of the embryonic somatic, visceral and heart musculature. *Mechanisms of Development* **50**(1):29–41. doi: https://doi.org/10.1016/0925-4773(94)00323-F.

Taylor, M. V. and Hughes, S.M. (2017). Mef2 and the skeletal muscle differentiation program. *Seminars in Cell and Developmental Biology* **72**:33–44. doi: https://doi.org/10.1016/j.semcdb.2017.11.020.

Taylor, M. V (2013). Comparison of Muscle Development in Drosophila and Vertebrates. Madame Curie Bioscience Database [Internet]. Austin (TX): Landes Bioscience; 2000-2013. https://www.ncbi.nlm.nih.gov/books/NBK6226/

Trimarchi, J.R. and Schneiderman, A.M. (1995). Initiation of flight in the unrestrained fly, Drosophila melanogaster. *Journal of Zoology* **235**(2):211–222. doi: https://doi.org/10.1111/J.1469-7998.1995.TB05138.X.

Tsao, C.K., Ku, H.Y., Lee, Y.M., Huang, Y.F. and Sun, Y.H. (2016). Long Term Ex Vivo Culture and Live Imaging of Drosophila Larval Imaginal Discs. *PLoS ONE* **11**(9). doi: https://doi.org/10.1371/JOURNAL.PONE.0163744.

Uchimura, Y., Ichimura, T., Uwada, J., Tachibana, T., Sugahara, S., Nakao, M. and Saitoh, H. (2006). Involvement of SUMO modification in MBD1- and MCAF1-mediated heterochromatin formation. *The Journal of biological chemistry* **281**(32):23180–23190. doi: https://doi.org/10.1074/JBC.M602280200.

Urbani, L., Piccoli, M., Franzin, C., Pozzobon, M. and de Coppi, P. (2012). Hypoxia

Increases Mouse Satellite Cell Clone Proliferation Maintaining both In Vitro and In Vivo Heterogeneity and Myogenic Potential. *PLoS ONE* **7**(11). doi: https://doi.org/10.1371/JOURNAL.PONE.0049860.

Verheyen, E.M. (2022). The power of Drosophila in modeling human disease mechanisms. *Disease models & mechanisms* **15**(3). doi: https://doi.org/10.1242/DMM.049549.

Vishal, K., Barajas Alonso, E., DeAguero, A.A., Waters, J.A., Chechenova, M.B. and Cripps, R.M. (2023). Phosphorylation of the Myogenic Factor Myocyte Enhancer Factor-2 Impacts Myogenesis In Vivo. *Molecular and cellular biology* **43**(6):241–253. doi: https://doi.org/10.1080/10985549.2023.2198167.

Vishal, K., Lovato, T.A.L., Bragg, C., Chechenova, M.B. and Cripps, R.M. (2020). FGF signaling promotes myoblast proliferation through activation of wingless signaling. *Developmental Biology* **464**(1):1–10. doi: https://doi.org/10.1016/J.YDBIO.2020.05.009.

Wang, D.Z., Renee Valdez, M., McAnally, J., Richardson, J. and Olson, E.N. (2001). The Mef2c gene is a direct transcriptional target of myogenic bHLH and MEF2 proteins during skeletal muscle development. *Development* **128**(22):4623–4633. doi: https://doi.org/10.1242/DEV.128.22.4623.

Wang, Jianbo, Sun, Z., Zhang, Z., Saadi, I., Wang, Jun, Li, X., … Amendt, B.A. (2013). Protein Inhibitors of Activated STAT (Pias1 and Piasy) Differentially Regulate Pituitary Homeobox 2 (PITX2) Transcriptional Activity. *The Journal of Biological Chemistry* **288**(18):12580. doi: https://doi.org/10.1074/JBC.M112.374561.

Wei, Q., Rong, Y. and Paterson, B.M. (2007). Stereotypic founder cell patterning and embryonic muscle formation in Drosophila require nautilus (MyoD) gene function. *Proceedings of the National Academy of Sciences of the United States of America* **104**(13):5461–5466. doi: https://doi.org/10.1073/pnas.0608739104.

Wen, Y., Bi, P., Liu, W., Asakura, A., Keller, C. and Kuang, S. (2012). Constitutive Notch Activation Upregulates Pax7 and Promotes the Self-Renewal of Skeletal Muscle Satellite Cells. *Molecular and Cellular Biology* **32**(12):2300. doi: https://doi.org/10.1128/MCB.06753-11.

Yang, S.H. and Sharrocks, A.D. (2004). SUMO promotes HDAC-mediated transcriptional repression. *Molecular cell* **13**(4):611–617. doi: https://doi.org/10.1016/S1097-2765(04)00060-7.

Young, P.E., Richman, A.M., Ketchum, A.S. and Kiehart, D.P. (1993). Morphogenesis in Drosophila requires nonmuscle myosin heavy chain function. *Genes and Development* **7**(1). doi: https://doi.org/10.1101/GAD.7.1.29.

Zack, G.W., Rogers, W.E. and Latt, S.A. (1977). Automatic measurement of sister chromatid exchange frequency. *The journal of histochemistry and cytochemistry : official journal of the Histochemistry Society* **25**(7):741–753. doi: https://doi.org/10.1177/25.7.70454.

Zappia, M.P., Castro, L. de, Ariss, M., Islam, A.B.M.M.K. and Frolov, M. (2019). A single-cell transcriptome atlas of the adult muscle precursors uncovers early events in fiber-type divergence in Drosophila. *bioRxiv*:806281. doi: https://doi.org/10.1101/806281.

Zappia, M.P. and Frolov, M. V. (2016). E2F function in muscle growth is necessary and sufficient for viability in Drosophila. *Nature Communications 2016 7:1* **7**(1):1–16. doi: https://doi.org/10.1038/ncomms10509.

Zhang, M., Zhu, B. and Davie, J. (2015). Alternative splicing of MEF2C pre-mRNA controls its activity in normal myogenesis and promotes tumorigenicity in rhabdomyosarcoma cells. *Journal of Biological Chemistry* **290**(1):310–324. doi: https://doi.org/10.1074/jbc.M114.606277.

Zhao, C. and Swank, D.M. (2013). An Embryonic Myosin Isoform Enables Stretch Activation and Cyclical Power in Drosophila Jump Muscle. *Biophysical Journal* **104**(12):2662. doi: https://doi.org/10.1016/J.BPJ.2013.04.057.

Zhao, M., New, L., Kravchenko, V. V., Kato, Y., Gram, H., di Padova, F., … Han, J. (1999). Regulation of the MEF2 Family of Transcription Factors by p38. *Molecular and Cellular Biology* **19**(1):21–30. doi: https://doi.org/10.1128/mcb.19.1.21.

Zhao, Y., van de Leemput, J. and Han, Z. (2023). The opportunities and challenges of using Drosophila to model human cardiac diseases. *Frontiers in Physiology* **14**:1182610. doi: https://doi.org/10.3389/FPHYS.2023.1182610/BIBTEX.

Zumstein, N., Forman, O., Nongthomba, U., Sparrow, J.C. and Elliott, C.J.H. (2004). Distance and force production during jumping in wild-type and mutant Drosophila melanogaster. *Journal of Experimental Biology* **207**(20):3515–3522. doi: https://doi.org/10.1242/JEB.01181.